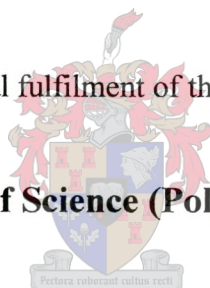# BLENDS WITH LOW-DENSITY POLYETHYLENE (LDPE) AND PLASTOMERS

By

ALLAN JOHN RABIE

Thesis presented in partial fulfilment of the requirements for the degree of

Master of Science (Polymer Science)

at the

University of Stellenbosch

Study Leaders:
Dr. P.E. Mallon
Dr A J van Reenen

Stellenbosch
December 2004

DECLARATION

I, the undersigned hereby declare that the work contained in this thesis is my own original work and has not previously, in its entirety or in part, been submitted at any university for a degree

ABSTRACT

This study describes the design, building and optimization of a fully functional preparative TREF (Prep-TREF) apparatus. This apparatus allows for the fractionation of semi-crystalline polyolefins according to the crystallizability of the molecules. Various factors, such as the sample cooling rate and the effect of on-support and off-support crystallization, are investigated.

The preparative TREF is used to fractionate a commercial low-density polyethylene (LDPE), two commercially available plastomers (polyethylene-1-octene copolymers), as well as blends of the LDPE and the respective plastomers. It is shown that in each case the samples fractionated by crystallizability. The fractions recovered from the Prep-TREF were characterized by CRYSTAF, DSC and NMR analysis. It is shown how the results of this preparative fractionation allow for a better understanding of the molecular heterogeneity in the LDPE and plastomers.

New ways of presenting the data from the preparative fractionation, in terms of 3-dimensional plots, are also investigated. These plots offer a novel way of presenting the molecular heterogeneity in the samples in terms of the molecular crystallizability. These plots highlight features that are difficult to detect in the conventional two-dimensional plots.

In conclusion, the influences of various blending ratios of LDPE and plastomer on the morphological and physical properties of the blends, such as haze, clarity, and tear-and impact strength are determined.

OPSOMMING

Die doel van hierdie studie was die ontwikkeling en optimisering van 'n ten volle funksionerende TREF. Hierdie tegniek word gebruik om polimeermengsels te fraksioneer deur gebruik te maak van die kristaliseerbaarheid van polimere. Verskeie faktore soos die afkoel spoed en die effect van met en sonder 'n ondersteuning(seesand) vir kristaliseering was ondersoek.

Hierna is navorsing gedoen om 'n beter begrip ten opsigte van die meganiese, fisiese en optiese eienskappe van lae-digtheid poliëtileen (LDPE) te ontwikkel. Hierdie LDPE is met die affiniteitsreeks plastomere van die maatskappy, Dow Chemicals, gemeng om tendense in die gefraksioneerde polimere te indentifiseer.

Een van Sasol se kommersiële LDPE produkte en twee van Dow Chemicals se plastomere is individueel gefraksioneer. Die mengsel van die twee ongefraksioneerde LDPE en plastomere is nog nooit voorheen op 'n molekulêre basis ondersoek nie. Dit is in hierdie studie gedoen deur van TREF gebruik te maak.

Nuwe maniere is ontwikkel om data op 'n nuwe manier voortestel deur middel van 3 Dimentionele grafieke te skep om resultate voortestel wat andersins baie moelilik was om voortestel in een dimensie agv die hoeveelheid data wat geinterpriteer word.

Ten slotte is die invloed van die verskillende mengverhoudings van LDPE en plastomere op die morfologiese en fisiese eienskappe soos deursigtigheid, helderheid, skeur- en impaksterkte, ook ondersoek.

This thesis is dedicated to my mother and father,

for their unwavering confidence in me over the years,

and to my fiancé.

ACKNOWLEDGEMENTS

LIST OF ABBREVIATIONS

AFM	atomic force microscopy
Br	branched carbon in NMR
CCD	chemical composition distribution
CH	carbon hydrogen bond
CRYSTAF	crystallization analysis fractionation
DMA	dynamic mechanical analysis
DSC	differential scanning calorimetry
2-D	two-dimensional
3-D	three-dimensional
EPDM	ethylene-propylene-diene monomer
FTIR	Fourier transform infrared
ΔG	Gibbs free energy
GC	gas chromatography
ΔH	enthalpy
HDPE	high density polyethylene
HT-SEC	high-temperature size exclusion chromatography
LCB	long-chain branching
LDPE	low density polyethylene
LLDPE	linear low density polyethylene
LMWPE	low molecular weight polyethylene
MD	machine direction
MFI	melt flow index
Mn	number average molecular weight
Mw	weight average molecular weight
MWD	molecular weight distribution
NMR	nuclear magnetic resonance spectroscopy
Plastomer A	Plastomer – Dow PL1881
Plastomer B	Plastomer – Dow VP8770
PP	polypropylene

ΔS	entropy
SCB	short-chain branching
SCBC	short-chain branching content
SCBD	short-chain branching distribution
SEC	size-exclusion chromatography
SEM	scanning electron microscopy
ΔT	temperature range
T_c	crystallization temperature
$T_{c\ (CRYSTAF)}$	CRYSTAF crystallization temperature at peak maximum
$T_{c\ (TREF)}$	TREF crystallization temperature at peak maximum
TCB	trichlorobenzene
TD	transverse direction
TEM	transmission electron microscopy
T_m	melting temperature
TREF	temperature rising elution fractionation
UHMWPE	ultra-high molecular weight polyethylene
VLDPE	very low-density polyethylene
W_i	weight fraction
$W_i\%$	weight fraction percentage
$\sum W_i\%$	sum of weight fraction percentage

LIST OF CONTENTS

LIST OF FIGURES

LIST OF TABLES

CHAPER 3

CHAPER 4

CHAPTER 1

INTRODUCTION AND OBJECTIVES

1.1) Introduction

Polyethylenes have a wide general structural variation: High Density Polyethylene (HDPE), Low Density Polyethylene (LDPE), Very Low Density Polyethylene (VLDPE) or Linear Low Density Polyethylene (LLDPE).

In South Africa, LDPE is mainly used in the film blowing industry. Sasol Polymers currently has 80% of the LDPE market in South Africa and plans to open a new high-pressure tubular reactor plant in 2005. This plant is expected to have a capacity of 220 000 tons per year. New markets for LDPE therefore have to be considered. One option is to blend the LDPE with a plastomer (an ethylene-octene copolymer with a relatively high octene content).

With the ever increasing compositional heterogeneity of polyethylene and ethylene-higher α-olefin copolymers and/or its blends, the knowledge of simply molecular weight vs. molecular weight distribution of a resin, as determined by Size-Exclusion Chromatography (SEC) is no longer sufficient to define the architecture of such a resin. Changes in the molecular properties of a resin will lead to changes in the morphological and physical properties of a resin. The research carried out for this thesis was done in an effort to better understand the structure property relationship of LDPE and its blends with plastomers, and to obtain worthwhile analytical data that could be useful in guiding the further development of LDPE and its blends. Blending LDPE with a plastomer will change the morphology and physical properties of the polymer blend. This blending will improve the draw-down properties and resistance to burn holing during shrinkage, increase the heat sealing range and improve sealing through contamination in extrusion film blowing.

The technique of Temperature Rising Elution Fractionation (TREF) involves the fractionation of a heterogeneous polymer by crystallizability. Preparative fractionation (Prep-TREF) by crystallizability allows for the recovery of relatively large fractions. These fractions can then be further characterized by other analytical techniques, such as CRYSTAF (Crystallization analysis fractionation), SEC, NMR (Nuclear Magnetic Resonance) and DSC

(Differential scanning calorimetry). This leads to a better understanding of the molecular heterogeneity of the polymers.

1.2) Objectives

The first and main objective of this project was to design and build a fully operational preparative TREF (Prep-TREF) apparatus. There were two main steps in the process that had to be considered. Various factors, such as cooling rate and crystallization on-support and off-support were investigated to determine the best procedure and technique for achieving optimum fractionation.

A further objective was to achieve a better understanding of the molecular heterogeneity of selected LPDE/plastomer blends. This was to be done by first fractionating the LDPE and the plastomers individually. These plastomers are metallocene catalyzed LLDPE-1-Octene (Linear low density polyethylene-1-Octene)polymers. The fractionation of the blends of these complex mixtures were also achieved, using Prep-TREF, and then determining the influence the two commercially available plastomers have on the molecular, morphological and physical properties of the respective LDPE/plastomer blends. By combining preparative fractionation with analytical techniques such as CRYSTAF and DSC, comparative techniques can be studied. It was possible with these techniques to study effects, such as co-crystallization, in the blends.

Lastly, new and useful ways of combining the data from the preparative fractionation with data from other analytical techniques were to be investigated. This data was to be summarized and presented in three-dimensional (3-D) plots.

CHAPTER 2

HISTORICAL AND THEORETICAL BACKGROUND

2.1) Early developments in the field of polyolefins

2.1.1) Introduction

The word 'polymeric' was first used by Berzeluis in 1832. [1] In 1832 Berthelot was the first to describe the polymerization of organic compounds. [2-4] The word olefin is based on the term 'olefiant' (oil-forming gas), first used by four pioneer Dutch chemists. The words alkene, ethene, propene, and so on are preferred in IUPAC nomenclature, but polymer scientists have chosen to use the equivalent trivial names: olefin, ethylene, propylene, and so on.

In 1858 Goryainov and Butlerov produced polypentene by the addition of a trace of boron trifluoride to pentene. In 1869 they published procedures used in their attempts to polymerize ethylene, propylene and pentene. [5] While they were able to polymerize propylene and isobutylene in the presence of traces of boron trifluoride [6], they were unsuccessful in their attempts to polymerize ethylene. Butlerov was the first to use the word 'polypropylene', in 1876. In 1894 Von Pechmann observed that a solution of diazomethane in ether, on standing, yielded a white substance, a linear low molecular weight polymer of ethylene, which could be recrystallized from chloroform. [7] In 1931 Taylor and Jones reported the successful polymerization of ethylene in the presence of diethylmercury. [8]

2.1.2) Early commercial production of polyolefins

During a study carried out in 1933 by Imperial Chemical Industries on the high-pressure chemistry of organic compounds, polyethylene was discovered as a trace of white powder in a reactor vessel. This discovery, first reported by Fawcett and Gibson in 1934 [9], resulted in the basic patent [10] for the high-pressure production of polyethylene. Commercialization was however delayed as the process involved numerous technical problems. The highly exothermic free-radical polymerization of ethylene required precise control and extensive safety procedures. In spite of this, and at the time that Hitler's troops invaded Poland, large quantities of LDPE

3

were being produced as insulation for coaxial cables used in radar. The first commercial plant constructed by ICI was ready in 1939. Upon the outbreak of war it was decided to double capacity and build a second new plant, which was also in full production by 1942. [11] During the war the polyethylene produced was exclusively for military use. After ICI started production, licenses were subsequently granted to Union Carbide and Du Pont. Today this peroxide-initiated, highly branched polymer, called low-density polyethylene (LDPE), is manufactured under pressures of up to 3000 bar and temperatures of 100-300 degrees Celsius. This is done preferably in continuous fashion in stirred autoclaves or in tubular reactors, with diameters less than 25 mm and lengths up to 30 meters, utilizing bulk or solution processes. [12]

Since LDPE has extensive branching the crystallinity is low, resulting in relatively low densities. Commercial density grades of between 0.915 and 0.945 g/cm^3 can be obtained by varying the reaction conditions. [13] Two types of branches have been identified:

- Long-chain branching (LCB), caused by intermolecular chain transfer reactions. In this reaction the active chain-end extracts a hydrogen from a neighboring chain, thereby initiating a growth centre for a new branch, and terminates itself. See Figure 2.1.

- Short-chain branching, identified through studies of infrared absorption and degradation under bombardment with high energy radiation. The result of intramolecular transfer reactions is shown in Figure 2.2.

When the active chain-end extracts hydrogen from its parent chain through a mechanism known as backbiting, butyl branches are formed. When further reactions occur with the hydrogen on the butyl branch, directly after the addition of ethylene to the active site, ethylene branches result. [12]

2.2) Polyethylenes

2.2.1) Polyethylene

Polyethylenes have a wide structural variation that depends on the degree and nature of the branching. Polyethylene can be HDPE with a density of 0.968 g/cm^3 and a high crystallinity of 70%, all the way down to VLDPE with a density of 0.86 g/cm^3 and a low crystallinity of 10%. The commercial LDPE that will be studied here has a broad heterogeneity resulting from its

preparation by the Ziegler Natta polymerized autoclave process. The uneven temperature ranges in the autoclave process cause the broad heterogeneity in this commercial LDPE product.
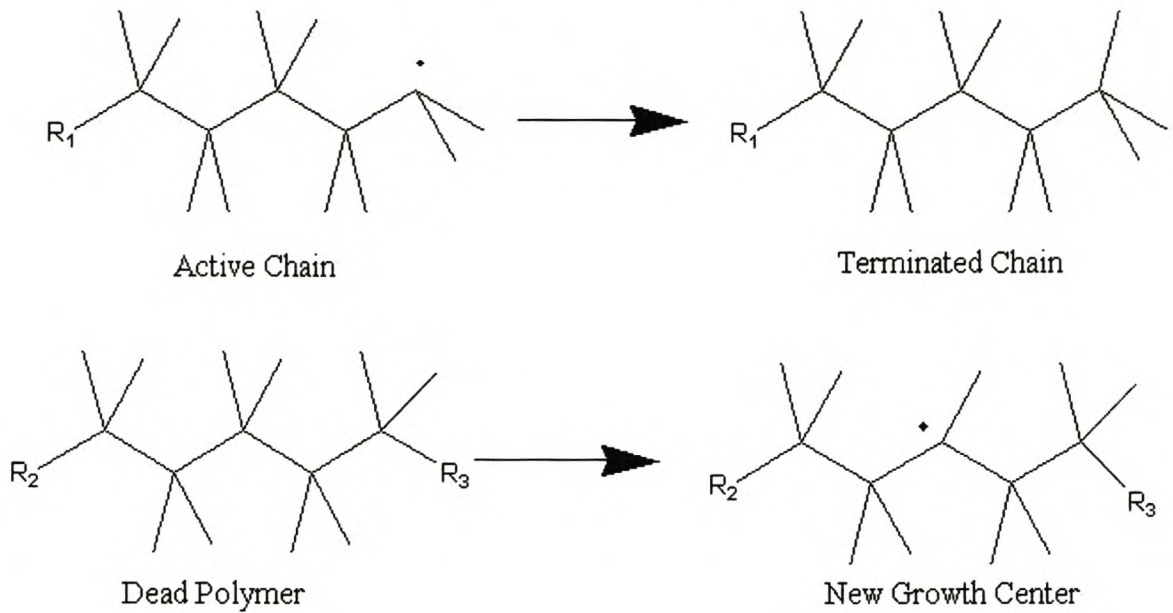
Figure 2.1 Branching in LDPE via intermolecular transfer.
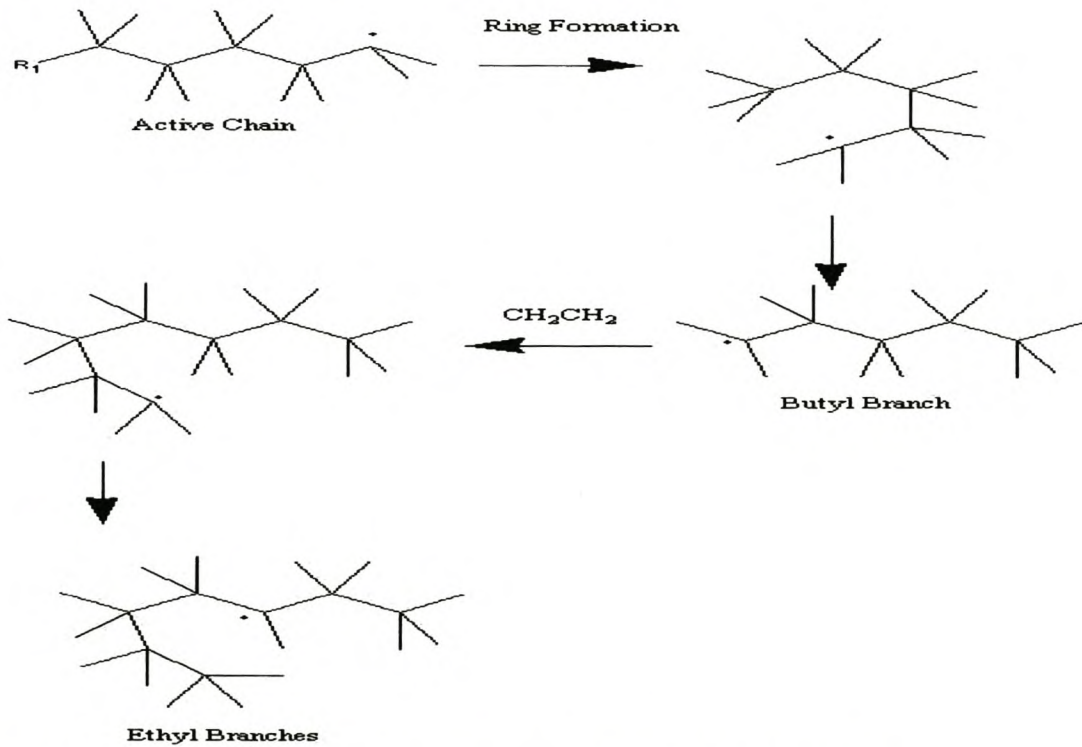
Figure 2.2 Intramolecular transfers through butyl and ethyl branches.

5

2.2.2) Metallocene catalyzed and Ziegler Natta catalyzed PE

In polymers such as linear low-density polyethylene (LLDPE), the comonomer distribution plays a critical role in influencing the ultimate properties of the polymer, e.g. clarity, toughness, tensile strength. There are differences between the properties of Ziegler Natta catalyzed LLDPE (as manufactured by Sasol Polymers) and metallocene (or single site) catalyzed LLDPE. This is because of the difference in distribution of the alpha olefin comonomer along the LLDPE backbone. Ziegler Natta catalyzed LLDPE is often thought of as consisting of three major fractions: a highly branched low molecular weight fraction, an intermediate molecular weight fraction with much less branching, and a high molecular weight (HDPE-like) fraction with very few branches. It is the latter fraction that gives rise to the high haze levels due to its ability to crystallize easily. Metallocene catalyzed PE shows a much more even distribution of comonomer. There is no HDPE fraction. Spherulite sizes are much smaller and light scattering and refraction is reduced compared to conventional LLDPE. Properties such as toughness and tear strength are also improved through this more even distribution of the comonomer.

2.3)   Polymer blends

2.3.1) Introduction

The individual members of the polyolefin family offer a fairly broad spectrum of structures, properties and applications. This spectrum can be expanded even further by blending individual polyolefins with other polymers. Several commercial blends are available. For example: Low molecular weight polyethylene (LMWPE) is added to ultra-high molecular weight polyethylene (UHMWPE) to improve processibility, and low density polyethylene (LDPE) is blended with linear low density polyethylene (LLDPE) to enhance and improve processibility. Furthermore, many other polymers can be improved by adding polyolefins to them. For example, ethylene-propylene-diene terpolymer rubber (EPDM) is added to polypropylene (PP) to improve low-temperature impact strength and PP is added to EPDM to produce thermoplastic elastomers.

Utracki *et al.* [14] compiled a detailed list that included 60 commercial polyolefin blends. This is clear proof of the large and rapid growing practical significance of these materials.

2.3.2) Miscibility and compatibility

For about the past five decades, polyblend scientists and engineers have used the terms miscibility and compatibility loosely and/or interchangeably. Many still do, and most of the literature is written in that way. In recent years however scientists have begun to recognize a very important distinction between these two terms. For absolute clarity and understanding, thermodynamic miscibility describes polymer blends that are completely miscible and homogeneous down to the molecular level and do not show any phase separation at all. In contrast, practical compatibility describes polymer blends that have properties useful in commercial practice. [15] It should be emphasized that most of the commercially useful polyblends have practical compatibility even through they do not have thermodynamic miscibility. For two polymers to be completely miscible down to the molecular level, the mixing process must produce a decrease in free energy ΔG. [16]

$$\Delta G = \Delta H - T\Delta S \leq 0$$

Enthalpy (ΔH) depends on the relative attraction/repulsion of the two polymers. Unlike molecules usually repel each other, thus ΔH is generally positive (unfavorable to mixing). Entropy (ΔS) results from the randomization, which occurs upon mixing. Since small solvent molecules produce great randomization, most solvents are miscible, whereas large polymer molecules produce very little randomization upon mixing. This little randomization is usually not enough to overcome the repulsion between unlike molecules ($+\Delta H$). Thus most polymer blends, lacking thermodynamic miscibility (compatibilization), separate into two or more micro phases. [17] When a polymer blend is thermodynamically immiscible it separates into two or more phases. This usually leads to poor practical properties. Generally it is assumed that either the particle size of the dispersed domains is not optimum, or else the immiscibility of the two phases produces weak interfaces, that fail under low stresses. The most popular way of trying to solve these problems is by the addition of a third ingredient. If this third ingredient succeeds it is then called a compatibilizer. In rare cases the compatibilizer actually produces complete

thermodynamic miscibility. In most cases however it simply acts as a surfactant to reduce the domain size, or as an adhesive to strengthen the interphase between the two immiscible polymer phases. Success is judged by improvement in practical properties. [17]

2.3.3) Polyolefin blends

Chem *et al.* [18] blended LDPE or long-chain branched VLDPE with VLDPE containing short branches. They then investigated the melting behavior of the pure copolymers and their blends. This was done using Differential Scanning Calorimetry (DSC) after applying stepwise isothermal crystallization ('thermal fractionation'). Thermal fractionation separates polymers according to their branching densities. The authors used fractioned curves to determine the short-chain branching distribution (SCB), crystallization and miscibility of blends. They then illustrated that when both polymers had similar unbranched segments, they could co-crystallize if they were miscible in the melt. They also showed that DSC fractionated curves allowed a detailed examination of co-crystallization and miscibility of blends. These DSC results were also comparable to the results they obtained using TREF. Shanks *et al.* [19] blended LLDPE and VLDPE with long chain branching, and prepared these blends by extrusion mixing. All their copolymers were commercial ethylene-octene copolymers and had similar branch lengths. Their copolymers and blends were subjected to crystallization ('thermal fractionation') by stepwise cooling, interspersed with isothermal periods, and the fractionated samples were examined using DSC. As mentioned, thermal fractionation by DSC separates copolymers and blends according to their branching densities. They used their thermal fractionation data to calculate branching distribution in polyethylenes using calibration curves obtained from the literature. They found that LLDPE contained a broad distribution of branching densities whereas the VLDPE contained a narrow distribution, though with shorter average lengths between branches. Their blends with high amounts of VLDPE showed some miscibility in the melt, suggesting that co-crystallization between the copolymers may have occurred.

Morgan *et al.* [20] investigated the crystalline texture of a blend of linear polyethylene and a blend of deuterated linear polyethylene with LDPE as a function of the rate of cooling from the melt. DSC, TEM(transmission electron microscopy) and FTIR(fourier transform infrared) were used to study co-crystallization and phase segregation. On the basis of their previous studies, their blend compositions were chosen so that the melt contained a single phase.

Segregation between components was found to occur, as a result of crystallization, during cooling at all rates other than rapid quenching. The degree of segregation was found to increase with decreasing cooling rate. The morphologies resulting from the phase segregation during crystallization were compared with the morphologies (previously determined by the authors) of blends of other compositions rapidly quenched from what was believed to be a phase-separated melt. Their scale of phase segregation was found to differ by more than an order of magnitude between the two types of morphologies. These results supported their argument that their rapidly quenched samples, which contained two crystal types, did so because of phase separation in the melt and not because of phase separation upon crystallization. These authors also made a comparison between two methods of sample preparation for transmission electron microscopy: permanganic etching/replication and chloro-sulfonic fixation/sectioning. They found the latter method better for revealing detailed morphological features between large lamellae.

Hedenqvist *et al.* [21] studied the fracture behavior of binary mixtures of low molar mass linear polyethylene (L2.5:M_w = 2500 g mol^{-1}, M_w/M_n = 1.15) and higher molar mass linear and branched polyethylenes. The average tie-chain concentration of the different samples had been indirectly estimated. They found that the true stress at fracture, fracture strain and fracture energy increased with the calculated average tie-chain concentration for all their binary blends. For their binary mixtures of L2.5 and the higher molar mass linear polyethylene there was no unique relationship between true stress at fracture and calculated average tie-chain concentration, suggesting that segregation of L2.5 was an important factor determining the strength of these samples. The fact that their L2.5 branched polyethylene blends with intimately mixed constituents exhibited higher strength than their L2.5/linear polyethylene mixtures, with a distinct segregation of L2.5, was explained as being due to the higher average tie-chain concentration in their former blends.

Fan *et al.* [22] studied the effects of branching characteristics of LDPE on its melt miscibility with HDPE. They used molecular dynamics to compute Hildebrand solubility parameters (δ) of models of HDPE and LDPE with different branch contents at five temperatures that were well above their melting temperatures. Their values computed for δ agreed very well with their experimental results. The Flory-Huggins interaction parameters (χ) for blends of HDPE and different LDPE models were then calculated using their computed δ values. The level of branch content for LDPE above which the blends were immiscible and segregated in the melt

was found to be around 30 branches/1000 long-chain carbons at their chosen simulation temperatures. These values were significantly lower than those of butene-based linear low-density polyethylene (LLDPE) (40 branches/1000 carbons) in blends with HDPE. The major difference between their LDPE and LLDPE models was that each modeled LDPE molecule had three long chains while each modeled LLDPE molecule had only one long chain. Their results together with those of the LLDPE/HDPE blends suggested that long-chain branching could have a significant influence on the miscibility of polyethylene blends at elevated temperatures.

Tanem *et al.* [23] investigated blends of LMWPE and several different ethylene-hexene copolymers, using DSC and TEM. All their blend components were the products of single-site catalysts. When cooling rates higher than 1°C/min were used, reorganization effects were generally present, making interpretation of their blends less clear. Organization effects were found to be dependent of the amount of comonomer in their branched blends.

Stori [24] examined the phase behavior in the melt in blends of a single-site catalyzed linear polyethylene and several single-site branched ethylen-1-alkene copolymers. They used an indirect technique based on the examination of rapidly quenched melts in the solid state, using DSC, TEM and AFM. The extent of phase separation was found to have increased if the amount of comonomer in the branched blend component was increased. These results were observed for ethyl and butyl type short chain branches and found to be valid as long the amount of comonomer was less than approximately 5%. For higher amounts of comonomer incorporation, the extent of phase separation was found to be approximately constant. These observations might be partly predicted from theory if an extra repulsive potential was added to the basic Flory-Huggins equation.

2.3.4) Plastomers

Metallocene plastomers are polyolefins with a very low density (= 0.915), a narrow molecular weight distribution and a narrow composition distribution. There are a number of ranges of plastomers that are commercially available. The two most notable suppliers are Exxon-Mobil, with their Exact plastomer range, and Dow Chemicals, with their Affinity plastomer range. These specific plastomers consists of LLDPE with octene as co-monomer, and the weight percentage comonomer content must be within the range 10-40%. These metallocene plastomers

are characterized by their excellent processability. The most important properties they bring to plastic films are: excellent sealability, very high toughness and good optics.

Almost every film property except stiffness is better in plastomers than in any other polyolefin. [25] The exceptional properties of these metallocene catalyzed plastomers are a result of the clean and organized molecular structure of these polymers. Indeed, every comonomer molecule introduced is effective in every one of the polymer chains. In conventional ethylene-based polymers many molecules are lost in low molecular weight chains, which in turn plays a negative role in terms of extractables and surface properties. [25] The ultimate mechanical properties will be achieved by using metallocene plastomers neat, but this is likely to be at the expense of throughput rates (speed of film blowing). The ultimate mechanical properties however are not always required and blending a plastomer with LDPE allows the film producer to optimize the material to the application and extruder requirements and tailor-make a material for maximum performance at the lowest possible cost. In this study two commercially available plastomers from the Dow Affinity range were selected for investigation. (See the experimental section, Section 3.1.1.)

2.4) Fractionation and characterization of polyolefins

2.4.1) Introduction

As polyolefins are of a heterogeneous nature they are often fractionated in order to understand the variations in molecular structure. Fractionation, followed by a detailed micro-structural analysis of the respective fractions, allows us to obtain a better understanding of the physical properties of the polyolefins.

Free radical polymerized polymers yields polymers with heterogeneity in the molecular weight (Mw), chemical composition distribution (CCD) and short-chain branching distribution (SCBD).

Examples of types of fractionation include: fractionation according to molecular weight, using preparative Size-Exclusion Chromatography (SEC), and solvent extraction and fractionation according to crystallizability, typically using Prep-TREF [26-29] or CRYSTAF. [30] The crystallization of polyolefins is influenced by: their molecular properties, molecular

weight (MW), molecular weight distribution (MWD), the comonomer type, comonomer amount and comonomer distribution. [31-34]

Using Prep-TREF one is able to obtain polymer fractions in sufficient quantities to study their mechanical and physical properties. Analysis of the respective fractions by DMA(dynamic mechanical analysis), DSC and microscopy provide valuable data about morphology, and information on the influence of molecular structure on morphology can be obtained. [35,36] Lee *et al.* [37] have shown that DMA is especially useful in determining the glass transition temperatures of various phases in a polymer sample. Smith *et al.* [38] also showed that spherulite size and size distribution could be correlated with surface and internal haze; a higher density polymer may have lower haze due to the effect of spherulite size and size distribution. All the above mentioned factors are responsible for the ultimate (mechanical) properties (haze, gloss, tensile strength, stress crack resistance) of a polymer. Nuclear magnetic resonance spectroscopy (NMR) can be used to determine the actual short-chain branching content (SCBC) of each fraction. Further, by isothermally crystallizing a polymer at various temperatures, information similar to that obtainable by TREF can be obtained via DSC.

Smith *et al.* [38] reported that spherulite size and size distribution of the various fractions of PE, and combinations of fractions, when quenched, could be followed by a standard microscopy technique or Atomic Force Microscopy (AFM). Scanning Electron Microscopy (SEM) and ordinary light microscopy could also be used as supporting techniques.

2.4.2) Separation mechanisms of fractionation

The early work of Desreux and Spiegels [39] pointed the way to fractionation by solubility as a means of eventual polymer structure evaluation. They recognized that both molecular weight and crystallinity separation come into play in the case of polyethylene, depending on whether the solvent composition or the temperature is varied, to achieve the fractionation. In the years that followed their pioneering efforts, the main objective of polymer fractionation was to establish molecular weight distributions. The emphasis was thus on the development of strategies for achieving solubility separations using differing solvent/non-solvent compositions. As time went by, efforts expanded and the need for a more practical and efficient system became of great importance. This led to the emergence of the elution of a polymer supported on packed columns in preference to approaches involving step-wise precipitation. The

advantages of using columns are described in a review by Schneider. [40] These included: experimental convenience with the opportunity for automation; the requirement for smaller volumes of solvent, even while maintaining the necessary condition of using dilute solutions; and the fact that fractionations take less time, particularly in comparison to fractionation by precipitation.

The need for information regarding the molecular weight distribution (MWD) of resins was eventually satisfied by size exclusion chromatography (SEC). SEC emerged as a powerful polymer characterization tool in the late 1960s and early 1970s. [41] Although MWD data was now readily available it did not provide all the explanations for the observed behavior of polymers, especially semi-crystalline polymers. Attention was therefore re-focused on structural features controlling solid state properties.

The term 'Temperature Rising Elution Fractionation' (TREF) was first coined by Shirayama et al. [42] to describe the method used to fractionate LDPE according to the degree of SCB. The actual technique that was used was first described by Desreux and Spiegels [39], who first recognized the potential of using elution at differing temperatures to achieve a crystallization separation. Although elution of amorphous polymers under conditions of rising temperature will also cause fractionation, it will be on the basis of molecular weight and not on the basis of crystallizability. SEC can be used for amorphous fractionation, thus there is little interest for an amorphous TREF. Thus TREF has come to be known as the technique for analyzing semi-crystalline polymers by separating the molecular species according to their crystallizabilities.

2.4.3) Theory of fractionation, using crystallizability

The free energy change for mixing two substances at a temperature T is given by the relationship:

$$\Delta G_{mix} = \Delta H_{mix} - T\Delta S_{mix} \tag{2.1}$$

The heat of mixing (ΔH_{mix}) is mostly a positive value for solutions, as the solution process is usually endothermic. The entropy of mixing (ΔS_{mix}) is also a positive value, relating to the higher random motion of solutions compared to the unmixed state. For a polymer to dissolve, $\Delta G_{mix} \leq 0$. This implies that ΔH_{mix} must be a small value.

In the case of highly crystalline polymers, which are insoluble at room temperature, Equation 2.1 has to be changed to accommodate the heat of fusion:

$$\Delta G_{mix} = (\Delta H_{mix} + \Delta H_f) - T(\Delta S_{mix} + \Delta S_f) \qquad (2.2)$$

where the subscripts *mix* and *f* denote mixing and fusion respectively.

Highly crystalline polymers comply with the solubility parameter rules at $T \geq T_m$. (T_m is the melting temperature of the polymer.) Crystalline polyethylene becomes soluble at elevated temperatures ($T \geq 80^\circ C$), depending on the choice of solvent. At room temperature these polymers obey the law of swelling.

Polymer fractionation or crystallization in solution can be explained on the basis of the Flory-Huggins statistical thermodynamic treatment, which accounts for the melting point decline in the presence of solvent:

$$\frac{1}{T_m} - \frac{1}{T_m^o} = \frac{R}{\Delta H_u} \frac{V_u}{V_1} (v_1 - \chi_1 v_1^2) \qquad (2.3)$$

where T_m^o is the melting temperature of the uncontaminated polymer; T_m is the equilibrium melting temperature of the polymer-solvent mixtures; ΔH_u is the heat of fusion per polymer repeat unit; V_u and V_1 are the molar volumes of the polymer repeating unit and the solvent respectively; $(v_1 - v_1^2)$ is the volume fraction of the solvent; and χ_1 is the Flory-Huggins thermodynamic interaction parameter.

The classical Flory equation can be applied in the case of random copolymers:

$$\frac{1}{T_m} - \frac{1}{T_m^o} = -\frac{R}{\Delta H_u} \ln(p) \qquad (2.4)$$

where T_m^o is the melting temperature of the homopolymer; ΔH_u is the heat of fusion for the homopolymer repeat unit and p the molar fraction of the crystallizing units. If the concentrations of the individual species are low and if they are not incorporated into the crystalline lattice, then the comonomer units and the polymer chain ends all have the same effect on the melting point decline. Flory proved that Equation 2.3 can be reduced to the same form as Equation 2.4. [43]

By replacing the term p with $(1 - N_2)$ in Equation 2.4, simplifications can be made to the equation, to yield Equation 2.5, where N_2 is the molar fraction of the comonomer that is not incorporated into the crystalline lattice structure. In that case were N_2 is a small value, the following term holds:

incorporated into the crystalline lattice structure. In that case were N_2 is a small value, the following term holds:

$$\ln(1 - N_2) \cong -N_2,$$

hence:

$$\frac{1}{T_m} - \frac{1}{T_m^o} \cong \frac{R}{\Delta H_u} N_2$$

(2.5)

Polyethylene with a Mw of 15 000 g/mol and higher crystallizes, independent of Mw in the solvent system. [44] Experiments have shown that PE with Mw as low as 1 000 g/mol can be fractionated by TREF in the case where end groups are considered as non-crystalline units. [27]

2.5) TREF

Prep-TREF can be used to resolve the heterogeneity of polymer blends. [45] The most known article in the field of TREF is that of Wild *et al.*, published in 1990. [29]

Mirabella et. al [46] used Prep-TREF to characterize polypropylene copolymers. These materials were a series of poly-(propylene-ethylene) co-polymers. Large fractions were obtained by Prep-TREF. The experimental procedure used by Mirabella *et al.* was as follows. [46] "The polymer was dissolved at a concentration of 4 g in 600 ml of *p*-Xylene at 130°C. The solution was cooled in a programmable bath at -5°C/hour from 120°C to room temperature. The best recovery of 93% was obtained. Free flowing solid was recovered and introduced back into the column. A time of an hour and a half was given between each elution of a fraction to let the system acquire equilibrium."

Wild *et al.* [29] recommend an uppermost cooling rate of -2°C/hour to avoid molecular weight and co-crystallization influences.

Mierau *et al.* [47] investigated graft-resistant polypropylene using temperature rising and elution fractionation. Once again xylene was used as solvent and the mixture was cooled at a rate of 5°C/hour. Three fractions, at 60°C, 96°C and 128°C, were recovered.

Monrabal [48] gives a good review of the TREF technique itself, focusing on the analytical TREF technique. The automation of TREF is extensively described (since most TREF apparatus built before 1990 were custom built). He further states the 2°C per hour cooling threshold and the importance thereof.

Xu *et al.* [28] have written a review article on the application of TREF in polyolefins, in which the fractionation mechanism is also well explained. This review includes the applications of TREF and tells us that polymers with homogeneous structure can be obtained to facilitate the study of polymer physics. The polyolefins that were included in the review were: polyethylene copolymers, polypropylene, polypropylene copolymers, polyolefin alloys and metallocene-based polyolefins. An interesting fact that emerged was that, working with polypropylene, Pref-TREF was preferred above analytical TREF since no reliable calibration curves could be found for PP. In actual fact PP fractionate according to tacticity and not short chain branching distribution of the polymer, which is the case in PE.

Wild [29] discussed a couple of possible systems with variable degrees of automation. The most robust and large scale TREF technique was developed by Shirayama *et al.* [42]; they placed their column, loaded with 4 grams of polyethylene, in a oil bath. Ten fractions were collected with good separation, thus benchmarking the basis for the development of the new Prep-TREF in the present study.

Galland [49] studied polyethylene copolymers prepared using the metallocene catalyst rac-Et[Ind]$_2$ZrCl$_2$. They used Prep-TREF, ^{13}CNMR, DSC and HT-SEM to characterize their polymers and to prove that inhomogeneity in the copolymers can be attributed to experimental conditions used during polymerization.

2.6)   CRYSTAF

Crystallization Analysis Fractionation (CRYSTAF), developed by Monrabal [50], is a method that complements the analyses that can be achieved from TREF. The unique set-up of the CRYSTAF system makes it possible to calculate the SCB of LLDPE from a standard calibration curve. [51]   Monrabal [27,30] also noted that the CRYSTAF analysis of PP and of LLDPE was much more effective than analysis by TREF. Most work that has been done to date on CRYSTAF has involved the basic analysis of standard polyolefin copolymers [52-57] and blend separation. [52,58] It has been found that a good correlation between the melting point (T_m), as determined by DSC, and the crystallization point (T_c) in solution exist, as determined by CRYSTAF. Calorimetric measurement is the newest and cheapest technique for the investigation of SCB in LLDPE and polyolefin blends. This method is based on DSC analysis, with a special

sample preparation procedure. Numerous researchers have shown that results obtained from DSC analysis are compatible with those obtained from CRYSTAF and TREF methods. [31,59] The only disadvantage of analysis by DSC is that the distribution curves cannot directly be converted into weight percentages of the components of different branching structures.

In all the studies that describe the development and use of TREF, it is assumed, either explicitly or implicitly, that the separation is taking place largely on the basis of crystallizability or melting. Very little work has been reported which deals with the theoretical aspects of the separation or even with the experimental limitations of the techniques as they are practiced. Monrabal [60] did raise some questions regarding factors which might influence TREF separation like molecular weight influences but were able to provide enough evidence supporting crystallizability as the dominant driving force for separation. They showed that for polyethylenes of various types one could construct a single and approximately linear relationship between separation temperature and degree of short-chain branching. It was suggested that this observed relationship was consistent with the theory of Flory concerning the effect of diluents on the depression of melting points. [59]

2.7) Comparison of TREF and CRYSTAF

TREF and CRYSTAF share the same principles of fractionation, namely fractionation on the basis of crystallization and through a slow cooling of a polymer solution. TREF is carried out in a packed column and demands two full temperature cycles - crystallization and elution - to achieve the analysis of the composition distribution. In CRYSTAF the analysis is performed in a single step - the crystallization cycle - which results in a faster analysis time and simple hardware requirements. [60] The use of stirred vessels and the fact that only crystallization plays a role in the separation process of CRYSTAF. In TREF there is the additional melting step where the polymer molecules have to melt out of the solid state. In TREF the polymer also experiences molecular entanglement effects between the polymer molecules and the support, which are probably the factors responsible for achieving in CRYSTAF [61], at faster crystallization rates, comparable resolution to the classical TREF.

TREF has the advantage that a continuous elution signal is obtained, as opposed to the discontinuous sampling of CRYSTAF. Discontinuous CRYSTAF sampling does however have

the advantage that multiple samples can be analyzed simultaneously. The main difference involved in comparing CRYSTAF and TREF results for the same polymer is the significant difference in the temperature scale. This difference is due to the 'under - cooling' effect; CRYSTAF data are collected during the precipitation of polymer out of solution, while TREF data are obtained in the melt dissolution. Both techniques can easily be calibrated by using results expressed in branches per 1 000 carbon units. Both Wild [29] and Monrabal [50] reported that the sample size, column dimensions, elution flow rate and elution temperature rate are all related, and all need to be optimized for a given TREF set-up. In general, the lowest concentration of sample (sample size) possible should be used in order to reduce co-crystallization, entrapment and entanglement effects. Monrabal further claims that the crystallization step can be carried out in a separate vessel, with or without a support, and that the absence of support during the crystallization results in a resolution improvement. [61]

Wild *et al.* [62] have patented the off-support crystallization and show that for LLDPE less tailing is achieved using off-support crystallization rather than on-support crystallization (with a support). We suspect the molecular entanglement and obstruction of the support is responsible for the improved results since LLDPE has homogeneous crystallization with and without a support, thus a heterogeneous crystallization environment cannot be responsible for the improved results. No relevant articles were found on the effect nucleating agents have on the crystallization cycle(step).

References:

1   Berzeluis, J., *Jahresber.* Fortsch. Phys. Wissensch., 1832, **11**: p. 44.

2   Berthelot, M., Soc. Chem. Paris, 1866, **148**: p. 44.

3   Mark, H., *Preface to History of Polyfins*, ed. R.B. Seymour and T. Cheng. 1985, Dordrecht, The Netherlands.

4   Berthelot, M., Ann. Chem. Phys., 1858, **3**(53): p. 158.

5   Buterlov, A., Annalen, 1876, **180**: p. 247.

6   Berthelot, M., Bull. Soc. Chim. Fr., 1869, **1**(11): p. 4.

7   Von Peckman, H., in *Berichte,* 1899, p. 2540.

8   Taylor, H.S., Jones, W.H., J. Am. Chem. Soc., 1931, **52**: p. 1111.

9   Fawcett, E.W., Gibson, R.O., J. Chem. Soc., 1934,**1**: p. 386.

10   Fawcett, E.W., Gibson, R.O., Perron, M.W., British Patent 471,590, 1937, Imperial Chemical Industries: Britain.

11   Raff, R., Lyle, E., *Historical Developments in Crystalline Olefin Polymers,* 1965, New York: John Wiley & Sons Ltd, part 1.

12   Billmeyer, H., (ed.), *Textbook of Polymer Science,* Second Edition, 1971, New York: John Wiley & Sons Ltd, p. 379.

13   Whelan, T., *Polymer Technology Dictionary,* 1994, London: Chapman & Hall, p. 240.

14   Utracki, L.A., *Polymer Alloys and Blends,* 1989, Munich: Hanser Publishers, p. 256-264.

15   Seymour, R.B., *Handbook of polyolefins*. History of Polyolefins, ed. Vasile C., 1993, New York: Marcel Dekker.

16   Scott, R.L., J. Chem. Phys., 1949, **17**: p. 279.

17   Seymour, R.B., *Handbook of polyolefins*. Polyolefin Polyblends, ed. Deanin, R., 1993, New York: Marcel Dekker. p. 779-786.

18   Chem, F., Shanks, R.A. and Amarasinghe, G., Polymer, 2001, **42**(10): p.4579-4587.

19   Shanks, R.A., Amarasinghe, G., Polymer, 2000, **41**(12):p. 4579-4587

20   Morgan, R.L., Hill, M.J., Barham, P.J., Polymer, 1999. **40**: p. 337-348.

21   Hedenqvist, M., Brana, M.T.C., Gedde, U.W., Polymer, 1996, **37**(23): p. 5123-5129.

22   Fan, Z.G.J., Williams, M.C., Choi, P., Polymer, 2002, **43**(4): p. 1497-1502.

23   Tanem, B.S., Stori, A., Polymer, 2001, **42**(12): p.5689-5694.

24   Stori, A., Polymer, 2001, **42**(13): p. 5689-5694.

25   Exxon, Chem.

26   Zhang, M., Lynch, D., Wanke, S., J. Appl. Polym. Sci., 2000, **75**: p. 960-967.

27   Monrabal, B., *Temperature rising elution fractionation and crystallization analysis fractionation*. Encyclopaedia of Analytical Chemistry. 2000.

28   Xu, J., Feng, L., Eur. Polym. J., 2000, **36**: p. 867-878.

29   Wild, L., *Temperature Rising Elution Fractionation*. Adv. Polym. Sci., 1990, **98**

30   Monrabal, B., *Chemical composition distribution analysis in polyolefins. Introduction to crystallization analysis fractionation. CRYSTAF*. New trends in polyolefin science and technology, ed. Hosoda, S., 1996, p. 119-133.

31   Stark, P., Polym. International, 1996, **40**: p.111-122.

32   Chem, F., Shanks, R.A., Amarasinghe, G., J. Appl. Polym. Sci., 2000, **78**: p.1009-1016.

33   Morgan, R.L., Hill, M.J., Barham, P.J., Polymer, 1999, **40**: p.337-348.

34   Yong-Man K., Jung-Ki, P., Jung-Whan, K., Tae-Ik M., J. Appl. Polym. Sci., 1996, **60**: p. 2469-2473.

35   Teh, W.J., Rudin, A., Polymer, 1994. **35**(8): p. 1680-1687.

36   Noda, I., Satkowski, M.M., Polymer Solutions, 1992 (Blends and interfaces): p. 109-131.

37   Lee, H., Cho, K., Ahn, T., Choe ,S., Park ,I., Lee, B.H., J. Polym. Sci.: Part B: Polym. Phys., 1997, **35**: p.1633-1642.

38   Smith, P.F., Dimitrivich, D., Rasburn, J., Vasco, G.J., Polymer Engineering and Sci., 1996, **36**(16): p.2129-2134.

39   Desreux, V., Spiegels, M.C., Bull. Soc. Chem. Belg., 1950, **59**: p. 476.

40   Schneider, N.S., J. Polym. Sci. C, 1965, **8**: p. 179.

41   Moore, J.C., J. Polym. Sci., Part 2A, 1964: p. 835.

42   Shirayama, K., Okada, T., Kita, S., J. Polym. Sci., Part 2A, 1965, **3**: p. 907.

43   Flory, P.J., *Principles of Polymer Chemistry*. Ithaca ed. 1953, New York: Cornel University Press.

44   Fatou, J.G., *Encyclopedia of Polymer Science and Engineering.*, ed. Mark, H.F., Korschwitz, J.I.,. 1989, **2**, New York: John Wiley & Sons Ltd: p. 231.

45   Chem, F., Shanks, R.A., Amarasinghe, G., Polymer, 2001, **42**: p. 4579-4587.

46   Mirabella, F., J. of Liq. Chromatography, 1994, **17**(15): p. 3201-3219.

47   Mierau, U., J. Appl. Polym. Sci., 1997, **63**: p. 238-288.

48   Monrabal, B., *Temperature rising elution fractionation and crystallization analysis fractionation.* Encyclopaedia of Analytical Chemistry, 2000, Chichester: John Wiley & Sons Ltd: p. 8074-8084.

49   Galland, G., J. Appl. Polym. Sci., 2002, **84**: p. 155-163.

50   Monrabal, B., 1991: US Patent 5,222,390.

51   Pasch, H., Brüll,R., Wahner., Monrabal, B., Macromol. Mater. Eng, 2000, **279**: p. 46-51

52   Monrabal, B., J. Appl. Polym. Sci., 1994, **52**: p. 491-499.

53   Kim, D.J., Soares, J.B.P., Macromol. Rapid. Com., 1999. **20**: p. 347-350.

54   Chu, K.J., Soares, J.B.P., Penlidis, A., Macromol. Chem. Phys., 2000. **201**: p. 340-348.

55   Chu, K.J., Soares, J.B.P., Penlidis, A., Ihm, S.K., Macromol. Chem. Phys, 1999, **200**: p. 2372-2376.

56   Chu, K.J., Shan, C.L.P., Soares, J.B.P., Penlidis, A., Macromol. Chem. Phys., 1999, **200**: p. 1298-1305.

57   Soares, J.B.P., Abbott, R.F., Kim, D.J., J. Polym. Sci., Part B: Polymer Phys., 2000, **38**: p. 1267-1275.

58   Brüll, R., Grumel., V., Pasch, H., Raubenheimer, H.G., Sanderson, R.D., Wahner, U., Macromol. Symp., 2002, **55**: p. 178.

59.   Flory, P., Trans Faraday Soc., 1955, **51**: p. 848.

60   Monrabal, B., J. Appl. Polym. Sci., 1994. **52**: p. 491-499.

61   Wild L., Trends in Polymer Sci., 1993 **1:** p. 50-55.

62   Wild, L., Knobeloch, D.C., 1991: US Patent 5,030,713.

CHAPTER 3
EXPERIMENTAL

3.1) Materials

3.1.1) LDPE and Plastomers A and B

The LDPE that was used in this study was a Sasol polymer (XHF 77/50), prepared in an autoclave reactor using free radical polymerization. This LDPE had a Melt Flow Index (MFI) of 1g/10min and a density of 0.922 g/cm^3. The commercial product contains an added anti-oxidant medium slip and anti-block, and is mainly used in the film-blowing industry. [1]

The two plastomers that were used were two different grades of the Affinity range of DOW Chemicals. Plastomer A (PL1881) had a MFI of 1g/10min and a density of 0.904 g/cm^3. Plastomer B (VP8770) had a MFI of 1g/10min and a density of 0.885 g/cm^3. The plastomers consisted of LDPE, with octene as comonomer. The percentage comonomer content ranged from 20-40%. The physical properties of plastomer A and Plastomer B are tabulated in Table 3.1

3.1.2) Blends

Blends of LDPE with the two different plastomers respectively were blended using extrusion filmblowing. Blend ratios of 10%, 20% and 40% plastomer relative to the LDPE were blended. The extrusion filmblowing blending produced films of 30 micrometers thick. The "barmag" extrusion film-blowing machine uses industrial quantities.

Table 3.1 Physical properties of the Plastomer A and Plastomer B [2]

Physical Properties	Test Method	Plastomer A	Plastomer B
Melt-Index g/10ml	*ASTM D 1238	1	1
Density g/cc	ASTM D 792	0.9035	0.885
DSC melt. pt. (°C)	Dow method	212	180
Tensile Yield psi (MPa)	[a]MD ASTM 1922	1170	1650
	[b]TD ASTM 1922	1040	n/a
Clarity	ASTM D 1746	83	n/a
Gloss, 20°C	ASTM D 2457	112	n/a
Haze	ASTM D 1003	3.2	n/a

*American Standard Test Method

[a] Machine Direction

[b] Transverse Direction

3.1.3) Solvents

Xylene (Aldrich, 99% purity) was used as the solvent in all TREF reaction procedures. Xylene was recycled and re-used.

3.1.4) Stabilizers

Irganox 1010 and Irgafos stabilizer mix (Sasol) were used in the TREF procedures to inhibit thermal degradation as high temperatures are used in the crystallization (cooling) step. These are amine-based stabilizers.

3.2) Analytical techniques

3.2.1) CRYSTAF

Figure 3.1 shows the typical profile obtained using Crystallization Analysis Fractionation (CRYSTAF). In CRYSTAF, the first data points taken at temperatures above any crystallization provide a constant concentration equal to the initial polymer solution concentration (Zone 1). As the temperature decreases, the most crystalline fractions, composed of molecules with zero or

very few branches, will precipitate first, resulting in a steep decrease in the solution concentration (Zone 2). This is followed by precipitation of fractions of increased branch content as the temperature continues to decrease (Zone 3). The last data point, corresponding to the lowest temperature of the crystallization cycle, represents the fraction that has not crystallized (mainly highly branched material) and remains soluble.

Crystallization analysis fractionation was carried out using a CRYSTAF commercial apparatus, model 200, manufactured by Polymer Char S.A. (Valencia, Spain). The crystallization was carried out in stirred stainless steel reactors (volume 60 ml) where dissolution and filtration takes place automatically. About 20 mg of a sample was dissolved in 30 ml 1,2,4-trichlorobenzene (TCB). The temperature was decreased at a rate of 0.10^{0}C/min from 100^{0}C to 30^{0}C. Fractions were taken automatically. The polymer concentration from solution was determined by means of an infrared detector, using 3.5μ as the chosen wavelength. Temperatures as low as 18°C were achieved using liquid nitrogen. TCB freezes at 18°C.
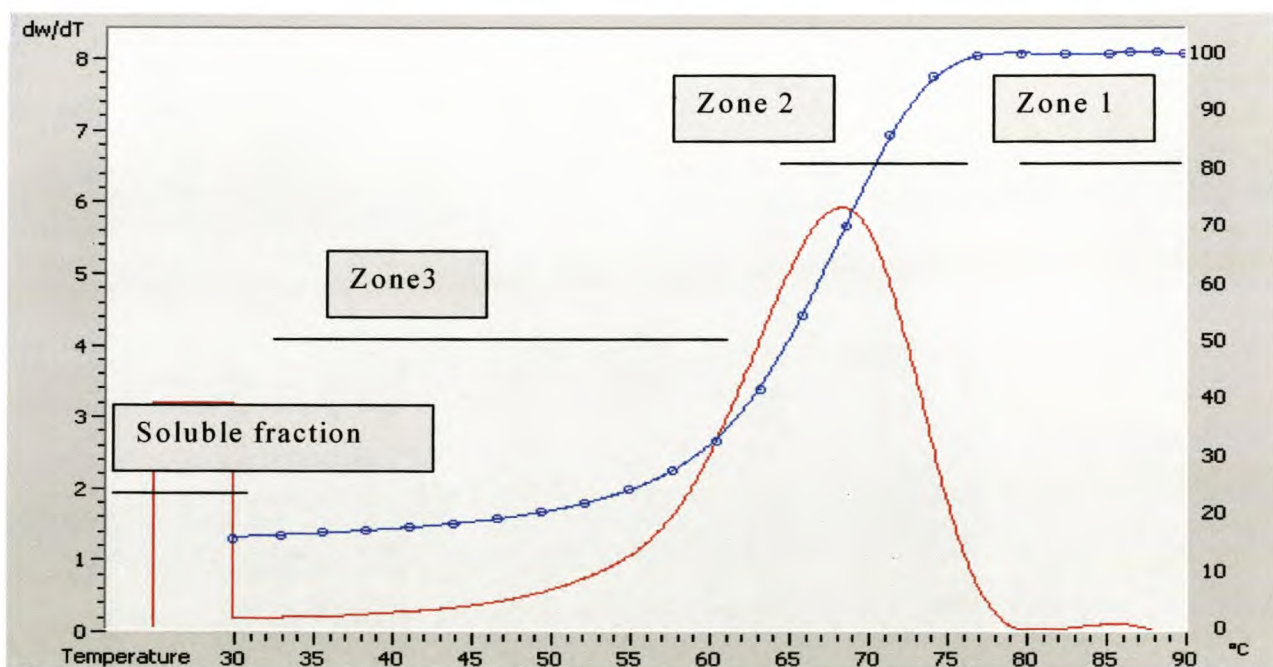
Figure 3.1 Typical temperature profile obtained using CRYSTAF.

3.2.2) TREF

TREF is a separation technique for fractionating crystallizable polymers based on crystallinity. [3] The experimental separation mechanism of TREF can be depicted as shown as in Figure 3.2. [3]
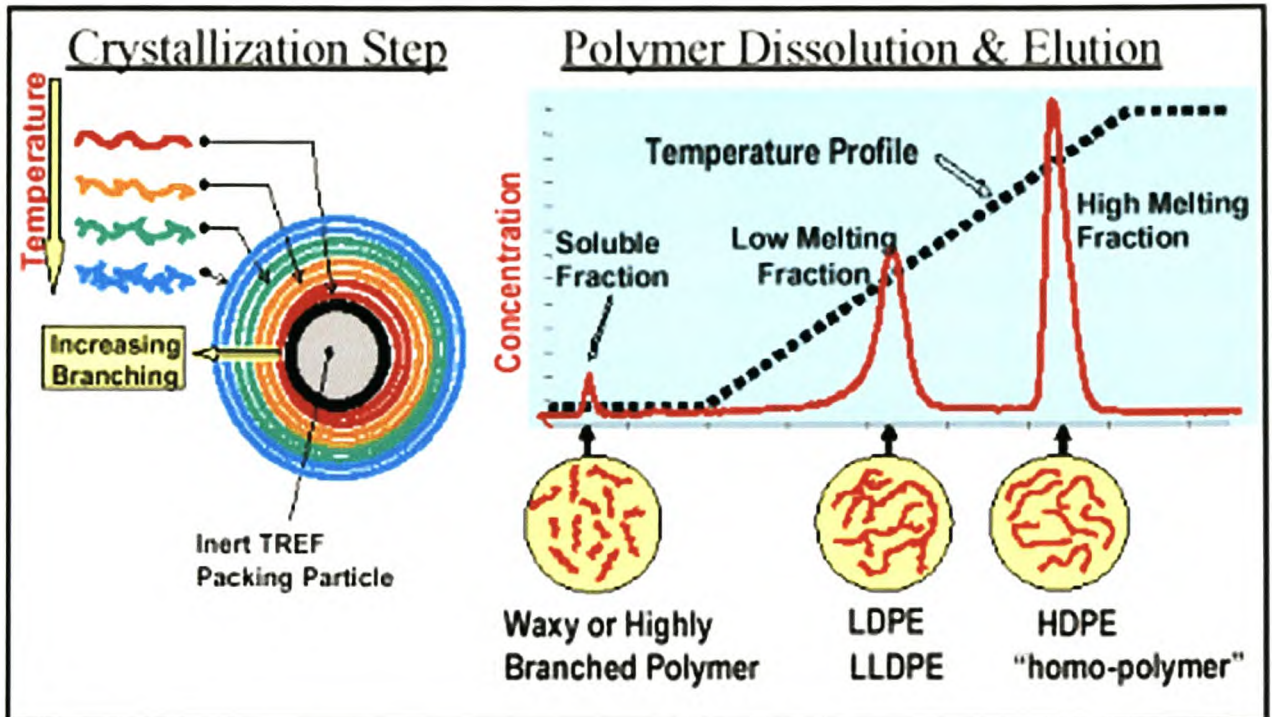
Figure 3.2 A schematic representation of the crystallization step in TREF.
Source: W.W Yau, D. Gillespie, Polymer 2001, 42, p. 8952

3.2.3) The separation mechanism of TREF

The operation of TREF is divided into two steps.

1. A dilute solution of a polymer is mixed with an inert support (for example, sea sand, glass beads, silica gel, etc.). This mixture is slowly cooled down to room temperature.[4] As the temperature decreases gradually the polymer fractions precipitate from the solution and coat the support in layers of different crystallinity. [3] The most easily crystallizable fraction precipitates first and deposits on the support in the innermost layer. On the contrary, the fraction with least crystallinity precipitates last and deposits on the outermost layer. This process is of great importance and a slow cooling rate is the key, since it ensures that polymer fractions

order according to their crystallinity. [4] A fast cooling rate may lead to co-crystallization of fractions with different crystallinity and therefore lead to less efficient fractionation.

2. In the second step, the precipitated polymer is eluted with a solvent using increasing or stepwise temperatures. At the lower temperatures, the fractions with less crystallinity dissolve. With increasing elution temperature the fractions of higher crystallinity dissolve.

There are two kinds of experimental TREF apparatus: analytical and preparative TREF. Analytical TREF is generally automated.

3.2.4) DSC measurements

The melting and crystallization properties of samples were determined on a DSC instrument, in a nitrogen atmosphere, using the following method. Approximately 5 mg of each sample was used in the analysis. The temperature of the DSC was increased ('ramped') at a rate of 10°C/min to 30°C, then left to equilibrate at 30°C, followed by further ramping at 10°C/min to 160°C. The sample was then cooled and the profile repeated. The data were only stored on the second run. The instrument used was a TA Instrument Thermal Analysis DSC standard cell. Data was baseline zeroed and normalized whenever 3-D plots were created.

3.2.5) HT-SEC measurements

Molecular weights were determined using Size Exclusion Chromatography (SEC). The measurements were preformed on a PL-GPC 220 High temperature chromatograph from Polymer Laboratories equipped with a PL gel 10 μm guard (50X7.5mm) and 3 PLgel mixed-B (300X7.5mm, particle size 10um) column. The packing material is a cross linked polystyrene/divinylbenzene copolymer. Elution was carried out at a flow rate of 1 ml/min with 1,2,4- trichlorobenzene containing 0.0125% of 2,6-di-tert-butyl-4-methylphenol(BHT) as stabilizer and flow rate maker, at a temperature of 160°C. The detector was a differential refractive index and molar mass determination was done relative to a calibration with narrow polystyrene standards.

This experimental procedure is illustrated using Figure 3.3 and Figure 3.4 as an example.
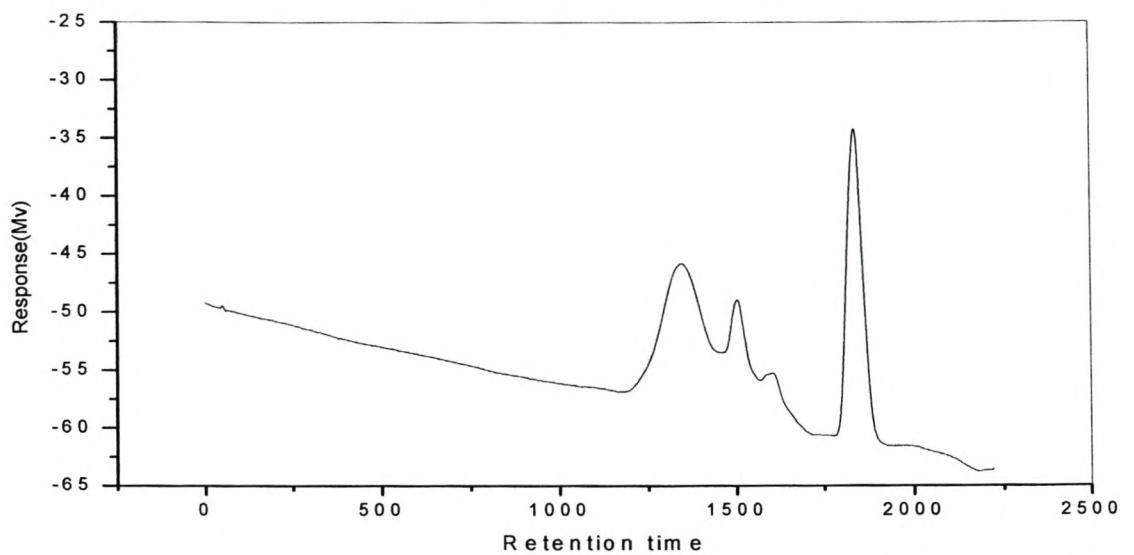
Figure 3.3 Raw data obtained from the HT-SEC.

In Figure 3.3 the baseline is uncorrected and has a response between -45 and -65Mv. The relative intensity is negative. Figure 3.4 shows the normalized baseline zeroed data
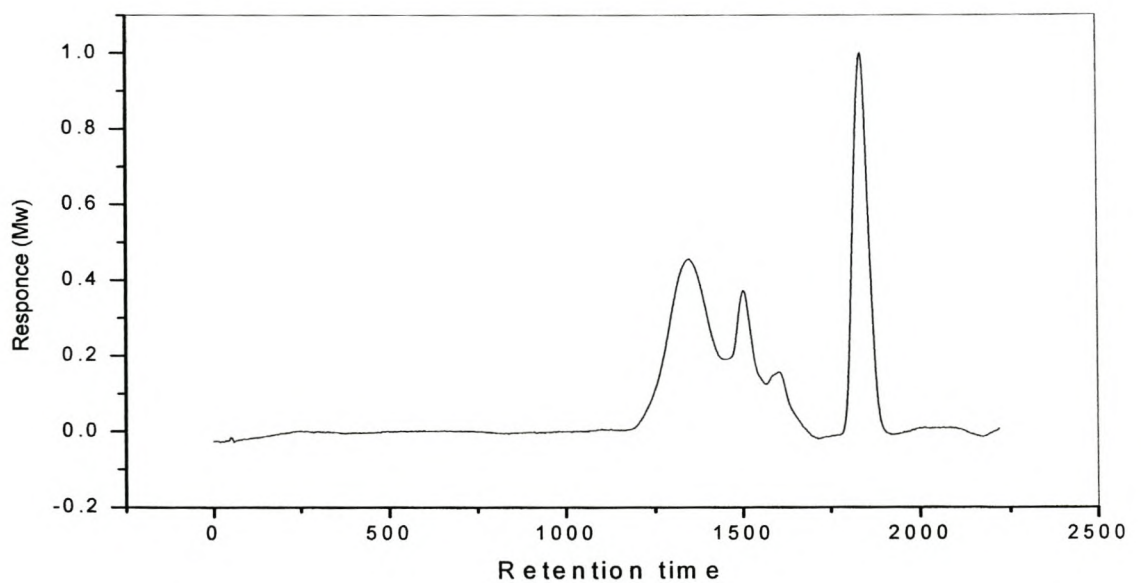
Figure 3.4 Baseline zeroed and normalized HT-SEC raw data.

28

It should be noted that in order to create 3-D plots with the HT-SEC data, obtained from analyzing the different TREF elution temperature fractions with HT-SEC, the individual HT-SEC traces were baseline zeroed. The HT-SEC traces were also normalized, by dividing each data point by the maximum point in the trace. The resulting baseline zeroed normalized data were then multiplied with the weight fractions of each trace as obtained from the Prep-TREF.

3.2.6) NMR measurements

^{13}C NMR spectra were recorded at 100^0C on a Varian VXR 300MHz instrument, in a 9:1 mixture of 1,2,4-trichlorobenzene/C_6D_6, using C_6D_6 at 127.9 ppm as internal secondary reference. The pulse angle was 45 degrees and the repetition time 0.82 seconds. For ^{13}C NMR a 75 MHz frequency was used.

3.2.7) Scanning electron microscopy

Scanning electron microscopy (SEM) results were achieved using a Leo 1430 VP scanning electron microscope. SEM was used to look at the surface of the LDPE, the plastomers and their blends.

3.3) Permanganic etching of polyolefins

The permanganic reagent used was a 7% mass/vol solution of potassium permanganate in concentrated sulfuric acid, prepared by adding the permanganate slowly to the acid in a conical flask with rapid agitation.[5] Once all the permanganate had been added, the flask was stoppered and shaken occasionally until all the crystals had dissolved, to yield a dark green solution. Samples of the films were cut to sizes of 1 cm x 1 cm x 40 μm and weighed before being etched and weighed again at 40 min, 60 min and 90-min intervals. These films are them washed in methanol.

References

1.   Chem, F., Shanks, R.A., Amarasinghe, G., J. Appl. Polym. Sci., 2000, **78**: p.1009-1016.

2.   http://www.dow.com/affinityga/index.htm., *September*, 2004.

3.   Junting, X. and Feng, L., *Application of Temperature Rising Elution Fractionation in Polyolefins.* Eur. Polym. J., 2000, **36**: p.867-878.

4.   Wild, L., *Temperature Rising Elution Fractionation.* Adv. Polym. Sci., 1990, **98**: p.1-47.

5.   Olley, R.H., *A Permanganic Etching for Polyolefins.* J. Polym. Sci., Part B: Polym. Phys., 1979. **17**: p. 627-643.

CHAPTER 4
RESULTS AND DISCUSSION

Summary

In this chapter the design, development and optimization of the preparative TREF (Prep-TREF) are discussed, followed by an evaluation of this technique. The operating procedure that was developed for using the Prep-TREF is also described. LDPE was used for proving the prep-TREF works. TREF results obtained from the LDPE and two selected plastomers is shown. The TREF results obtained from the analysis of LDPE/plastomer blends is also shown. The effect of the cooling rate on fractionation is also considered. Solution crystallization and the morphology of LDPE and the LDPE/plastomer blends is also investigated and changes in the morphology of the blends discussed, relative to the LDPE and plastomers. Physical properties of the blends are also described.

4.1)   Design and development of the preparative TREF

4.1.1) Introduction

A number of options for the design and building of a preparative TREF were investigated. One option that was considered was the design in which both the cooling and elution steps would take place in one column, in a temperature controlled GC-oven. In the second option, the option subsequently chosen, the crystallization and elution steps were separated. This was achieved by using an oil bath with a temperature profiler for the crystallization step and using a GC-oven for the elution step. This option was chosen as it has several advantages.

1.)   It allows better control over the critical cooling step. A slow cooling rate is the most important factor in achieving good separation. A slow cooling rate minimizes the effects of co-crystallization and molecular weight influences. This better control of the cooling step was achieved with a Cole-Parmer Temperature Controller r/s (Advanced Model)

8900-15, attached to an oil bath. Using this option, a cooling rate of 1°C/h is possible - which is otherwise difficult to achieve and control with a GC oven.

2.) By separating the cooling and elution steps a continuous crystallization cycle can be maintained, leading to improved productivity. It takes approximately 6 days for the cooling step and only about 6 hours for the elution. The use of a temperature-controlled oil bath allows for the simultaneous cooling of four different samples. The main practical advantages of this include the following: it is possible to prepare large numbers of samples continuously and only standard, inexpensive laboratory glassware is required for the crystallization cycle step. The main disadvantage of this approach is that it is a more labour-intensive technique, yet it is more time efficient. There is, however, also a possibility of loosing some sample during the transfer step into the metal eluting column.

It is worth mentioning here that an in-situ detector system for the preparative TREF was not required since the fractions were collected and weighed, then analytical CRYSTAF run on each fraction.

It should also be mentioned here that the polymer used in the development of the TREF and operating procedure was LDPE (see Experimental section, 3.1.1).

4.1.2) Design of a reactor for the cooling step

The cooling step is the most important step in the TREF. The basis of the cooling step is a controllable temperature environment. The components that were chosen to achieve this were a Labcon water bath type WBH with a built - in element. The bath was filled with silicon oil and a R50D CAT overhead stirrer was inserted into the oil bath. A Cole Palmer Digi-Sence Temperature Controller model 8900-15 was used to create the temperature profile for the cooling step. The temperature profiler was attached directly to the oil bath element. A temperature probe was submerged into the silicon oil to enforce the temperature profile settings. Four 1-liter round bottom flasks were submerged into the silicon oil and kept in place with clamps attached to retort stands. Water coolers were attached to the flasks. All the water coolers were purged with a positive nitrogen pressure then sealed.

4.1.3) Design of the elution step

The elected two-step procedure provided an opportunity to explore new creative ideas in designing the elution step, in such a way as to optimize productivity yet contain costs. The following were used for carrying out the elution step: a controlled-temperature environment and a rugged, durable column. An GC-oven (Variant, model 3700) was used for the controlled temperature environment.

The column was designed to fit into this GC-oven. Due to the fragility of glass it was decided to design a metal column (seen Figure 4.3). The column consisted of four components:

1) a stainless steel shaft with the pre-solvent and post-solvent copper coil attached to it

2) a stainless steel lid

3) iron hardened or copper screws (not stainless steel screws, as they will damage the bore holes) to close the column

4) a Teflon seal placed between the lid and the metal shaft to seal the column airtight.

Attached to the column, but still inside the GC-oven, was a copper coil (volume 100mL) wrapped around the column. The coil had a radius of 4 mm and a length of 1 meter. The main function of the coil was to pre-heat the solvent that entered the column. The column had a radius of 3 cm and was 20 cm high. The column was designed with an empty capacity of 600 mL. This capacity was required to accommodate the 350 mL of column space required for the 500 g of dry sea sand (-50 +70 mesh, Aldrich). Once the sea sand was wetted and loaded with polymer it required an additional 50 mL of column space. The column was also loaded with glass beads and glass wool in order to create a uniform elution flow pattern through the column and to prevent channeling during the elution step. The column was first loaded with a layer of glass beads, followed by glass wool. The packing material loaded with the polymer was then placed in the column. Another layer of glass wool was placed on top and the column then sealed.

The elution step is not the time-limiting step. Using the design described above, five elution steps could be run for a single crystallization step, doing one 6-hour elution step per day.

4.1.4) Preliminary experimental procedures

The experimental procedure was developed largely by a trial and error method. Different cooling rates were tried, with mixed results. Different elution temperatures were used, depending

on preliminary CRYSTAF results and the amount of polymer exiting the preparative TREF at the chosen temperatures. Figure 4.1 shows an example of the CRYSTAF trace used to identify the TREF elution temperatures. If the step-wise temperature increase in the elution step of the prep-TREF is to large, the recovery of to large fractions (in mass) occurs. It should be noted that when using the un fractionated CRYSTAF trace to determine the elution temperatures for TREF, the "under cooling" effect should be taken into account, i.e. about $+10^{o}C$ needed to be added to the desired CRYSTAF temperature. To improve our accuracy and further optimize the prep-TREF technique, it was decided to elute at every 5°C, to give a larger number of plots and thus improve our weight fraction curves. It is much easier to simply blend two 5°C elution range fractions, if a larger mass fraction is needed at a later stage, than separating a 10°C elution range fraction into two five - degree elution fractions. The second reason is that the narrower an elution fraction temperature, the narrower is the SCBD of the polymer that is obtained, which shows as a narrower CRYSTAF peak width in the results.
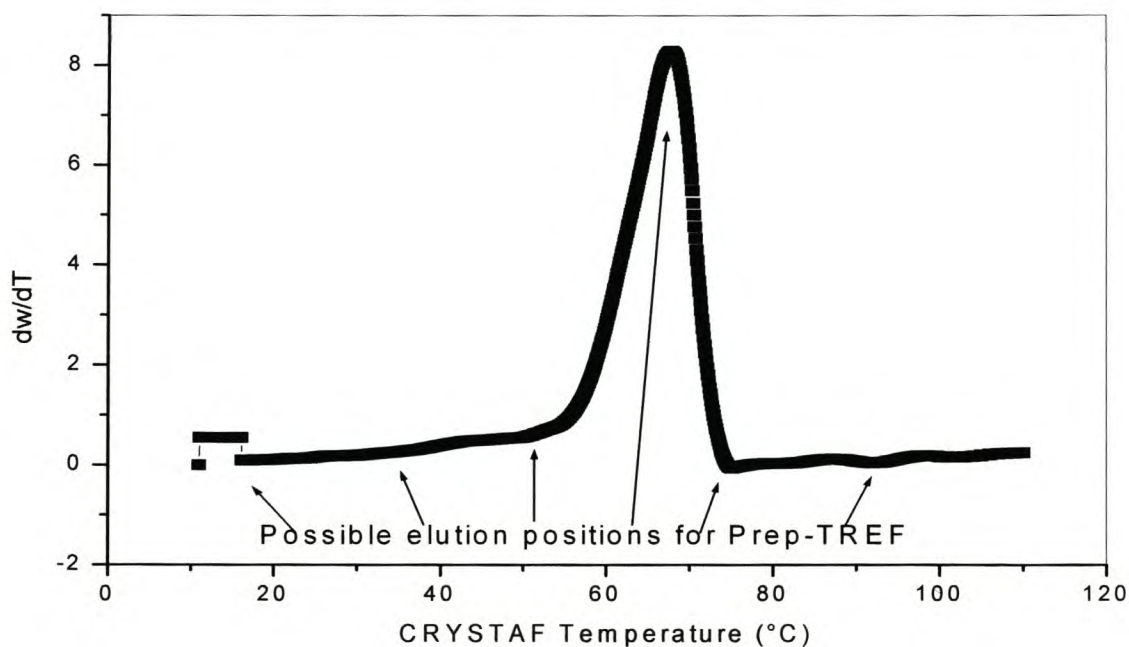

Figure 4.1 Possible elution positions for the Prep-TREF.

During the cooling step care was taken to totally cover the polymer solution with sea sand to ensure that no polymer crystallized on the top of the support of sea sand, and thus causing an inhomogeneous crystallization environment.

Factors that were investigated and optimized for the Prep-TREF were:

- Column loading (amount of polymer relative to support material)
- Cooling rate
- Elution temperature equilibration time
- Elution volume
- Elution rate
- Fraction recovery.

The final operating and experimental procedures that were arrived at were the results of the development (Section 4.1.4) and subsequent optimization (Section 4.1.5) of all the above factors in our system.

4.1.5) Further optimization of the Prep-TREF

Results of this study to date lead to the design of a new Prep- TREF system to further optimize the fractionation of LDPE. The improvements included in the new design were the following:

1.)   The 1-litre round bottom flasks were replaced with glass reactors that could easily be opened by separating the two parts. This change made the removal of the polymer loaded on the packing material much less labour intensive. These new reactors also had necks through the lids, for the addition of stirrers and probes for future application, should they be required. The latest modifications made to the cooling step of the Prep- TREF are shown in Figure 4.2.

2.)   To solve the problems arising from fluctuating nitrogen pressure and the possible shortage of pre-heated xylene for the elution step, a new column was designed to increase the volume of pre-heated xylene. This was done by increasing the length of the copper coil inside the oven, in order to pre-heat more solvent. The copper coil is shown in Figure 4.3.
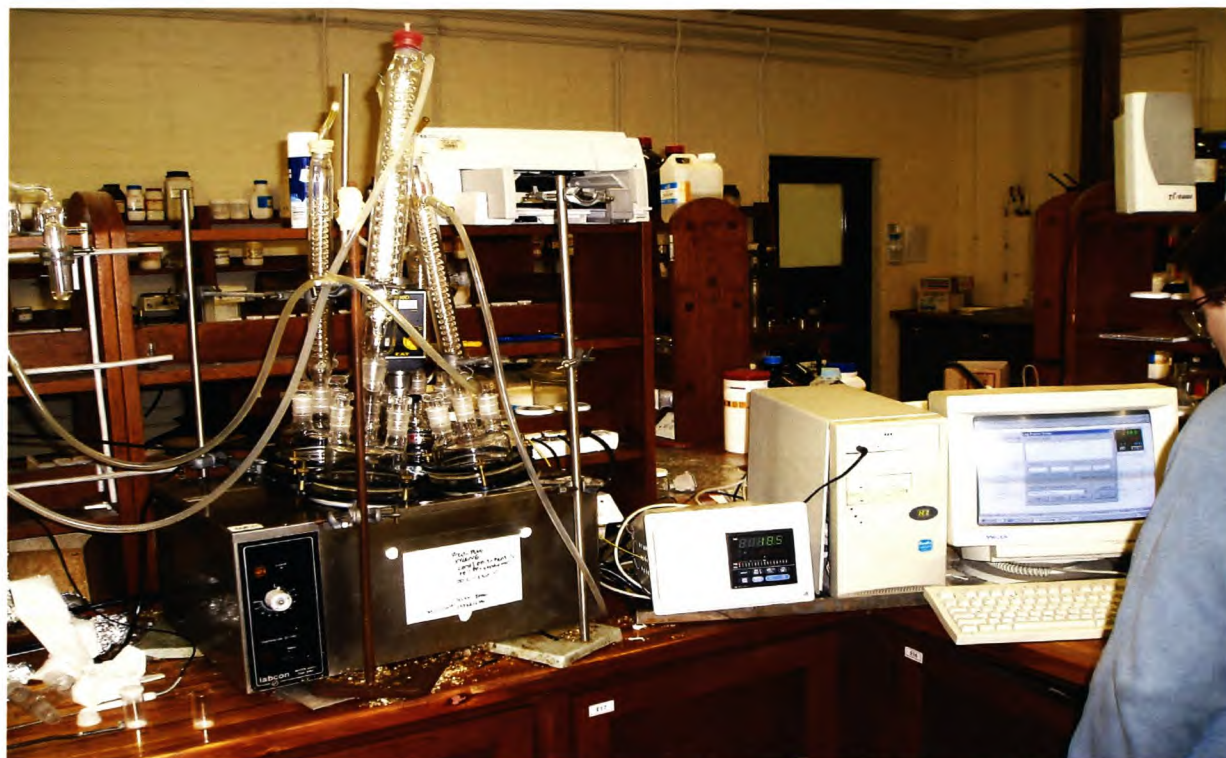
Figure 4.2 The latest modifications made to the cooling step of the Prep-TREF.

Figure 4.3 The old and new columns, with probe shown inside the new column (top left).

3.)   The first column did not have an opening for a probe to measure the internal column temperature. This forced us to wait one hour in between each elution to ensure that the oven and column internal temperature had equilibrated. The new column had a probe inserted into it to continuously measure the internal column temperature, thus increasing the elution speed of the Prep-TREF and confirming that the oven temperature and column internal temperature concurred.

4.)   In the first design no heating tape was wrapped around the exit pipe. Upon determining for the high-temperature fractions that the fractions recovered after elution showed a decrease in the weight average molecular weight (Mw), it had to be ensured that this was not due to crystallization occurring in the exit pipe. Hence heating tape was wrapped around the pipe carrying the polymer solution out of the oven. The exit pipe and heating tape are shown in Figure 4.4. After repeating the fractionation there was still a decrease in the Mw for the higher elution temperature fractions. At this point it was concluded that this was occurring because of fractionation and it was not due to experimental error.
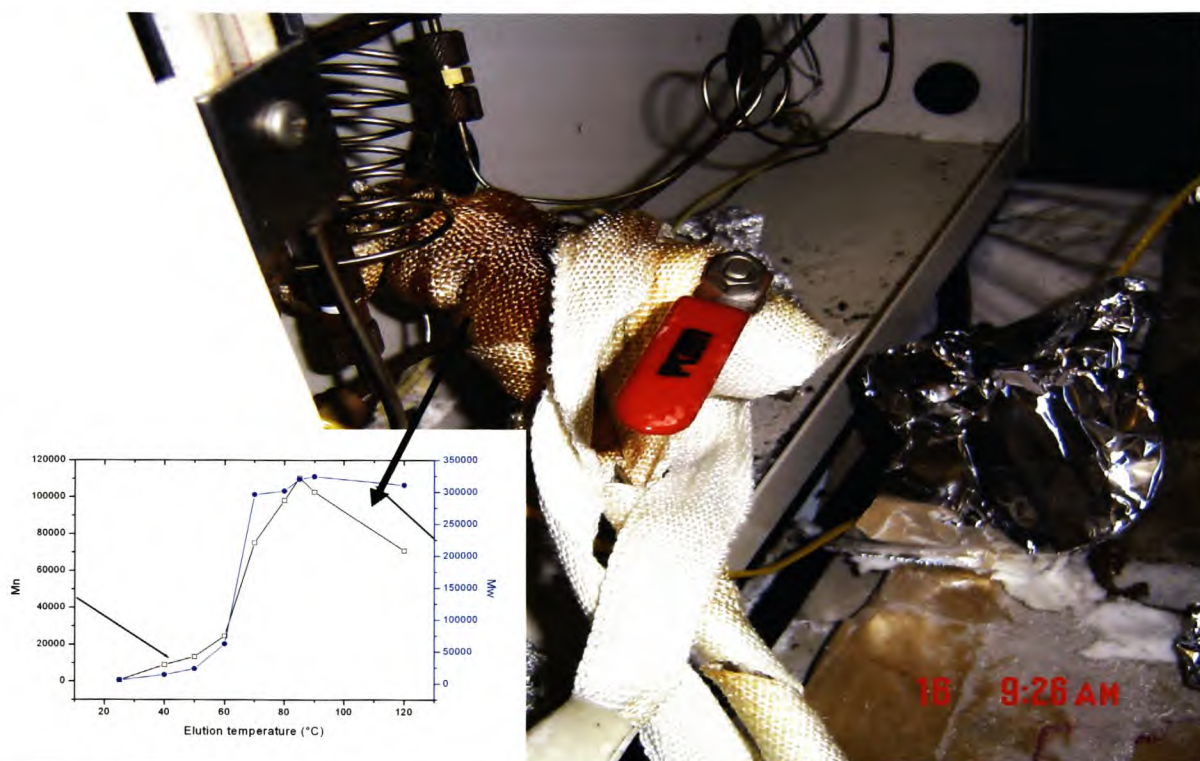

Figure 4.4 The heating tape wrapped around the exit pipe.

Figure 4.5 shows the different LDPE fractions after Prep-TREF. It was interesting to see that the fractions looked different; some were brittle films, some were porous powder and some were elastic films. The weight fractions recovered are shown as weight fraction curves, in the top of Figure 4.5.

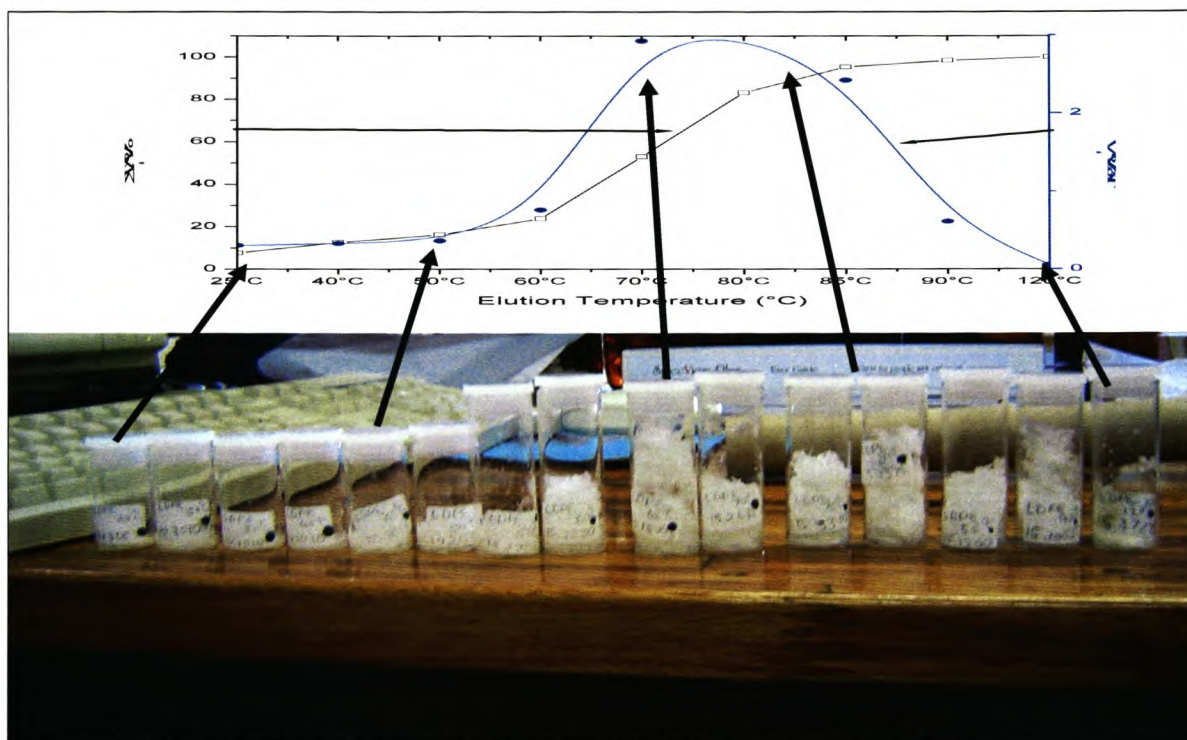**Figure 4.5 The fractionated LDPE polymer samples after Prep-TREF.**

4.2) Operating procedure of the Preparative TREF

4.2.1) Introduction

The operating procedure reached for the use of the Prep-TREF, based on the optimization of the factors mentioned in the previous section (4.1), is described. The procedure is divided into four main steps:

Step 1 - cooling, Step 2 - elution, Step 3 – transfer, Step 4 - recovery.

4.2.2) The cooling step

First, about 4kg of the sea sand support (mesh 50 – 70)is placed in a 5-liter round bottom flask, in an oil bath, and pre-heat to 140°C. This should ensure enough sand for all four reactors. Second, into a 1-liter round bottom flask 2g of the LDPE polymer is added into 200 mL of xylene or 3g of LDPE polymer into 300mL of xylene, then 2% of an Irganox 1010 and Irgafos stabilizer mix (SASOL's premixed batch) is added. This flask plus content is then placed in an oil bath with attached temperature profiler. A maximum of four 1-liter round bottom flasks can be placed in an oil bath. A cooler is added at the top of the flask and a positive nitrogen pressure applied. The oil bath is heated to 140°C to dissolve the polymer completely in the xylene. Once the oil bath has reached a temperature of 140°C, the pre-heated sea sand is added to the solution until the xylene is completely covered. The amount will depend on the initial amounts of polymer and xylene used. Lastly the temperature profiler is set on the first profile and the slow-cooling step is started. The cooling setup is shown in Figure 4.6.
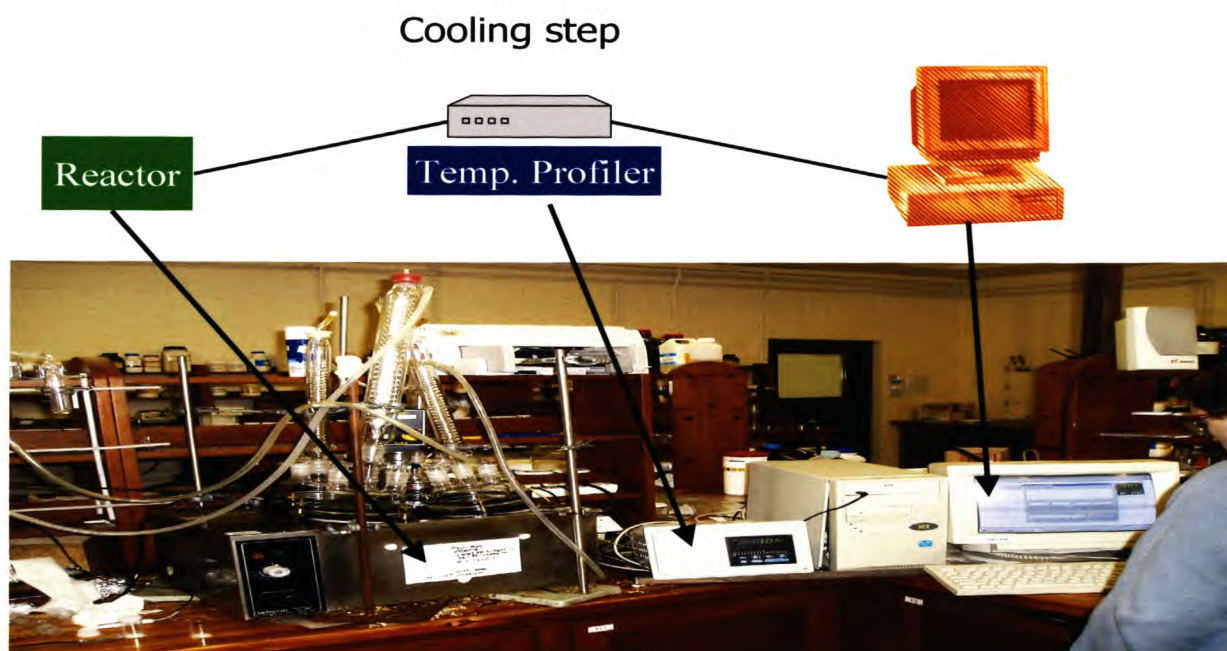

Figure 4.6 The cooling setup used in Prep-TREF.

4.2.3) The elution step

In the elution step the polymer is eluted from the packing material. Once the cooling step is completed, the column is prepared by transferring the cooled support (sea sand)/solvent mixture to the steel elution column. The elution column is prepared by placing some glass wool in the bottom, followed by some glass beads to prevent any flow currents in the column, followed by some more glass wool. The sand is loaded into the column, followed by some more glass wool and glass beads to fill up the column.
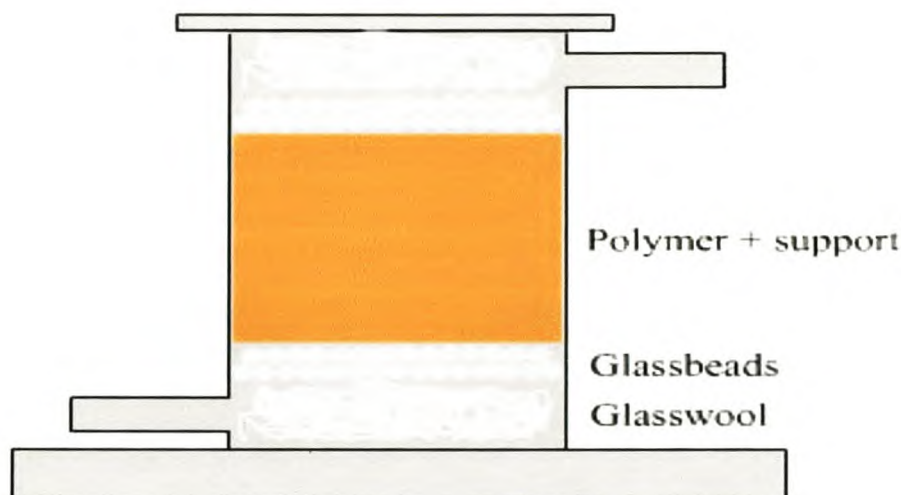
Figure 4.7 Loading the column of the Prep-TREF in the elution step.

4.2.4) Transfer of the column

In this step the column is sealed and transferred to the GC-oven. The entire GC-oven stands inside a fume hood to limit xylene fumes. The column is heated, using a stepwise heating profile at 2°C/minute, to a predetermined elution temperature. The column is allowed to equilibrate at this temperature for 1 h. The column is then eluted with solvent at a rate of 20 mL/min so as to give the eluting xylene a chance to pre-heat before entering the column. Nitrogen pressure is used to elute our solvent mixture. A nitrogen bottle with regulator is

coupled to a gas flow valve that is, in turn, coupled to the column, and calibrated to deliver a flow rate of 20 mL/min. The eluent is collected in 500-mL Berzeluis beakers and transferred to a rotary evaporator. The elution setup is show in Figure 4.8.
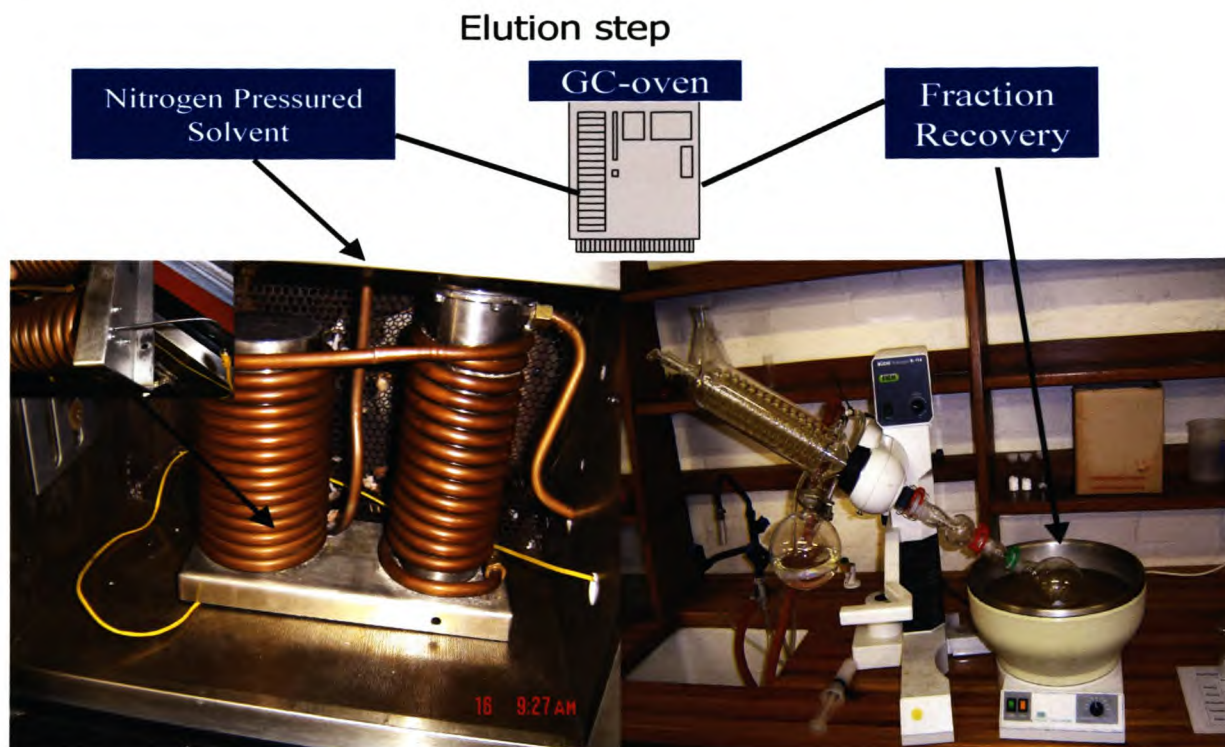

Figure 4.8 The elution setup used in Prep-TREF.

4.2.5) Recovery of the fractions

The final step involves recovering the polymer. The xylene solution of each polymer fraction is transferred from the 500-mL Berzeluis beaker into a 500-ml round bottom flask and the xylene removed by evaporation under reduced pressure on a rotary evaporator at 70°C. The polymer is removed from the flask with 10 ml of acetone. The polymer/acetone samples are placed in pre-weighed poly-top vials and dried in a vacuum oven at room temperature. The poly-tops are then re-weighed to calculate the mass fraction recovered. Great care must be taken when weighing, since one experimental error here will be magnified and reflected in the 3D-plots later. The fractions can be washed with methanol if catalyst traces need to be removed.

4.3) Evaluation of the Preparative TREF, using LDPE

4.3.1) Fractionation techniques (TREF and CRYSTAF) and analytical techniques (CRYSTAF, HT-SEC, NMR and DSC)

In this study we combined two fractionation techniques to study the structure of the LDPE, namely Prep-TREF and CRYSTAF. Both of these techniques fractionate samples according to their crystallizability. Although the mechanisms of separation are slightly different, a combination of these two techniques offers the opportunity to carry out a more detailed analysis of the polymers. It is, for example, possible to examine effects such as co-crystallization since molecules that co-elute in Prep-TREF fractionation may appear as a bimodal peak in the CRYSTAF trace for that fraction.

In order to evaluate the effectiveness of the preparative TREF that was designed and developed in this study, a detailed discussion of the LDPE and its fractions obtained using the Prep-TREF will be discussed. A wide variety of techniques were used to analyze the fractions: CRYSTAF, HT-SEC, NMR and DSC.

4.3.2) Prep-TREF results

Figure 4.9 shows the sum of the weight fractions recovered for each TREF elution temperature as well as the weight fraction/temperature plot. A broad peak of the weight fraction percentage devided by the elution temperature ($W_i\%/\Delta T$) curve (blue) is seen. This was important since in Prep-TREF the broader the peak the better the fractionation. The peak maximum $Tc_{(TREF)}$ was at 70°C. The onset temperature was at 50°C. The second curve (black) is the curve of the sum of the weight fractions ($\sum W_i\%$). Table 4.1 shows the raw data that was used in Figure 4.9.
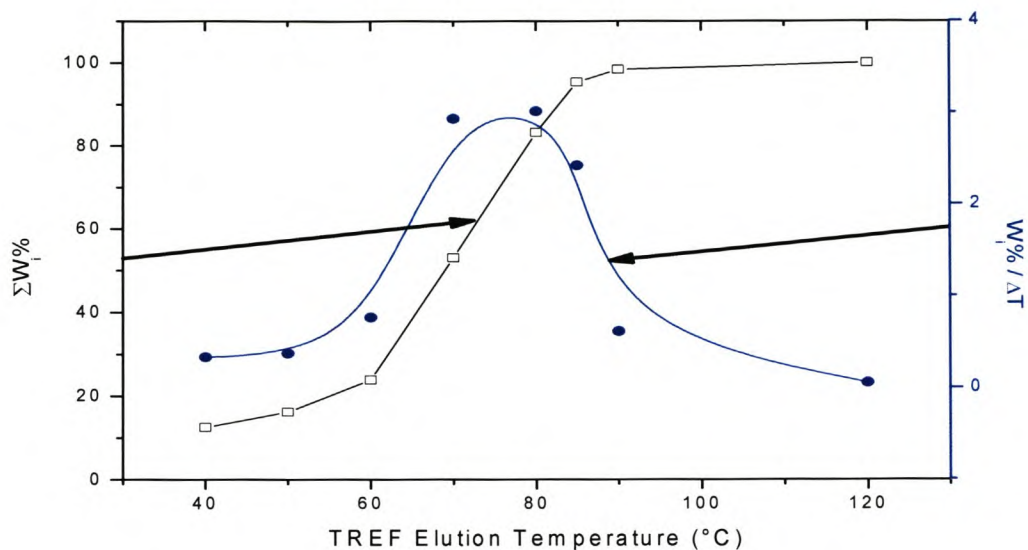
Figure 4.9 The $\sum W_i\%$ and $W_i\%/\Delta T$ vs the TREF elution temperature.

Table 4.1 Raw data of the LDPE obtained after fractionation by Prep-TREF

Elution temp. (°C)	Mass recovered from 3 g sample (g)	Weight fraction[a] W_i	Weight fraction %[b] W_i (%)	Sum of the weight fractions% $\sum W_i\%$	ΔT [c] (°C)	$W_i\%/\Delta T$[d]
25	0.227	0.08	7.60	7.60	n/a	n/a
40	0.148	0.05	4.94	12.54	15	0.33
50	0.111	0.04	3.65	16.19	10	0.37
60	0.228	0.08	7.61	23.80	10	0.76
70	0.876	0.29	29.26	53.06	10	2.93
80	0.902	0.30	30.13	83.18	10	3.01
85	0.362	0.12	12.10	95.28	5	2.42
90	0.091	0.03	3.07	98.35	5	0.61
120	0.049	0.02	1.65	100	30	0.05

[a] mass of each fraction / total mass recovered

[b] mass / total (3g) x 100

[c] the elution temperature range between each fraction

[d] weight fraction percentage divided by the elution temperature range between each fraction.

4.3.3) CRYSTAF results

Figure 4.10 shows the CRYSTAF traces for the eight different temperature fractions of the LDPE sample, obtained using the Prep-TREF. The CRYSTAF trace for the unfractionated LDPE is also included.

The following were seen:

- The CRYSTAF trace for the unfractionated LDPE showed a relatively broad crystallization peak between 55°C and 78°C.

- The 25°C fraction showed no peak. It was totally soluble, even at 20°C. (TCB freezes at 18°C.)

- The 40°C TREF fraction appeared as the first crystallizable trace, between 2°C and 40°C.

- The 50°C trace appeared between 40°C and 50°C.

- The $60°$C trace appeared between 50°C and 70°C.

- The 70°C trace had the narrowest peak, between 45 and 60°C, and a peak maximum at 52°C.

- The 80°C trace had a peak maximum at 53°C. It was broader than the 70°C trace.

- The 85°C trace had a peak maximum at 55°C.

- The 90°C trace has a peak maximum at 60°C.

The CRYSTAF traces for each of the fractions showed that the Prep-TREF was successful in fractionating the sample according to crystallizability. The maximum in the first derivative of the concentration curve from CRYSTAF moved progressively to a higher temperature with increasing TREF fraction temperature. The broad shoulders on the lower temperature fractions could possibly be due to co-crystallization. Figure 4.10 was later plotted as a 2-D-plot seen in three dimensions. (It is shown in Figure 4.12.) In future this will be referred to as the unweighted CRYSTAF curves (as seen in Figure 4.12).
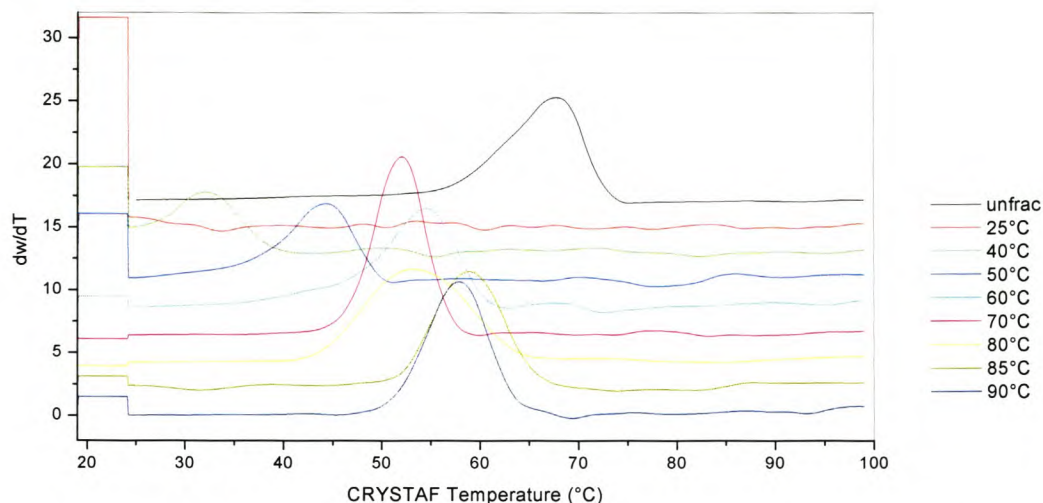
Figure 4.10 CRYSTAF traces for the eight different LDPE temperature fractions obtained using Prep-TREF, and one unfractionated trace, obtained using a waterfall plot with the Y-axis offset for clarity purposes.

Figure 4.11 shows the $Tc_{(CRYSTAF\ peak\ maxima)}$ vs. the TREF elution temperature for each of the Prep-TREF LDPE fractions recovered. The LDPE Tc values increased with an increase in the TREF elution temperature. A direct comparison of the CRYSTAF traces for each of the TREF fractions could be misleading however, since each of the peaks appeared to have similar intensities. This was because approximately the same quantity of sample was used to obtain the CRYSTAF traces, regardless of the quantity of polymer obtained in the fraction. This was clearly seen in Figures 4.10 and 4.12.
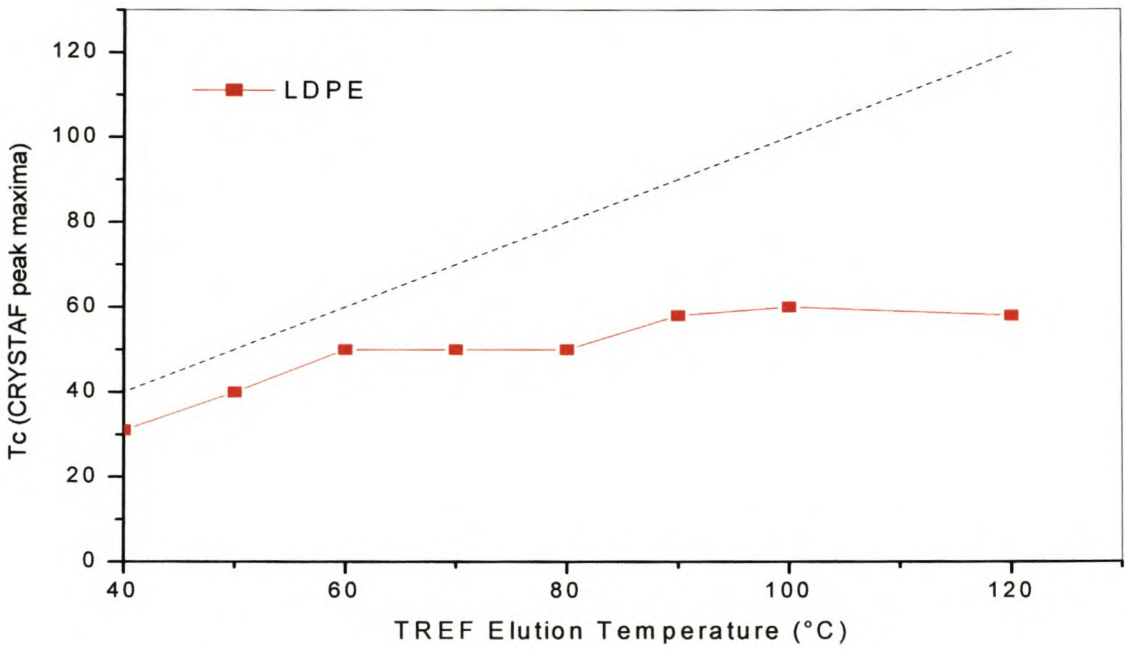
Figure 4.11 The CRYSTAF peak maxima (Tc) vs. the TREF elution temperature for each LDPE fraction recovered.
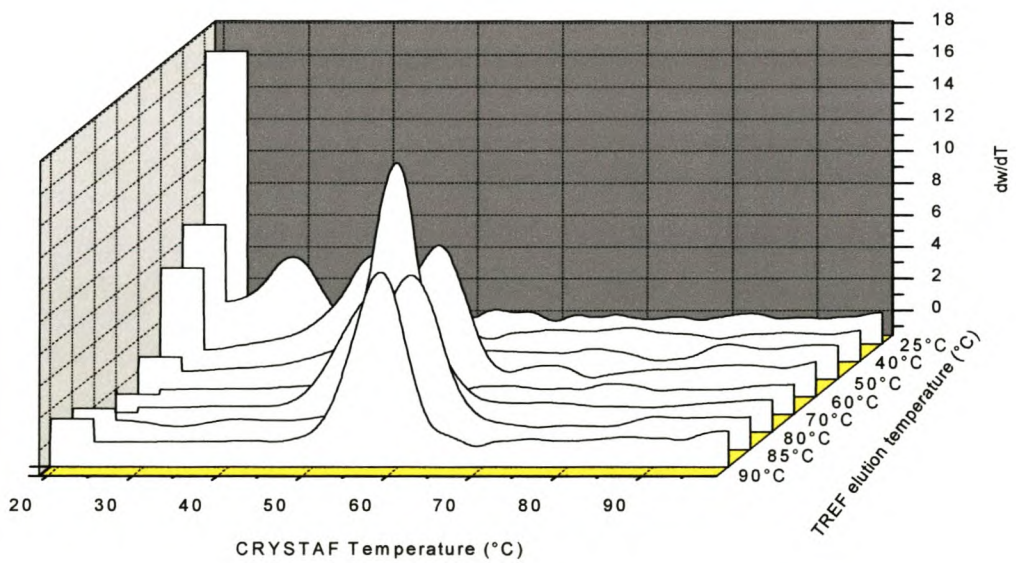

Figure 4.12 The 2-D unweighted CRYSTAF waterfall plot shown in 3-D. (See also Fig 4.10)

In order to make a better comparison of the CRYSTAF traces for each of the TREF fractions we weighted each CRYSTAF trace according to the weight fraction of the polymer recovered in that fraction from the Prep-TREF. This gave a more visual and accurate idea of the sample composition, since the data now contained information on the relative quantity of material in the fractions as well as the CRYSTAF profiles. An example of a weighted CRYSTAF plot is shown in Figure 4.13. (The 80°C data was omitted as it was suspected that it contained experimental error.) The data obtained in the above manner was combined with the TREF elution data to produce a 3-dimentional plot that contained information on the TREF elution temperature, CRYSTAF traces, as well as the quantity of material eluted in each TREF fraction. These types of plots made it easier to visualize the molecular heterogeneity in a LDPE sample, based on the two fractionation techniques, as seen in Figure 4.14.
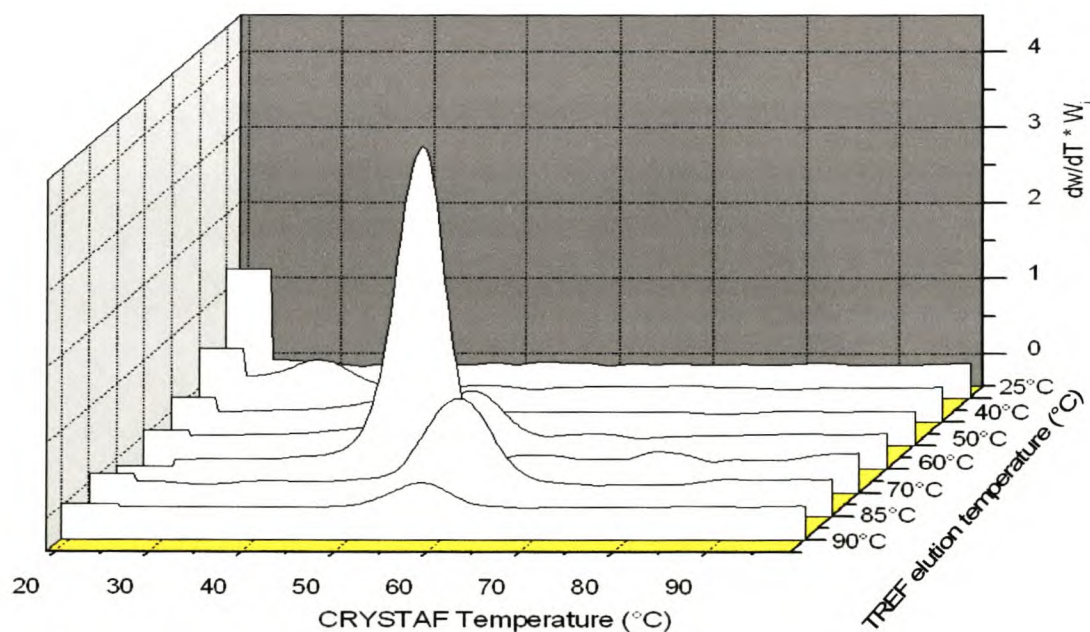

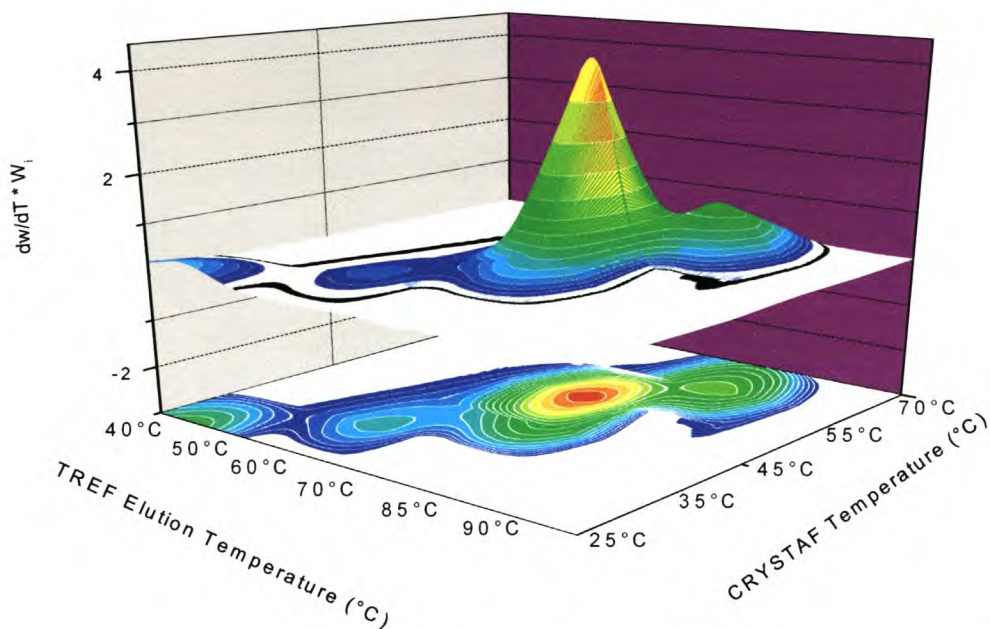**Figure 4.13 The weighted LDPE curves presented as 2D graphs in 3-D.**

Figure 4.14 The 3-D CRYSTAF plot of the weighted LDPE curves presented as 3-D graphs.

Figure 4.14 shows a true 3-D graph, illustrating the heterogeneity of the LDPE. The graph has a contour plot in the bottom so as to show the data that is hidden in the cone-like structure graph. There was broad distribution along the TREF elution temperature axis and narrower distribution along the CRYSTAF temperature axis. It should be noted that the axis in the 3-D plot was not linear for the TREF elution temperature since only the following TREF fractions were used: 40°C, 50°C, 60°C, 70°C, 85°C and 90°C. The 80°C fraction was omitted. For the sake of being able to compare all the 3-D plots of the LDPE, only the following TREF fractions were now to be used: 40°C, 50°C, 60°C, 70°C, 85°C and 90°C. A linear comparison can be created only if all the TREF fractions that are collected have a constant temperature increase of either 5°C or 10°C.

Figure 4.15 illustrates the CRYSTAF plot of the unfractionated LDPE in comparison with the weight fraction percentage divided by the fraction temperature range, obtained from the Prep-TREF.
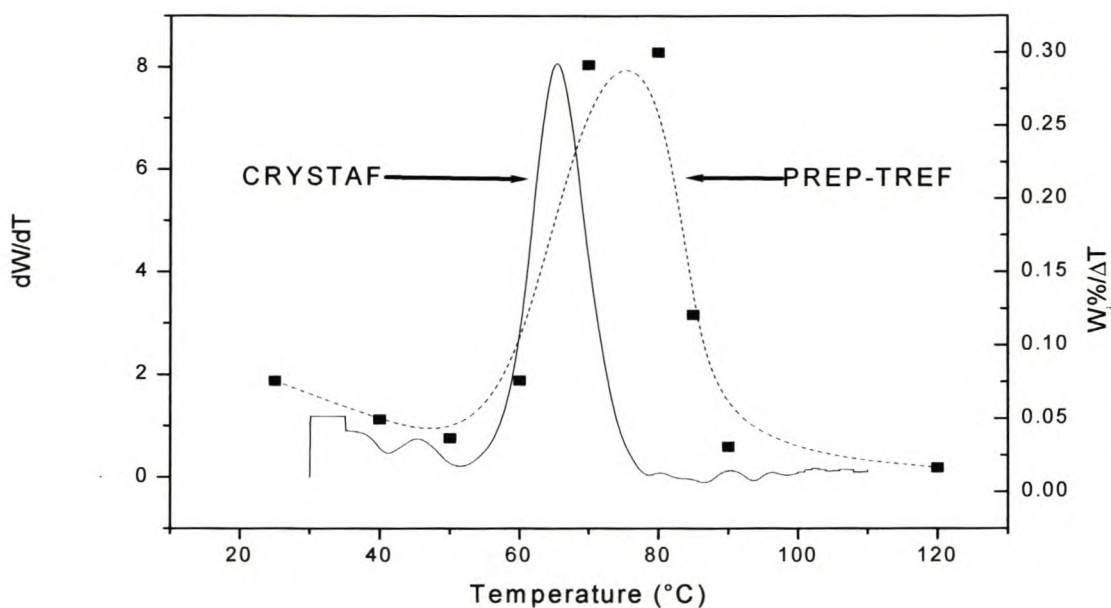
Figure 4.15 Schematic representation of the CRYSTAF plot of the unfractionated LDPE in comparison to the Prep-TREF plot.

In Figure 4.15 the CRYSTAF plot had a peak maximum at 66°C. The TREF had a peak maximum at 78°C. The higher value for the TREF peak is a well-known phenomenon; this phenomenon is attributed to the so-called "under cooling" effect. According to Monrabal [1], both the techniques fractionate via short chain branching distribution (SCBD) but there is a difference in the crystallization and elution steps. In CRYSTAF, first one precipitates the polymer out of solution and then one detects the concentration of the polymer remaining in solution, using FTIR. In TREF however, one needs to dissolve the polymer in solution and then precipitate it out of solution onto a support particle (in our case sea sand), where the polymer is then reheated and eluted in the elution step. There is thus a secondary melting (dissolution) effect in TREF that do not occur in CRYSTAF. This effect most probably accounts for the difference in peak maxima of the dw/dT curves shown in Figure 4.15. Although a solvent effect can not be discounted in this case, since xylene was used for the TREF elution, while TCB is used in the CRYSTAF analysis. The Prep-TREF and CRYSTAF peaks however correlate in shape, once

again showing that the Prep-TREF is separating according to the same principles as a commercially available CRYSTAF.

4.3.4) HT-SEC results

Table 4.2 summarizes the HT-SEC and CRYSTAF Tc data for each LDPE fraction.

Table 4.2 The HT-SEC and CRYSTAF peak maxima results for LDPE fractions

Temperature[a] (°C)	Mn	Mw	PD	Tc[b]	W_i
25.00	670	5600	8.4	no Tc	0.08
40.00	7200	13000	1.8	31.00	0.05
50.00	7900	14000	1.9	40.00	0.04
60.00	8200	15000	1.8	50.00	0.08
70.00	20000	63000	3.2	50.00	0.29
80.00	70000	250000	3.5	50.00	0.30
85.00	78000	250000	3.2	58.00	0.12
90.00	86000	250000	2.8	60.00	0.03
120.00	90000	230000	2.6	broad	0.02
unfractionated	29000	210000	7.3	58	1

[a] Internal column temperature of the Prep-TREF for each fraction

[b] Tc: CRYSTAF peak maxima.

Figure 4.16 shows the HT-SEC results for each of the TREF fractions for the slow-cooled LDPE.
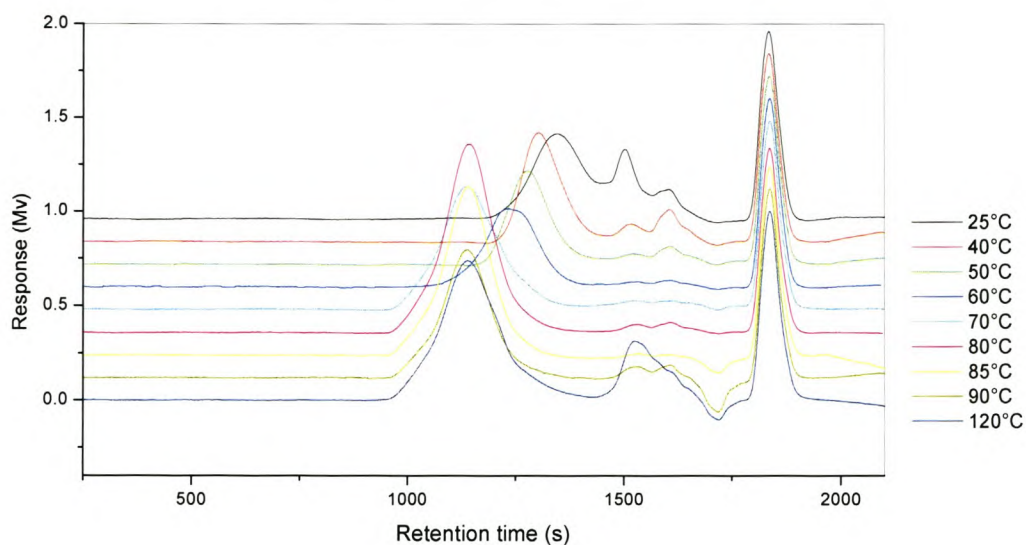
50

Figure 4.16 HT-SEC baseline corrected and normalized results for the slow-cooled LDPE.

The narrow high-intensity peak seen in each trace between 1750 and 2000 seconds is the BHT peak used as a flow rate marker. As done for the CRYSTAF trace (Section 4.3.3) we could weight each SEC trace to give a visual representation of the relative amounts of polymer recovered in each fraction. Figure 4.17 shows a representation of these results – it shows the weighted baseline corrected and normalized 2D-LDPE results. The data in Figure 4.17 will be discussed in greater detail in Section 4.4.
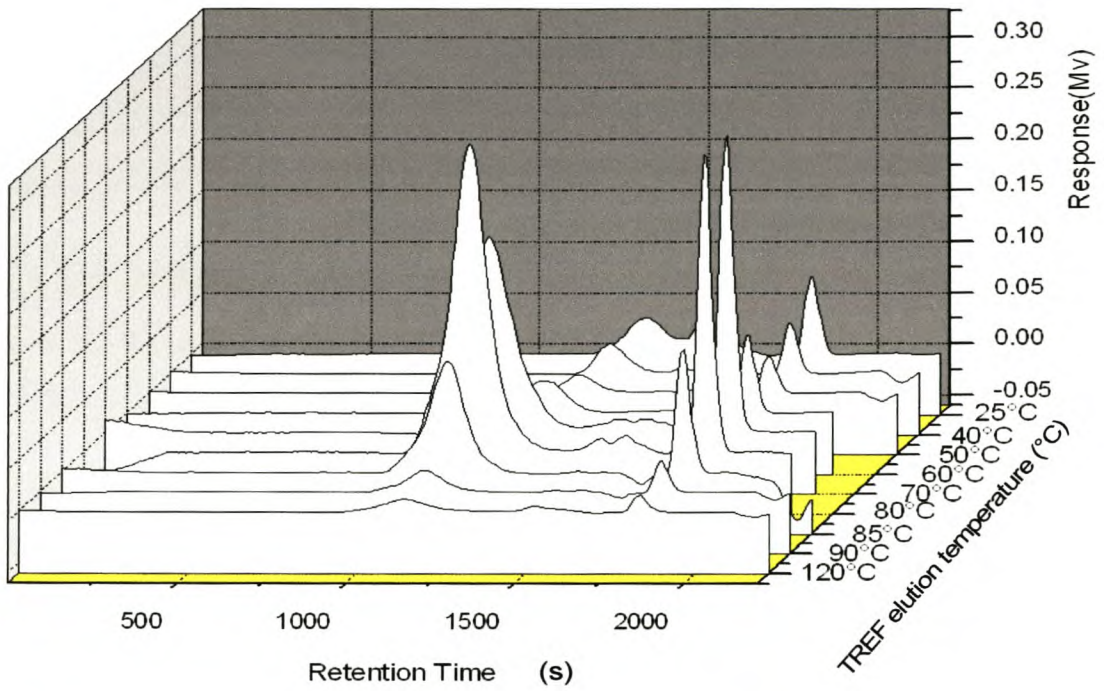
Figure 4.17 The LDPE HT-SEC results of the weighted, baseline corrected Prep-TREF fractions as a 2-D waterfall plot.
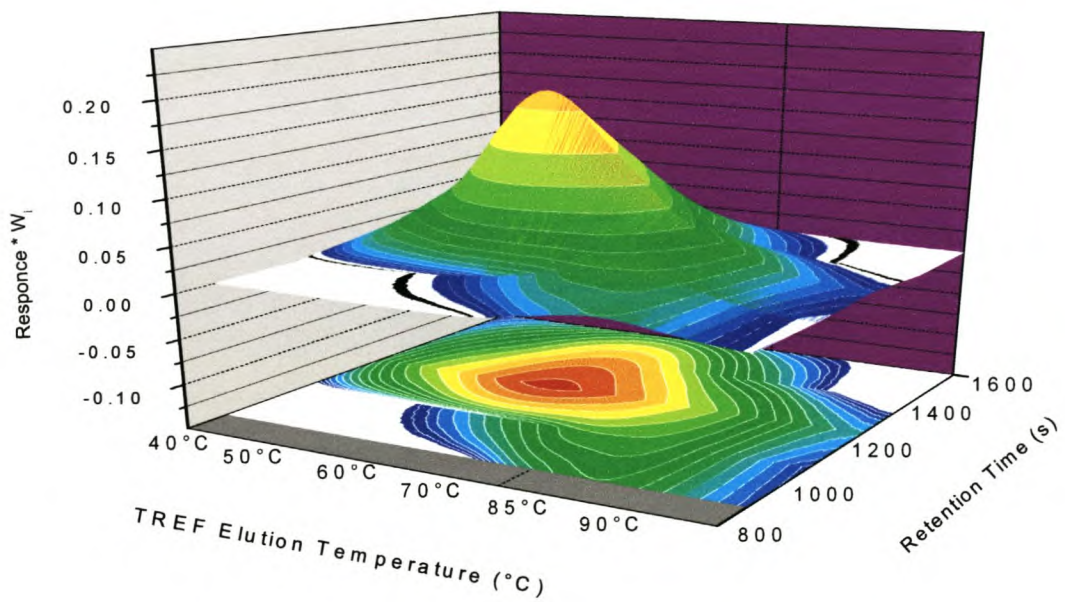

Figure 4.18 The 3-D HT-SEC results for the slow-cooled LDPE.

Figure 4.18 shows the 3-D HT-SEC results for the Prep-TREF fraction using a matrix to replace the x-axis of conventional graphs with a 3-D plot presenting the data of three variables. This graph was plotted using the normalized, baseline corrected and weighted HT-SEC data of the Prep-TREF fractionated 40°C, 50°C, 60°C, 70°C, 85°C and 90°C traces. This type of plot provides a simple visual representation of the heterogeneity with respect to the TREF and SEC data.

Figure 4.19 shows the plot of the LDPE molecular weight vs. the TREF elution temperature.
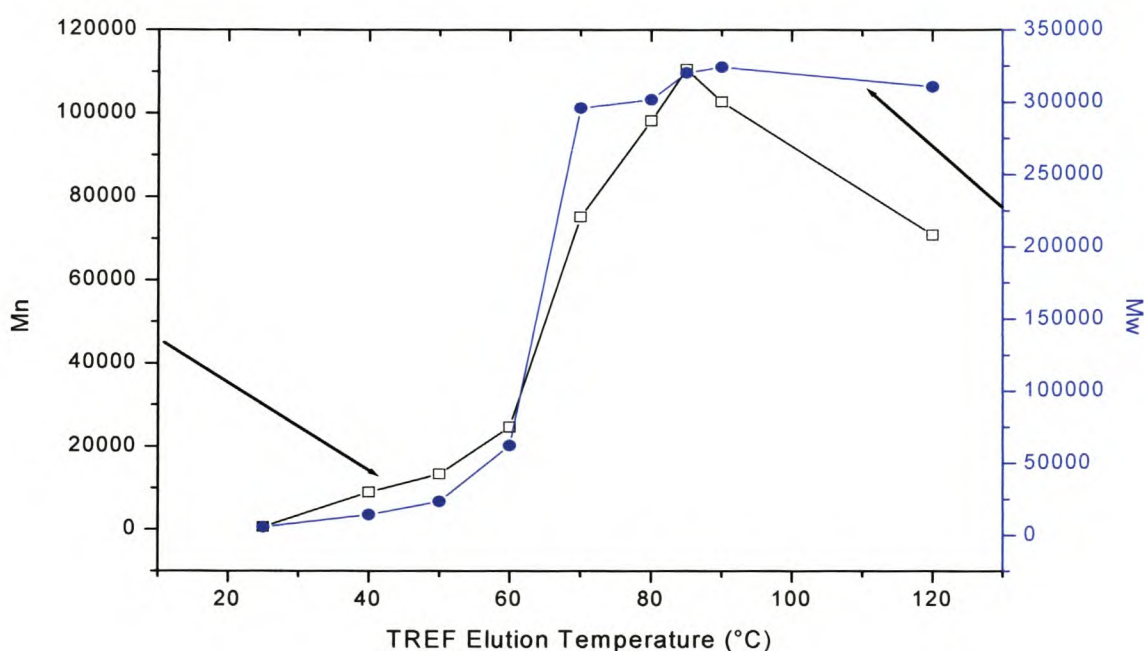
Figure 4.19 The number average and weight average molecular weight vs. the TREF elution temperature for each fraction for the LDPE sample.

The 25°C TREF fraction has a bimodal MMD with Mn = 670 and Mw 5600 and PD greater than 8. The Mn of the 25°C-40°C trace had increased to 7200 and the Mw has increased to 13200, with a PD of 1.826. The Mn and Mw values of the 40°C-50 °C trace had also increased, while the PD values were less than that of the unfractionated LDPE. The Mn and Mw values of the

50°C-60°C, 60°C-70°C, 70°C-80°C and 80°C-85°C traces also showed increases and the PD values were again below that of the unfractionated LDPE sample. The Mn of the 85°C-90°C trace had decreased slightly, but there was an increase in Mw, relative to the lower temperature traces. These increases of Mn and Mw relative to elution temperature did not necessarily suggest that the separation mechanism occurred via molecular weight. The results did show however that the low molecular weight fractions were the more branched and that the high molecular weight fractions were the least branched.

4.3.5) NMR results

Figures 4.20-4.22 show the ^{13}C NMR spectra of the unfractionated LDPE, the 60°C TREF fraction and the 85°C TREF fraction, respectively.
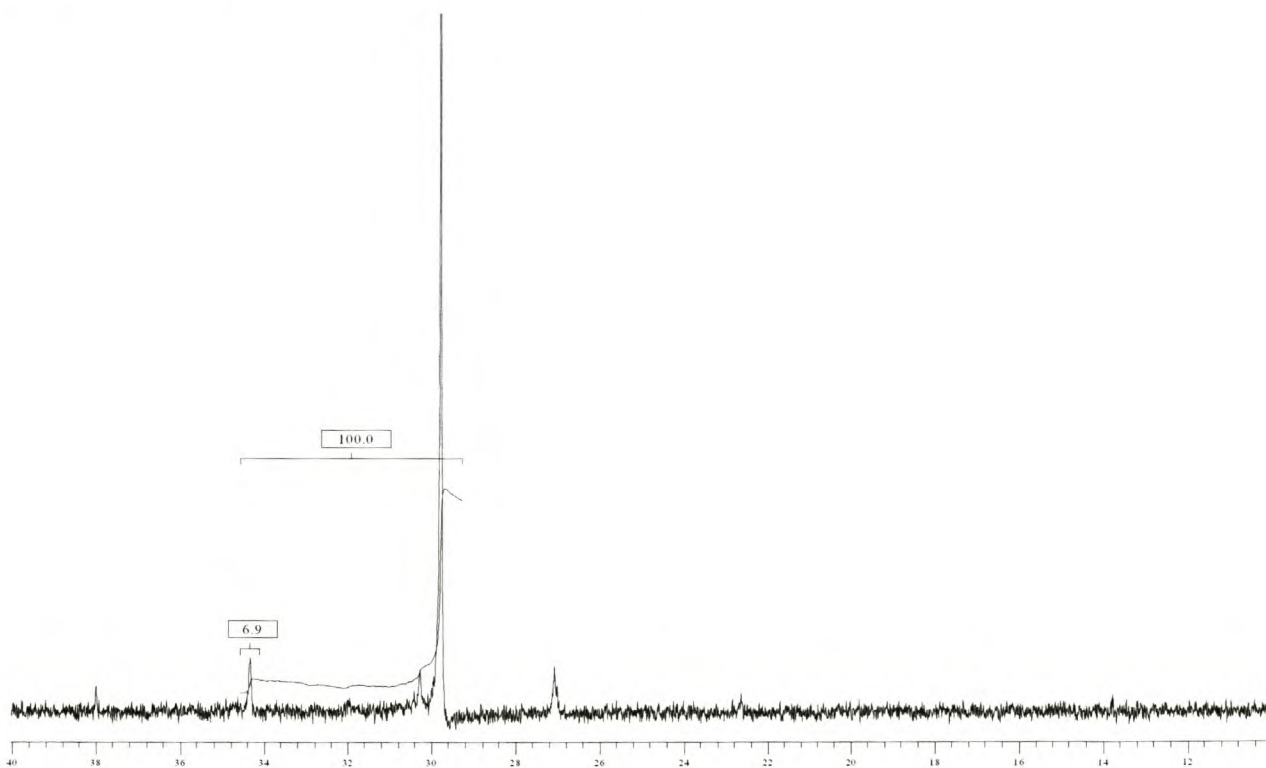

Figure 4.20 ^{13}C NMR spectrum of the unfractionated LDPE.

Figure 4.20 shows the signal of the methylene groups in the main chain at 29.98 ppm. The relative degree of branching was calculated to be 3.45%. To calculate the relative degree of

branching of the LDPE the integration value of the branched peak was divided by the value of the whole main chain branched x 200, to get a relative degree of branching percentage. The second peak used for the integration was the branching peak at 34 ppm. This peak included all the α-branched (ethylene, butene, hexene) peaks. Hanson et al. [2] have shown where all the branched peaks occur in the NMR spectrum of LDPE.
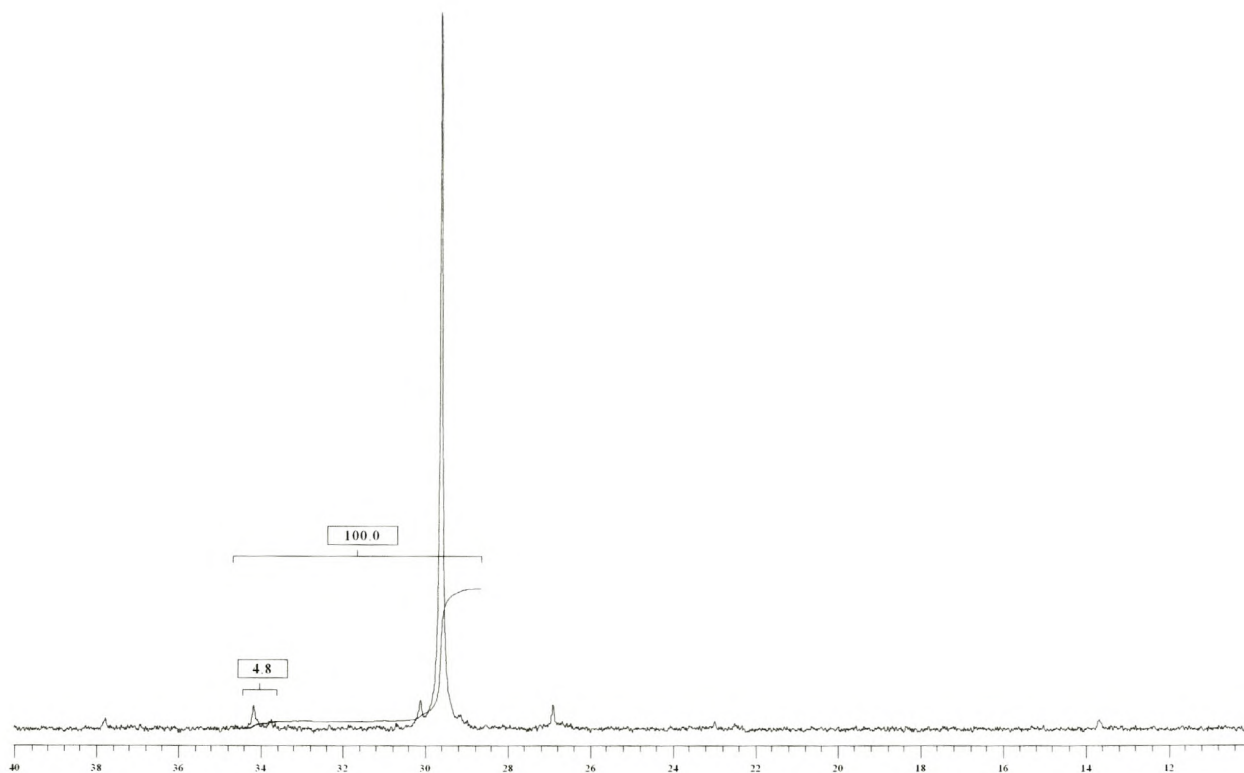
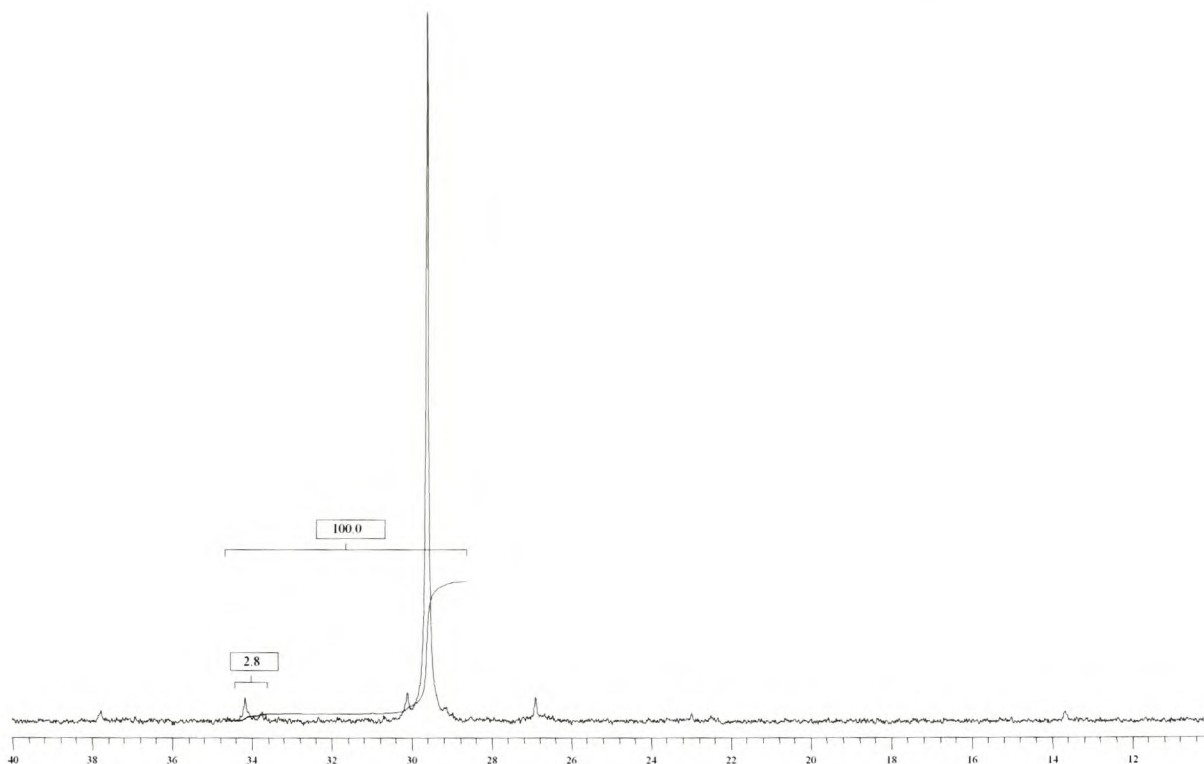

Figure 4.21 ^{13}C NMR-spectrum of the 60°C fractionated LDPE trace.

Figure 4.22 ^{13}C NMR-spectrum showing the 85°C fractionated LDPE trace.

From Figure 4.21 it was calculated that the relative degree of branching for the 60°C fraction was 2.45%. This represented a decrease in the relative branching content of the 60°C fraction of LDPE relative to the unfractionated LDPE. From Figure 4.22 it was calculated that the relative degree of branching for the 85°C fraction was 1.45%. This decrease in the relative degree of branching was again illustrated by the further decrease in branching content with an increase in elution temperature from the 60°C fractionated LDPE trace to the 85°C fractioned LDPE trace, as seen in Figure 4.22. These NMR results proved that increasing the Prep-TREF elution temperature lead to a decrease in the relative degree of branching of LDPE.

4.3.6) DSC results

Figures 4.23 and 4.24 show the DSC crystallization and DSC melting peaks for the Prep-TREF fractions of LDPE, respectively. DSC's results have all been baseline zeroed and normalized.
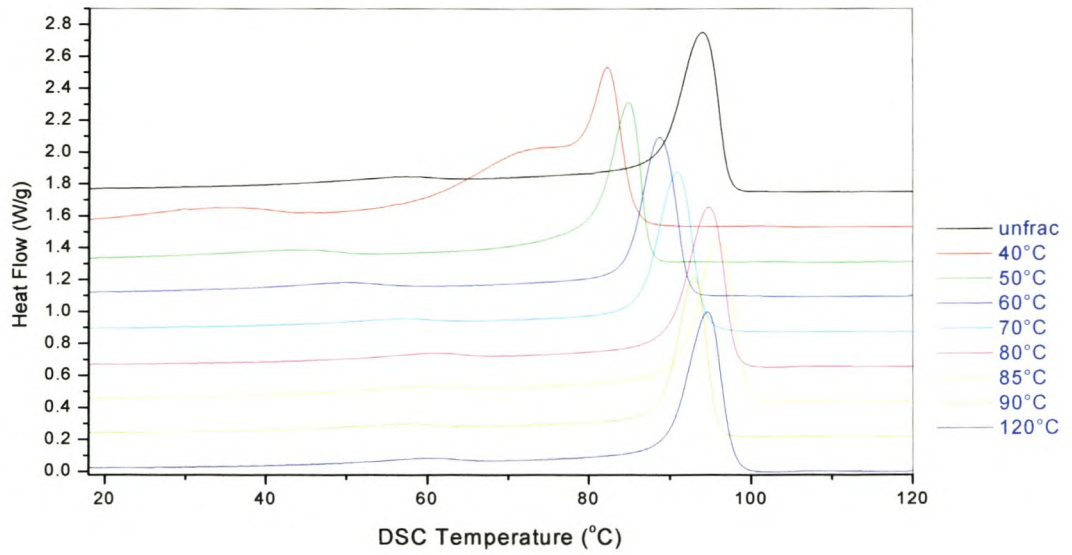
Figure 4.23 DSC crystallization peaks for the unfractionated and Prep-TREF fractionated LDPE traces.
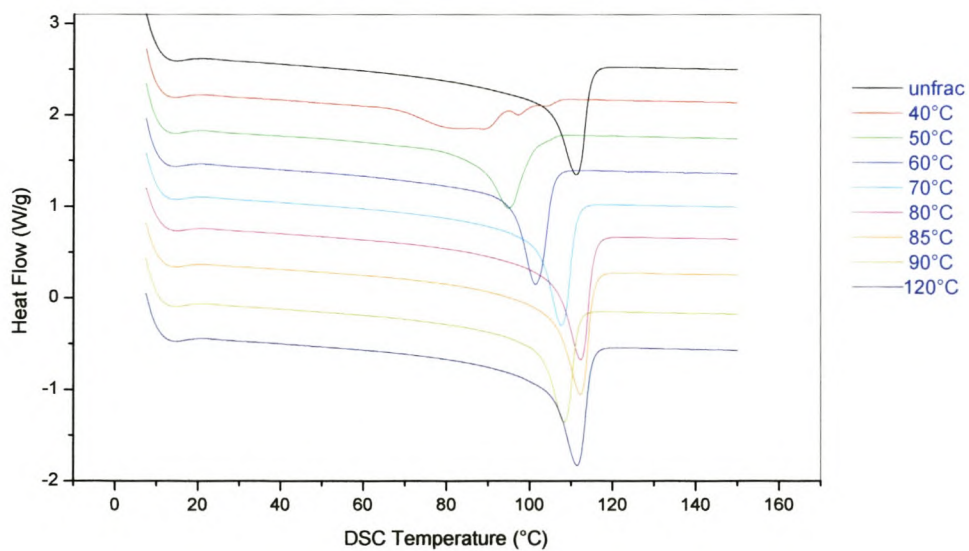

Figure 4.24 DSC melting peaks for the unfractionated and Prep-TREF fractionated LDPE traces.

The unfractionated DSC crystallization peak is shown at the top of the Figure 4.23. The DSC crystallization peak for the 40°C trace had a large shoulder between 60°C and 80°C. There was an increase in the peak maxima $Tc_{(DSC\ crystallization\ peak\ maximum)}$ of the other peaks with an increase in the Prep-TREF fraction temperature. Figure 4.24 shows the DSC melting peaks for the unfractionated and Prep-TREF fractionated LDPE fractions. The unfractionated LDPE DSC melting peak is shown first, followed by those of the fractionated fractions. The DSC melting peaks all had a broad shoulder on the left-hand side.

Figure 4.25 shows the $Tc_{(DSC\ crystallization\ peak\ maximum)}$ values for each of the Prep-TREF fractionated fractions of LDPE.
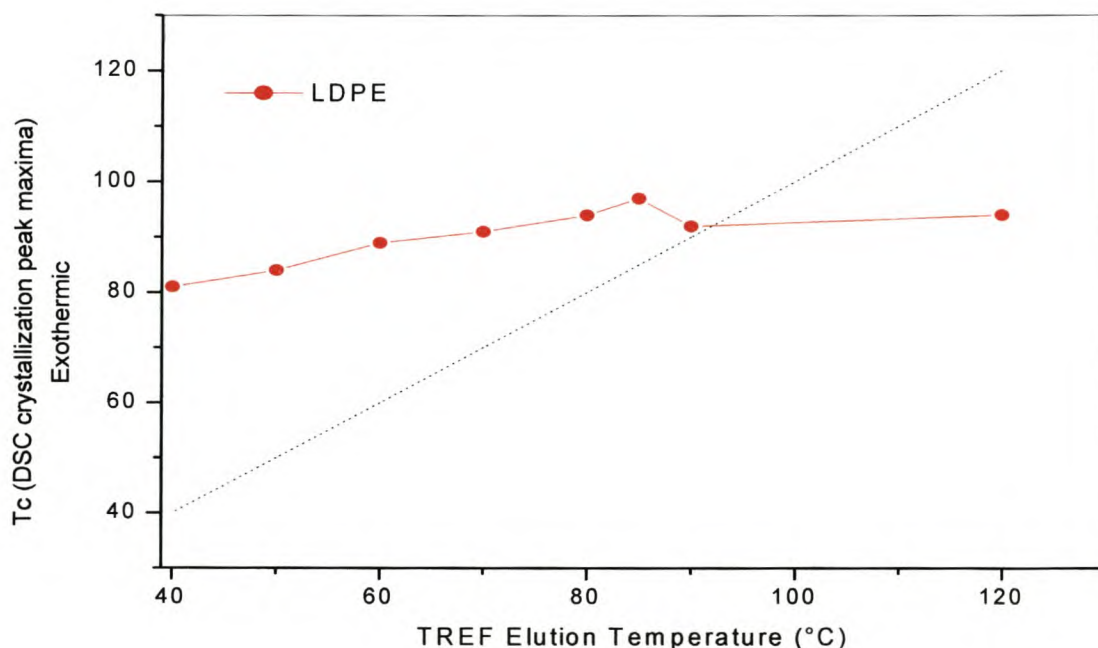

Figure 4.25 The DSC crystallization peak maxima vs. the TREF elution temperature for each Prep-TREF fractionated LDPE fraction recovered.

The DSC $Tc_{(crystallization\ peak\ maximum)}$ values were higher for the 40°C-90°C Prep-TREF fractions than the dotted line representing the $Tc_{(DSC)}$ crystallization peak maxima $= Tc_{(TREF)}$, and lower for the DSC Tc of the 120°C Prep-TREF fraction than the dotted line representing the $Tc_{(DSC)}$ crystallization peak maxima $= Tc_{(TREF\ elution\ temperature)}$.

Figure 4.26 shows the DSC $Tc_{(melting\ peak\ maximum)}$ values for each of the Prep-TREF fractionated LDPE fractions. The DSC $Tc_{(melting\ peak\ maximum)}$ values for the 40 - 90°C Prep-TREF fractions are higher than the dotted line representing the $Tc_{(DSC)}$melting peak maxima = $Tc_{(TREF)}$, and lower for the DSC $Tc_{(melting\ peak\ maximum)}$ of the 120°C Prep-TREF fraction than the dotted line representing the $Tc_{(DSC)}$ melting peak maxima = $Tc_{(TREF)}$.

Unlike the $Tc_{(CRYSTAF)}$ (Figure 4.11) where the values were below the dotted line, both the $Tc_{(DSC)}$ melting and $Tc_{(DSC)}$ crystallization were above the dotted line. It should also be noted that the $Tc_{(DSC)}$ crystallization varied by a much lesser degree than the $Tc_{(CRYSTAF)}$ and $Tc_{(DSC)}$ melting temperature as a function of TREF elution temperature.

As was the case for the Tc(CRYSTAF) temperature (Figure 4.11) there was a relatively small increase in the Tc(DSC) crystallization and Tc(DSC) melting for the higher temperature fractions (80°C-120°C fractions).
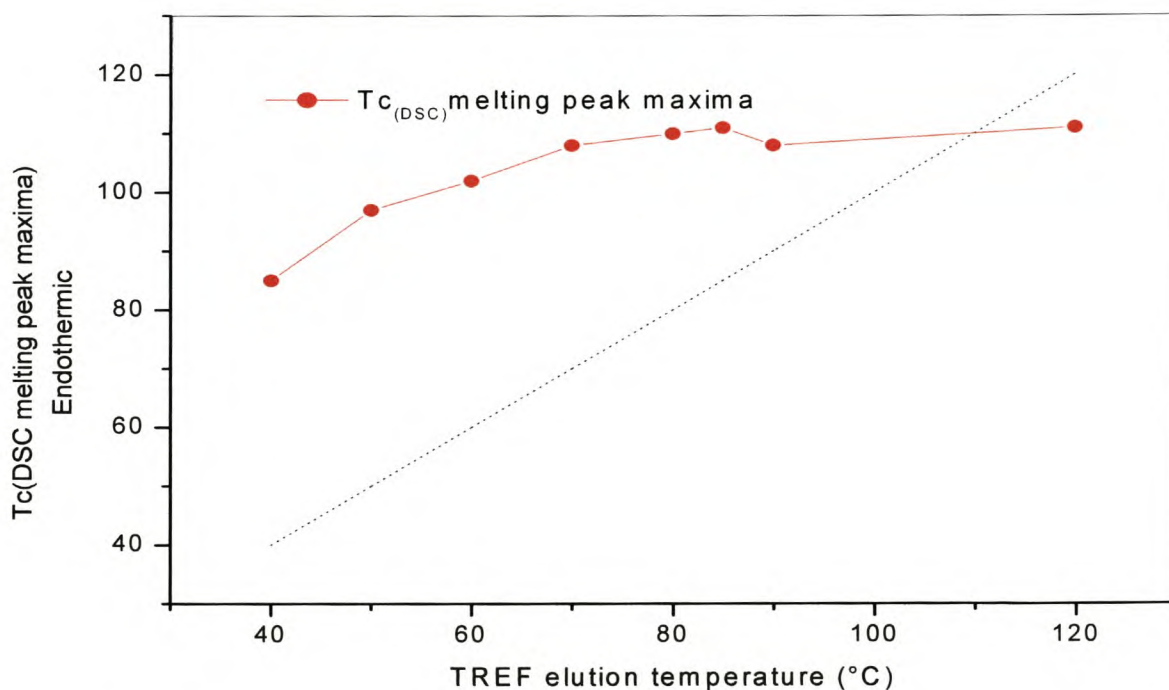

Figure 4.26 The DSC melting peak maxima vs. the TREF elution temperature for each LDPE fraction recovered.

Figure 4.27 shows the 2-D waterfall plot of the weighted, baseline zeroed and normalized DSC results for the Prep-TREF LDPE fractions. Figure 4.28 shows another novel 3-D plot, created to allow for easy visual representation of the heterogeneity of the LDPE with respect to the TREF and DSC data.
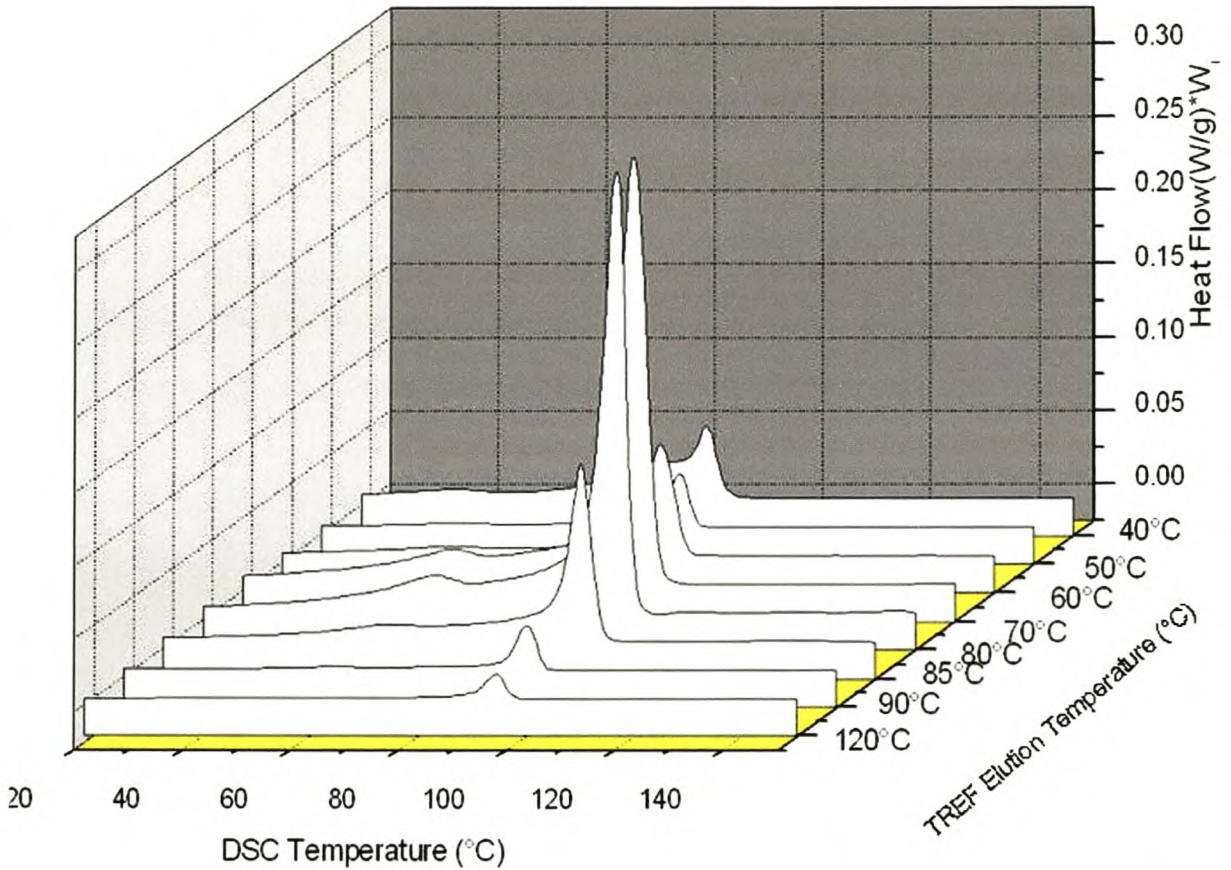

Figure 4.27 The 2-D waterfall plot of the weighted, baseline zeroed and normalized DSC results for the Prep-TREF LDPE fractions.
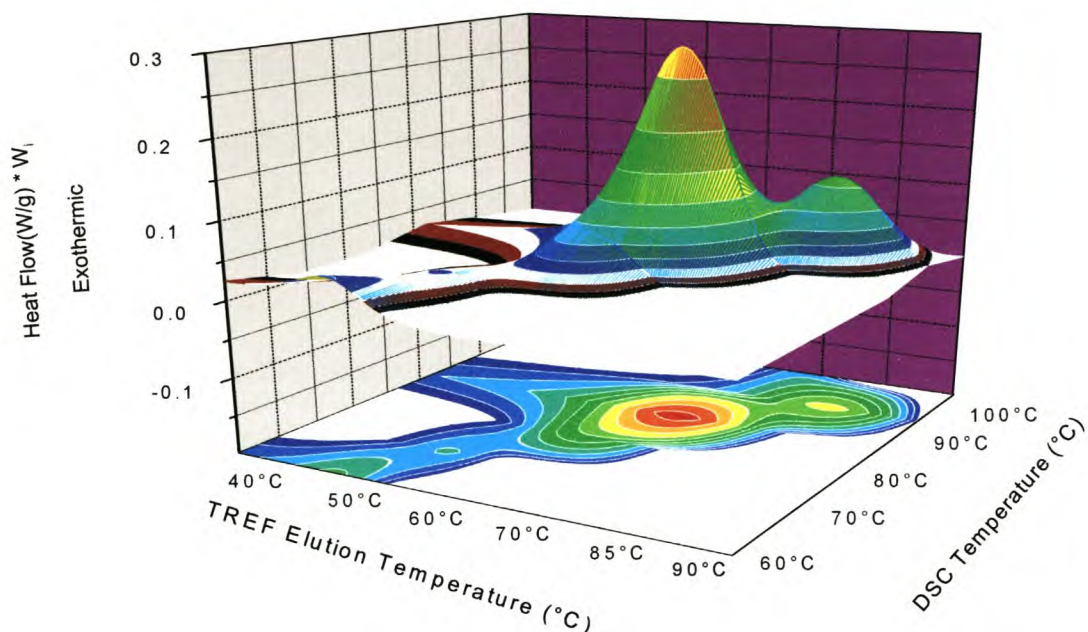
Figure 4.28 The 3-D presentation of the above DSC data obtained from the Prep-TREF LDPE fractions.

Similar to the 3-D plot of the TREF-CRYSTAF data, the DSC crystallization peak data showed a large conical distribution between the 60°C and 85°C TREF fractions and smaller distribution at higher and lower temperatures. A comparison of the 3-D plots will be discussed in detail later in Section 4.11.

4.4) Effect of cooling rate on fractionation.

The effect of the TREF cooling rate on the fractionation of LDPE samples was examined and reported on here. This was done by comparing the quenched-cooled (LDPE polymer and support mixture at 130°C cooled rapidly using an ice-bath) to the slow-cooled (1°C per hour) LDPE. The results were to be used to determine the significance, if any, of the effect of the cooling rate on the crystallization and fractionation process. Figure 4.29 also shows the sum of the weight fractions % ($\sum W_i\%$) in order to compare the weight fractions with weight fractions of other samples, since more fractions can easily change the shape of the W_i curves but not the

shape of the sum of the weight fraction curve, at different temperatures, for slow-cooled and quench-cooled LDPE .
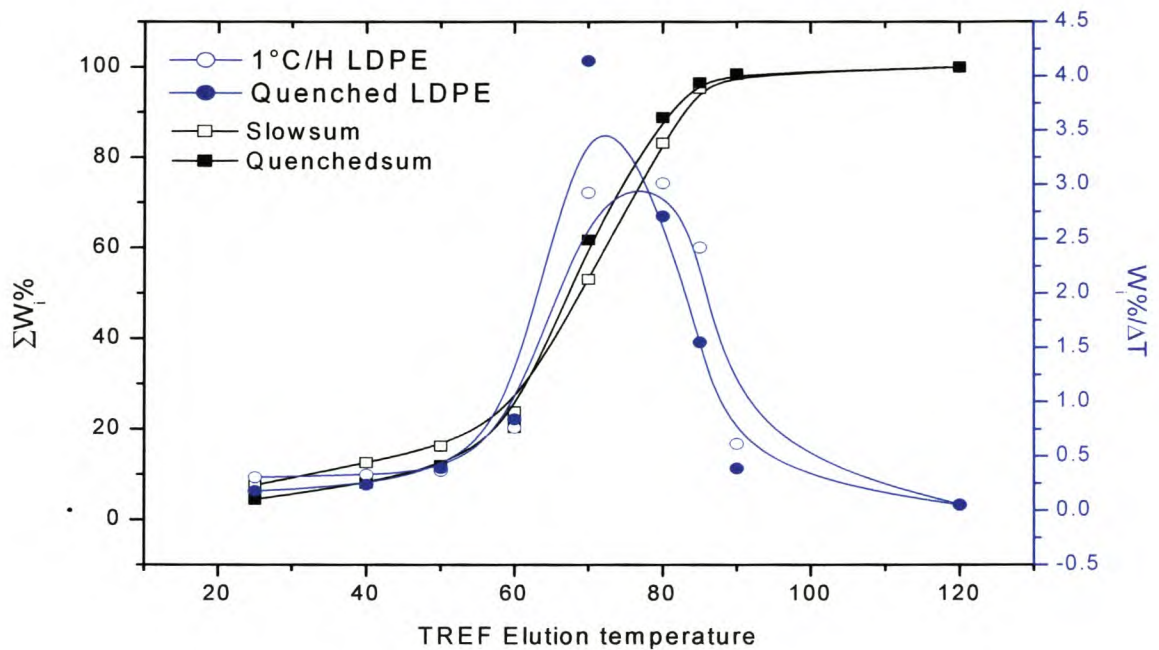

Figure 4.29 Prep-TREF comparison between the slow-cooled and quench-cooled LDPE.

Figure 4.29 shows that the quench-cooled fraction had a $Tc_{(TREF)}$ peak maximum lower than the $Tc_{(TREF)}$ of the slow-cooled polymer fraction 72°C and 78°C respectively. This was expected since the fast cooling rate is favourable for co-crystallization; the fractions did not have time to fractionate prior to the onset of crystallization. This results in a lower $Tc_{(TREF)}$ peak.

It would also be expected that if co-crystallization is forced by quench cooling, this would result in a more disperse molecular fraction, which in turn should lead to a broader CRYSTAF peak.

Figures 4.30 and 4.31 show the comparative CRYSTAF traces of the quench-cooled LDPE fractions and the corresponding slow-cooled fraction. The broader peak width of the quenched fractions was most noticeable for the 40°C and 50°C fractions shown in the figures.

Table 4.3 tabulates the results of the quench-cooled Prep-TREF LDPE fractions.

Table 4.3 Prep-TREF data for the quench-cooled LDPE fractions

Elution temperature (°C)	Mass (g)	Weight fraction[a] W_i	Weight fraction %[b] W_i (%)	Sum of the weight fractions % $\sum W_i\%$	ΔT[c] (°C)	$W_i\%/\Delta T$[d]
25	0.130	0.044	4.44	4.44	n/a	n/a
40	0.104	0.03	3.57	8.02	15	0.23
50	0.114	0.03	3.89	11.91	10	0.38
60	0.245	0.08	8.39	20.31	10	0.83
70	1.213	0.41	41.40	61.71	10	4.14
80	0.793	0.27	27.08	88.80	10	2.70
85	0.227	0.07	7.74	96.54	5	1.54
90	0.057	0.01	1.93	98.47	5	0.38
120	0.045	0.01	1.52	100	30	0.05

[a] mass of each fraction / total mass recovered

[b] mass / total (3g) x 100

[c] the elution temperature range between each fraction

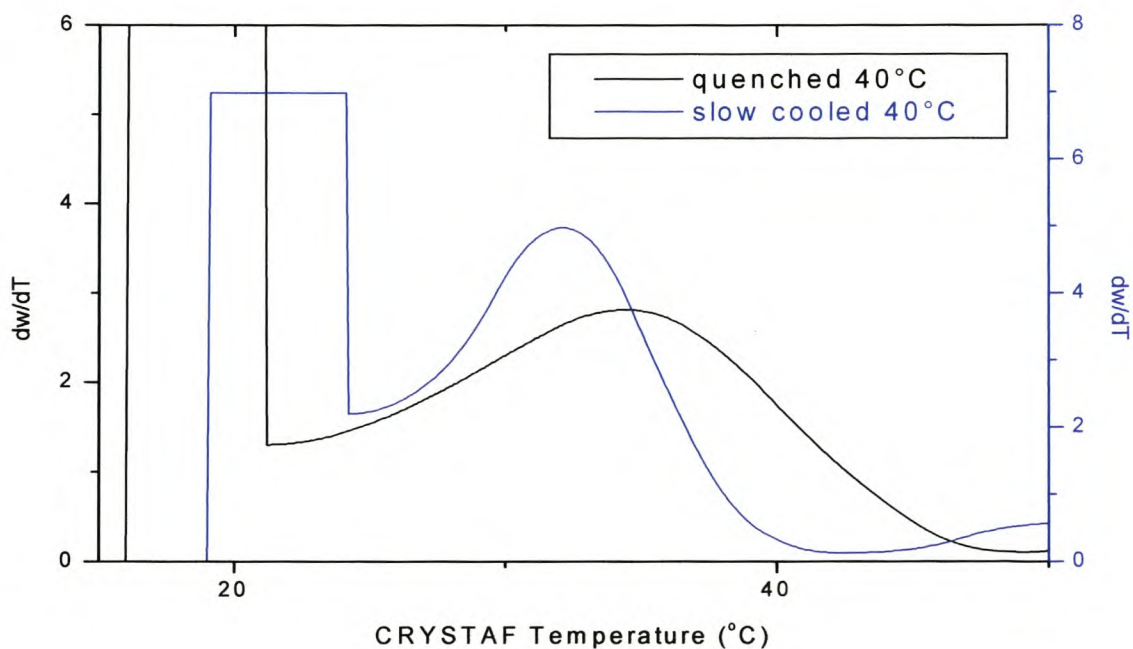[d] weight fraction percentage divided by the elution temperature range between each fraction.

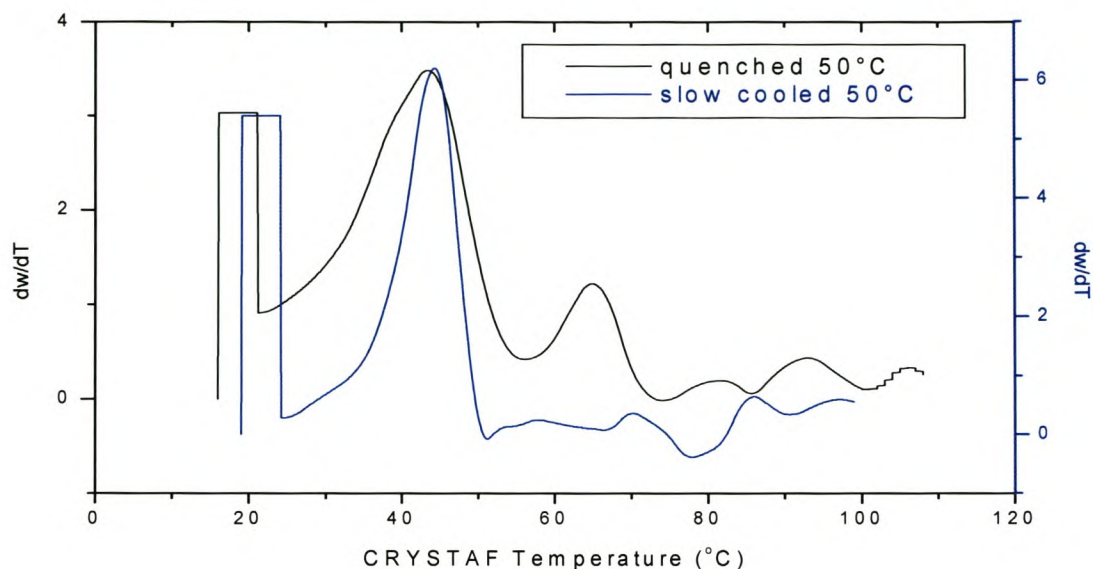**Figure 4.30 Comparison of CRYSTAF traces of 40°C Prep-TREF fractions of slow- and quench-cooled LDPE.**

Figure 4.31 Comparison of CRYSTAF traces of 50°C Prep-TREF fractions of slow- and quench-cooled LDPE.

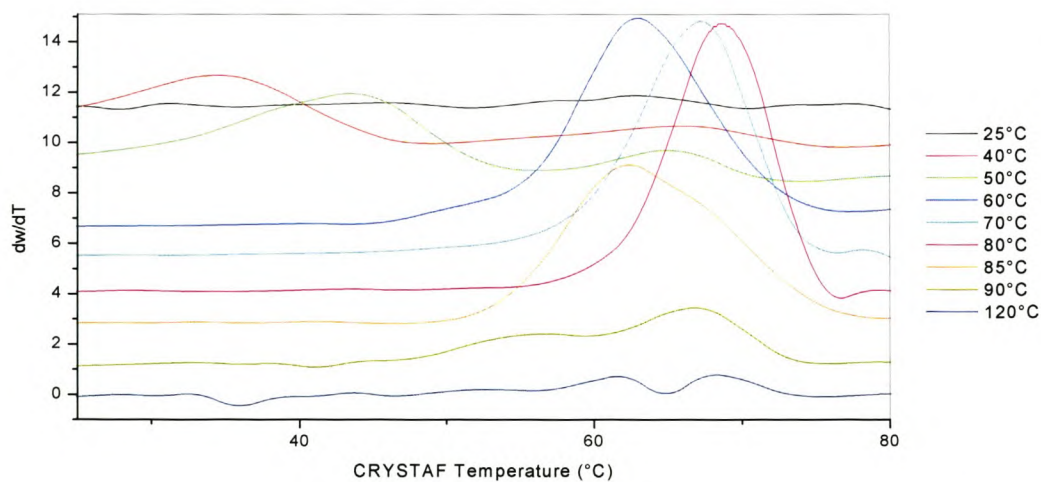Figure 4.32 shows the CRYSTAF traces for each of the fractions recovered from the quench-cooled sample.

Figure 4.32 CRYSTAF traces of the quench-cooled Prep-TREF LDPE fractions.

64

Figure 4.32 shows that the fractionation via crystallizability in the quench-cooled sample followed the same pattern as for the slow-cooled fractions, but the CRYSTAF traces lacked the narrow Gaussian curve peak distribution. This illustrated the decrease in the homogeneity of the fractionation via crystallization with an increase in the cooling rate of the elution step. Figures 4.10 and 4.11 in Section 4.3.3 showed the CRYSTAF results for the slow-cooled LDPE. In these latter two figures we could clearly see the shifting of the Prep-TREF CRYSTAF traces [$Tc_{(CRYSTAF\ peak\ maximaa}$] with an increase in TREF elution temperature.

In order to quantify the degree of molecular distribution (as illustrated by the CRYSTAF peak width) of the TREF fractions we quantified the breath (or broadness) of each of the CRYSTAF traces for the different temperature fractions by fitting a simple Gaussian curve to the data. From these fitted curves the full width at half the maximum (FWHM) could be determined. A larger value indicates a broader peak and therefore broader distribution. Figure 4.33 shows the plot of the full width at half the maximum (FWHM) vs. the TREF elution temperature for the slow- and quench-cooled fractions of the LDPE. Error bars in Figure 4.33 show the statistical uncertainty. In Figure 4.33 it was seen that in each of the equivalent TREF fractions the quench-cooled fraction had a broader peak distribution. This clearly illustrated that the slower cooling rate lead to a narrower distribution within the TREF fraction. This was probably due the slower cooling rate allowing time for the separation of homogeneously crystallizable molecules.
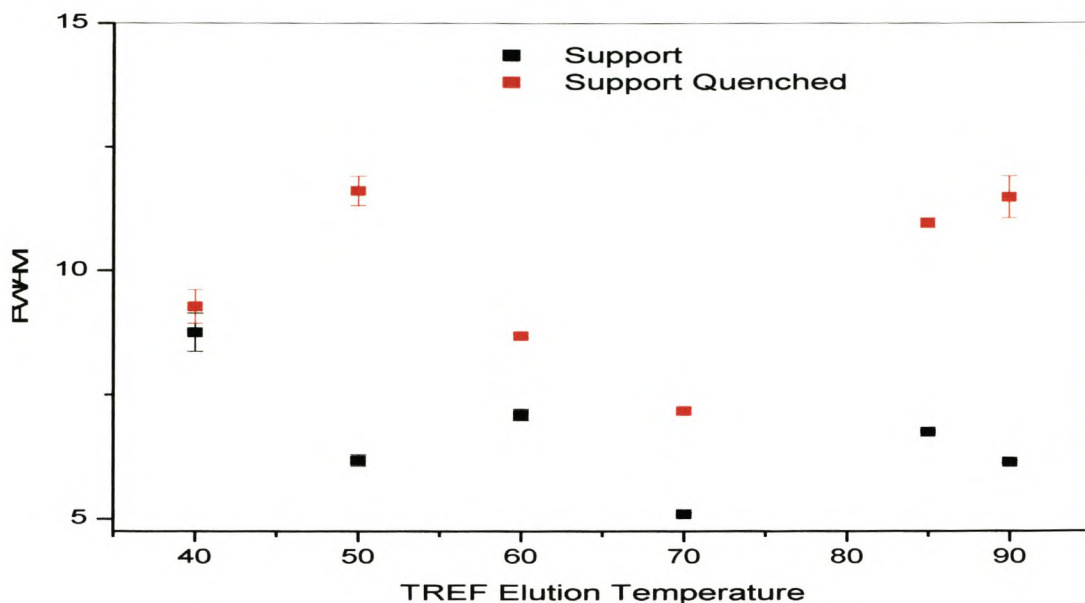
Figure 4.33 Plot of the full width at half the maximum (FWHM) vs the TREF elution temperature for the slow- and quench-cooled fractions of the LDPE.

In Figure 4.34 the $Tc_{(CRYSTAF\ peak\ maxima)}$ values of the slow- and quench-cooled LDPE are compared.
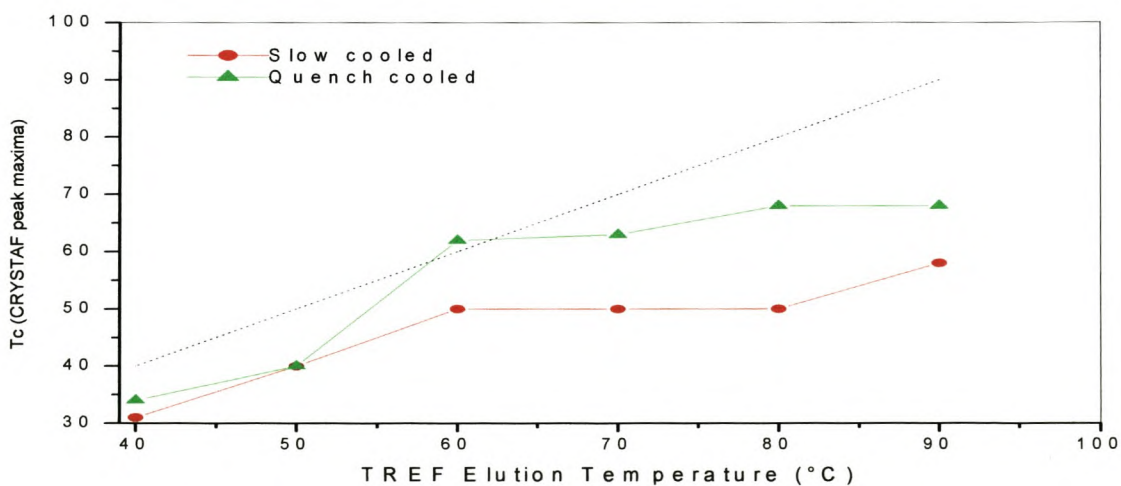

Figure 4.34 Comparison of the CRYSTAF peak maxima of the slow-cooled vs. quenched-cooled Prep-TREF fractions of LDPE.

Once again we could see that the Tc values for the quench-cooled and slow-cooled samples fell below the dotted line for Tc = TREF elution temperature, and once again this was attributed to the 'under cooling' effect discussed previously. Figure 4.34 also showed that the Tc values for the quench-cooled sample were greater than those recorded for the slow-cooled sample. This suggests that the quench cooling forced progressively more crystallizable fraction to elute at lower temperatures, in addition to broader fractions, as discussed earlier

Figure 4.35 shows the 3-D plot for the quench-cooled, weighted CRYSTAF traces. There was a broad distribution along the CRYSTAF temperature axis and a narrower distribution along the TREF elution temperature axis.
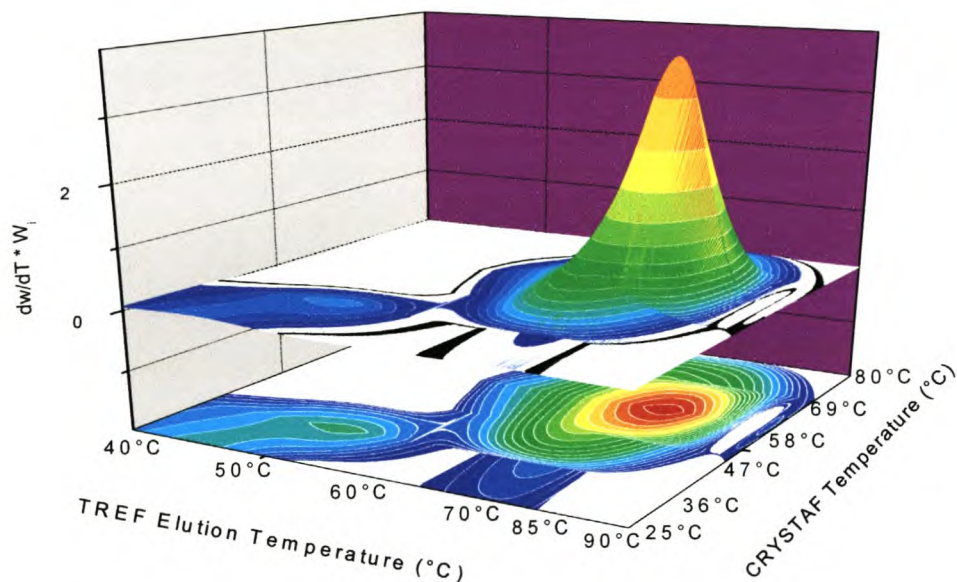
Figure 4.35 A 3-D plot for the quench-cooled CRYSTAF result for LDPE.

It was also interesting to note that the distribution peak observed at the higher temperature fractions in the slow cooled samples(Figure4.14) was not observed for the quench cooling, while the smaller distribution at lower temperature fractions was still evident.

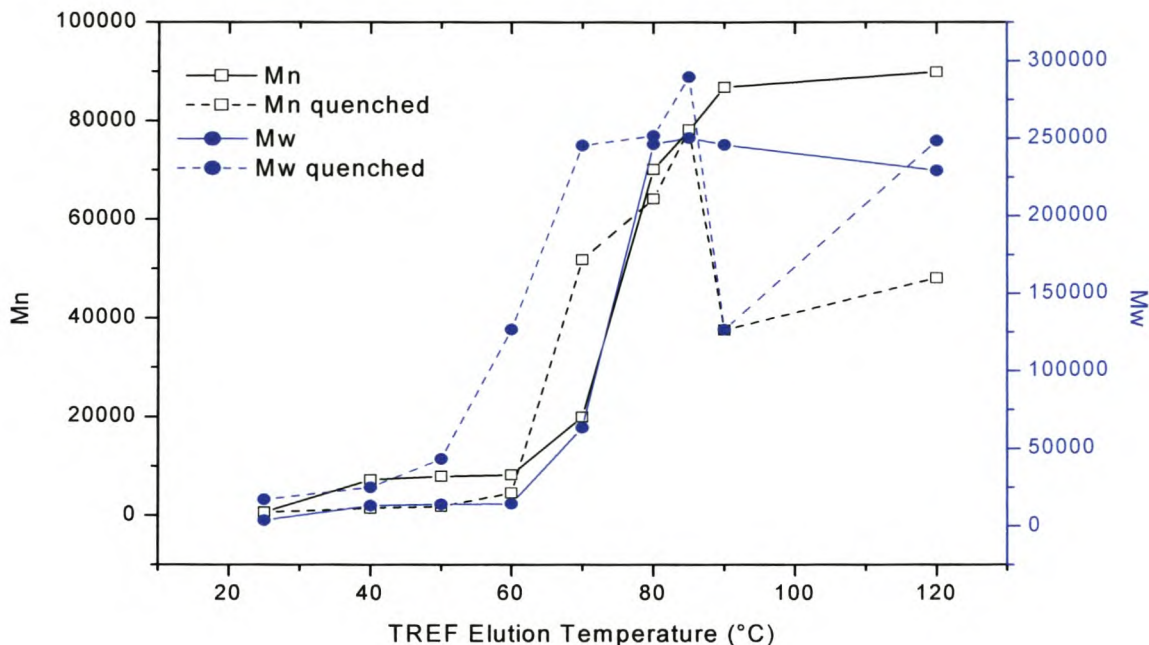In Figure 4.36 the Mn and Mw results of the slow-cooled and quench-cooled Prep-TREF fractions of LDPE are compared.

Figure 4.36 The number average (Mn) and weight average molecular weights (Mw) of the slow-cooled and quench-cooled Prep-TREF fractions of LDPE.

There was an increase in the Mn and Mw of the slow-cooled LDPE with an increase in elution temperature, except at very high temperatures - where there was a slight decline in the Mw. The Mn of the quench-cooled fractions showed a steady increase from 25°C to 80°C, but with a further increase in TREF elution temperature there was a decrease in Mn. The Mw followed the same trend as the Mn. Figure 4.36 further showed that the slow-cooled Mn and Mw data were more linear than the quench-cooled Mn and Mw data, which had a step-wise trend.

Figure 4.37 shows the HT-SEC curves for the quench-cooled Prep-TREF fractions of LDPE.
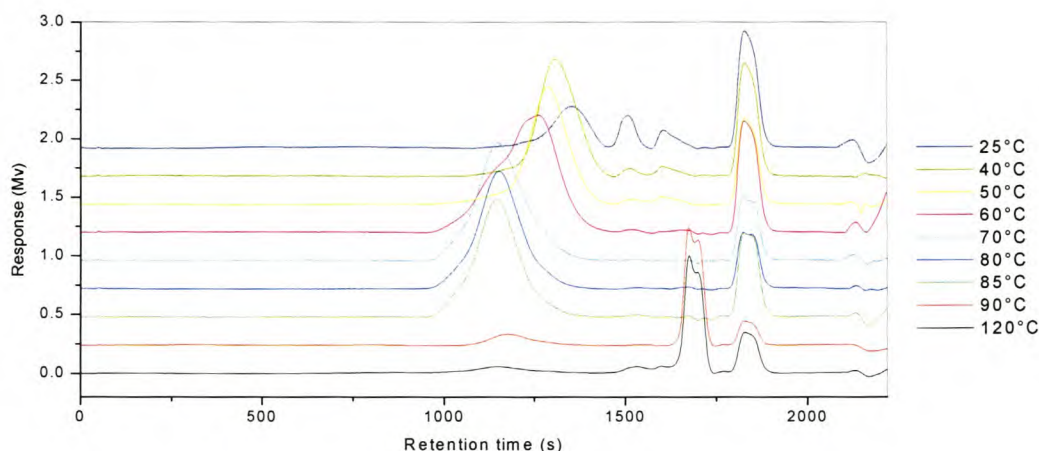

Figure 4.37 HT-SEC curves of the retention time vs. response for the quench-cooled Prep-TREF fractions of LDPE.

In Figure 4.16 it was seen that the 25°C Prep-TREF HT-SEC trace had bimodality, with peaks in the low molecular and high molecular weight ranges. As the temperature of the Prep-TREF fraction traces increased the following was seen: there was a decrease in the low molecular weight fractions in the HT-SEC and narrower, more intense high molecular weight fractions. In the very high Prep-TREF elution temperature traces, indications of low molecular weight polymer began to appear. Figure 4.37 showed that the 25°C Prep-TREF HT-SEC trace also had bimodality. The main differences between Figures 4.16 and 4.37 were the following: a) there was less shifting of the peak maxima in the quench-cooled traces relative to the slow-cooled traces, b) higher molecular weight peaks were absent in the 90 and 120°C fractions of Figure 4.37, and c) there was an increase in low molecular weight peaks for the 90 and 120°C Prep-TREF fractions of the quench-cooled traces relative to those of the slow- cooled LDPE traces. All data is summarized in Table 4.4.

Figure 4.38 shows the 3-D plot of the baseline corrected and normalized weighted results of the quench-cooled HT-SEC fractions of LDPE.

Table 4.4 shows the tabulated results of the HT-SEC data.

Table 4.4 HT-SEC data for the quench-cooled LDPE

Temperature (°C)	Mn	Mw	PD	Tc(CRYSTAF maximum)	Weight fraction Wi
25	620	17000	27.6	0	0.044
40	1400	25000	17.2	34	0.035
50	1800	43000	23.8	40	0.038
60	4600	130000	27.8	62	0.084
70	52000	250000	4.7	63	0.414
80	64000	250000	3.9	68	0.271
85	78000	290000	3.7	60	0.077
90	37000	130000	3.4	68	0.019
120	48000	250000	5.2	broad	0.015
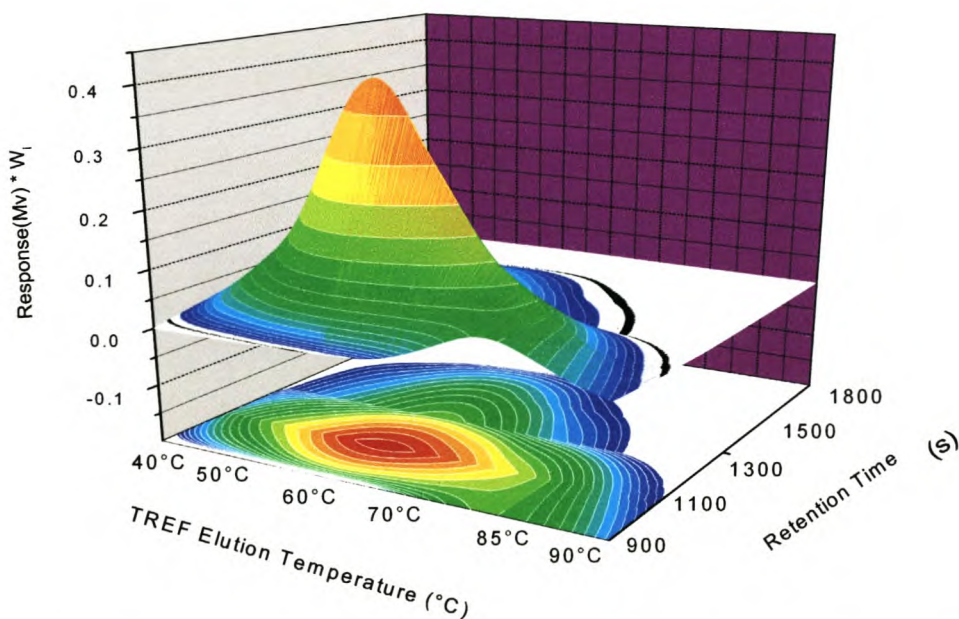
Figure 4.38 3-D plot of the weighted results of the quench-cooled HT-SEC fractions.

When the results in Table 4.4 were compared with the results in Table 4.3 it was seen that the PDs of the Prep-TREF fractions for the quench-cooled LDPE were higher than the PDs of the slow-cooled Prep-TREF fractions.

4.5)   Comparing the slow-cooled LDPE with and without support (sea sand)

It was further necessary to determine whether crystallization occurred better with a support, such as sea sand, which lends the polymer a homogeneous crystallization environment, or without a support.

When considering any crystallization process it is important to understand that it does not occur under conditions of thermodynamic equilibrium. In particular, it is well accepted that crystallization processes are controlled to a great degree by an initiation (nucleation), which may be due to the complexity of the process. [4] Thus the crystallization rate is considered to be not only dependent on the rate of crystal growth but also on the rate of nucleation. Since crystallization takes place through an initiation process (nucleation) it is likely that the environment in which crystallization takes place will influence the separation. One can therefore expect the column packing material to play a significant role in TREF. It is particularly difficult to dismiss the possibility of the influence of column packing particularly in the case of polypropylene (PP), whose crystallization behaviour in the melt is strongly affected by nucleation agents. This is because, for polypropylene, the nucleation step is heterogeneous, in contrast with the homogeneous nucleation observed for polyethylene and its copolymers. [4]

In order to investigate the influence of the support a solution crystallization set-up similar to that used for the crystallization step of the polymer with support was used. The only difference was that the support was now removed and the solution was stirred with an overhead stirrer to minimize nucleation via the glass reactor surface. All other parameters were kept constant, hence: the cooling rate was 1°C/h, a starting mass of 3 grams was used, and the same elution temperature fractions were obtained and recovered. Furthermore, since solution crystallization does not require a support, much larger quantities could be fractionated. The initial volume of xylene, relative to the quantity of polymer, could simply be increased to keep the polymer

solvent concentration constant. One then only needed to filter the polymer solution onto a bit of support (sea sand), which was placed on top of a piece of filtration paper. Thus the sand acted as a filter, the crystallized polymer was trapped on the sea sand and the soluble polymer solution was separated. The polymer, trapped on the support, was then transferred into the column. The latter was packed with cotton wool and beads at the bottom, to eliminate any flow-currents, and at the top, to fill the column. The effect of the polymer solution concentration is discussed in detail in the next section.

Table 4.5 and Figure 4.39 show the Prep-TREF results for the off-column crystallized LDPE (exp. 3 g solution and 1°C/h cooling rate). In Figure 4.38 the sum of the weight fraction percentage recovered is shown on the left Y-axis and the weight fraction percentage recovered divided by the temperature range (ΔT) as the right Y-axis of each fraction.
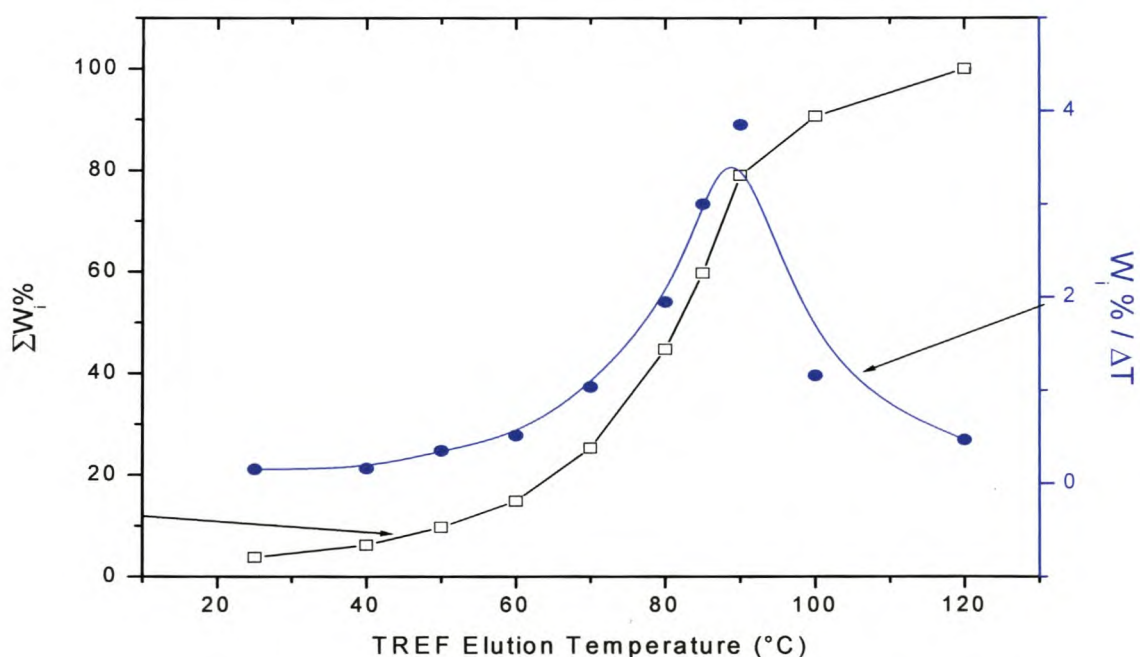
Figure 4.39 Prep-TREF weight fractions of the off-column solution crystallized LDPE (3 g solution, 1°C/h cooling rate).

Table 4.5 Prep-TREF results for the off-column solution crystallized LDPE (3 g solution, 1°C/h cooling rate)

Elution temperature (°C)	Mass (g)	Weight fraction[a] W_i	Weight fraction %[b]	Sum of the weight fractions % $\sum W_i\%$	ΔT[c] (°C)	$W_i\%/\Delta T$[d]
25	0.165	0.037	3.79	3.79	n/a	n/a
40	0.115	0.024	2.42	6.21	15	0.16
50	0.153	0.035	3.52	9.73	10	0.35
60	0.224	0.051	5.16	14.89	10	0.52
70	0.451	0.103	10.38	25.27	10	1.04
80	0.846	0.194	19.48	44.75	10	1.95
85	0.652	0.150	15.01	59.76	5	3.0
90	0.837	0.192	19.27	79.03	5	3.9
100	0.503	0.115	11.59	90.62	10	1.16
120	0.408	0.093	9.38	100	20	0.47
Total			100			

[a] mass of each fraction / total mass recovered

[b] mass / total (3g) x 100

[c] the elution temperature range between each fraction

[d] weight fraction percentage divided by the elution temperature range between each fraction.

Figure 4.40 shows the CRYSTAF traces of the Prep-TREF fractions of the solution crystallized, or off-column crystallized, LDPE.

Figure 4.41 shows the Tc (CRYSTAF peak maxima) vs. TREF elution time for the solution crystallized and support crystallized LDPE.
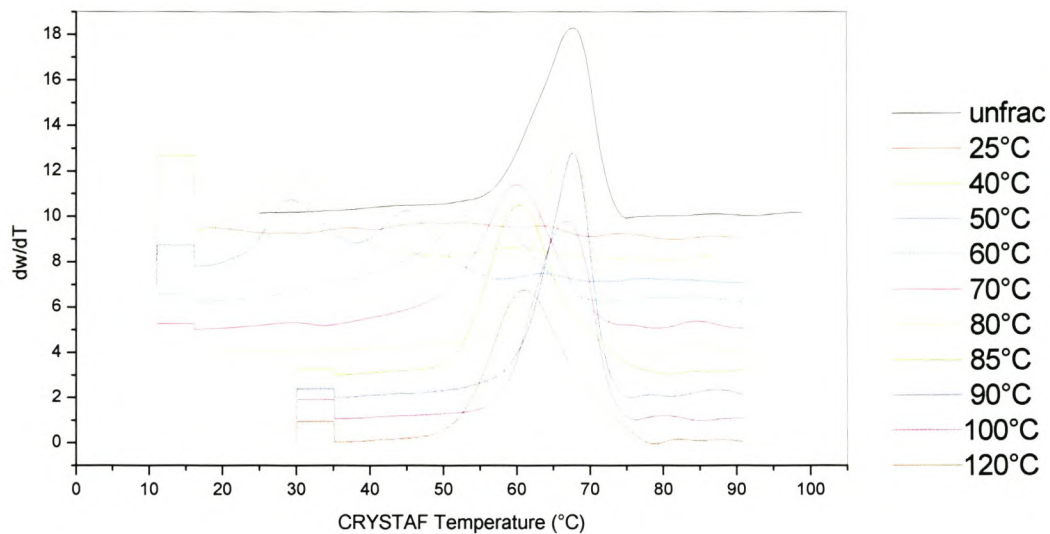
Figure 4.40 CRYSTAF traces of the off-column (solution crystallized) LDPE.
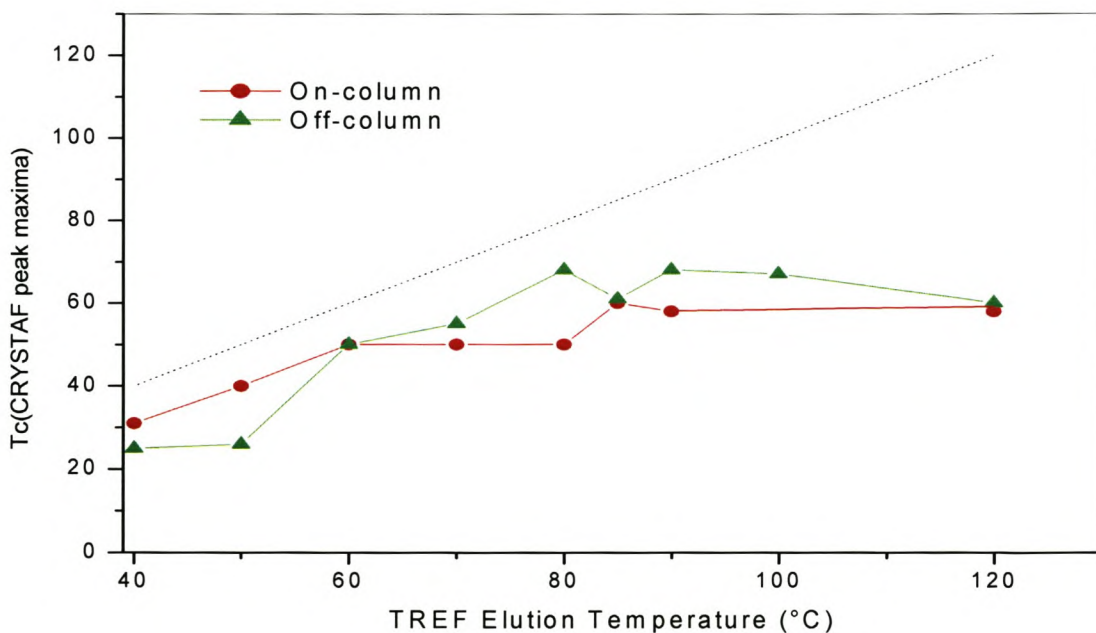
Figure 4.41 Tc (CRYSTAF peak maxima) **vs. TREF elution time for the solution crystallized and support crystallized LDPE.**

In Figure 4.40 the unfractionated LDPE CRYSTAF trace is presented first (top), followed by the 25°C trace that is soluble and shows no crystallization peak. Further:

- The 40°C trace showed a peak maximum at 25°C.
- The 50°C trace showed bi-modality with peak maxima at 25°C and 40°C. (This is probably due to experimental error.)
- The 60°C trace showed a peak maximum at 50°C.
- The 70°C trace showed a peak maximum at 55°C.
- The 80°C trace showed a peak maximum at 64°C.
- The 90°C trace had a peak maximum at 60°C.
- The 100°C trace had a peak maximum at 61°C.
- The 120°C trace had a peak maximum at 56°C.

Figure 4.41 shows the $Tc_{(CRYSTAF\ peak\ maxima)}$ vs. TREF elution time for the off-support (solution) crystallized LDPE and the support crystallized LDPE. There was not much difference between the Tc values of the slow-cooled LDPE (with support) and solution cooled LDPE (without support). The $Tc_{(CRYSTAF\ peak\ maxima)}$ values of the solution crystallized LDPE were, overall, closer to the dotted line for the higher temperature fractions.

In Figure 4.42 a comparison is made between the weight fraction curves for the slow-cooled (1°C/h) LDPE with and without support, also referred to as on- and off-column crystallization. In appeared that the latter (i.e. solution crystallized LDPE) had a narrower half peak width. The Tc(TREF) for the solution crystallized sample occured at a higher temperature compared to the support cooled sample.

Chapter 4: Results and Discussion
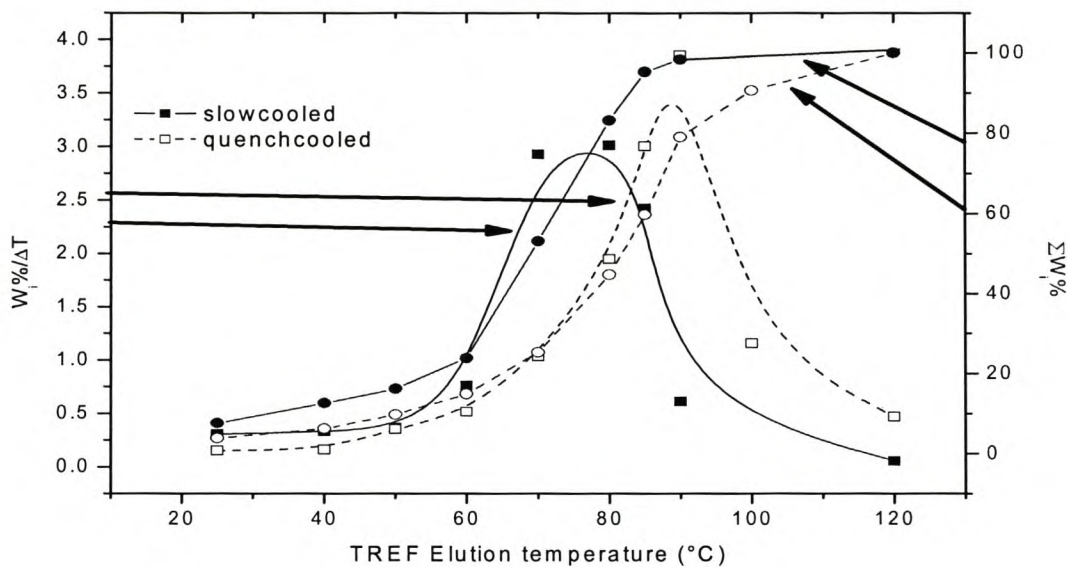
Figure 4.42 Comparison of the weight fraction figures of the slow-cooled LDPE with support (on-column crystallization) and without support (off-column crystallization).

In Figures 4.43-4.46 the individual Prep-TREF traces (of various temperatures) are compared, to compare the slow-cooled LDPE (on/with-support) with the solution crystallized LDPE (off/without-support).

The LDPE traces for the 40°C fractions (so called 40°C traces) are shown in Figure 4.42.

The LDPE traces for the 60°C fractions (so called 60°C traces) are shown in Figure 4.43.

The LDPE traces for the 70°C fractions (so called 70°C traces) are shown in Figure 4.44.

The LDPE traces for the 85°C fractions (so called 80°C traces) are shown in Figure 4.45.
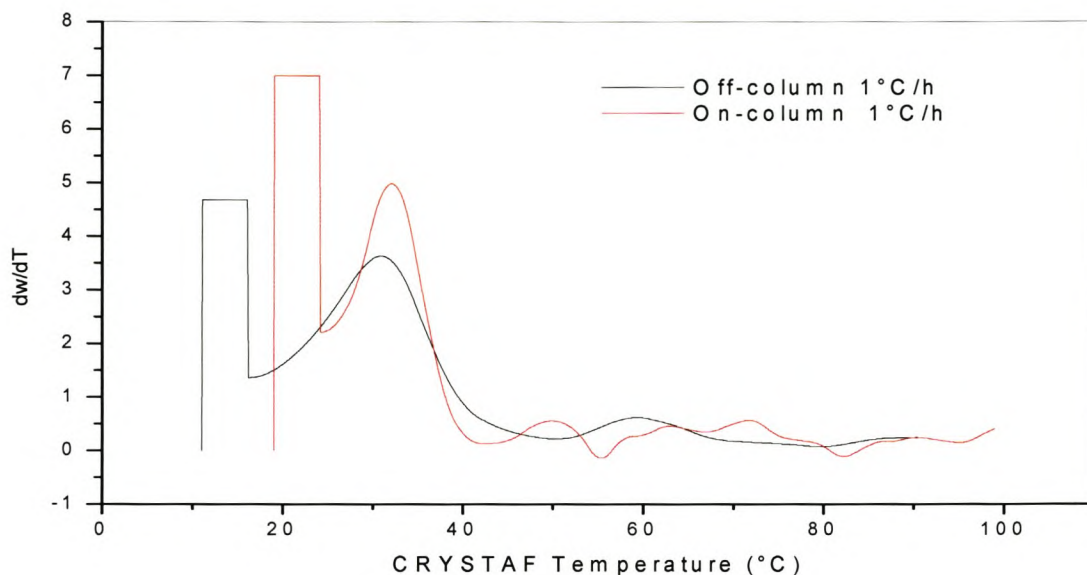
Figure 4.43 Comparison of the 40°C traces for the slow-cooled (1°C/h) LDPE (with support) compared to the LDPE without support.

In the 40°C traces it was seen that better fractionation was achieved for the LDPE that was cooled on-support, since the half peak width was narrower. (Note: Here slow-cooled LDPE refers to a 1°C/h crystallization rate (step) using a support (sea sand) in the crystallization step.) Solution crystallization or off-support LDPE in this case has a 1°C/h crystallization rate (step) but, without support. Both the solution and slow-cooled crystallization made use of a support during the elution step.
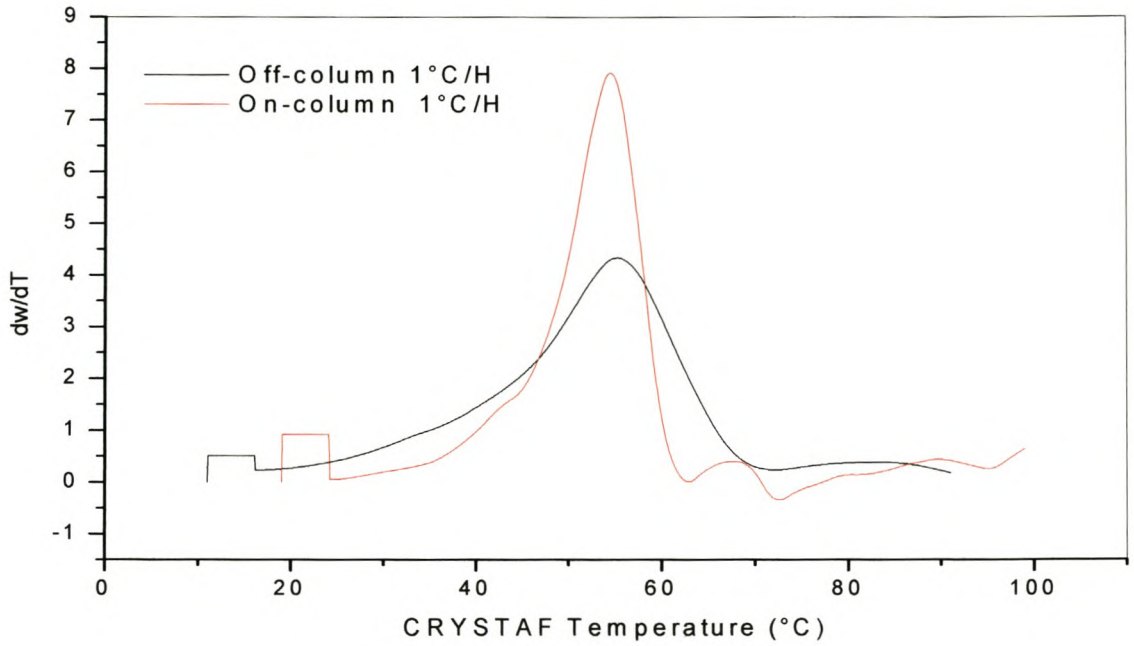
Figure 4.44 Comparison of the 60°C traces for the slow-cooled (1°C/h) LDPE (with support) compared to the LDPE without support.
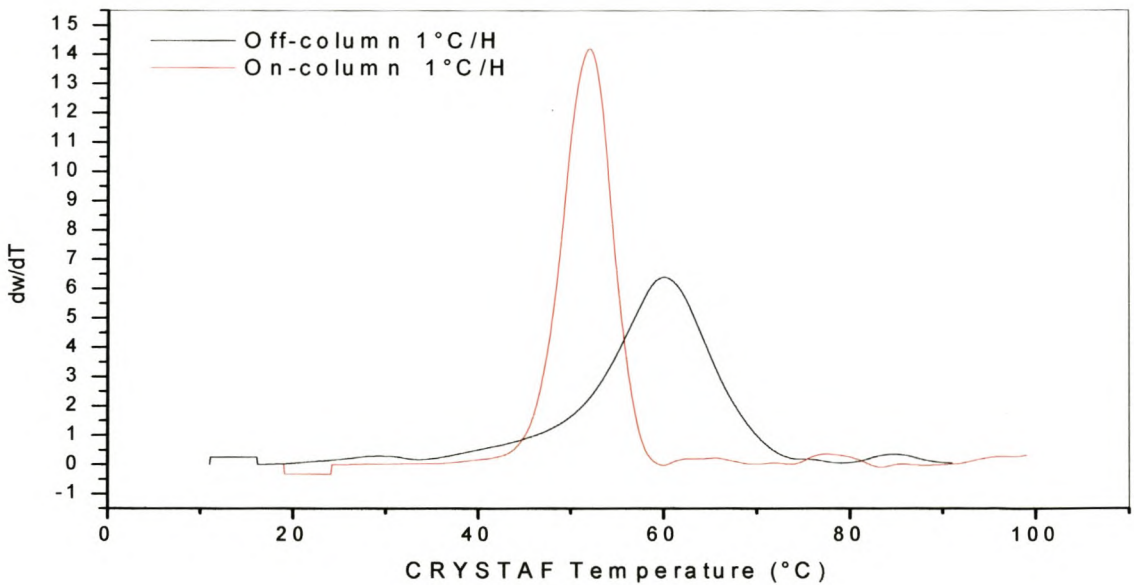
Figure 4.45 Comparison of the 70°C traces for the slow-cooled (1°C/h) LDPE (with support) compared to the LDPE without support.
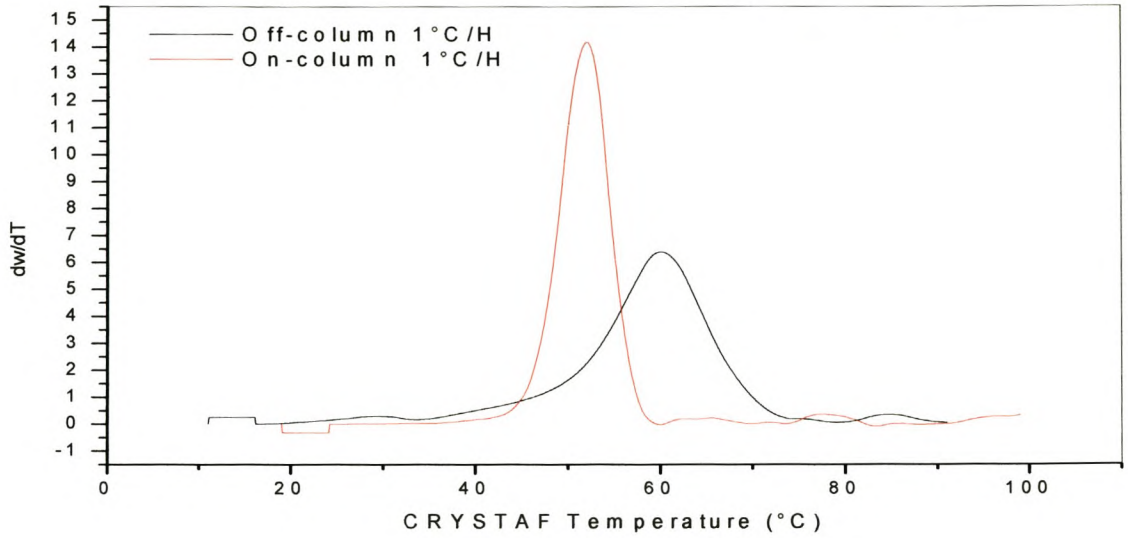
Figure 4.46 Comparison of the 85°C traces for the slow-cooled (1°C/h) LDPE (with support) compared to the LDPE without support.

Figure 4.47 shows a FWHM comparison for the on- and off-support crystallized LDPE.
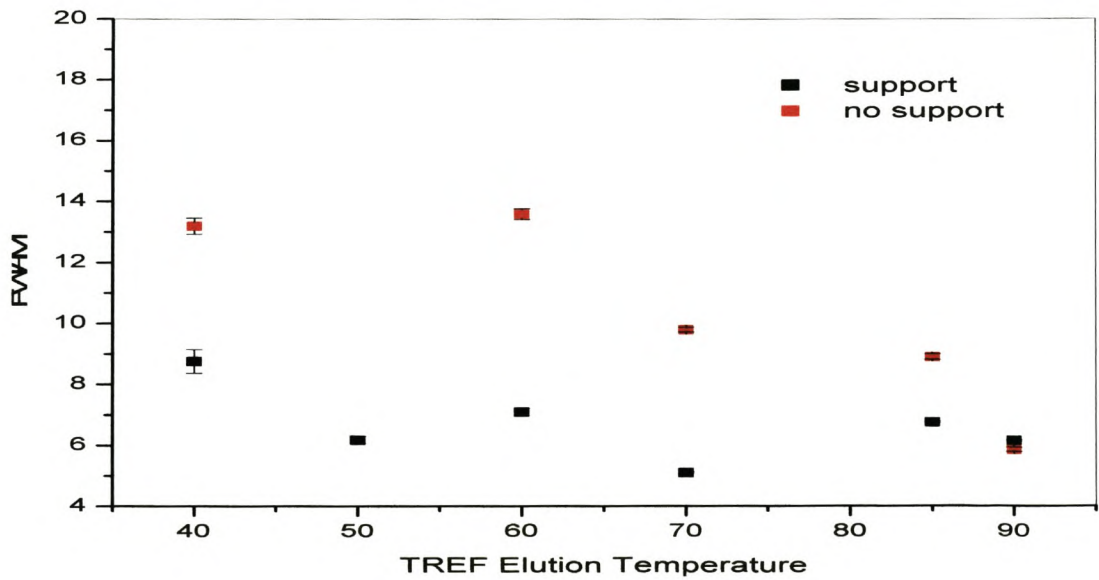
Figure 4.47 FWHM comparison of the on- and off-support slow-cooled LDPE.

The LDPE crystallized with support had a narrower CRYSTAF FWHM for the individual TREF fractions than the LDPE crystallized without support had. These results suggested that in the case of the LDPE sample, narrower molecular fractions are recovered when the crystallization step occurs on a support.

The next results to be presented are the High Temperature Size Exclusion Chromatography (HT-SEC) data for the slow-cooled LDPE without support. Figure 4.48 shows the data of all the different temperature traces in the form of a waterfall plot.
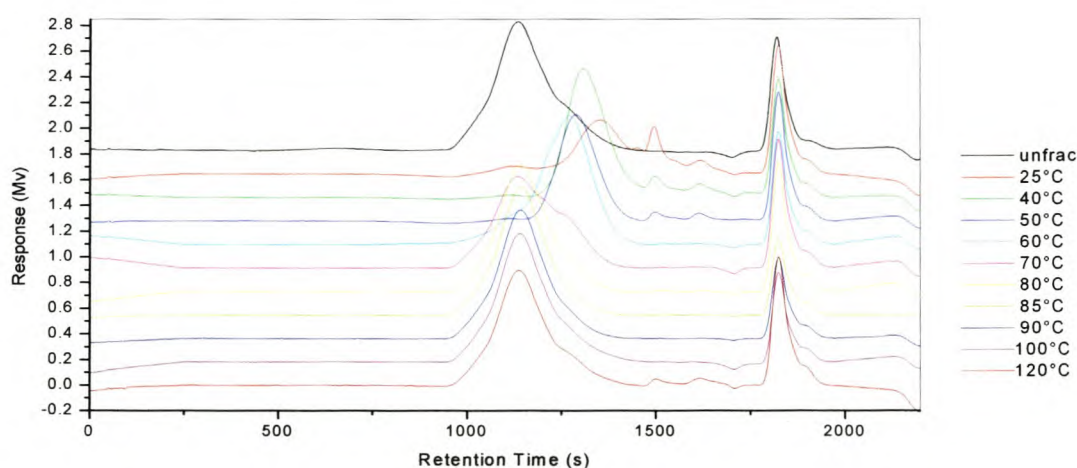
Figure 4.48 Retention time vs. response for the LDPE slow-cooled (1°C/h) without support.

At a retention time of 1500 seconds/25 minutes there were some low molecular weight residues in the 25°C, 40°C and 50°C Prep-TREF elution traces. There was also a progressive increase in the peak maxima with an increase in the Prep-TREF elution traces, up to the 70°C trace. The 70-120°C traces all had the same peak maxima as the unfractionated LDPE trace.

Table 4.6 shows the HT-SEC data for the off-support crystallized LDPE.

Table 4.6 HT-SEC data and CRYSTAF peak maxima for the off-support crystallized LDPE

Temperature (°C)	Mn	Mw	PD	Tc(CRYSTAF maximum)	W_i
25	1600	9900	6.4	n/a	0.04
40	7800	13000	1.6	25	0.02
50	8700	14000	1.6	26	0.04
60	9500	15000	1.6	50	0.05
70	11000	20000	1.8	55	0.10
80	14000	38000	2.6	68	0.19
85	19000	47000	2.5	61	0.15
90	26000	89000	3.4	68	0.19
100	41000	200000	4.8	67	0.12
120	53000	290000	5.4	60	0.09

There was an increase in the number average molecular weight (Mn) with an increase in TREF elution temperature for all the fractions. This was the first time in this study that this was observed. The weight average molecular weight (Mn) also increased with an increase in TREF elution temperature for all the fractions.

The following conclusions could be made. Using the Tc(CRYSTAF peak maximum) comparisons, use of the off-support crystallization for the LDPE (LDPE being a homogeneously crystallizable semi-crystalline polymer) resulted in the fractionation that was achieved being as good, as using on-support crystallization. In both case there was a increase in the Tc(CRYSTAF) with an increasing TREF elution temperature. However, looking at the FWHM of the CRYSTAF traces of the Prep-TREF fractions of LDPE in Figure 4.47, the on-support crystallization seemed to be the better technique, leading to more homogeneous fractionation. The HT-SEC results for both the on-and off-support crystallization appeared to be quite similar.

4.6) The effect of the solution concentration and cooling speed of the off-support crystallized LDPE

In continued efforts to optimize the solution Prep-TREF under development I compared the on- and off-support crystallized LDPE using different masses (3 g and 6 g) and cooling rates

(1°C/h and 6°C/h). Increasing the mass of the polymer fractionated has the advantage that a larger mass of polymer is recovered in each fraction which makes further analysis of these fractions much easier. These are preliminary results.

Figure 4.49 shows the TREF results. The on-support crystallized LDPE had a broad distribution, indicating good fractionation. The '3g_6°C/h off-support' showed similar results, with only the peak maximum increasing to a higher temperature. This increase in peak maximum with an increase in crystallization cooling rate could be caused by the homogeneous nucleation of LDPE. Hence, since LDPE crystallizes homogeneously both on- and off-support, it would be better to compare the solution technique using polypropylene that has heterogeneous nucleation, using the off-support way in the Prep-TREF. The narrowing of the peak width observed with an increase in the quantity of polymer from 3 g to 6 g, yet at the same cooling rate as used for the '3g off-support', shows that with the 6 g quantity more co-crystallization and entrapment, and possible entanglement effects, were occurring, thus decreasing the efficiency of fractionation. Concentration ratio's where kept constant as to prevent concentration effects(3g/300mL or 6g/600mL).
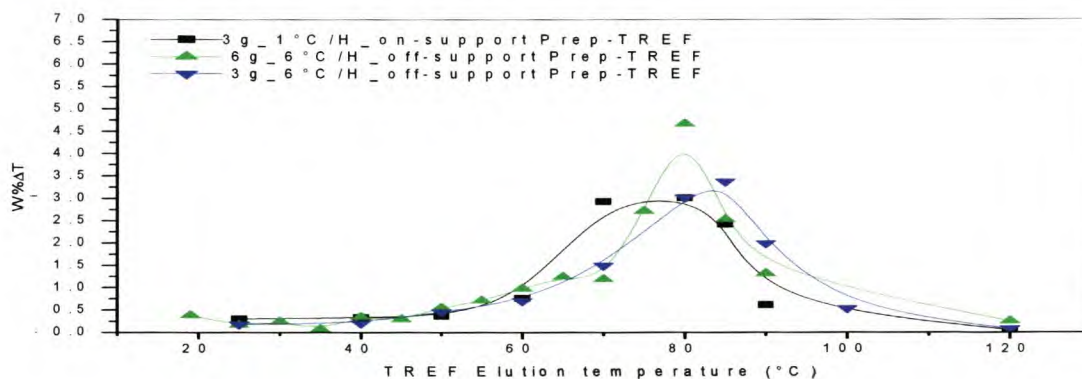
Figure 4.49 Comparison of Prep-TREF curves for on- and off-support crystallized LDPE.

This suggests that although we used solution crystallization, a quantity of 6 g was probably too much for the dimensions of our elution column to handle. Using 3 g, without a support, and cooling at 6°C/h, seemed just as effective as the 1°C/h on-support if the increase in peak maxima difference between the two options is ignored. To confirm the Prep-TREF results we further compared the individual CRYSTAF results for the '3 g_6°C/h off-support' and '3 g_1°C/h on-support'.

Table 4.7 shows the Prep-TREF results for the '6 g_6°C/h off-support' crystallized LDPE, fractionated at intervals of every 5°C and Table 4.8 shows results for the '3 g_6°C/h off-support' crystallized LDPE, fractionated at intervals as tabulated. It should be noted here that in order to compare the 6 g Prep-TREF traces with the 3 g Prep-TREF traces were combined and added the appropriate weight fractions then divided by 2, so creating the same intensities.

Table 4.7 The '6g_6°C/h' off-support Prep-TREF raw data for LDPE

Elution temperature (°C)	Mass (g)	Weight fraction W_i	Weight fraction %[a] Wi%	Sum of the weight fractions %[b] $\sum Wi\%$	ΔT[c] (°C)	Wi%/ΔT[d]
19	0.432	0.072	7.18	7.18	n/a	n/a
25	0.059	0.01	0.98	8.16	6	0.2
30	0.072	0.012	1.2	9.35	5	0.2
35	0.022	0.004	0.36	9.71	5	0.1
40	0.104	0.017	1.73	11.44	5	0.3
45	0.089	0.015	1.47	12.91	5	0.3
50	0.165	0.027	2.75	15.66	5	0.5
55	0.215	0.036	3.57	19.23	5	0.7
60	0.295	0.049	4.9	24.12	5	1
65	0.373	0.062	6.2	30.32	5	1.2
70	0.359	0.06	5.95	36.28	5	1.2
75	0.819	0.136	13.59	49.87	5	2.7
80	1.406	0.233	23.34	73.21	5	4.7
85	0.761	0.126	12.63	85.84	5	2.5
90	0.396	0.066	6.58	92.42	5	1.3
120	0.456	0.076	7.58	100	30	0.25

[a] mass of each fraction / total mass recovered

[b] mass / total (6g) x 100

[c] the elution temperature range between each fraction

[d] weight fraction percentage divided by the elution temperature range between each fraction.

Table 4.8 showed that by using 6 g we could obtain more mass for each fraction. However, as seen later in Figure 4.50, we began to experience some problems.

Table 4.8 The '3g_6°C/h' off-support PREP-TREF raw data for LDPE

Elution temperature (°C)	Mass (g)	Weight fraction W_i	Weight fraction %[a] Wi%	Sum of the weight fractions %[b] $\sum Wi\%$	ΔT[c] (°C)	Wi%/ΔT [d]
25	0.140	0.05	4.56	4.56	n/a	n/a
40	0.097	0.03	3.14	7.70	15	0.21
50	0.141	0.05	4.58	12.28	10	0.46
60	0.218	0.07	7.07	19.35	10	0.71
70	0.461	0.15	14.99	34.34	10	1.50
80	0.929	0.31	30.19	64.52	10	3.02
85	0.520	0.17	16.89	81.41	5	3.4
90	0.307	0.10	9.98	91.39	5	2.0
100	0.165	0.06	5.37	96.76	10	0.54
120	0.051	0.02	1.67	98.43	20	0.08

[a] mass of each fraction / total mass recovered

[b] mass / total (3g) x 100

[c] the elution temperature range between each fraction

[d] weight fraction percentage divided by the elution temperature range between each fraction.

Figure 4.50 shows the Prep-TREF weight fractions curves for the '3g_6°C/h off-support' and '3g_1°C/h on-support' Prep-TREF fractions.
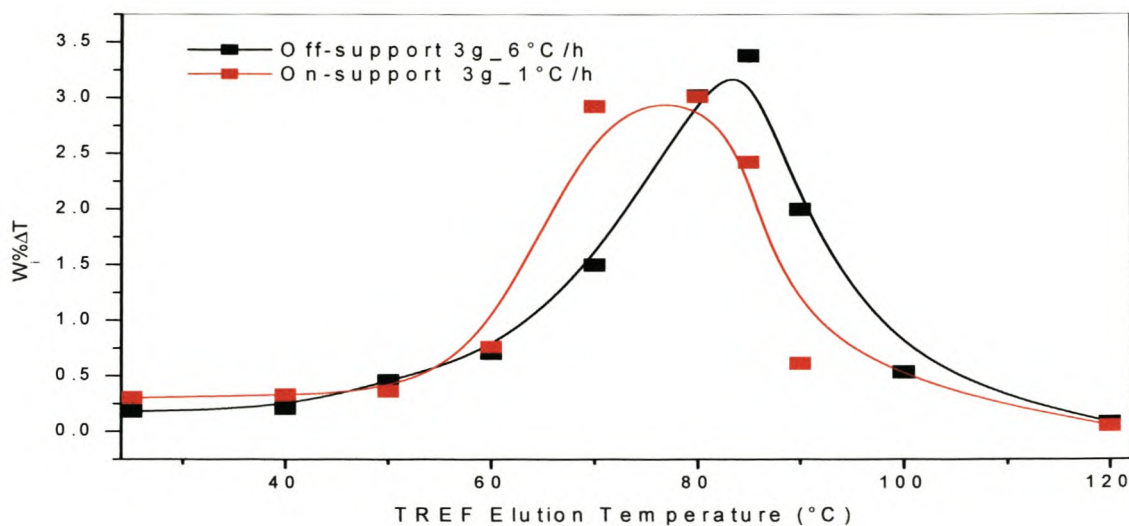
Figure 4.50 Prep-TREF traces for the '3g_6°C/h off-support' and '3g_1°C/h on-support' Prep-TREF fractions.

Figures 4.51-4.53 compare the CRYSTAF traces for the '3g_6°C/h off-support' and '3g_1°C/h on-support' Prep-TREF traces.
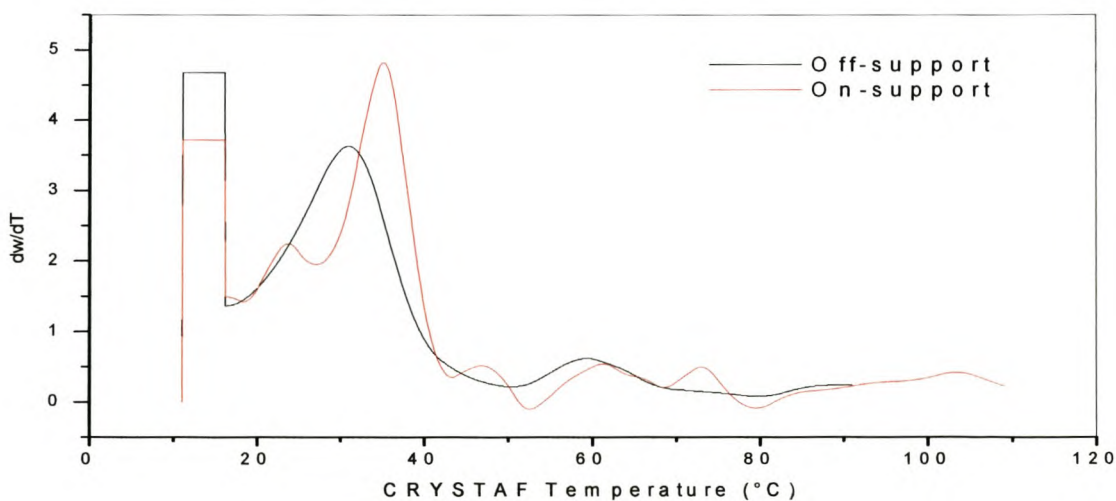
Figure 4.51 The 40°C CRYSTAF traces for the '3g_6°C/h off-support' and '3g_1°C/h on-support' Prep-TREF traces.
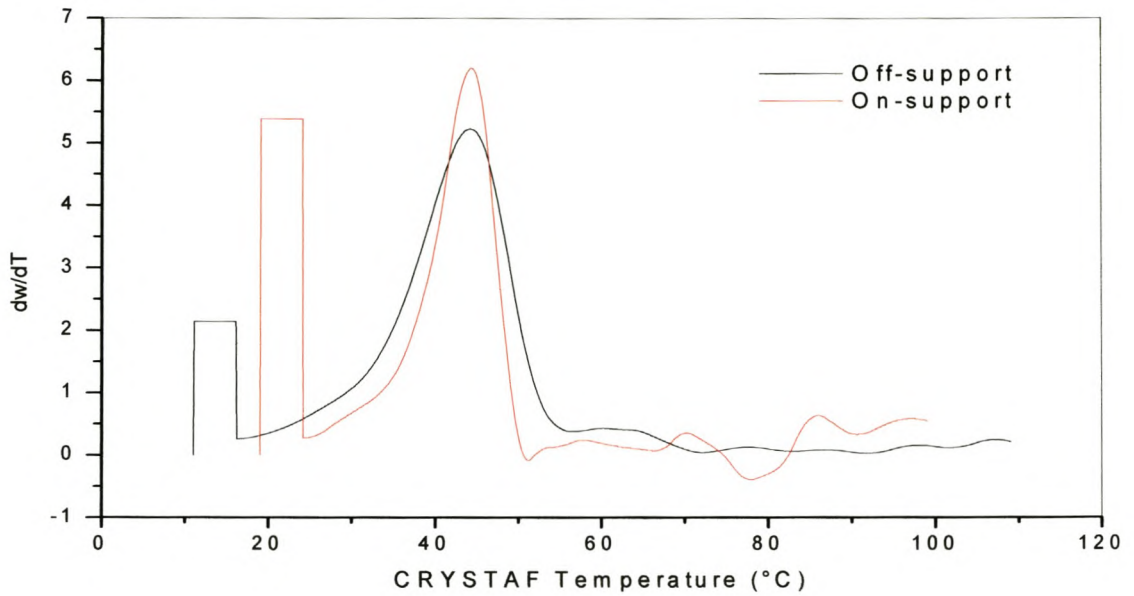
Figures 4.52 The 50°C CRYSTAF traces for the '3g_6°C/h off-support' and '3g_1°C/h on support' Prep-TREF traces.
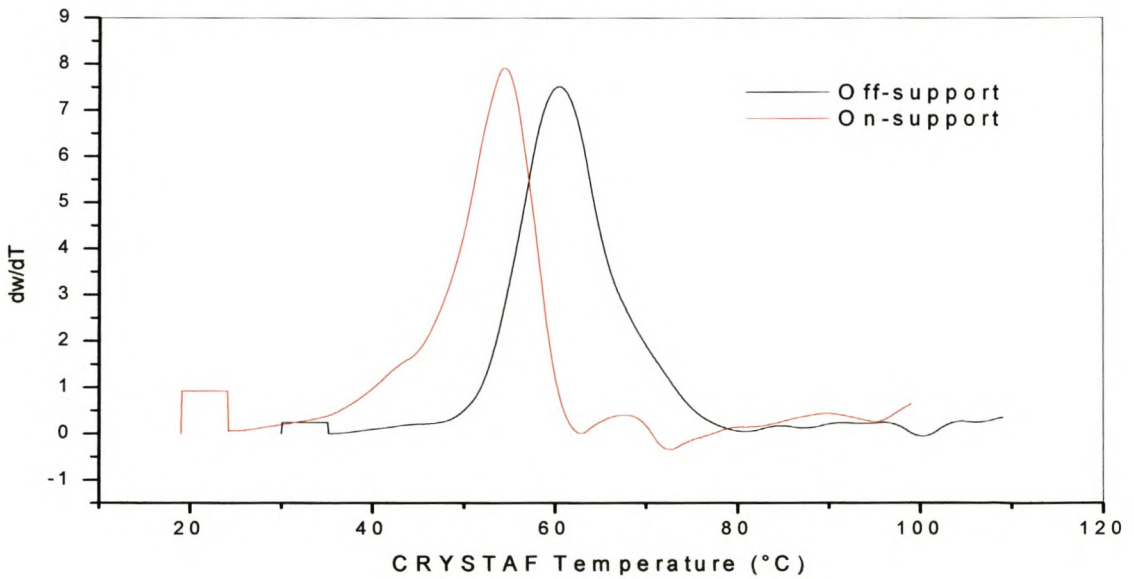
Figures 4.53 The 60°C CRYSTAF traces for the '3g_6°C/h off-support' and '3g_1°C/h on support' Prep-TREF traces.

In Figure 4.51 the off-support crystallization peak maximum moved to an even higher TREF elution temperature relative to the on-support crystallization. In their patent, Wild et. al. [3] report that off-support crystallization leads to less tailing - but this does not give an answer for the increase in the peak maximum. This figure also showed that the on-support appeared to have a narrower crystallization peak.

In Figure 4.52 the CRYSTAF peak maxima appeared at the same temperature, and the on- support had the narrower of the two crystallization peaks.

In Figure 4.53, showing the 60°C Prep-TREF CRYSTAF traces, there was a further increase in the crystallization peak maxima of the off-support trace relative to the on-support peak. This meant that we were getting closer to the ideal situation, namely $Tc_{(CRYSTAF\ peak\ maximum)}$ = $Tc_{(TREF\ peak\ maximum.)}$

Figure 4.54 shows the Prep-TREF fractionated CRYSTAF curves for a '6g_6°C/h' LDPE sample. It showed the effects of possible overloading of the column, even though fractions were taken every 5°C.
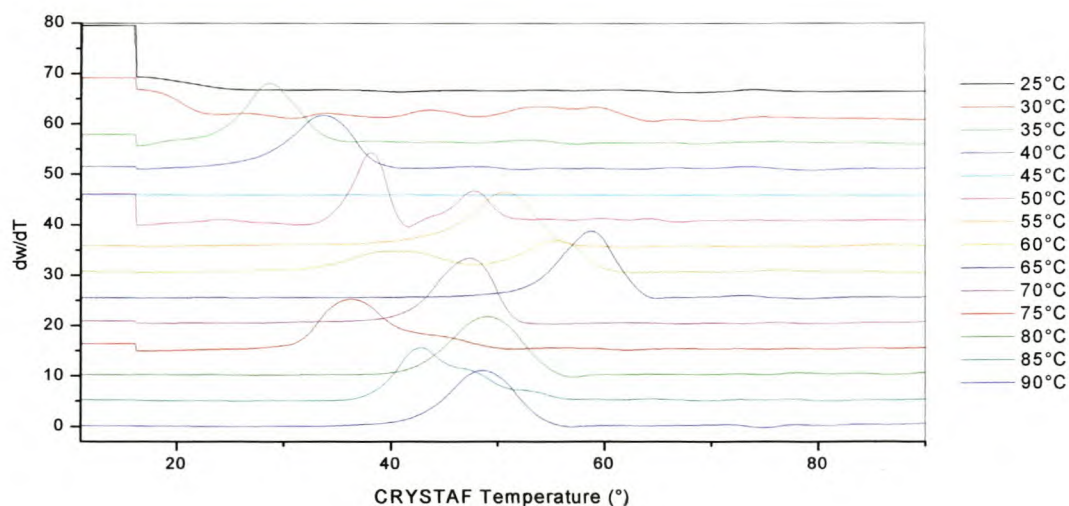
Figure 4.54 Prep-TREF fractionated CRYSTAF curves for a '6g_6°C/h' LDPE sample.

Fractionating larger amounts of polymer seemed to decrease the quality of fractionation due to possible entanglement effects, resulting in significant unexplained decreases in the CRYSTAF

peak maxima of the 70°C and 75°C Prep-TREF plots. In most cases each of the fractions had a relatively broad CRYSTAF peak. It is therefore concluded at this point that a quantity of 6 g could possibly be overloading the column since the solution concentration is to high. Further studies should however be carried out before any conclusive results can be made regarding the maximum quantity of polymer suitable for use on this newly developed TREF.

4.7) Analysis of the plastomers

4.7.1) Introduction

This section describes the systematic characterization of Plastomer A and Plastomer B. First the two materials were analyzed by ^{13}C NMR analysis, then Prep-TREF and CRYSTAF results are given for Plastomer A, both unfractionated and fractionated. The results for the plastomer fractions will be shown in various ways: waterfall plots, 2-D waterfall plots set in 3-D, and finally novel 3-D plot of the fractionated, weighted CRYSTAF traces vs. the TREF elution temperature. Similar CRYSTAF and preparative TREF results will be shown for Plastomer B. HT-SEC data will also be given for the unfractionated and fractionated traces for Plastomer A and Plastomer B, shown in normal, waterfall and 2-D waterfall plots, and finally as 3-D plots. DSC results of the fractions of the plastomers are also given. Section 4.7 will be concluded with an analysis of comonomer content of the fractions of Plastomer A.

4.7.2) NMR analysis of the plastomers

The plastomers used in this study were polyethylene-1-octene random co-polymers. The comonomer composition of the plastomers (octene content) was determined by determining the ratios of the characteristic peaks of the different monomers in the ^{13}C NMR spectrum of the copolymeric plastomer. This entailed comparing the peak area of the signals for the carbon atoms at which the branching took place (branching CH) with that of the carbon atoms in the backbone (backbone C). Peak assignments were done by making use of data in the literature where possible, and checked against chemical shift assignments predicted by the 'additive' rules described by Grant and Paul. [4]Results are shown in Table 4.9.

Chemical shift predictions of a specific carbon atom, according to the additive rules of Grant & Paul, are made by determining the combined effects of the neighbouring (α up to ε) carbons. Thus, the relative amount of carbon in the α, β, γ, δ and ε positions relative to the carbon for which the chemical shift is being determined is counted, and each fraction multiplied by its respective correction factor and added together. Apart from the standard influences of the neighbouring carbons, different types of carbons also affect each other differently. In this regard, for example, a tertiary carbon having a secondary neighbour, 3(2), a secondary carbon having a tertiary neighbour, 2(3), and a primary carbon atom having a tertiary neighbour, 1(3), have specific influences on the chemical shifts. To complete the calculation for a certain carbon, its direct neighbour (in the α position) is determined and each multiplied by their respective correction factors. This value is added to the value obtained from the first calculation and the constant of -1.87 ppm added to give the predicted chemical shift in ppm. For all ethylene/α-olefins copolymers, the comonomer content in mole percent [C] was calculated according to the following formula[4]: [C] = 50 Branched Carbons / (Total Backbone Carbons). For α-olefins larger than 1-heptene, the β-CH_2 in the chain also appears at the same chemical shift as the backbone β-carbons. In these cases, the intensity of the branching CH was subtracted from those of the α and β carbon intensities. Figures 4.55 and 4.56 show the ^{13}C NMR spectra for the two plastomers used in this study.

Table 4.9 The predicted NMR shifts for Plastomer A and B (ethylene/1-octene) as predicted with the Grant and Paul rules

Ethylene/1-Octene	1	2	3	4	5	6	Br	α	β	γ	δ	ε
Grant and Paul	14.1	22.7	32.5	30	27.5	34.9	38	34.9	27.6	30.4	30.1	30
Observed	13.9	22.8	32.1	30	27.2	34.5	38.2	34.5	27.2	40.4	30.1	3 0

Plastomer A has a 4,89% octene content, thus giving the most crystallinity of the two plastomers. Plastomer B has a 9,26% co-monomer content, with almost no crystallinity.
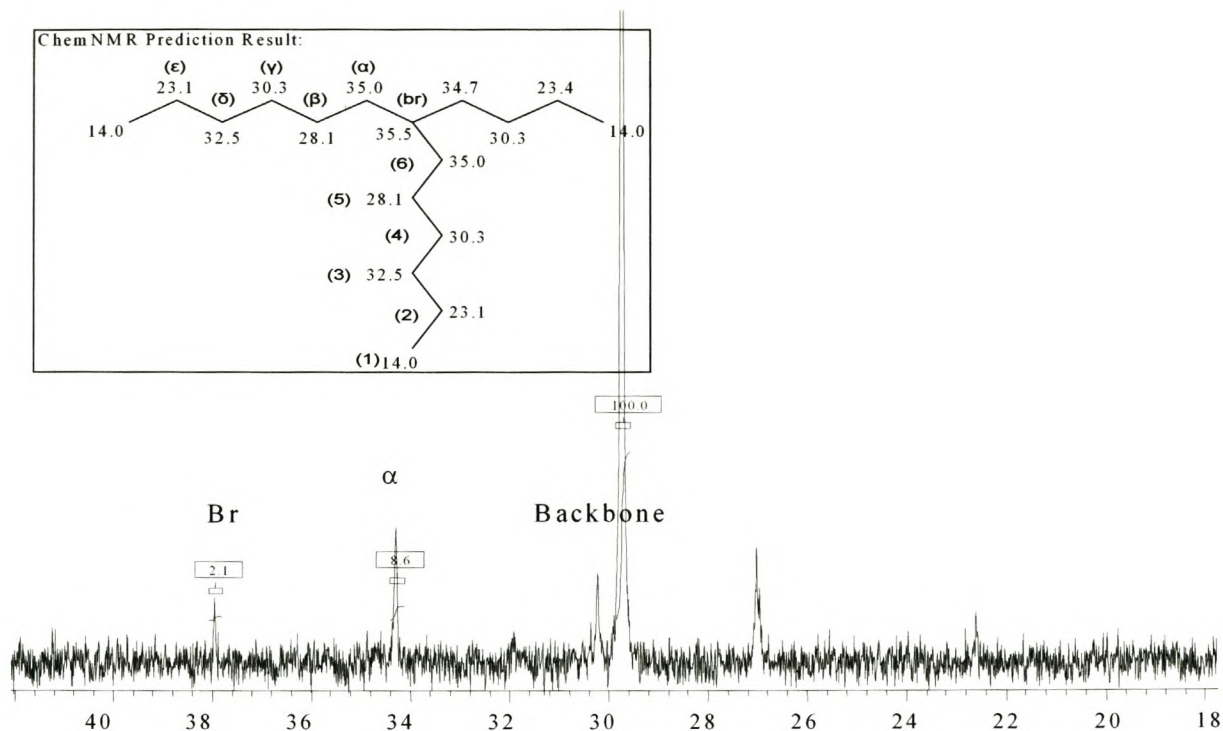
Figure 4.55 The ^{13}C NMR spectrum of Plastomer A.
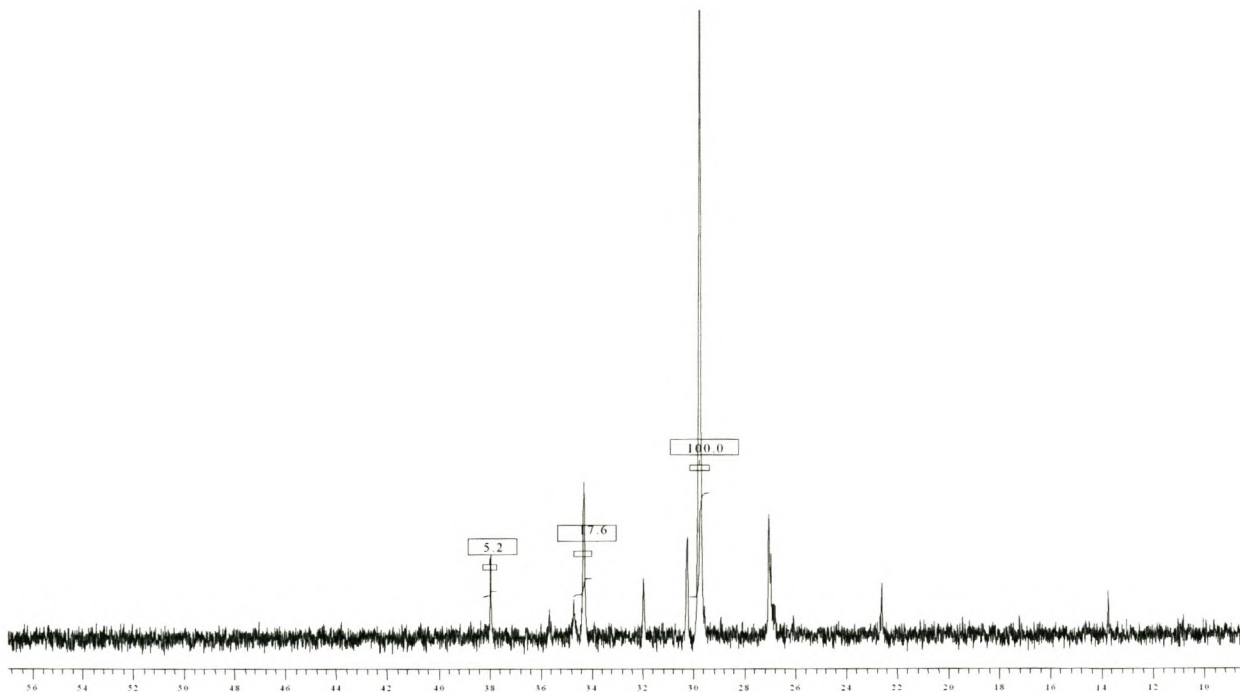
Figure 4.56 The ^{13}C NMR spectrum of Plastomer B.

90

4.7.3) CRYSTAF and Prep-TREF Results

The CRYSTAF runs were carried out in two modes:

1) the normal CRYSTAF run between 110^oC and 35^oC, and

2) the sub-ambient mode, in which the CRYSTAF was run at temperatures as low as 10^oC (achieved with the use of liquid nitrogen).

The limiting factor was the freezing point of the solvent TCB (18^oC). As TCB freezes at 18^oC, any results lower than 18°C should be treated with caution as they could possibly be due to freezing of the solvent.

4.7.3.1) Plastomer A

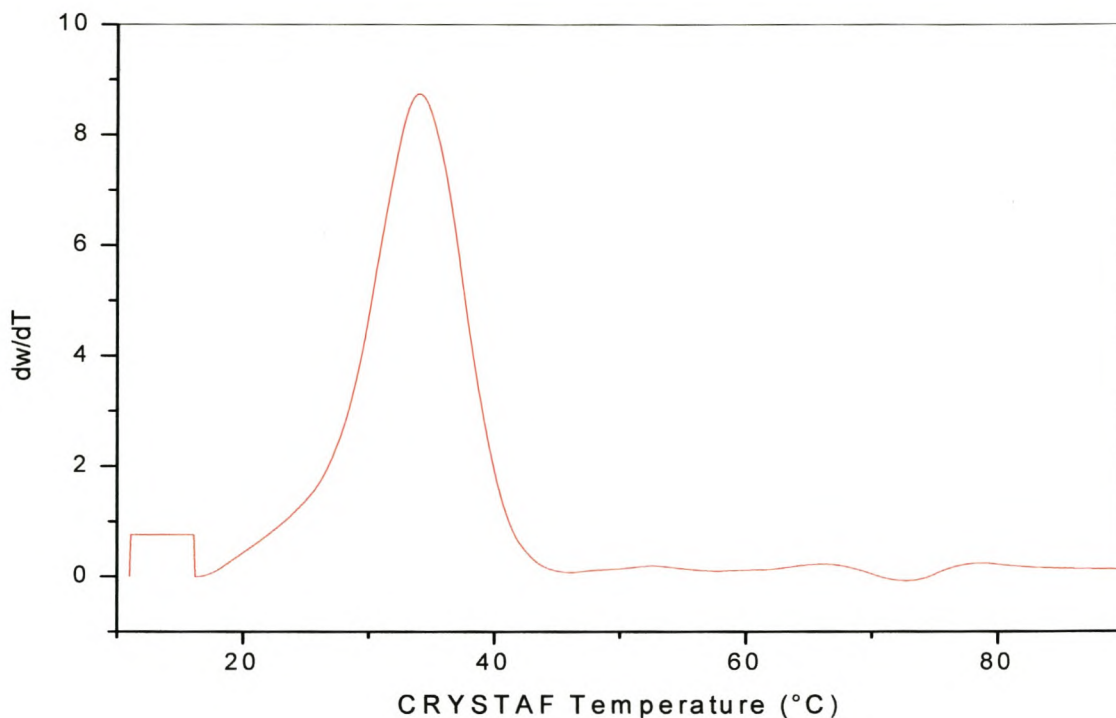Figure 4.57 shows the CRYSTAF trace for Plastomer A.
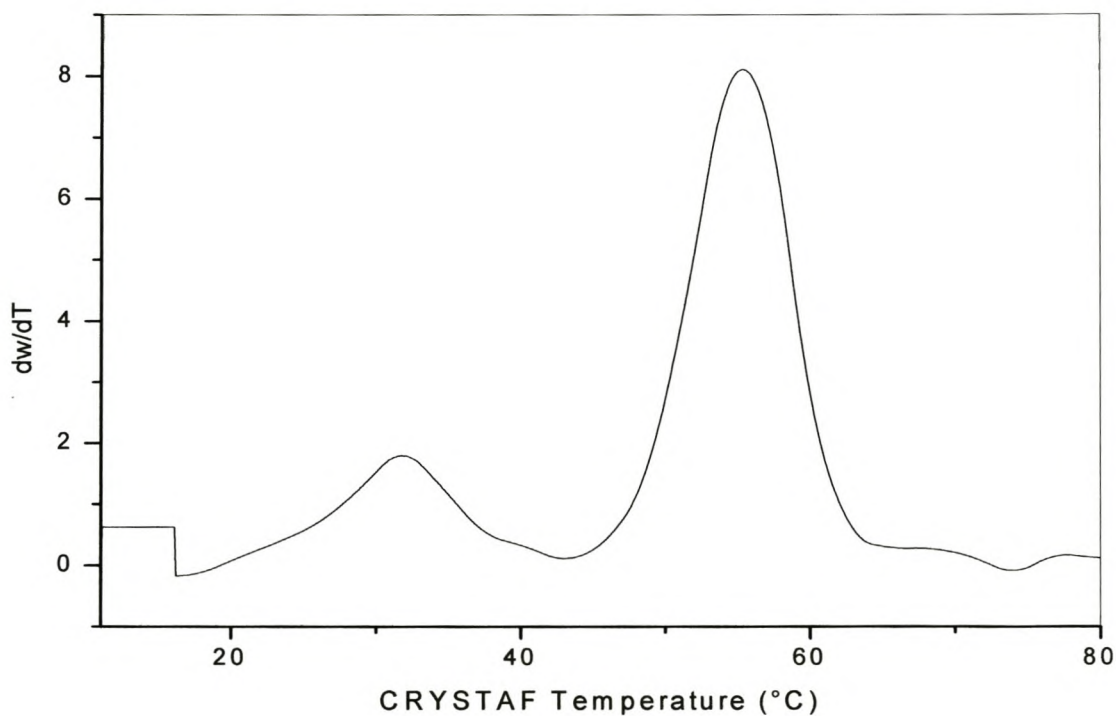
Figure 4.57 The CRYSTAF result for 100% Plastomer A

The trace represents the first derivative of the concentration curve and had a maximum at 58°C. The plastomer trace indicated a bimodal distribution, showing one crystallization peak between 20°C and 40°C and the other between 40°C and 62°C.

Figure 4.58 shows the weight fraction of the preparative TREF fractions and the sum of weight fractions vs. the TREF elution temperature. The sum of the weight fractions allowed for a comparison to be made between individual Prep-TREF weight fraction figures, since different elution temperatures were used for different materials.
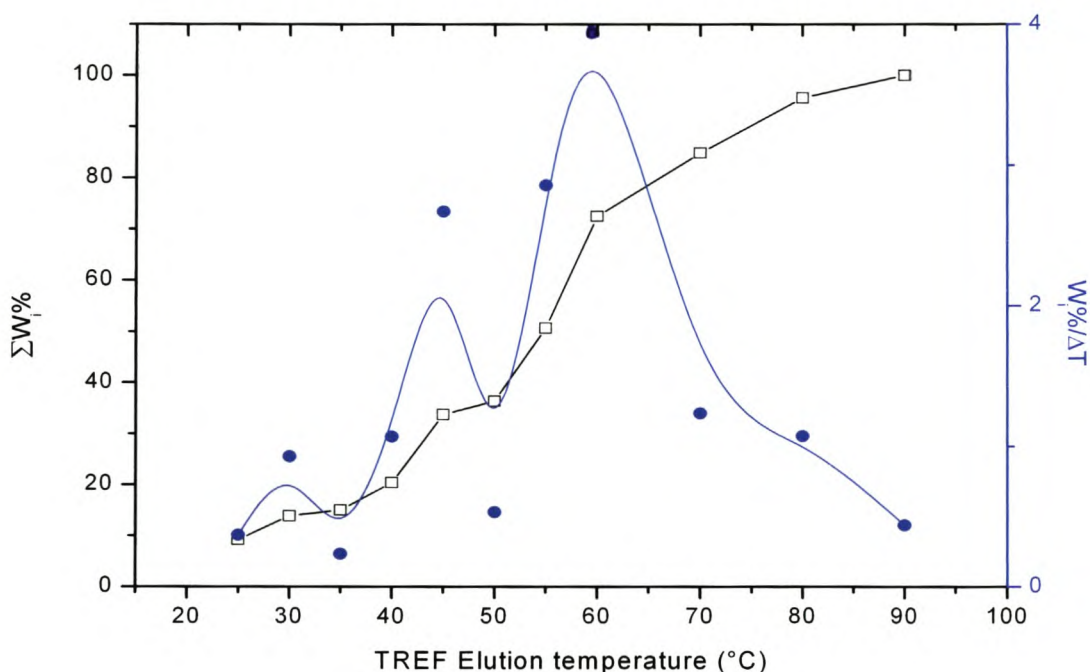
Figure 4.58 The weight fraction percentage and sum of the weight fractions percentage divided by the elution temperature range vs. the elution temperature of the Prep-TREF for Plastomer A.

The preparative TREF results showed bimodality in the derivative curves. In this case there was a smaller peak between 40°C and 50°C and a larger, broader peak between 50°C and 75°C. This corresponded with the CRYSTAF results; there was only a shift of the peak in the TREF results to a higher temperature, due to the under-cooling effect. The bimodality in the TREF and CRYSTAF traces/curves can be explained as being due to factors responsible for the broad SCBD of the metallocene-catalyzed LLDPE. These factors are:

1) The active sites in metallocene catalysts are not homogeneous, and more than one type of active site is present.

2) The fluctuation in local polymerization environment may also result in compositional heterogeneity of copolymers.[5]

Table 4.10 summarizes the data obtained for the Prep-TREF fractionation of Plastomer A.

Table 4.10 Prep-TREF data for Plastomer A

Temperature (°C)	Mass (g)	W_i	Wi(%)	∑Wi%	ΔT	Wi%/ΔT
25	0.263	0.09	9.23	9.23	n/a	n/a
30	0.132	0.05	4.64	13.87	5	0.9
35	0.033	0.01	1.17	15.04	5	0.2
40	0.153	0.05	5.35	20.39	5	1.1
45	0.381	0.13	13.35	33.74	5	2.7
50	0.076	0.03	2.66	36.41	5	0.5
55	0.407	0.14	14.28	50.69	5	2.9
60	0.622	0.22	21.81	72.5	5	4.4
70	0.353	0.12	12.37	84.87	10	1.23
80	0.316	0.11	10.74	95.61	10	1.07
90	0.125	0.04	4.39	100	10	0.43

Figure 4.59 shows a comparison of the traces for the unfractionated Plastomer A and for the unfractionated LDPE sample.
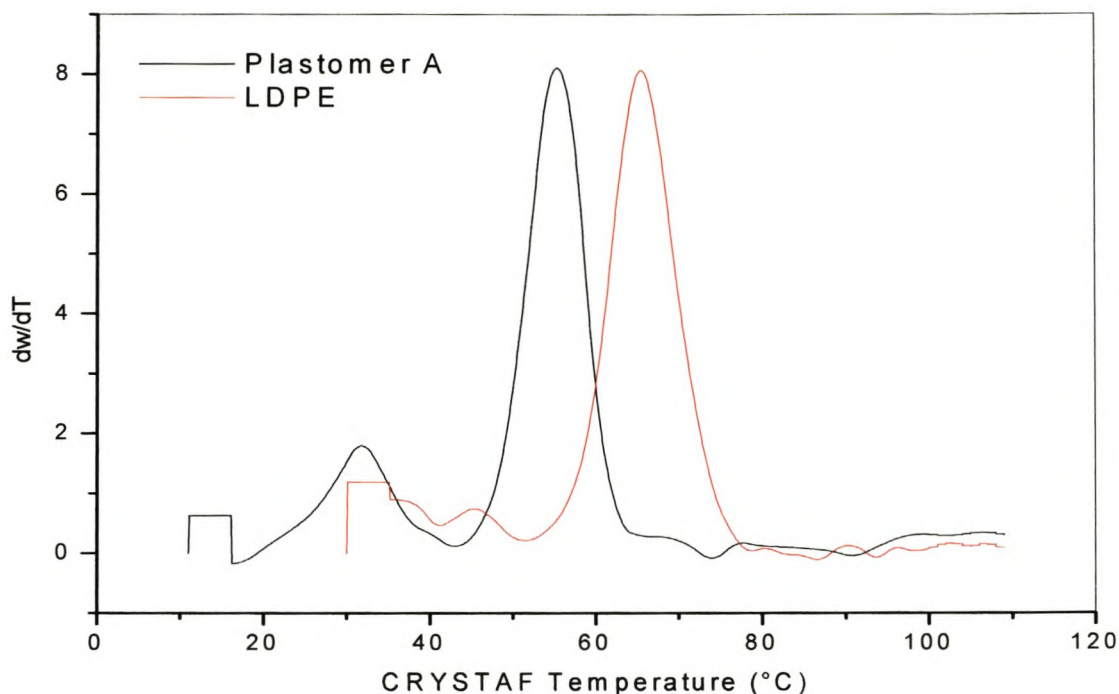
Figure 4.59 CRYSTAF traces of the 100% Plastomer A (Affinity PL1881) and the CRYSTAF trace of the 100% LDPE trace (extruded).

The LDPE sample had a CRYSTAF peak maximum at a higher temperature than that of the plastomer. Figure 4.59 showed significant overlapping of the LDPE and Plastomer A traces in the 55°C-65°C region. This overlapping area had the possibility to co-crystallize in the blend if the branching distributions of the polymer chains overlap. This will be discussed in more detail in Section 4.6. Figure 4.60 shows the CRYSTAF traces for each of the different temperature fractions recovered from the preparative TREF for Plastomer A.
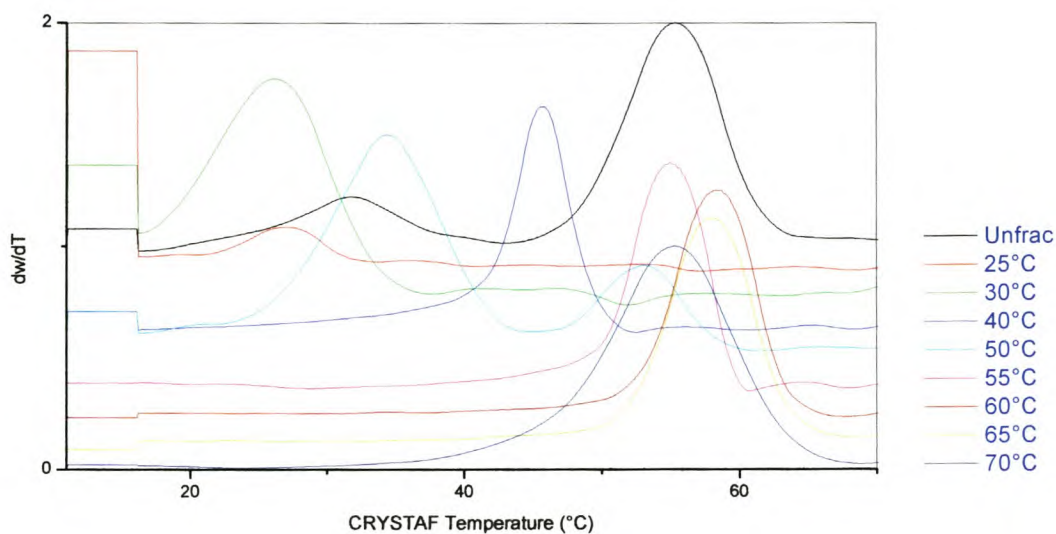
Figure 4.60 CRYSTAF traces for the preparative TREF fractions of 100% Plastomer A.

In Figure 4.60 the following were seen:

- The 25°C trace showed a small peak maximum at 25°C.
- The 30°C trace showed a peak maximum at 35°C.
- The 40°C trace showed a narrow peak maximum at 48°C.
- The 50°C trace showed bimodality, with peak maxima at 30°C and 52°C.
- The 55°C trace showed a single peak maximum at 58°C.
- The 60°C and 65°C traces both showed peak maxima at 60°C.
- The 70°C trace showed a peak maximum at 54°C.

Figure 4.61 shows a 2-D waterfall plot for Plastomer A, for which each of the CRYSTAF traces was weighted to account for the quantity of polymer in each fraction. Figure 4.62 shows the weighted 3-D CRYSTAF plot for Plastomer A. There was a narrow distribution along the CRYSTAF temperature axis and a broad distribution along the TREF elution temperature. This novel 3-D plot clearly showed that the heterogeneity could not be seen as clearly using one dimension.
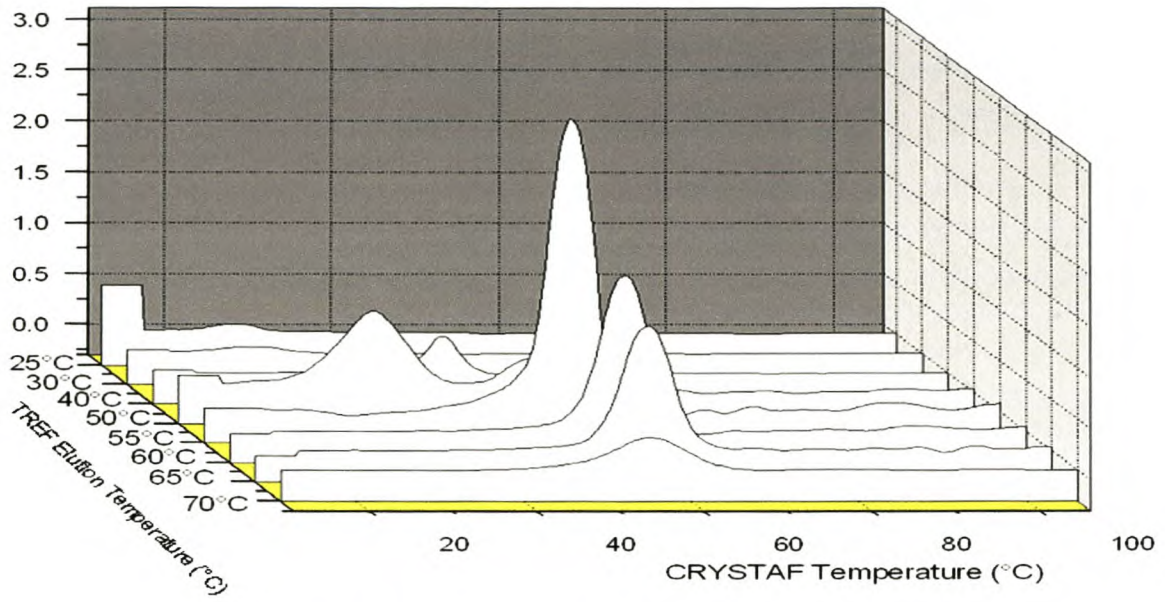
Figure 4.61 The 2-D weighted Plastomer A CRYSTAF traces.
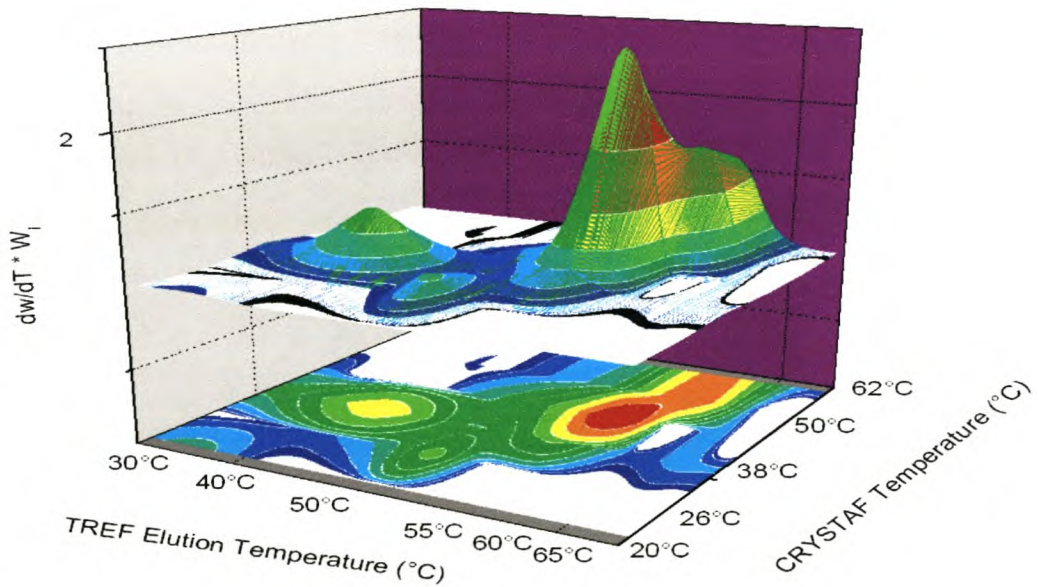
Figure 4.62 The 3-D CRYSTAF plot of Plastomer A.

The 3-D plot clearly illustrated that the plastomer consisted of at least two identifiable fractions - one occurring in the lower TREF elution area (a lower crystallinity fraction) and the other at a higher temperature more crystallisable fraction.

4.7.3.2)   Plastomer B

Figure 4.63 shows the CRYSTAF trace for Plastomer B.

Figure 4.63 The CRYSTAF result for the 100% Plastomer B.

The trace represented the first derivative of the concentration curve and had a maximum at 37°C. It had a broad peak between 15°C and 40°C, with a peak maximum at 37°C. No bimodality in the curve was observed. As expected, the peak maximum in the first derivative for this sample occurred at a lower temperature than in the case of Plastomer A. This was expected, since Plastomer B has an higher octene content, and therefore a larger degree of SCB.

Figure 4.64 shows the weight fractions and sum of the weight fraction curves vs. the TREF elution temperature of the Prep-TREF fractions of Plastomer B.
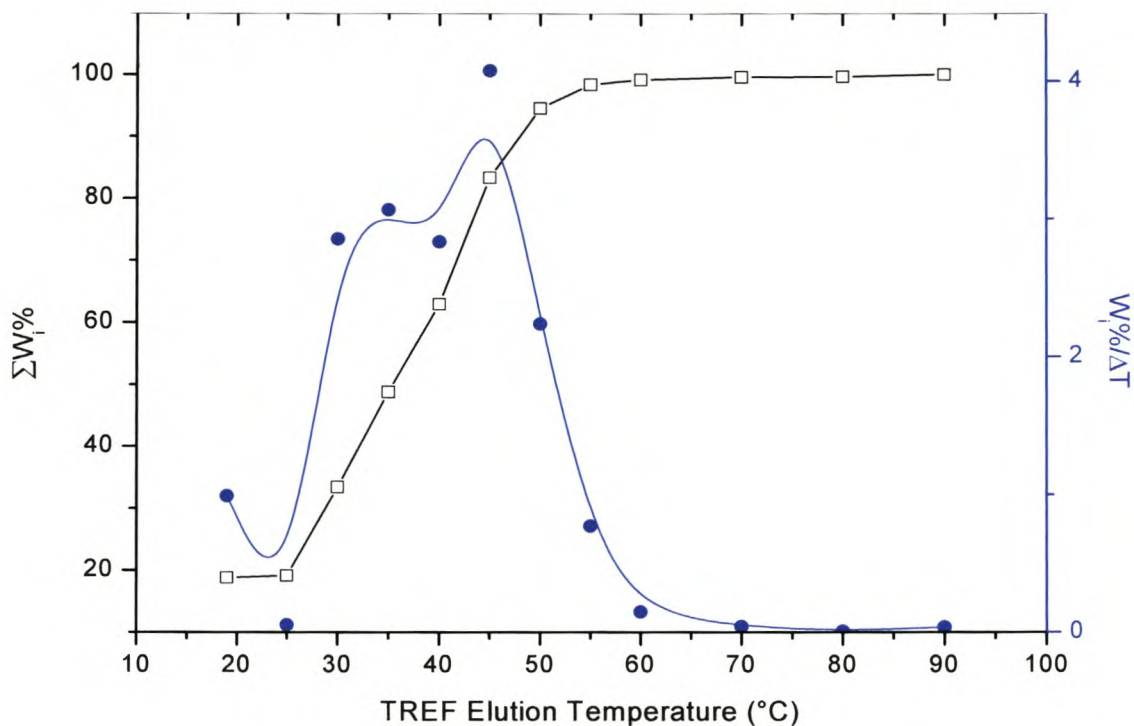
Figure 4.64 Preparative TREF weight fractions of Plastomer B.

It should be noted that the above plots lines (the weight fraction figures) should only be used as a visual guide, they should not be used in further calculations - it is preferable to use the sum of the weight fractions. The Prep-TREF results for Plastomer B showed a broad peak in the derivative curve between 25°C and 55°C, with a peak maximum at 45°C. Once again this peak occurred at higher temperature than the CRYSTAF peak and was once again attributed to the 'under-cooling' effect.

Table 4.11 summarizes the data obtained for the Prep-TREF fractionation of Plastomer B.

Table 4.11 Prep-TREF data for Plastomer B

Temperature (°C)	Mass (g)	W_i	Wi%	∑Wi%	ΔT	Wi%/ΔT
19	0.531	0.19	18.82	18.82	n/a	n/a
25	0.009	0.0032	0.33	19.15	6	0.1
30	0.403	0.14	14.28	33.43	5	2.8
35	0.433	0.15	15.33	48.76	5	3.0
40	0.401	0.14	14.17	62.94	5	2.8
45	0.576	0.20	20.40	83.33	5	4.0
50	0.316	0.11	11.19	94.52	5	2.2
55	0.109	0.04	3.86	98.39	5	0.7
60	0.021	0.01	0.74	99.13	5	0.1
70	0.012	0.00	0.42	99.55	10	0.042
80	0.002	0.00	0.08	99.62	10	0.0075
90	0.011	0.00	0.38	100	10	0.038

Figure 4.65 shows the CRYSTAF traces for the LDPE and Plastomer B, respectively. Figure 4.66 shows the CRYSTAF traces for each of the temperature fractions recovered from the Prep-TREF for Plastomer B.
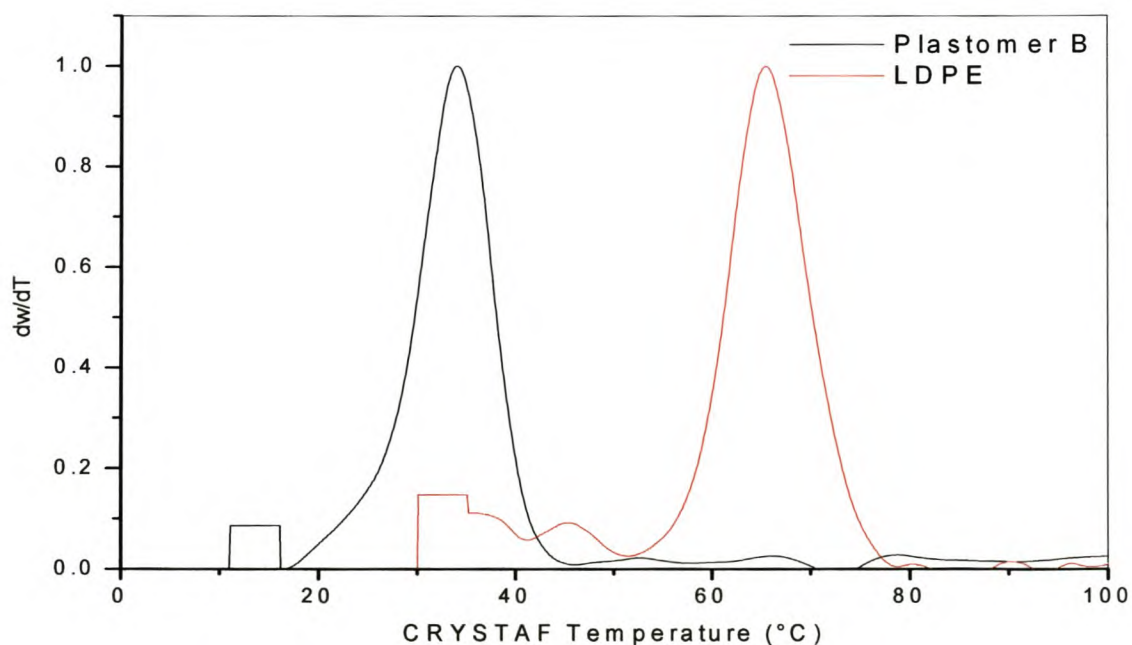
Figure 4.65 CRYSTAF traces for the 100% Plastomer B and 100% LDPE (extruded).
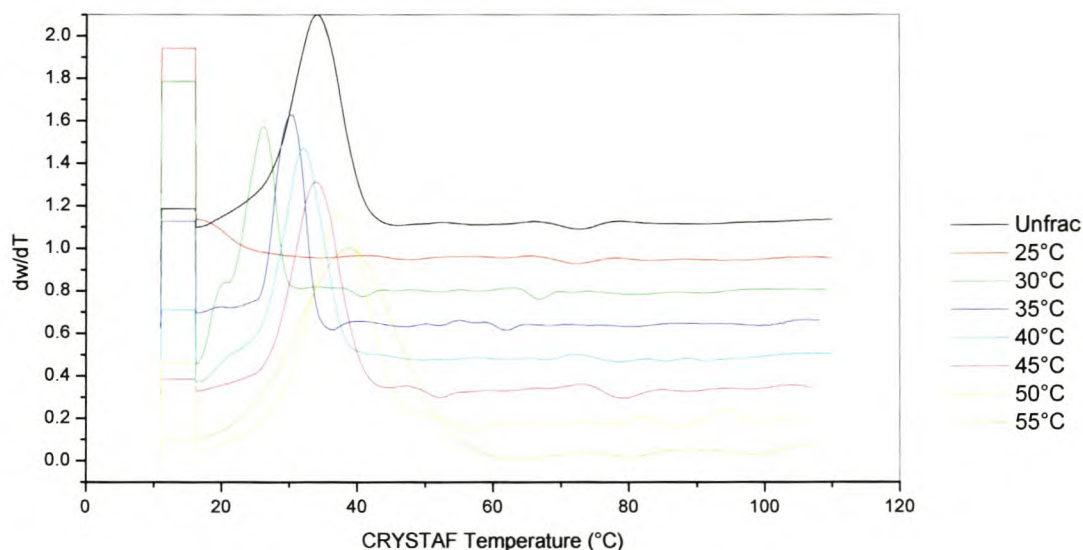
Figure 4.66 The CRYSTAF traces for the Prep-TREF traces of Plastomer B.

In Figure 4.65 there was a significant difference in the peak positions of Plastomer B and the LDPE. Unlike for Plastomer A, there was little overlap in the CRYSTAF derivative peaks, and only a small degree of overlap in the region between 20°C and 40 °C. In Figure 4.66 there was a progressive shift of the CRYSTAF peak maxima to higher temperatures with increasing TREF elution temperature.

In Figure 4.66 the following were seen:

- In Plastomer B the unfractionated trace showed a peak maximum at 38°C.
- The 25°C trace showed a slight peak at 20°C.
- The 30°C trace showed a peak maximum at 25°C.
- The negative values(30°C trace) below 20°C could possibly be due to freezing of the solvent TCB.
- The 35°C, 40°C, 45°C and 50°C traces showed a progressive shift of the peak maxima to higher temperature with an increasing TREF elution temperature.
- The 55°C trace showed a broad peak with a peak maximum at 38°C. The TREF plots showed broadening of the peak half width with an increase in CRYSTAF temperature.

The intensities of the CRYSTAF traces could however be misleading, as they were not weighted.

Figure 4.67 shows the 2-D weighted waterfall plot of Figure 4.66 , in which each trace is now weighted.
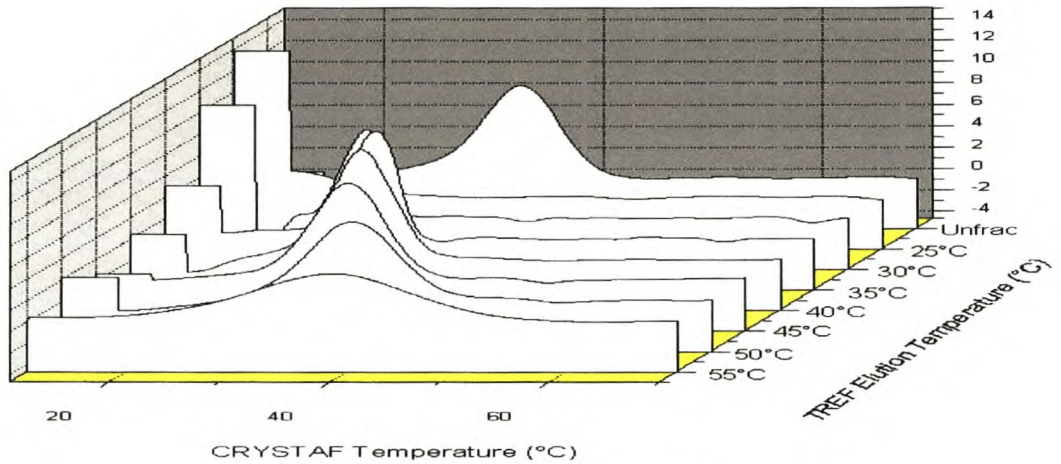
Figure 4.67 The weighted traces for Plastomer B in a 2-D waterfall plot.

Figure 4.68 shows the 3-D CRYSTAF plot of the Prep-TREF fractions of Plastomer B. Again there was a narrow distribution along the CRYSTAF temperature axis and a broad distribution along the TREF elution temperature axis.
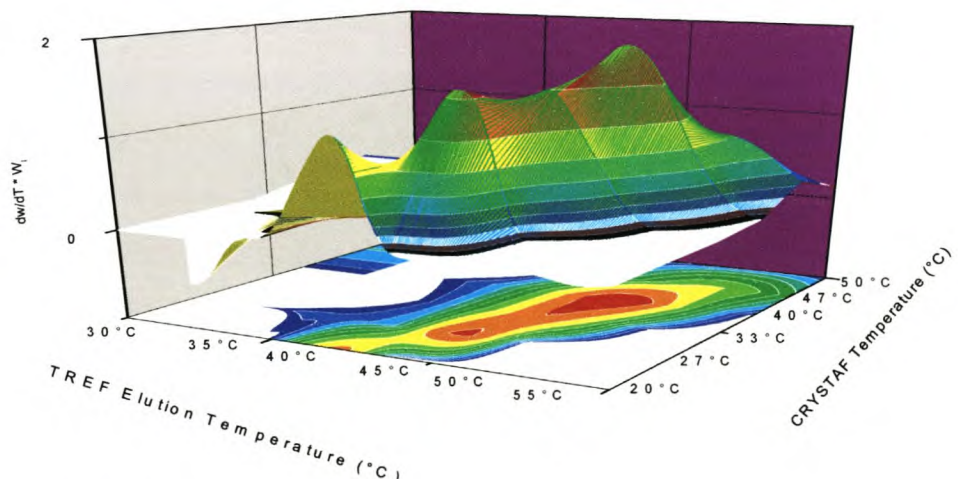
Figure 4.68 3-D CRYSTAF plot of the Prep-TREF fractions of Plastomer B.

4.7.4) HT-SEC results

HT-SEC results for the Prep-TREF fractions of Plastomer A are given here.

4.7.4.1) Plastomer A

Figure 4.69 shows the raw data of the HT-SEC results for the 100% Plastomer A that were baseline corrected and normalized. There were low molecular weight traces in the low and the high Prep-TREF fractions of Plastomer A. The soluble 25°C trace showed low molecular weight polymer. Bimodality was seen in the 25°C and 30°C traces – probably due to the presence of very low molecular weight polymer and medium molecular weight polymer. There was also low molecular weight polymer in the 90°C trace.
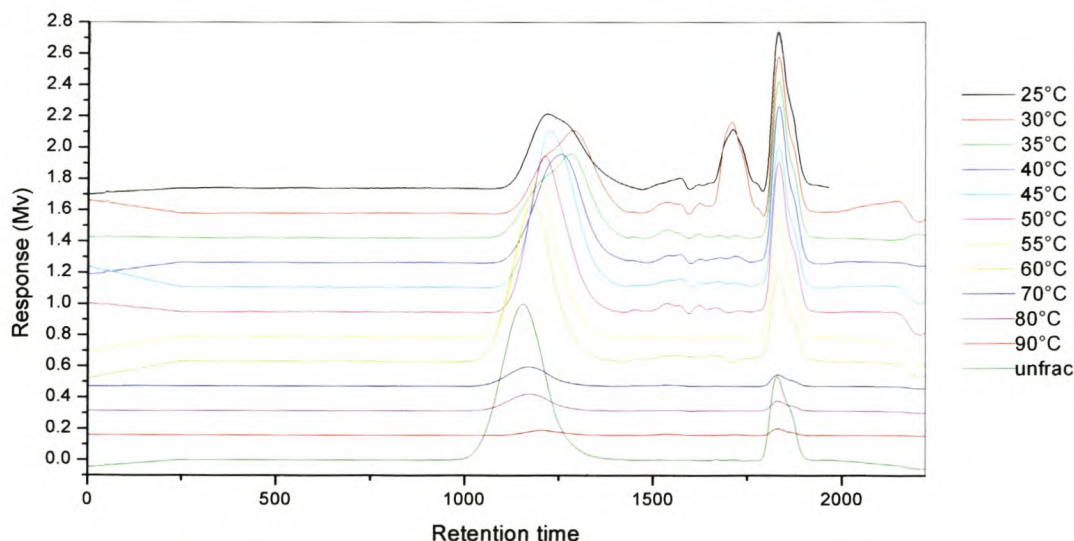
Figure 4.69 The HT-SEC raw data for the unfractionated and fractionated Plastomer A traces.

Figure 4.70 shows the weighted, baseline corrected Plastomer A HT-SEC results in a 3-D plot.
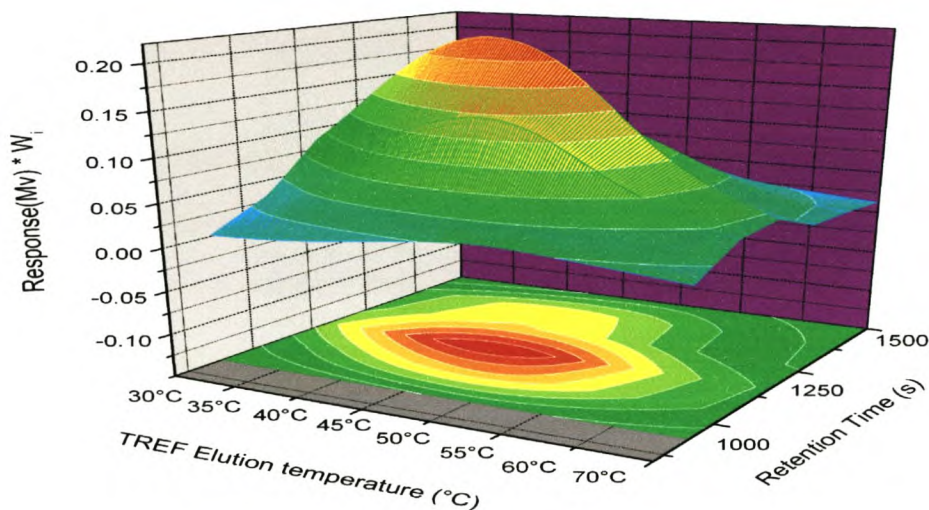
Figure 4.70 3-D plot of the HT-SEC data for Plastomer A.

Figure 4.71 shows the Mn and Mw of the 100% Plastomer A Prep-TREF fractions.
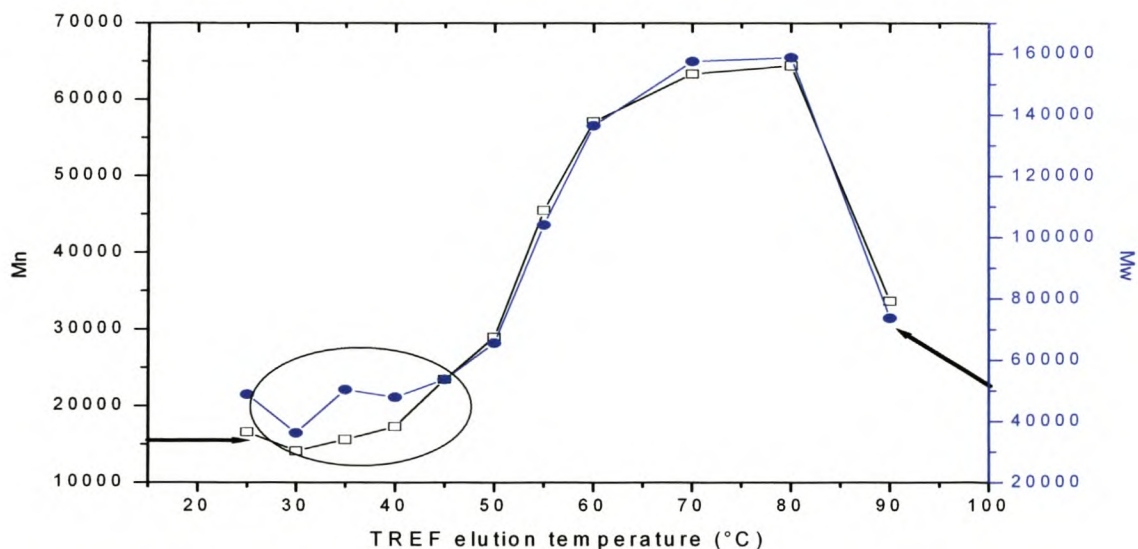
Figure 4.71 Mn and Mw vs. TREF elution temperature for the Prep-TREF Plastomer A fractions.

There were peak maxima at 80°C for the Mn and Mw, followed by a decrease in Mn and Mw. This increase was consistent with the shift to shorter retention time for each fraction seen in the 3-D plot (Figure 4.70). In Figure 4.71 the small peak between 30°C and 50°C on the x-axis is indicated. This peak could be associated with the lower molecular distribution that was observed for this plastomer in the 3-D CRYSTAF plot.

Table 4.12 shows the tabulated HT-SEC results for Plastomer A.

Table 4.12 HT-SEC results of the Prep-TREF fractions for Plastomer A

Temperature (°C)	Mn	Mw	PD	W_i
25	17000	49000	2.9	0.09
30	14000	36000	2.6	0.05
35	16000	50000	3.2	0.01
40	17000	48000	2.8	0.05
45	23000	54000	2.3	0.13
50	29000	66000	2.3	0.03
55	46000	100000	2.3	0.14
60	57000	140000	2.4	0.22
70	63000	160000	2.5	0.12
80	64000	160000	2.5	0.11
90	33000	74000	2.2	0.04
unfrac	75000	210000	2.8	

The polydispersities of all the fractions were quite similar, as expected for a metallocene-catalyzed plastomer.

4.7.4.2)   Plastomer B

Figure 4.72 shows the raw HT-SEC data for the unfractionated 100% Plastomer B, followed by the Prep-TREF fractions of the 100% Plastomer B acquired at different elution temperatures. It also shows low molecular weight polymer in the 19°C trace. The 25°C fraction trace showed little to no low molecular weight polymer. The peak maxima will be discussed in more detail as molecular weight graphs.
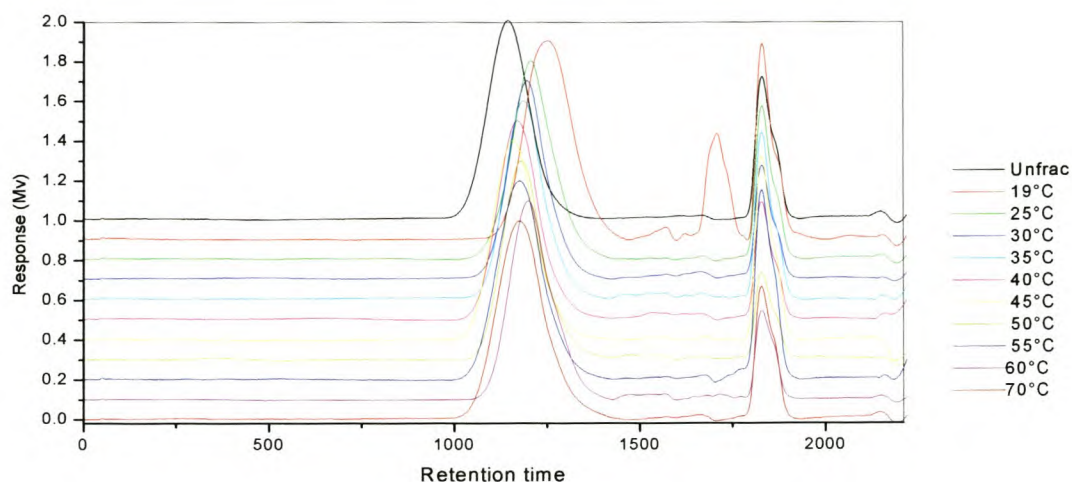
Figure 4.72 Raw data obtained from the HT-SEC for the 100% Plastomer B.

Table 4.13 shows the tabulated HT-SEC results for the Prep-TREF fractions of Plastomer B. The PDs of the Plastomer B traces were in the range of, metallocene-catalyzed polymers, which usually have a PD of between 2 and 3.

Table 4.13 HT-SEC results of the Prep-TREF fractions for Plastomer B

Temperature (°C)	Mn	Mw	PD	Wi
19°C	16000	40000	2.6	0.20
25°C	33000	87000	2.6	0.003
30°C	42000	97000	2.3	0.14
35°C	48000	101000	2.3	0.15
40°C	59000	150000	2.5	0.14
45°C	69000	180000	2.6	0.20
50°C	48000	120000	2.5	0.11
55°C	52000	150000	2.9	0.04
60°C	34000	86000	2.5	0.007
70°C	40000	140000	3.6	0.004
unfrac	96000	240000	2.5	

Figure 4.73 shows the 3-D plot for the HT-SEC data of the 100% Plastomer B.
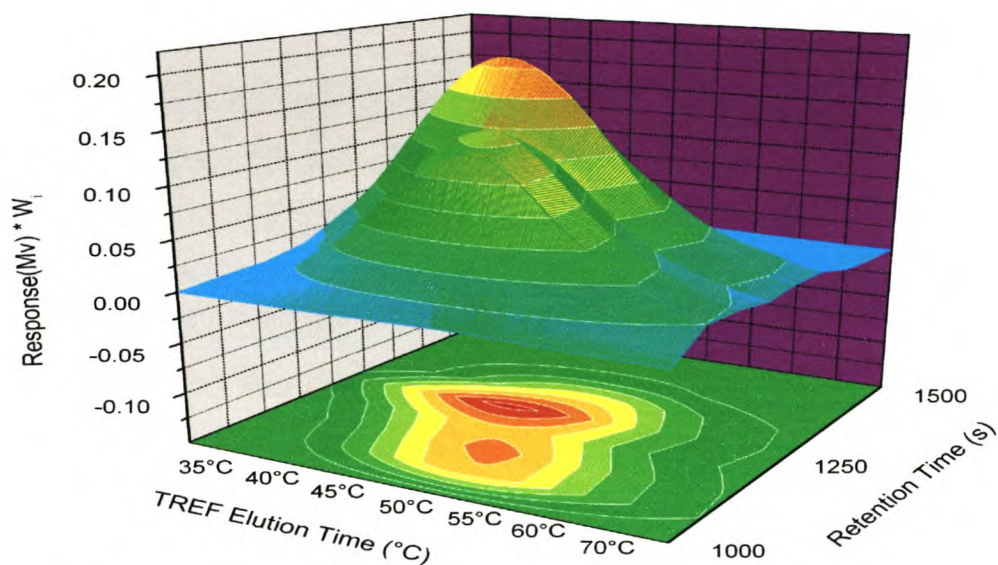
Figure 4.73 3-D plot of the weighted, normalized and baseline-corrected HT-SEC data vs. TREF elution time for Plastomer B.
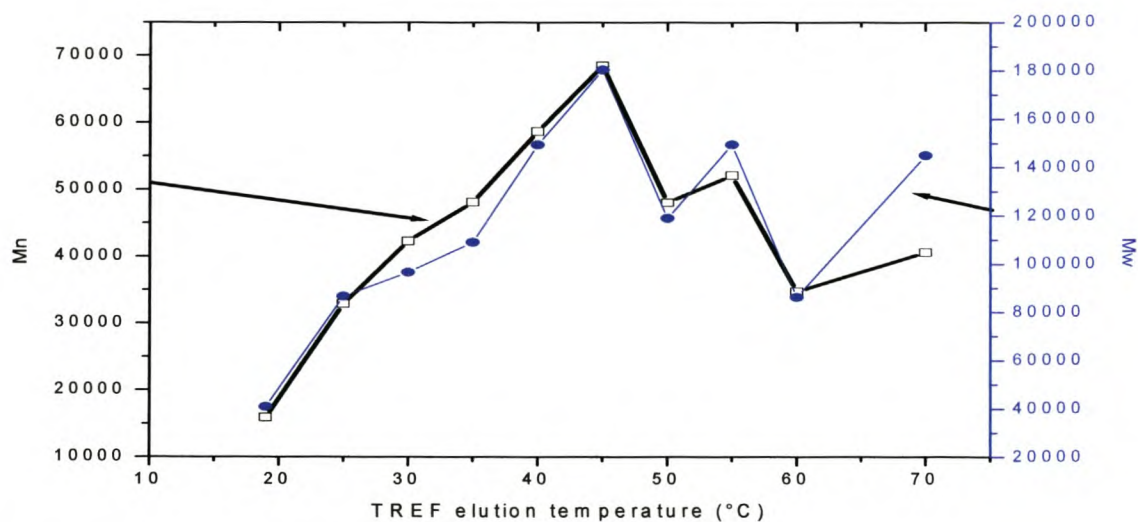
Figure 4.74 Comparison of Mn and Mw of Prep-TREF fractionated plots for Plastomer B.

In Figure 4.74 the Mn and the Mw of the Prep-TREF fractionated plots for Plastomer B are compared. Both the Mn and Mw had peak maxima at 45°C, followed by a gradual decrease in the Mn and Mw.

4.7.5) DSC results

DSC results of Prep-TREF fractions of Plastomer A and Plastomer B are given here. All fraction traces are normalized and baseline zeroed.

4.7.5.1) Plastomer A

Figure 4.75 shows the DSC crystallization peaks for the unfractionated and fractionated fractions of Plastomer A. There was an increase in the DSC $Tc_{(crystallization\ peak\ maximum)}$ with an increase in the Prep-TREF elution temperature. These DSC results confirmed that Plastomer A was fractionated via crystallizability. There was a slight shoulder on the left side of the crystallization peaks but this was not as great as in the case of the LDPE.
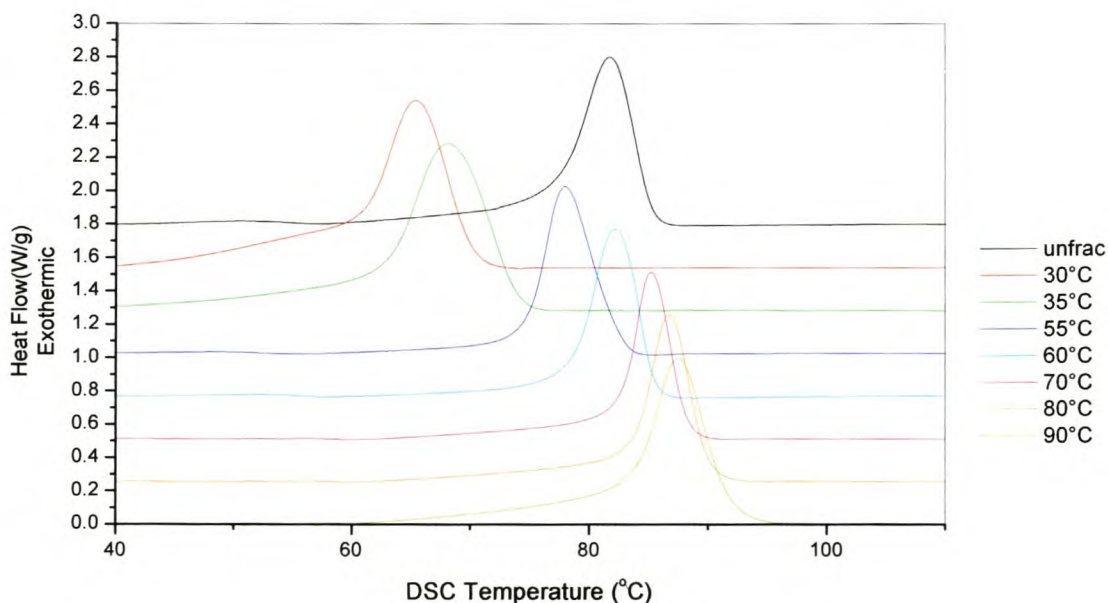
Figure 4.75 Waterfall plot of the DSC crystallization peaks for the unfractionated and fractionated Prep-TREF fractions of Plastomer A.

Figure 4.76 shows the DSC melting peaks for the unfractionated and fractionated Prep-TREF fractions of Plastomer A. There was a gradual increase in the $Tc_{(DSC\ melting\ peak\ maxima)}$ with

an increase in the Prep-TREF elution temperature for the Plastomer A fractions. The melting peaks all had a shoulder on the left hand side. The melting peaks also became progressively broader for each of the higher temperature fractions.
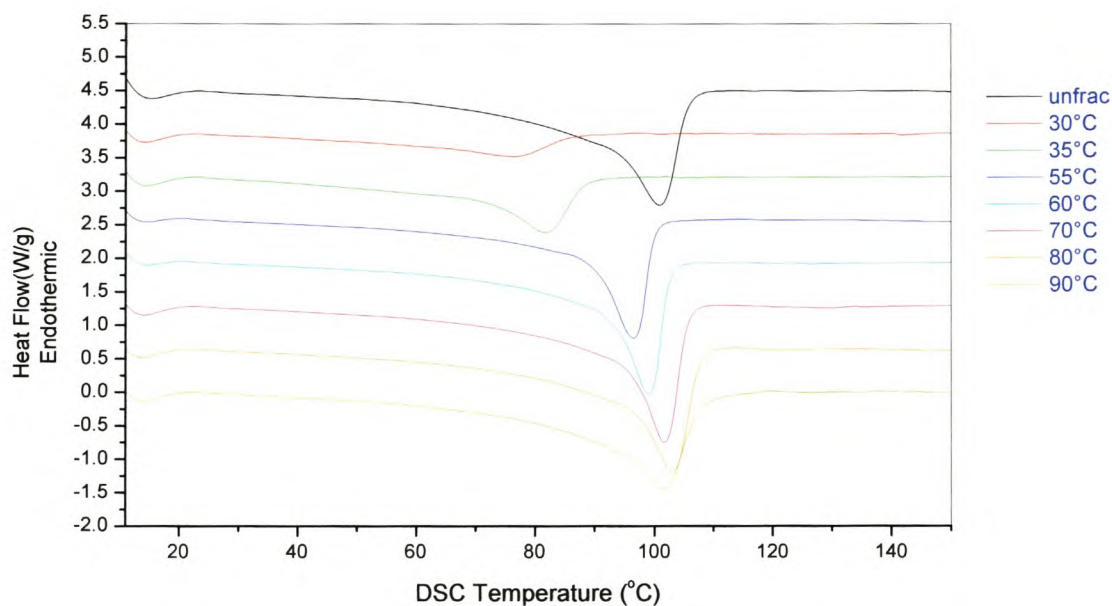
Figure 4.76 DSC melting peaks for the unfractionated and fractionated Prep-TREF fractions of Plastomer A.

Figure 4.77 shows the DSC crystallization peaks of the unfractionated LDPE and of the unfractionated Plastomer A. There was a large area of overlapping between the LDPE's DSC crystallization peak and the Plastomer A's DSC crystallization peak. Figure 4.77 confirmed the CRYSTAF results shown earlier in Figure 4.59.
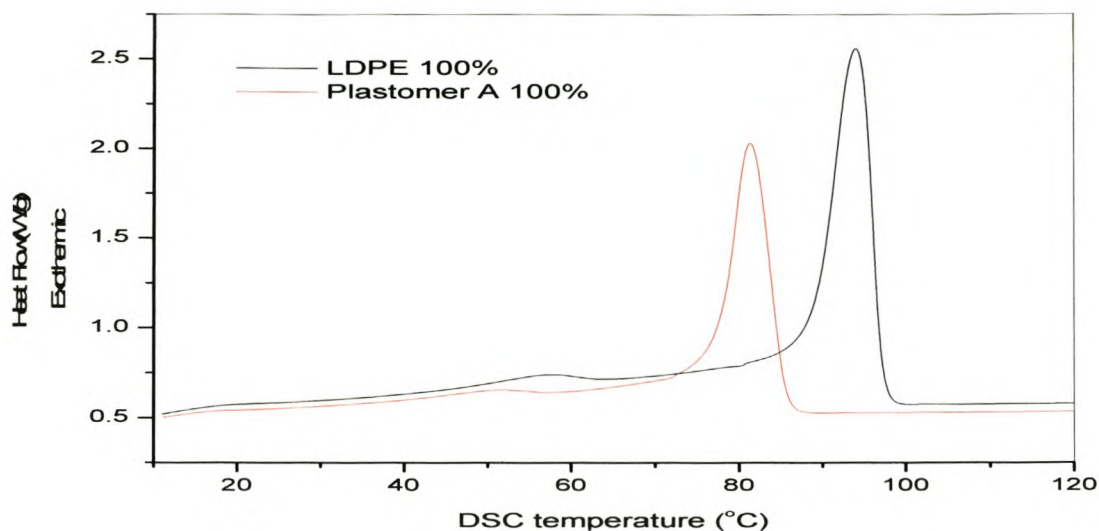
Figure 4.77 DSC crystallization peaks of the unfractionated LDPE and the Plastomer A.

4.7.5.2) Plastomer B

Figure 4.78 shows the DSC crystallization peaks for the unfractionated and Prep-TREF fractionated Plastomer B traces, on the same x-axis. There was an increase in the $Tc_{(DSC}$ $_{crystallization\ peak\ maxima)}$ with a increase in TREF elution temperature.
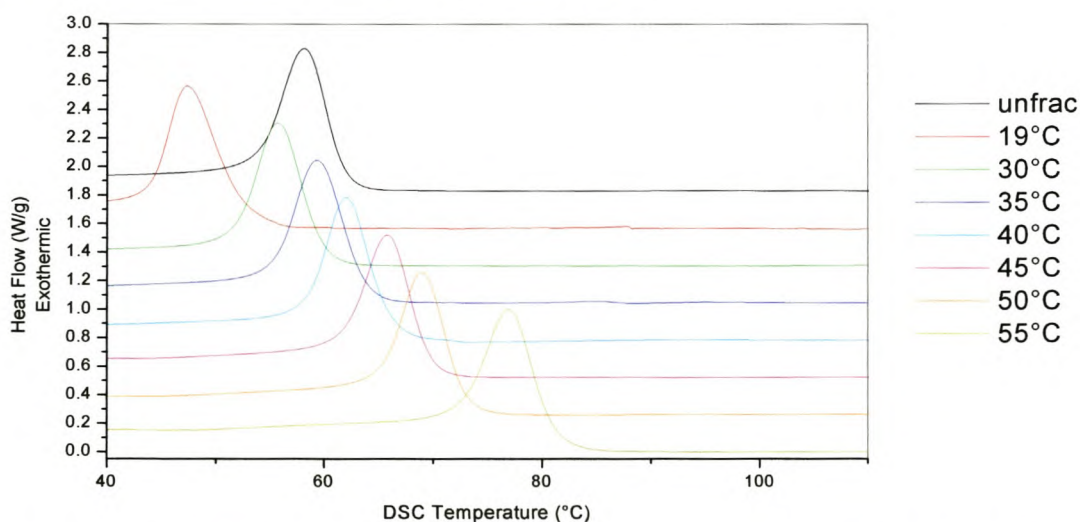
Figure 4.78 Waterfall plot of the DSC crystallization peaks for the unfractionated and fractionated Prep-TREF fractions of Plastomer B.

109

Figure 4.79 shows the DSC melting peaks for the Plastomer B fractions in a waterfall plot. There was a gradual increase in the $Tc_{(DSC\ melting\ peak\ maxima)}$ with an increase in the Prep-TREF elution temperature. It is interesting to note that while there was a progressive shift to higher $Tc_{(DSC\ melting\ peak\ maxima)}$ values, the total area of the melting peaks was much smaller than that for Plastomer A. This illustrated the overall small amount of crystallinity in each corresponding Plastomer B fraction.
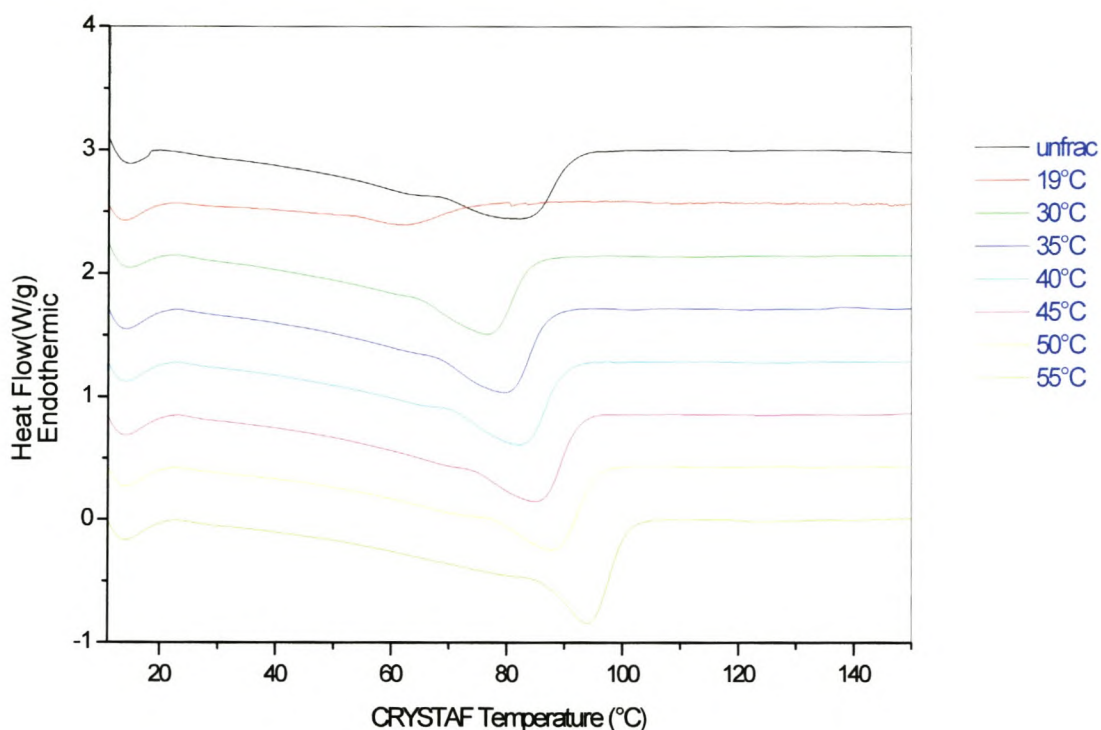
Figure 4.79 DSC melting peaks for the unfractionated and fractionated Prep-TREF fractions of Plastomer B.

Figure 4.80 shows the DSC crystallization peaks for the unfractionated LDPE and Plastomer B fractions, shown on the same x-axis.
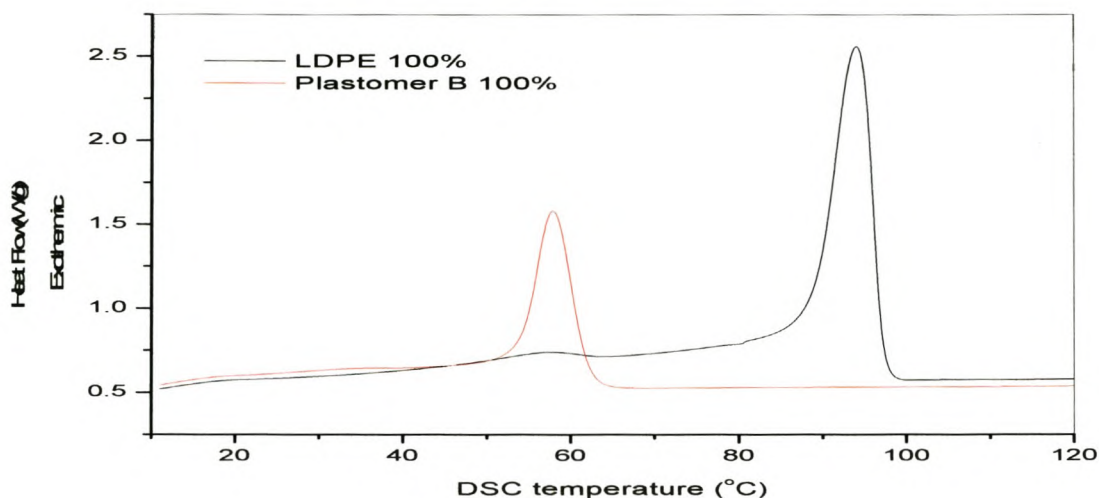
Figure 4.80 DSC crystallization peaks for the unfractionated LDPE and Plastomer B fractions.

4.7.6) Co-monomer content of Plastomer A fractions, as determined by NMR

Figure 4.81 shows the percentage comonomer content in the fractions of Plastomer A.
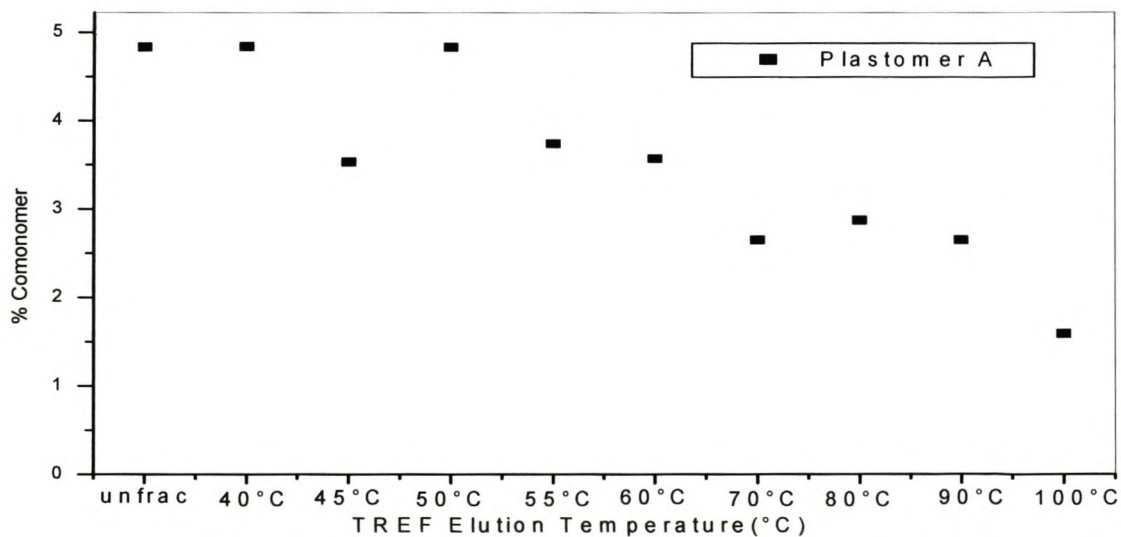
Figure 4.81 Percentage comonomer content of Prep-TREF fractionated traces of Plastomer A.

There was a gradual decrease in comonomer content with an increase in the TREF elution temperature. This figure also showed that the metallocene-catalyzed Plastomer A did not have a uniform distribution of comonomer content in the Prep-TREF fractions. The progressive decrease in co-monomer content for higher elution fractions showed the effect of progressive larger amounts of comonomer on crystallizability.

4.8) Analysis of LDPE / Plastomer blends

4.8.1) LDPE / Plastomer A blends

In this section a blend of 40% Plastomer A and 60% LDPE is analysed, using the results obtained earlier for Plastomer A and for LDPE, respectively. First, the CRYSTAF traces of the unfractionated LDPE, Plastomer A, and a blend of 40% Plastomer A and 60% LDPE, will be considered. Results are shown in Figure 4.82. The CRYSTAF trace for the blend was deconvoluted as shown on Figure 4.83.
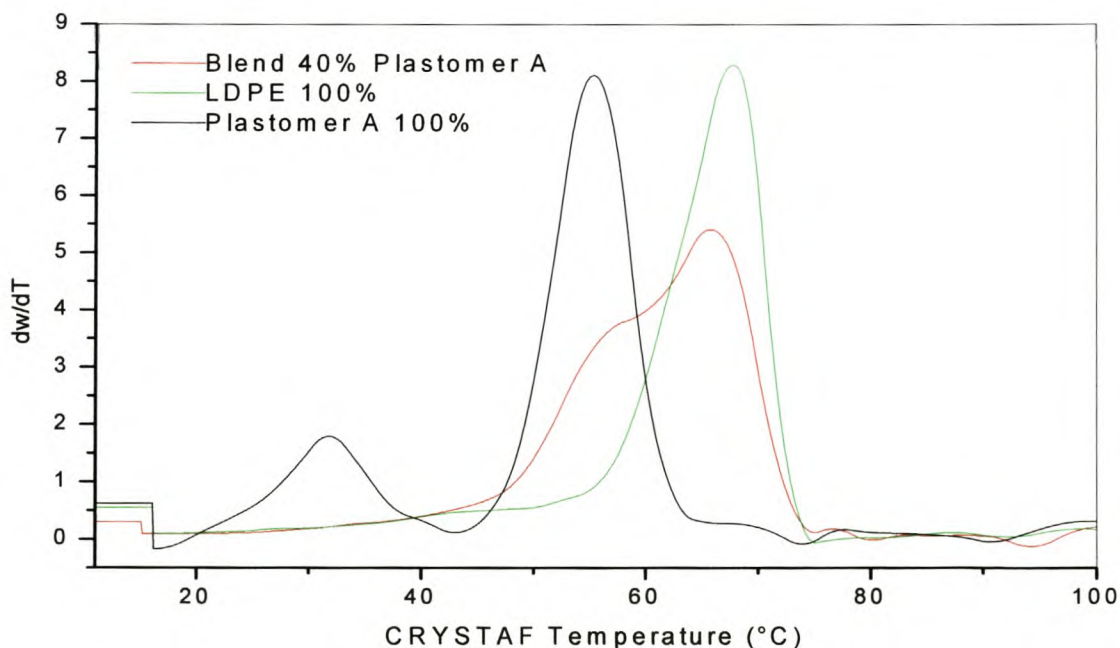
Figure 4.82 CRYSTAF traces for: LDPE, Plastomer A, and a blend of 40% unfractionated Plastomer A and 60% LDPE.

Figure 4.82 shows that 100% Plastomer A had bi-modality, resulting from a peak between 20°C and 40°C and a larger more intense peak between 45°C and 65°C. The CRYSTAF trace of unfractionated LDPE had a single peak between 55° and 75°C. The unfractionated blend had a bi-modal peak between 45°C and 75°C. The shoulder on the peak suggested that the two components were crystallizing in CRYSTAF as separate fractions The traces for unfractionated LDPE and for unfractionated Plastomer A overlapped in the area between 55°C and 65°C. This area represented the possible fraction that could co-crystallize in the 40% blend during the TREF cooling step.

Figure 4.83 shows the deconvolution of the 40% Plastomer A trace into two overlapping Gaussian curves (indicated in the figure by the green curves). The deconvoluted peaks exactly matched the unfractionated LDPE and Plastomer A in terms of the position of the peak maxima.
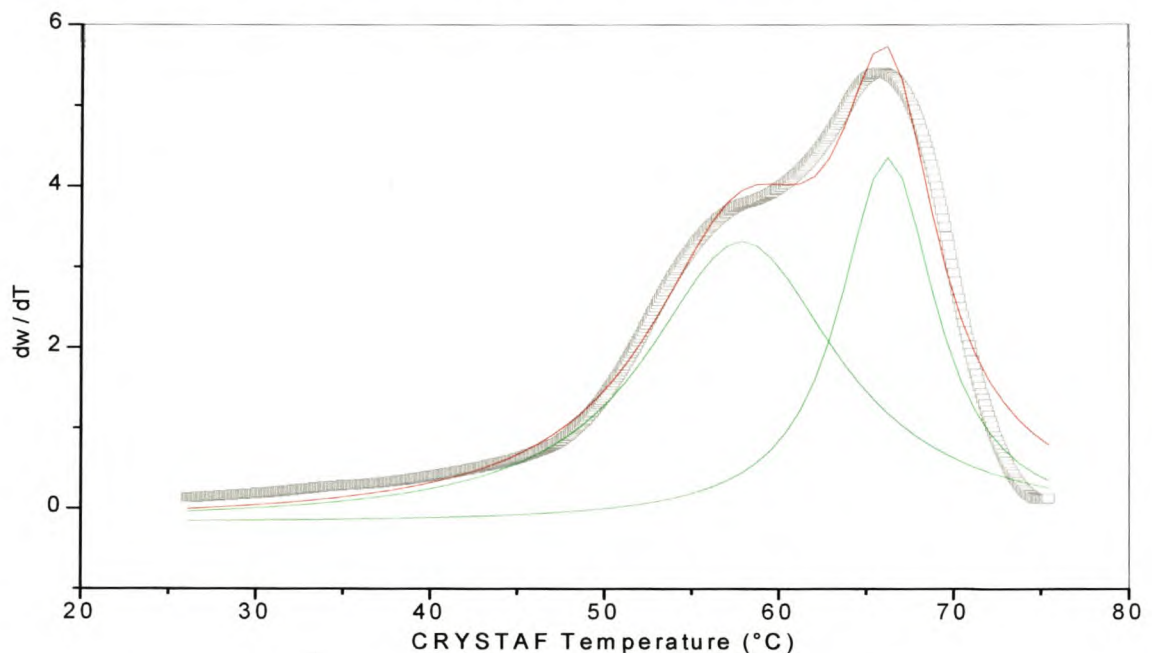
Figure 4.83 Deconvolution of the blend containing 40% unfractionated Plastomer A.

Figure 4.84 shows the Prep-TREF result of the fractionated 40% Plastomer A trace. It shows the Prep-TREF weight fraction curves and the sum of the weight fractions. The shape of the weight fraction curve in Figure 4.84 resembled the shape of the CRYSTAF trace of blend.
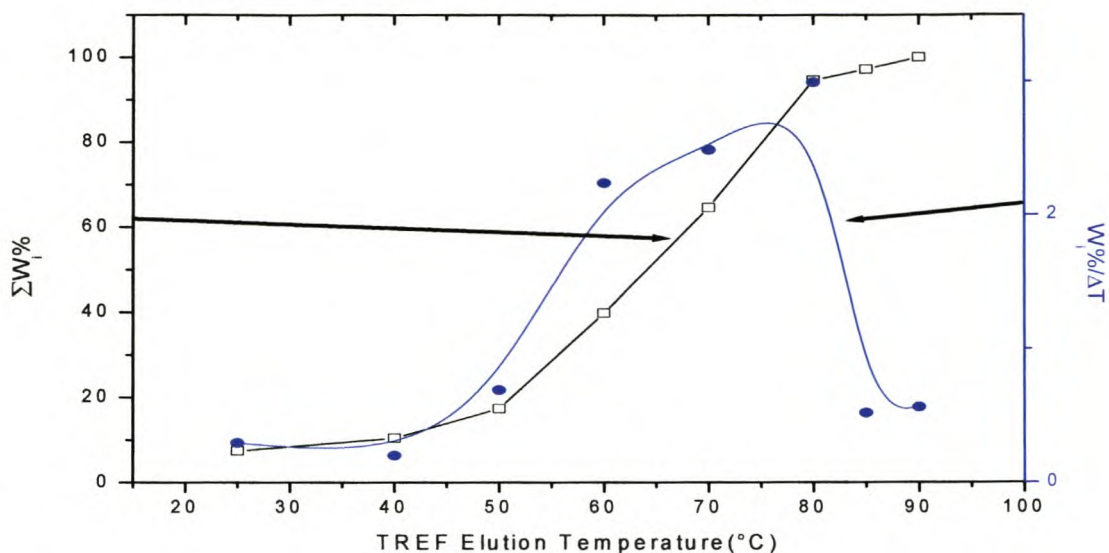
Figure 4.84 Prep-TREF trace of the blend containing 40% fractionated Plastomer A.

Table 4.14 shows the Prep-TREF results obtained for the 40% Plastomer A blend.

Table 4.14 Prep-TREF data for the 40% Plastomer A blend

Temperature (°C)	Mass (g)	Wi	Wi (%)	∑Wi%	ΔT	Wi%/ΔT
25	0.2074	0.0741	7.40	7.40	n/a	n/a
40	0.0851	0.0304	3.03	10.44	15	0.20
50	0.1935	0.0691	6.91	17.35	10	0.69
60	0.6268	0.2239	22.38	39.74	10	2.24
70	0.6968	0.2489	24.88	64.63	10	2.49
80	0.8382	0.2994	29.94	94.57	10	2.99
85	0.0728	0.0260	2.60	97.17	5	0.5
90	0.079	0.028218	2.82	100	5	0.6

Figure 4.85 super-imposes Prep-TREF weight fraction curves of the fractionated LDPE, 100% Plastomer A and the 40% Plastomer A blend. The figure showed definite bi-modality in the 100% Plastomer A. The 40% Plastomer A did not have bi-modality but overlapped clearly in areas of both the unblended Prep-TREF traces. This overlapping area meant that co-

crystallization between the plastomer and LDPE was possibly taking place. The Prep-TREF results were very similar to the comparative CRYSTAF results shown in Figure 4.82.
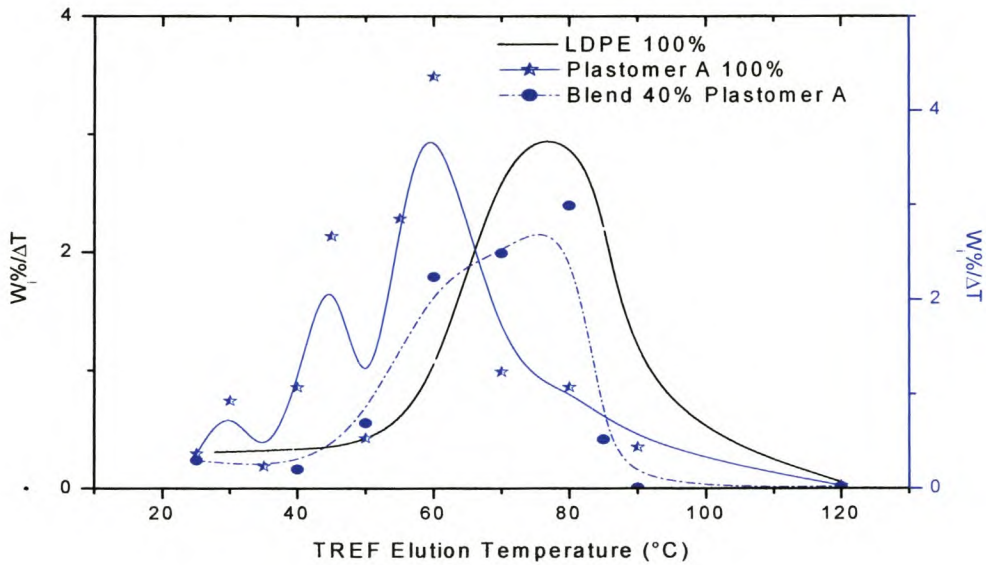
Figure 4.85 Weight fractions for the Plastomer A, LDPE and 40% Plastomer A blend.

Figure 4.86 shows the sum of the weight fraction curves for the LDPE, Plastomer A and the 40% blend. Such a presentation is useful should comparisons in Figure 4.85 need to be drawn, since different TREF elution temperatures are present in that figure (4.85).
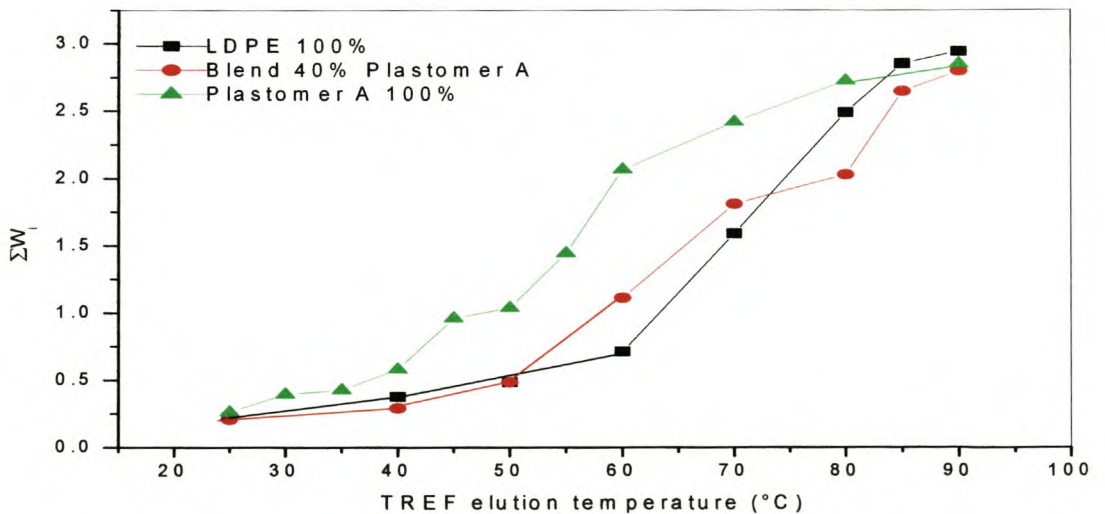
Figure 4.86 Sum of the weight fractions for the Plastomer A, LDPE and the 40% blend.

In Figure 4.86 the sum of the weight fractions curve for Plastomer A had the greatest incline. The LDPE had the lowest incline in the beginning of the trace but increased dramatically between 60°C and 80°C. The 40% blend had a lower incline between 25°C and 50°C than the LDPE curve. Between 50°C and 70°C the blend trace was above the LDPE trace, then dropped below the LDPE curve until 90°C.

Figure 4.87 shows the CRYSTAF traces of the Prep-TREF fractions for the 40% Plastomer A blend. The unfractionated trace showed a broad bi-modal peak as discussed above. The 25°C trace was soluble. The 40°C Prep-TREF fractionated CRYSTAF trace showed a small CRYSTAF peak maximum at 40°C. The 50°C trace had a narrower peak maximum than the unfractionated trace. The 60-85°C traces showed a progressive increase in the $Tc_{(CRYSTAF)}$ with an increase in TREF elution temperature, as will be shown in Figure 4.88. The 60°C trace was relatively narrow, while the higher temperature traces showed a broader CRYSTAF peak.
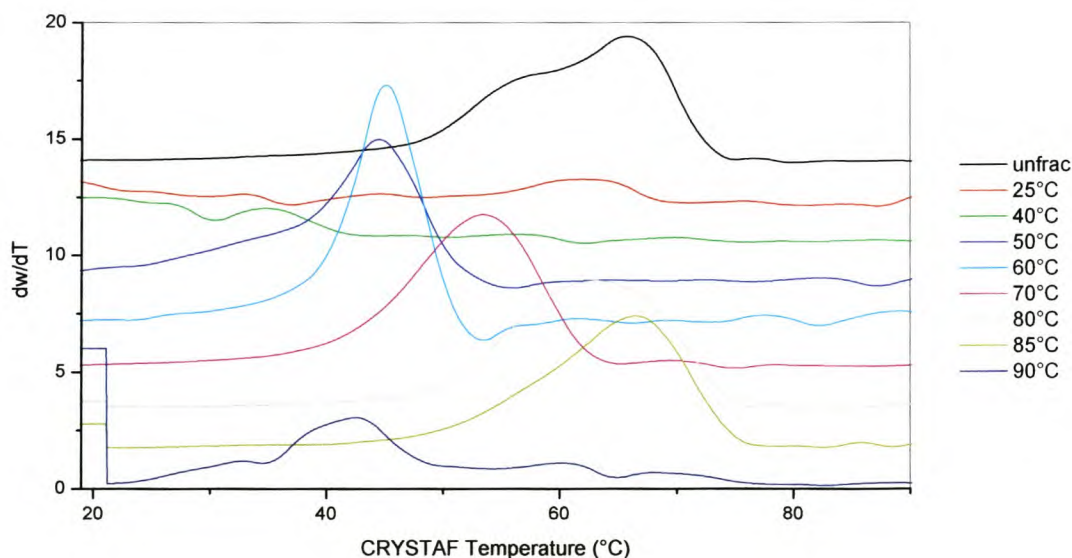
Figure 4.87 CRYSTAF traces of the Prep-TREF fractions for the 40% Plastomer A blend.
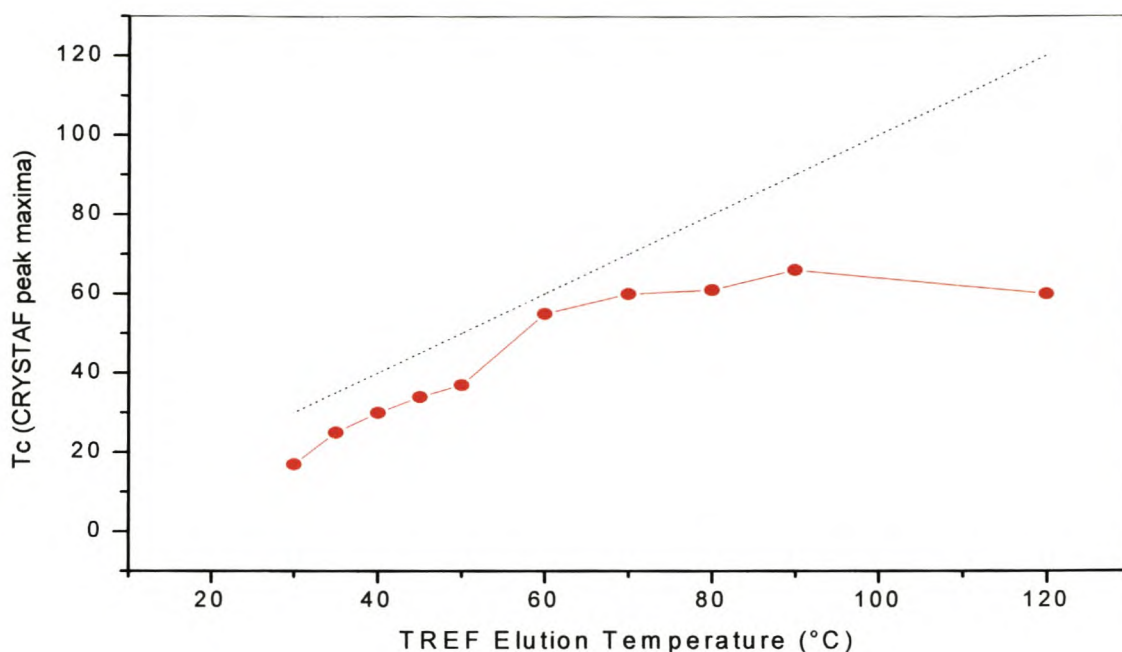
Figure 4.88 Tc (CRYSTAF peak maxima) for the 40% Plastomer A blend.

In Figure 4.88 the red curve represents the $Tc_{(CRYSTAF\ peak\ maxima)}$ for the Plastomer A and LDPE blend and the dotted line represents a linear increase of the Tc values. Once again the $Tc_{(CRYSTAF\ peak\ maxima)}$ (red curve) is lower than the dotted line $Tc_{(CRYSTAF\ peak\ maxima)}$ = TREF elution temperature due to the under-cooling effect.

Figure 4.89 shows the 3-D CRYSTAF plot for the 40% Plastomer A blend. It showed more than one peak maximum due to the presence of both the Plastomer A and the LDPE. The possibility of co-crystallization is emphasized in the 3-D polt, as in Figures 4.83 and 4.84. Great care should be taken when interpreting these blends since the appearance of multiple peaks can be misleading, since it could be inhomogeneous blending causing the bi-modality.
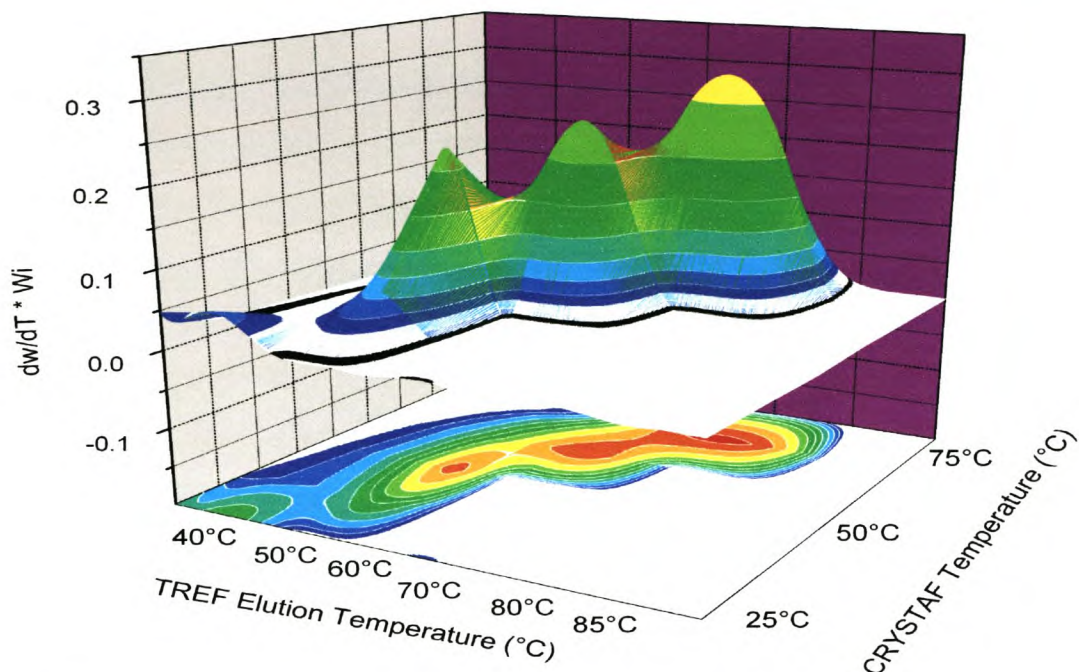
Figure 4.89 3-D CRYSTAF traces for the 40% Plastomer A blend.

Figure 4.90 shows the HT-SEC results for the Prep-TREF fractions of the 40% Plastomer A blend.
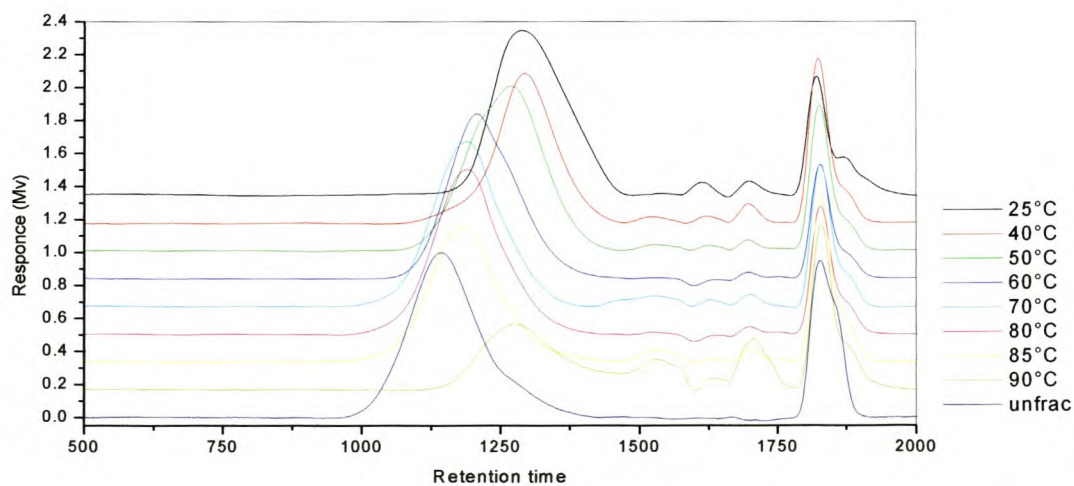
Figure 4.90 HT-SEC trace results for Prep-TREF fractions of the 40% Plastomer A blend.

Figure 4.90 is presented as a waterfall plot to increase the clarity of the traces. If the unfractionated 40% blend was bimodal, then we could determine the percentage co-crystallization using the areas under the bimodal peaks

There was an increase in the molecular weight distributions of the Prep-TREF fractions of the Plastomer A blend with a increase in the TREF elution temperature of the fractions, except for the 90°C fraction that showed a decrease in molecular weight relative to the 85°C trace. The 25-50°C Prep-TREF were low molecular weight material coming out as small peaks just after the solvent peaks, between the retention times of 1500 and 1750. The solvent peaks could be seen between the retention times of 1750 and 2000 seconds. The 90°C HT-SEC trace seemed to have a large quantity of low molecular weight material between the retention times of 1500 and 1750 seconds.

Figure 4.91 shows the HT-SEC results of the baseline zeroed, normalized and weighted, matrix generated 3-D plot of the Prep-TREF traces of 40% Plastomer A blend.
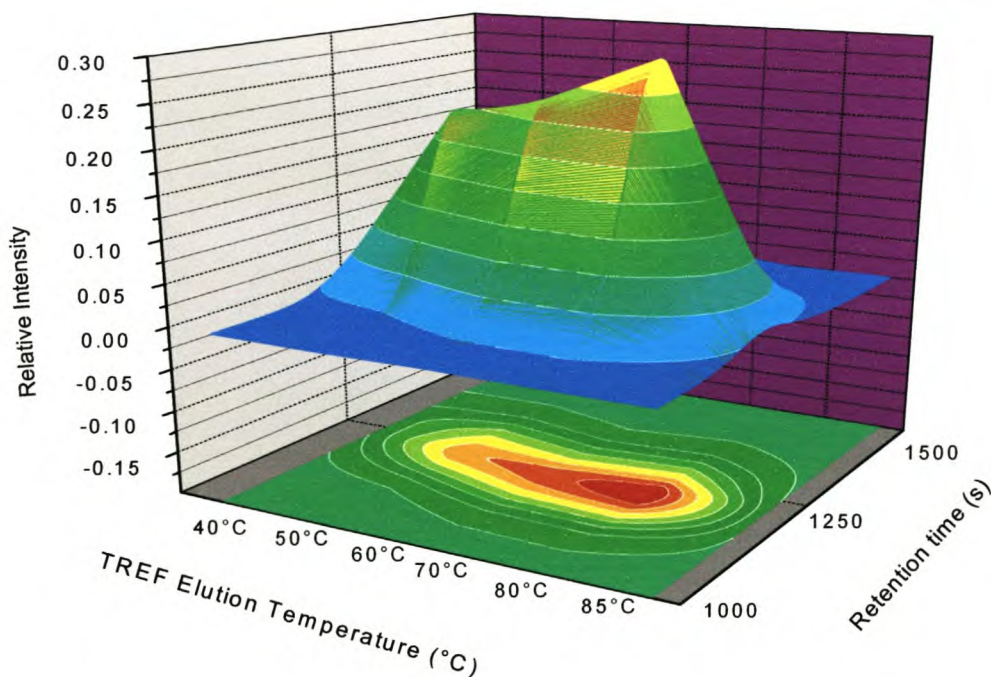
Figure 4.91 3-D HT-SEC results of the Prep-TREF traces of 40% Plastomer A blend.

4.8.2) LDPE / Plastomer B blends

In this section a blend containing 40% Plastomer B and 60% LDPE is analysed, using results obtained earlier for Plastomer B and for LDPE. Prep-TREF, CRYSTAF and HT-SEC results will be used to interpret the molecular structure heterogeneity.

Figure 4.92 shows the respective CRYSTAF (normalized) traces for the unfractionated LDPE, Plastomer B, and the blend containing 40% unfractionated Plastomer B. The figure showed that the Plastomer B and LDPE could overlap in the area between 40°C and 60°C.
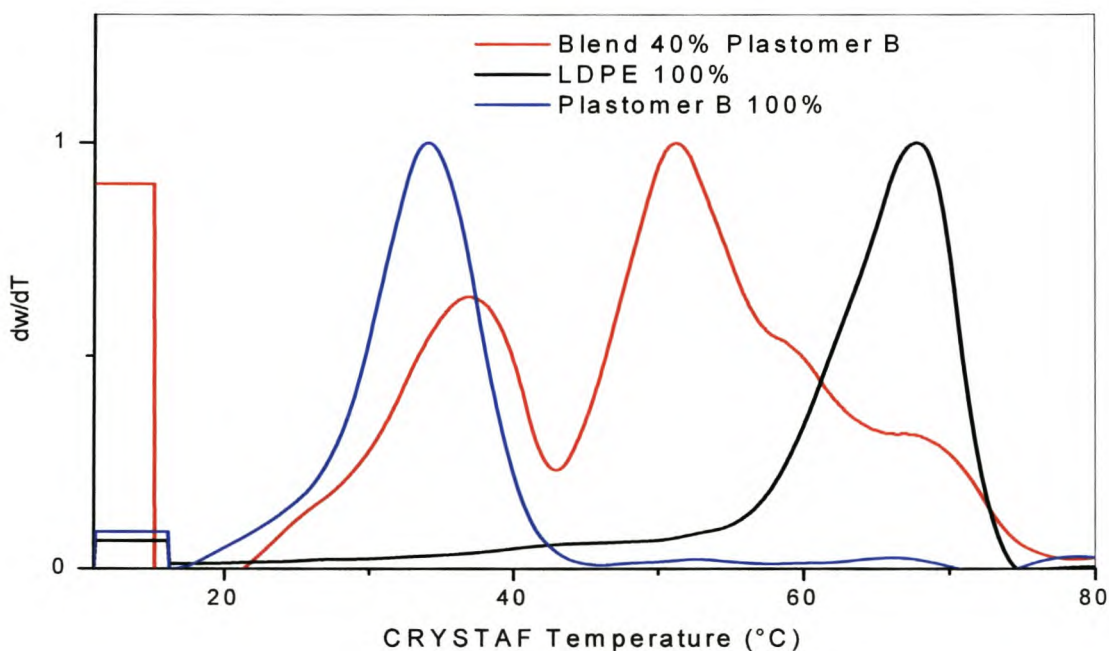
Figure 4.92 CRYSTAF traces for the LDPE, Plastomer B, and blend containing 40% unfractionated Plastomer B.

Figure 4.93 shows the deconvolution of the CRYSTAF trace of unfractionated 40% Plastomer B. The CRYSTAF traces were deconvoluted by fitting a series of four overlapping Gaussian curves. The deconvoluted peaks showed four distinct peaks. The first peak, as indicated with an arrow, corresponded to Plastomer B. The second and third peaks could possibly be the co-crystallized area. The fourth peak corresponded to the LDPE peak. These predictions still needs to be confirmed with NMR data to provide absolute certainty.
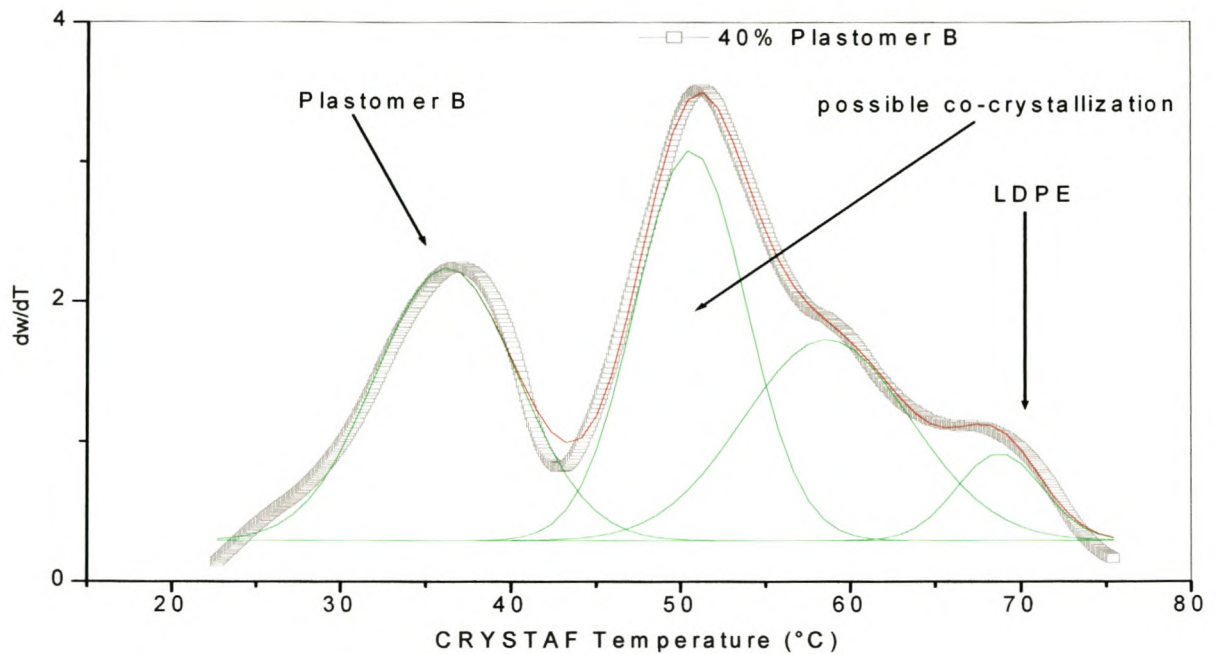
Figure 4.93 Deconvolution of the 40% unfractionated Plastomer B blend.

Figure 4.94 shows the sum of the weight fraction % of the 40% Plastomer B blend on the left Y-axis, the weight fraction % divided by elution temperature range on the right Y-axis, and the Prep-TREF elution temperature on the right X-axis. Figure 4.94 showed multiple peaks. The first peak was assigned to the Plastomer B, the second peak was possibly due to co-crystallization, and the third peak was probably due to the LDPE.
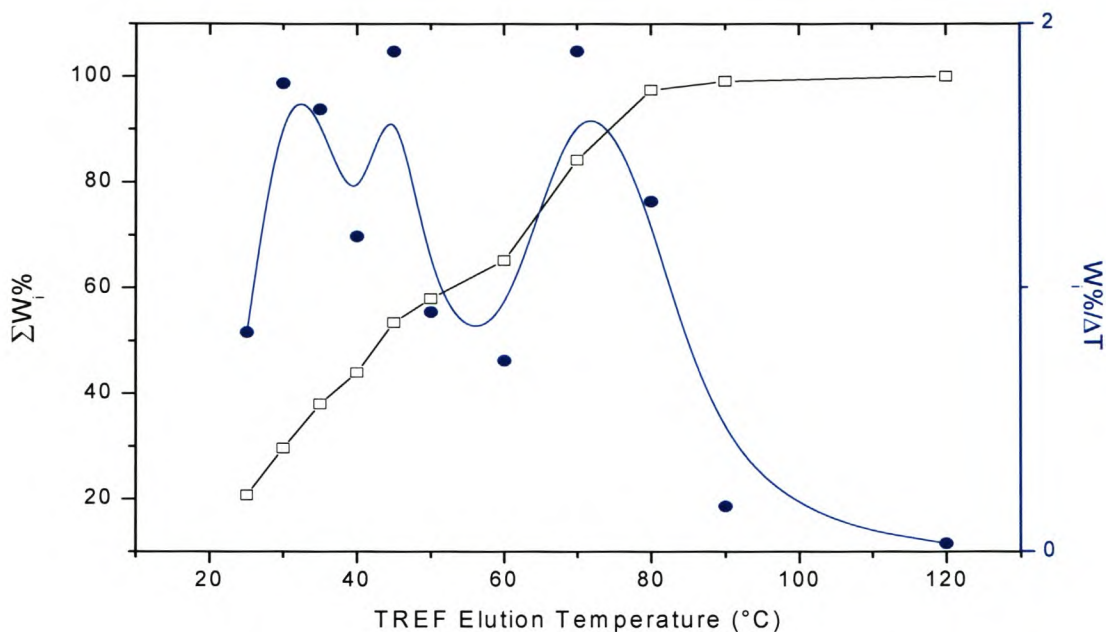
Figure 4.94 Sum of the weight fraction % of the 40% Plastomer B blend as the left Y-axis and weight fraction % divided by elution temperature range on the right Y-axis.

Table 4.15 shows data of the TREF fractions of the 40% Plastomer B blend.

Table 4.15 Data of the TREF fractions of the 40% Plastomer B blend

Temperature (°C)	Mass (g)	Wi	Wi (%)	$\sum Wi\%$	ΔT	Wi%/ΔT
25	0.551	0.207	20.74	20.74	n/a	n/a
30	0.236	0.088	8.86	29.6	5	1.8
35	0.222	0.083	8.37	37.98	5	2.7
40	0.158	0.059	5.96	43.95	5	1.2
45	0.252	0.094	9.47	53.42	5	1.9
50	0.12	0.045	4.53	57.95	5	0.9
60	0.192	0.072	7.21	65.17	10	0.72
70	0.504	0.189	18.95	84.12	10	1.9
80	0.352	0.132	13.26	97.38	10	1.33
90	0.045	0.017	1.7	99.09	10	0.17
120	0.024	0.009	0.9	100	30	0.03

Figure 4.95 shows the combination of the weight fractions curves for the Prep-TREF traces of Plastomer B, the 40% Plastomer B blend, and the 100% LDPE. As was the case for the CRYSTAF traces, here again the blend showed peaks corresponding to those for Plastomer B and for LDPE, and a possible co-crystallization between 50°C and 60°C.
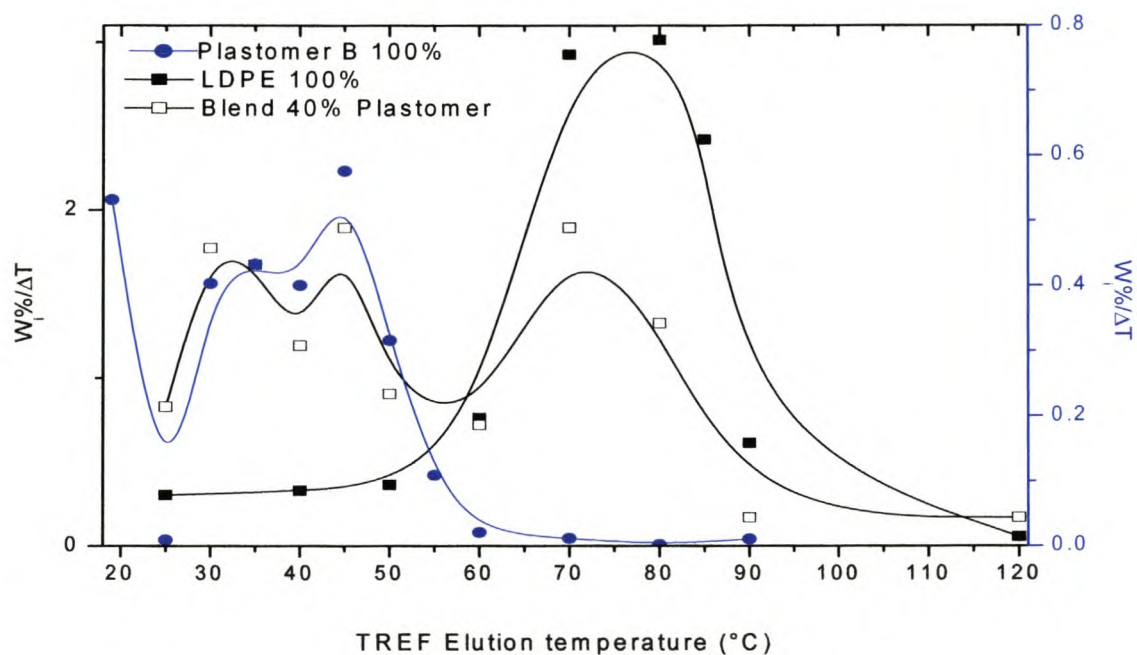
Figure 4.95 The combination of the weight fractions curves for Plastomer B, 100% LDPE, and the 40% Plastomer B blend vs. the Prep-TREF elution temperature.

Figure 4.96 shows the CRYSTAF traces for the Prep-TREF of the blend comprising 40% Plastomer B and 60% LDPE. The unfractionated 40% blend CRYSTAF trace is shown first, followed by the 25°C Prep-TREF CRYSTAF trace that had a crystallization peak just appearing at 20°C. The CRYSTAF peak maxima of all the Prep-TREF fractions will be discussed after Figure 4.97. The 60°C Prep-TREF fractionated CRYSTAF trace had bi-modality and will also be discussed in more detail after Figure 4.97.
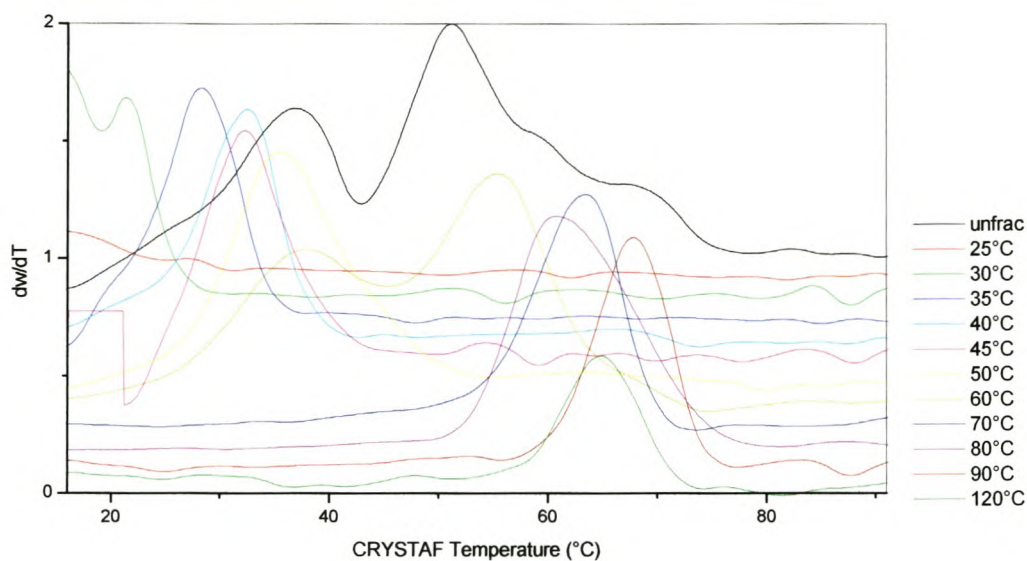
Figure 4.96 The CRYSTAF traces for the Prep-TREF fractions of the blend comprising 40% Plastomer B and 60% LDPE.

Figure 4.97 shows the CRYSTAF peak maxima vs. TREF elution temperature for the Prep-TREF fractions of the 40% blend. The T_c (CRYSTAF peak maximum) increased with an increase in Prep-TREF elution temperature for all the fractions except the 120°C Prep-TREF trace, that had a T_c(CRYSTAF peak maximum) lower than the previous data point. The T_c(CRYSTAF peak maxima) for all the Prep-TREF fractions were also below the $T_{c(TREF)}$ due to the under-cooling effect.
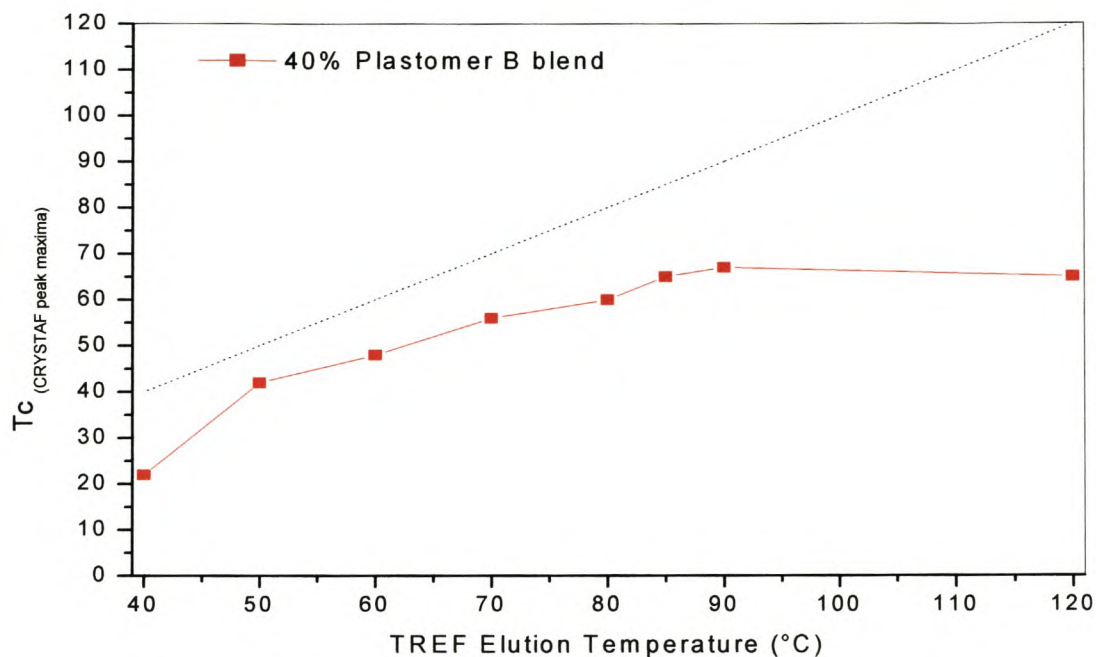
Figure 4.97 The Tc (CRYSTAF peak maxima) for the Prep-TREF fractions of the blend of 40% Plastomer B and 60% LDPE.

Figure 4.98 shows the deconvoluted 60°C Prep-TREF fractionated 40% Plastomer B CRYSTAF trace into two curves by fitting a series of two Gaussian curves. This bi-modality was not expected for a Prep-TREF fraction. The bi-modality can however be explained by the possible presence of co-crystallized crystals that could have eluted in the Prep-TREF elution stage and separated in the CRYSTAF. The mechanisms for TREF and CRYSTAF are similar, although not identical.
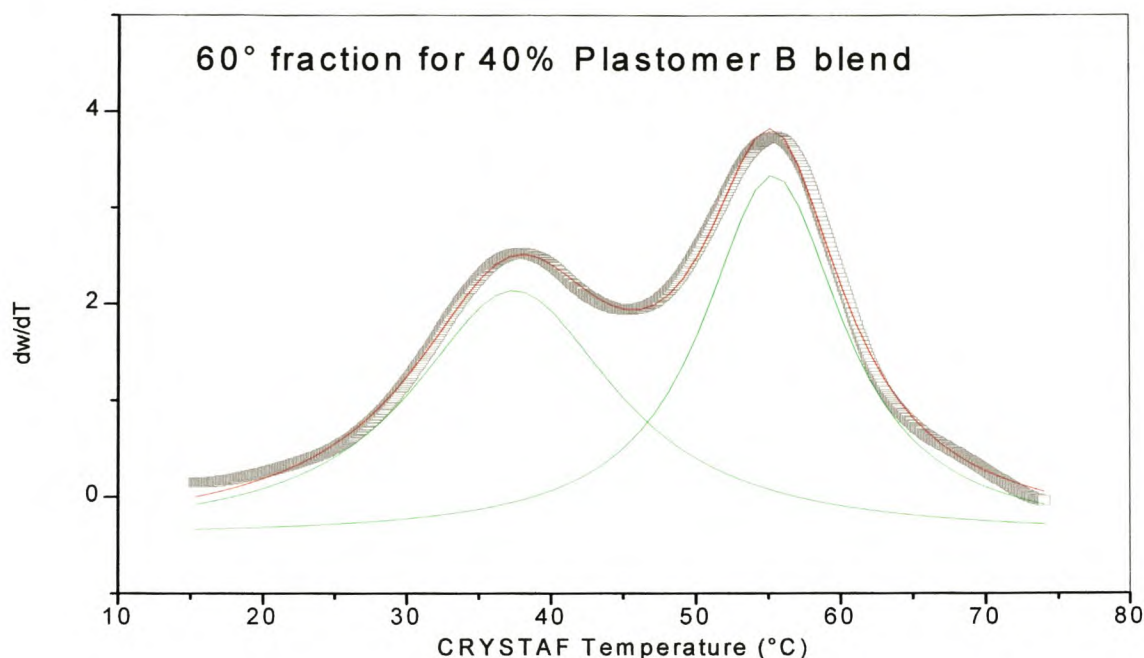
Figure 4.98 The deconvoluted 60°C Prep-TREF fractionated 40% Plastomer B CRYSTAF trace.

Figure 4.99 shows the 3-D plot of the CRYSTAF traces of the Prep-TREF fractions of the 40% Plastomer B and 60% LDPE blend. It showed the heterogeneity of this blend. Figure 4.99 had two peaks. The smaller of the two peaks was a cone-like structure in the low TREF elution temperature, and is probably due to the Plastomer B. The second peak was a single, cone-like structure in the higher TREF elution temperature, and is probably due to the LDPE. It was interesting to see that the two main peaks were connected. This area corresponds to the area where co-crystallization between two materials is possible.
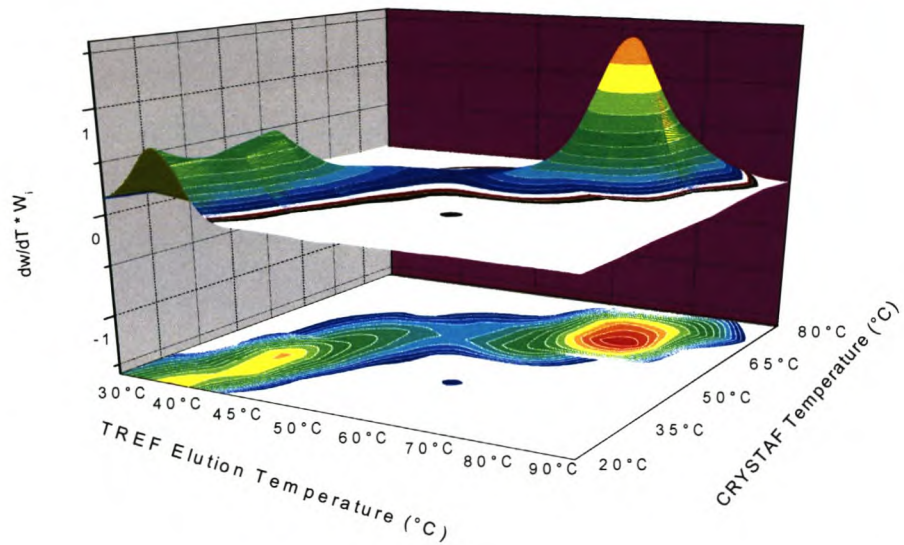
Figure 4.99 3-D plot of the CRYSTAF traces of the Prep-TREF fractions of the 40% Plastomer B and 60% LDPE blend.

Figure 4.100 shows the unfractionated, and the 50°C, 60°C, 70°C and 90°C fraction CRYSTAF (normalized intensities) traces for the 40% Plastomer B and 60% LDPE blend.
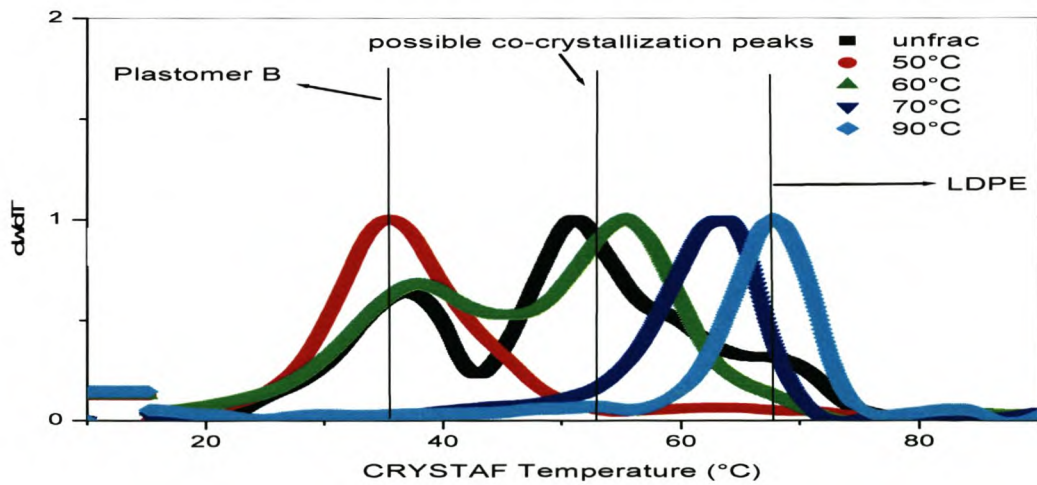
Figure 4.100 The unfractionated, and the 50°C, 60°C, 70°C and 90°C fractionated CRYSTAF traces for the 40% Plastomer B and 60% LDPE blend.

In Figure 4.100 the first line drawn in the figure corresponded to the peak maximum of Plastomer B. The second line drawn in the figure corresponded to a possible co-crystallization peak, and the third line to the peak maximum of the LDPE. Figure 4.100 showed that everything left of the first line could only be 100% Plastomer B. The area of possible co-crystallization was between the first and third lines and only LDPE could be found to the right of the third line. This means that the 50°C trace was probably only Plastomer B and the 60°C trace was probably co-crystallized polymer with a higher concentration of Plastomer B. The 70°C trace was probably also co-crystallized polymer material, but with a higher concentration of LDPE than Plastomer B, hence the peak maximum was shifted to a higher CRYSTAF temperature. The 90°C trace was probably only due to LDPE.

Figure 4.101 shows the HT-SEC traces of the Prep-TREF fractions for the 40% Plastomer B blend.
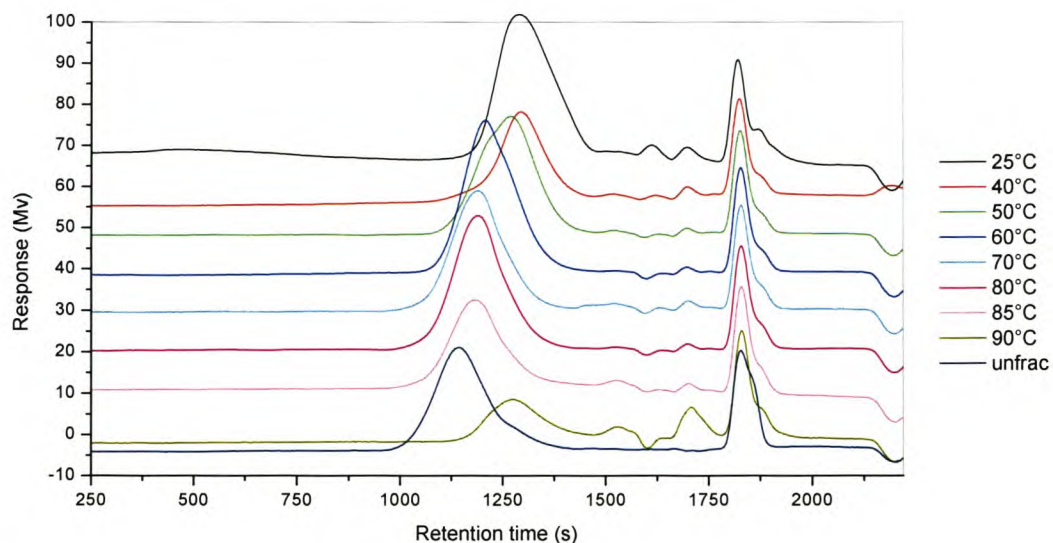
Figure 4.101 HT-SEC traces for the unfractionated and Prep-TREF fractions of the 40% Plastomer B blend.

In Figure 4.101 the 25°C Prep-TREF fractionated HT-SEC trace showed low molecular weight peaks between retention times of 1500 and 1750 seconds. All the traces showed a solvent trace between the retention times of 1750 and 2000 seconds. The higher molecular weight peaks appeared between the retention times of 1500 and 1000 seconds, with a gradual increase in the high molecular weight peak maximum with an increase in the Prep-TREF fraction temperature.

Figure 4.102 shows the 3-D plot for the HT-SEC traces of the Prep-TREF fractions of the 40% Plastomer B blend.
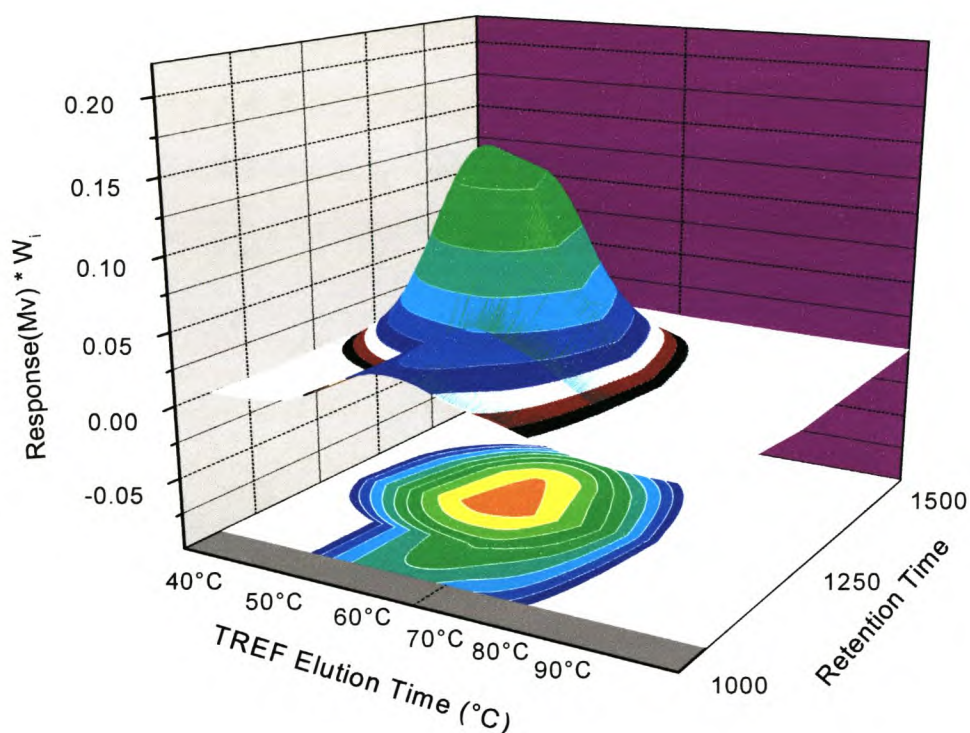
Figure 4.102 3-D plot for the HT-SEC traces of the Prep-TREF fractions for the 40% Plastomer B blend.

The DSC analysis of the TREF fractions is discussed and presented in Section 4.11.

4.9) Characterization of the morphology of LDPE and LDPE/plastomer blends

In this section the effect of various blending ratios of the two plastomers to the LDPE on the morphology of the blends was investigated. DSC was used to monitor the effects of the amount of plastomer on the crystallization and melting characteristics of the blend. Etching and SEM analysis were used to monitor how the nature of the crystallinity varied. Finally the effect of the blending ratios on the physical and mechanical properties were investigated.

4.9.1) DSC

Figure 4.103 shows the overlay of the melting and crystallization curves of the LDPE with different ratios of blending with Plastomer A (PL1881).

Figure 4.104 shows the DCS results of the LDPE and Plastomer B (VP8770) blends.

Figure 4.105 shows the DSC results for the 100% Plastomer A (PL1881) and 100% Plastomer B (VP8770).
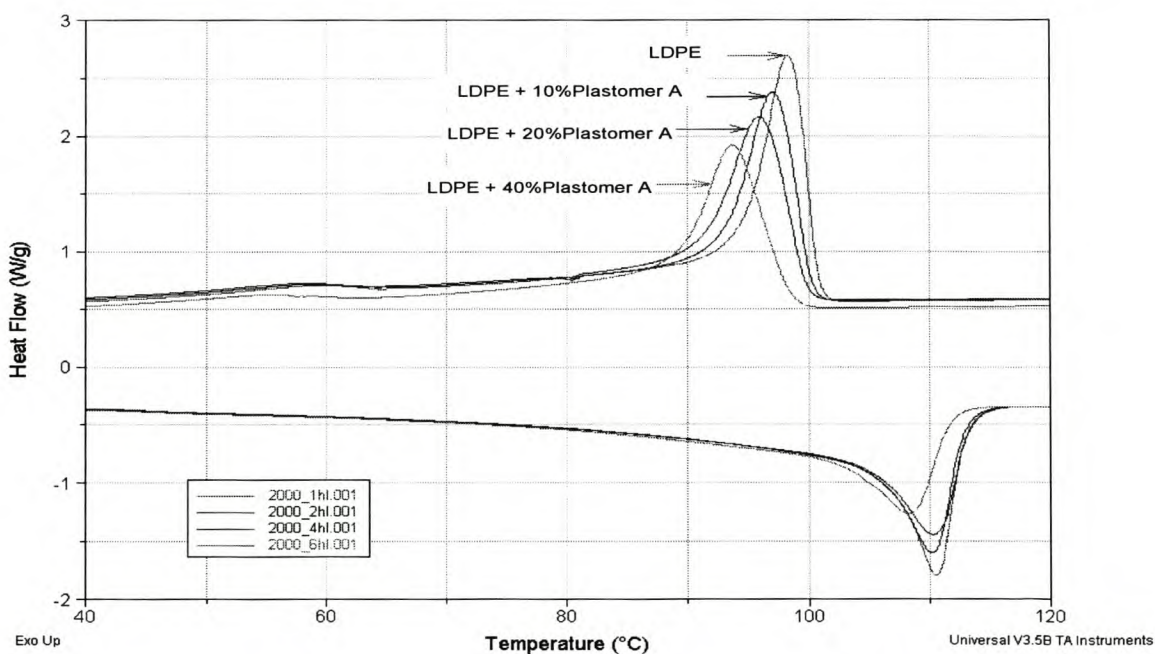
Figure 4.103 The overlay of melting and crystallization curves of LDPE blended with Plastomer A at different levels.

130
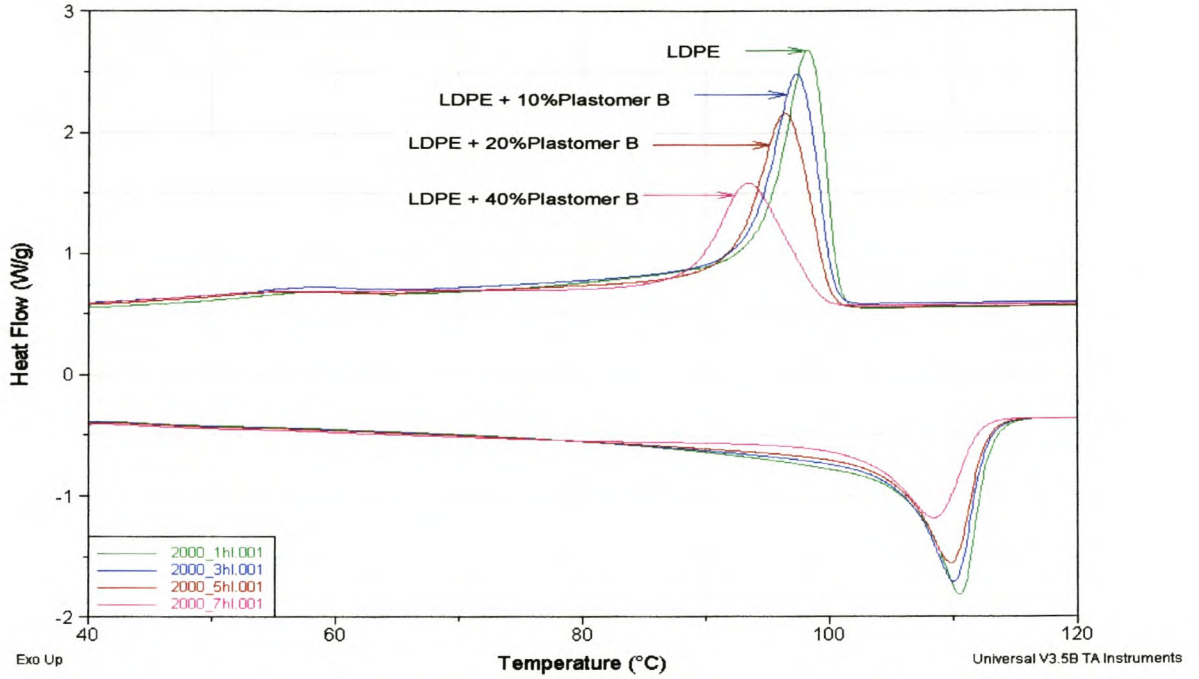
Figure 4.104 The overlay of melting and crystallization curves of LDPE blended with Plastomer B at different levels.
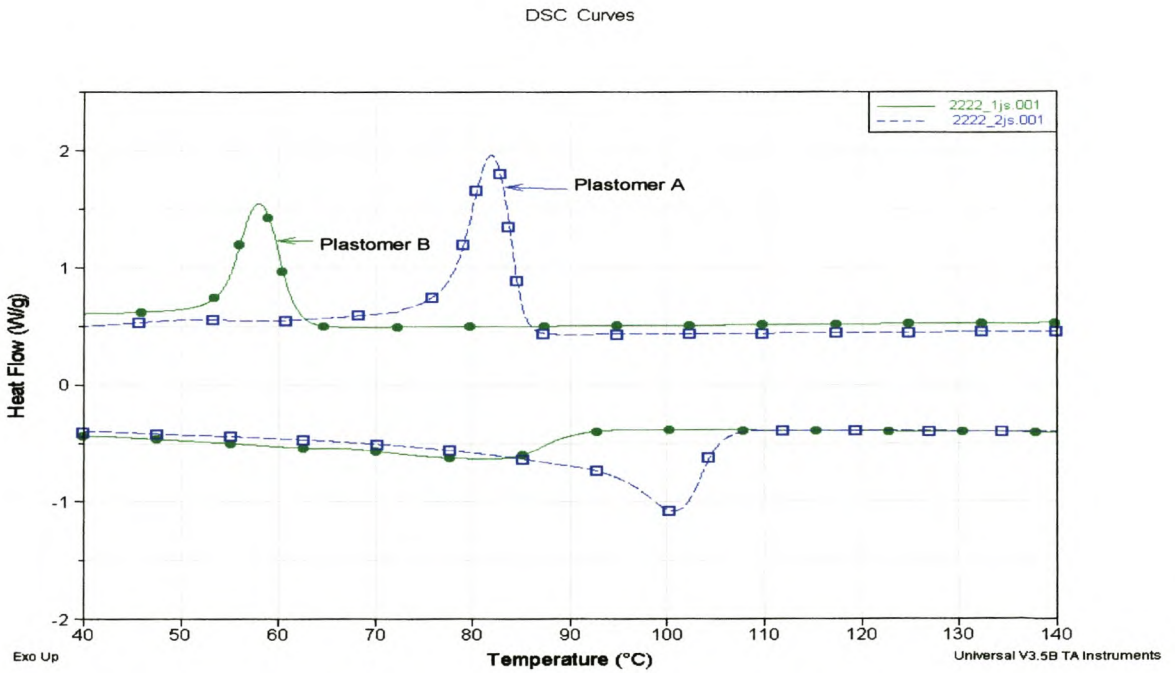
Figure 4.105 Overlay of the melting and crystallization curves of the plastomers (A and B).

Figures 4.103 – 4.105 show the DSC results of the blending ratios of 10%, 20% and 40%. Plastomer A and Plastomer B blends did not phase separate during crystallization, since there was only one melt and crystallization peak for the unfractionated blends. The crystallization and melting peaks broadened with increasing amount of each plastomer. It was therefore concluded that as the concentration of the plastomer increased, the peak temperature of melting of LDPE, its onset, the final temperatures of melting, and the crystallinity, would decrease notably.

Figure 4.105 shows that Plastomer B (higher octene content polymer) had a crystallization peak at a lower temperature than Plastomer A and, as expected, a lesser degree of crystallinity.

Tables 4.16 and 4.17 show the DSC raw data for the melting and crystallization properties of LDPE and its blends with Plastomer A and with Plastomer B, respectively, at different blending ratios.

Table 4.16 The melting and crystallization properties of LDPE and its blends with Plastomer A (PL 1881) at different blending ratios

Melting properties	100% LDPE	10%A	20% A	40% A	100%A
Maximum Temp of melting Tm (°C)	113.02	112.89	113.37	111.82	105.54
Peak temperature(s) (°C)	110.61	110.23	110.44	108.38	88.06; 100.87
Onset temperature of melting (°C)	105.37	104.27	103.25	100.06	90.81
Heat of melting (J/g)	71.46	66.60	65.39	59.66	50.71
% Crystallinity	24.39*	22.73*	22.32*	20.36*	-
Crystallization properties:					
Starting temperature Tc (°C)	100.79	100.22	99.79	98.44	85.3
Peak temperature(s) (°C)	98.31	97.14	95.99	93.79	82.03
Final temperature (°C)	94.43	92.89	90.89	89.38	77.57
Heat of crystallization (J/g)	61.28	54.52	64.56	51.67	52.58
% Crystallinity	20.91*	18.61*	22.04*	17.64*	-
Supercooling (Tm-Tc) (°C)	12.23	12.67	13.58	13.38	20.24

*Based on the theoretical value of 293J/g for 100% crystalline polyethylene

Table 4.17 The melting and crystallization properties of LDPE and its blends with Plastomer B (VP8770) at different blending ratios

Melting properties	100% LDPE	10%B	20%B	40%B	100%B
Maximum Temp of melting Tm (°C)	113.02	112.75	112.68	112.16	90.63
Peak temperature(s) (°C)	110.61	110.10	109.89	108.61	63.04; 82.48
Onset temperature of melting (°C)	105.37	104.87	104.45	102.86	56.42
Heat of melting (J/g)	71.46	63.45	56.35	30.65	34.38
% Crystallinity	24.39*	21.66*	19.23*	10.46*	-
Crystallization properties:					
Starting temperature Tc (°C)	100.79	100.38	100.10	99.36	61.86
Peak temperature(s) (°C)	98.31	97.45	96.47	93.57	58.1
Final temperature (°C)	94.43	93.50	92.34	88.75	54.1
Heat of crystallization (J/g)	61.28	53.36	51.03	38.15	33
% Crystallinity	20.91*	18.21*	17.42*	13.02*	-
Supercooling (Tm-Tc) (°C)	12.23	12.37	12.58	12.80	28.77

*Based on the theoretical value of 293J/g for 100% crystalline polyethylene

Figure 4.106 shows the onset of melting vs. the weight fraction of LDPE. The presence of plastomer in LDPE lowered the melting properties of the blends. The LDPE and Plastomer B blends seemed less affected by the onset of melting than the Plastomer A and LDPE blends.

Figure 4.107 shows the % crystallinity vs. the weight fraction of LDPE. Plastomer A displayed higher melting and crystallization temperatures than Plastomer B. Plastomer A also had a higher heat of melting, implying that Plastomer A is more crystalline than Plastomer B.
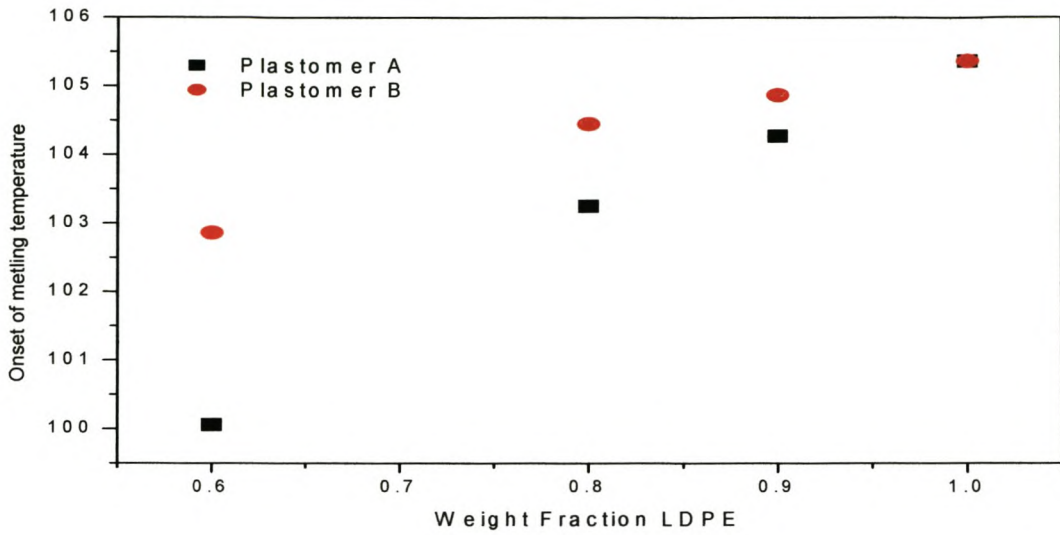
Figure 4.106 The onset of melting vs. the weight fraction LDPE in blends.
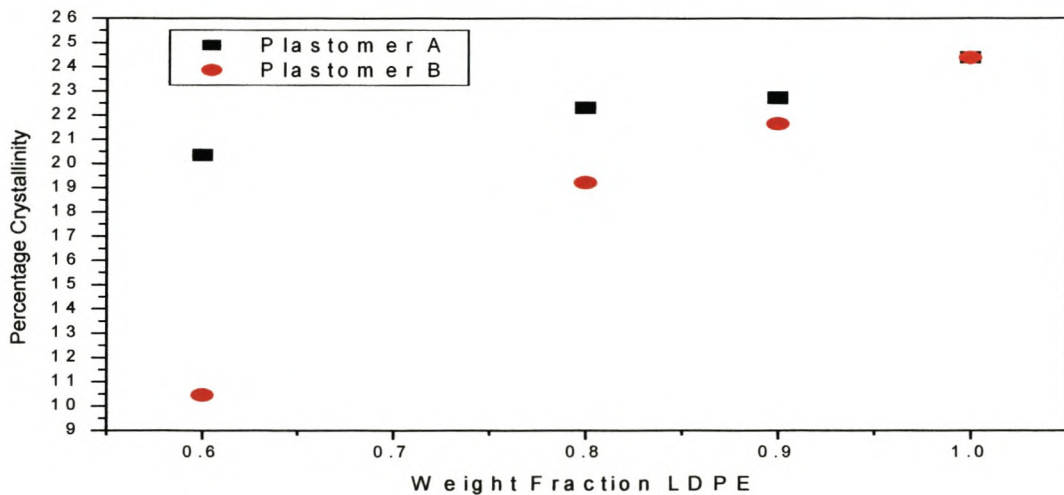
Figure 4.107 The percentage crystallinity vs. the weight fraction LDPE in blends.

The presence of Plastomer B had a more dramatic effect on the decrease in % crystallinity than Plastomer A. This is expected since Plastomer B has a much higher octene content than Plastomer A.

4.9.2) Scanning electron microscopy

Scanning electron microscopy was used to actually look at the surfaces of polymer samples and see the morphological changes that resulted from the blending of our LDPE and the plastomers. It was necessary to first etch the polymer films, for two reasons. The first was to remove the amorphous polymer and show the crystal structure and the second was to create less flat surfaces, since the scanning electron microscope requires uneven surfaces for high resolution pictures. The literature describes two ways in which polymers can be etched[6,7]: permanganic etching and chloro-sulfonic fixation. The experimental procedure followed in the present study was described in the experimental section (Section 3.3). The most efficient etching time was determined by calculating the % weight loss after X minutes of etching:

% weight loss = (mass after X minutes of etching) / (mass at beginning) x 100.

Table 4.18 shows the results for the % mass fraction after different etching times. Upon looking at the mass lost during the different etching times it was clearly seen that the greatest mass loss was at 90 minutes. The SEM pictures for the 90-minutes etching also showed the best results. All the SEM pictures are shown in Appendix A. The SEM results confirmed that the blend ratios did indeed affect the morphology of the blends.

Table 4.18 Percentage mass fraction after different etching times for LDPE and LDPE/plastomer blends

	Weight loss after various times		
	40 min	60 min	90 min
LDPE (100%)	0.099	0.1173	0.1212
LDPE (90%) + (10%) PL1881	0.0977	0.102	0.1113
LDPE (80%) + (20%) PL1881	0.1162	0.1189	0.1278
LDPE (60%) + (40%) PL1881	0.1198	0.1289	0.1309
LDPE (90%) + (10%) VP8770	0.1253	0.1289	0.1408
LDPE (80%) + 20%) VP8770	0.1289	0.1301	0.1434
LDPE (60%) + (40%) VP8770	0.1336	0.1387	0.1567
PL1881 (100%)	0.1198	0.1298	0.1301
VP8770 (100%)	0.5443	0.5543	0.5546

4.10) Physical properties of the LDPE and plastomer blends

The physical properties of the blends of LDPE and Plastomer A and LDPE and Plastomer B are a direct result of changing the morphology of the blends. The morphology of the blends was altered by changing the molecular structure of the blends. This was achieved by changing the blend ratios. Table 4.19 shows the results of some physical properties of LDPE and the blends, including the following:

- There was no significant difference in the Haze measurements with an increase in plastomer content.

- The gloss of blends that included Plastomer A and Plastomer B decreased slightly as the plastomer content increased.

- The tear strength in the machine direction (MD) decreased with an increase in plastomer content.

- The tear strength was indirectly proportional to the machine direction and increased with an increase in plastomer content.

Table 4.19 Physical properties of LDPE and some blends of LDPE/Plastomer A (PL1881) and LDPE/Plastomer B (VP 8770)

Grade:	Haze (%) ASTM D1003	Gloss (units) ASTM D2457	Tear Strength (g/um)ASTM D1922	
			MD	TD
LDPE	9.92	55.5	18.3	3.68
LDPE +10% Plastomer A	10.5	52	14.7	4.16
LDPE +10% Plastomer B	9.81	55.1	6.25	3.92
LDPE +20% Plastomer A	10.7	51.2	4.92	4.3
LDPE +20% Plastomer B	10.1	53.8	4.32	7.25
LDPE +40% Plastomer A	10.7	49.3	2.5	19.2
LDPE +40% Plastomer B	9.65	49.3	2.16	15.8

Table 4.20 shows some further physical properties of LDPE and the blends with the two plastomers.

Table 4.20 Further physical properties of LDPE and some blends of LDPE/Plastomer A (PL1881) and LDPE/Plastomer B (VP 8770)

Grade	Impact Strength F50 ASTM D1709	Thickness Variation (μm)			Static and Dynamic Coefficients of Friction ASTM D1894	
	(g)	Min	Max	Mean	uS	uD
LDPE	88	25	34	30.3	0.12	0.08
LDPE + 10% Plastomer A	88	29	34	31.4	0.13	0.09
LDPE + 10% Plastomer B	103	25	31	28.9	0.13	0.1
LDPE + 20% Plastomer A	100	27	32	28.8	0.12	0.09
LDPE + 20% Plastomer B	100	29	35	32.2	0.12	0.09
LDPE + 40% Plastomer A	160	27	34	30.2	0.13	0.09
LDPE + 40% Plastomer B	448	28	32	29.9	0.13	0.1

It showed that in the case of both plastomers the impact strength increased with an increase in plastomer content. It was evident that the most dramatic changes occured between the 20% and 40% plastomer blending ratios. For all the blending ratios it was evident that plastomer B (higher octene content) has a greater influence on the impact strength of the materials.

4.11) Comparing 3-D CRYSTAF results with 3-D DSC results

In this section DSC data will be presented for Plastomer B and a 40% Plastomer B + 60% LDPE blend, followed by 3-D DSC plots for the Plastomer B and the 40% Plastomer B + 60% LDPE blend. The DSC 3-D data will be compared with the 3-D CRYSTAF data. (Unfortunately DSC results for Plastomer A and the 40% blend were not available for inclusion in this document.)

Figure 4.108 shows the DSC crystallization peaks for the Prep-TREF fractions of the blend of 40% Plastomer B + 60% LDPE. The first line in the figure corresponded to the peak

maximum of the unfractionated Plastomer B. The second line corresponded to the peak maximum of the unfractionated LDPE. The peak maxima of the DSC crystallization peaks moved to higher temperatures with an increase in the Prep-TREF fraction elution temperature. Similar to the CRYSTAF traces, the 25°C and lower temperature fractions showed broad peaks.
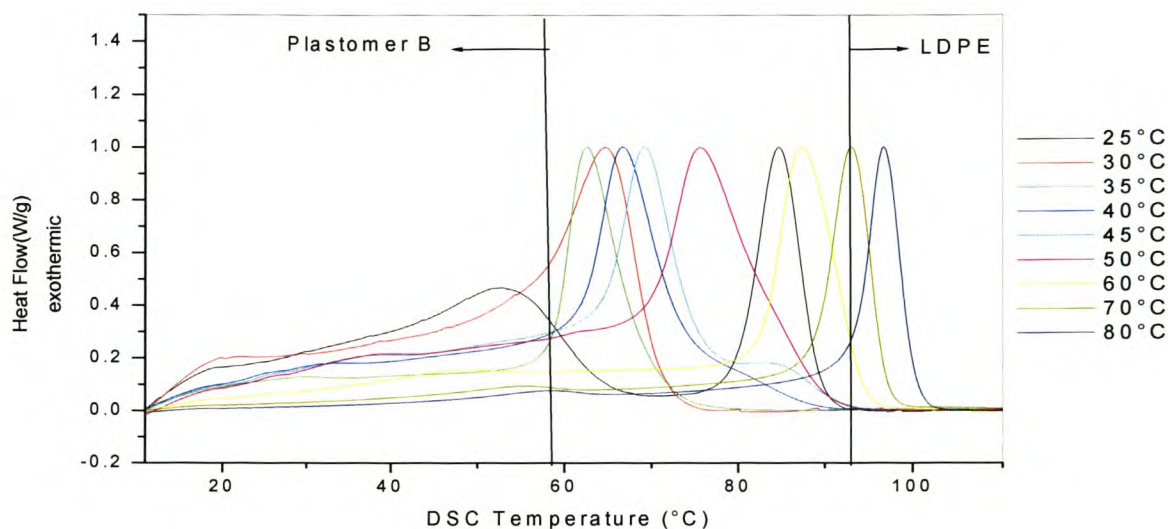
Figure 4.108 The DSC crystallization peak traces of the blend of 40% Plastomer B and 60% LDPE.

The information on this heterogeneity seen in these 3-D graphs is much clearer and user friendly, and provides more immediate information than any 1-D graph could ever do.

Figures 4.109-111 show the 3-D DSC and CRYSTAF plots of the LDPE, Plastomer B and the 40% blend. These 3-D CRYSTAF plots have been presented previously (Sections 4.3; 4.7; 4.8: Figures 4.14; 4.67; 4.99) but are shown again here - to simplify the comparison between the 3-D CRYSTAF and 3-D DSC data.
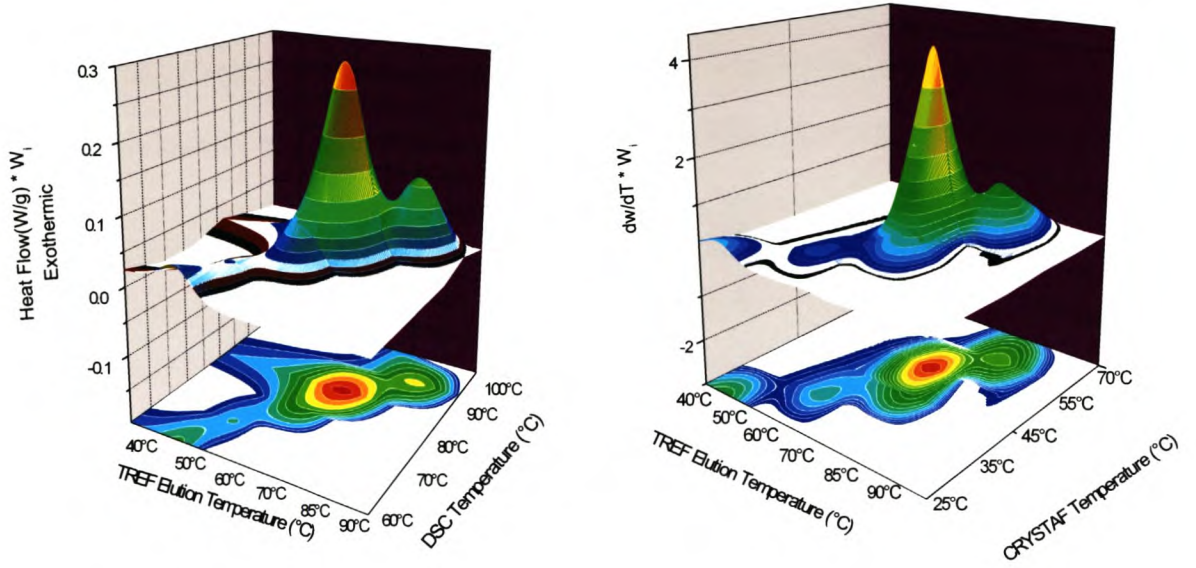
Figure 4.109 The 3-D DSC and CRYSTAF plots of the LDPE.
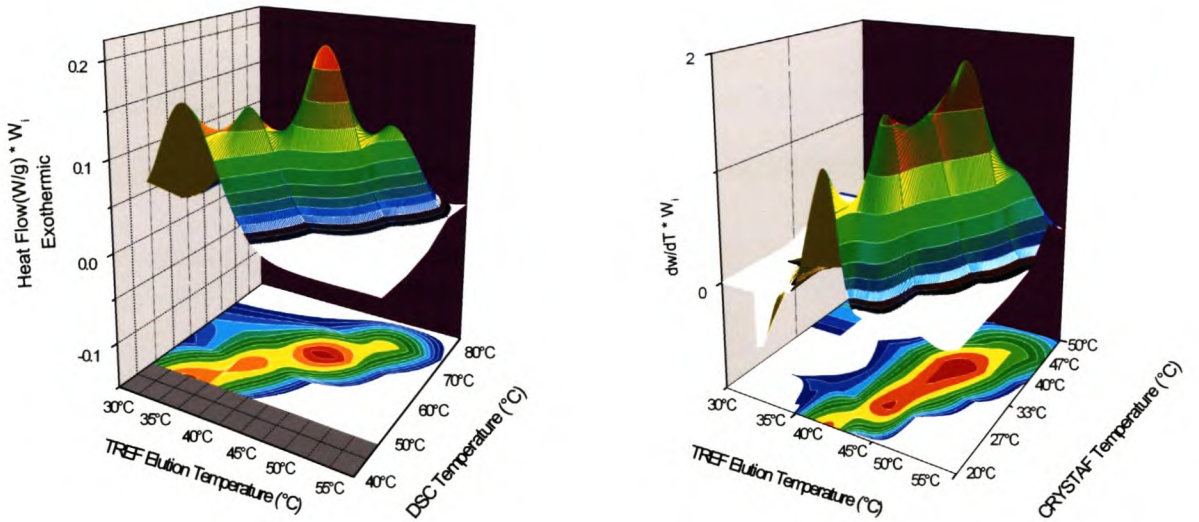
Figure 4.110 The 3-D DSC and CRYSTAF plots of the Plastomer B.
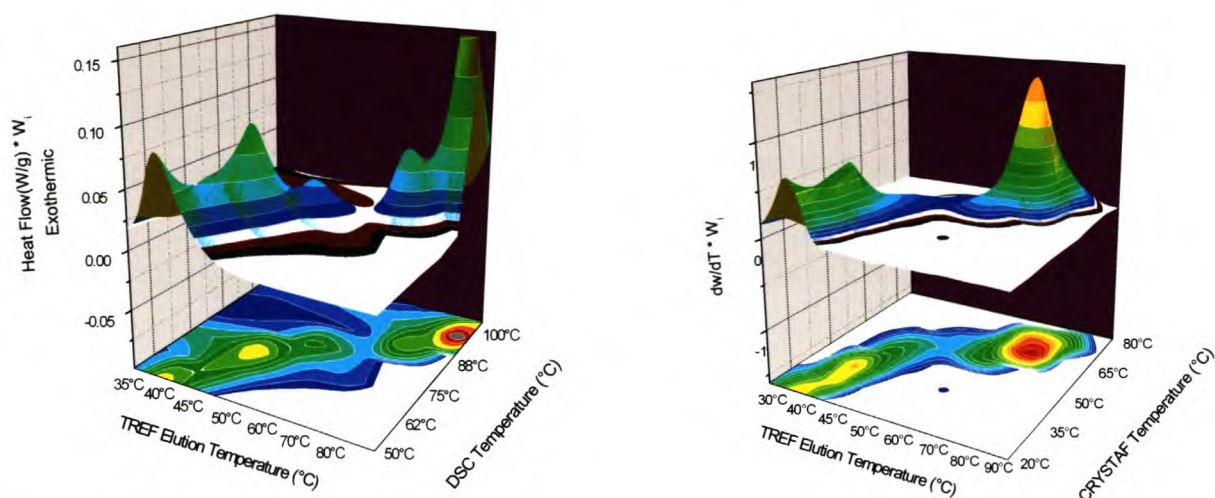
Figure 4.111 3-DSC and CRYSTAF plot showing the heterogeneity of the LDPE and 40% Plastomer B blend.

When the 3-D plots of the TREF elution temperature versus CRYSTAF and TREF elution temperature versus DSC (crystallization) for the LDPE are compared (Figure 4.109), the two figures show remarkable similarities in the features that are observed. The main difference is the shift of the features position on the CRYSTAF and TREF axis, with the main peak appearing at about 65°C on the CRYSTAF axis and 85°C on the DSC axis.

A comparison of the 3-D plots (Figure 4.110) for the Plastomer B also shows remarkable similarity with, once again, the shift in the peak position on the CRYSTAF and DSC axes. The 40% Plastomer B blend also have similar feature in each of the blends.

It is clear from the plots that, as expected, there is a correlation between the TREF elution temperature and the two techniques for monitoring the crystallizability, namely CRYSTAF and DSC. Presenting this data in the 3-D plots allows for an easy visualization of the molecular heterogeneity in the polymer samples with regards to their crystallizability. These plots, for example, show features that are not easily identifiable in simple 1 or 2 dimensional plots. However great care needs to be taken in interpreting these plots as the appearance of individual peaks and bimodality can be misleading and can be a result of experimental factors. It should be noted that in the case of the 3-D DSC plot, each thermogram was first baseline zeroed,

normalized and then weighted to produce the 3-D plots. No correlation however could be made using 3-D SEC graphs, between TREF and SEC. This is not unexpected since the fractionation mechanism in TREF is based on crystallizability and not molecular weight.

References:

1.   Monrabal, B., *Temperature rising elution fractionation and crystallization analysis fractionation.* Encyclopaedia of Analytical Chemistry. 2000, p.8074-8094.

2.   Hanson, E., *N.m.r characterization of polyethylene with emphasis on internal consistency of peak intensities and estimation of uncertainties in derived branch distribution numbers.* Polymer, 1997, **17**: p.4295-4304.

3.   Wild, L. and Knobeloch, D.C., (1991) US Patent 5,030,713

4.   Randall, J., *Long-Chain Branching in Polyethylenes. Polymer Characterization by ESR and NMR*, 1980, **6**: p.93.

5.   Junting, X., and Feng, L., *Application of temperature rising elution fractionation in polyolefins.* Eur. Polym. J., 2000, **36**: (5) p.868

6.   Morgan, R.L., Hill, M.J., and Barham, P.J., *Morphology,melting behaviour and co-crystallization in polyethylene blends:the effect of cooling rate on two homogeneously mixed blends.* Polymer, 1999, **40**: p.337-348.

7.   Olley, R.H., *A Permanganic Etching for Polyolefins.* J. Polym. Sci.: Part B Polym. Phys., 1979, **17**: p.627-643.

CHAPTER 5

CONCLUSIONS AND RECOMMENDATIONS

5.1)   Conclusions

A new, fully functional Prep-TREF apparatus was designed, built and optimized. It successfully fractionated LDPE according to its crystallizability. This Prep-TREF was optimized by designing improved, more specific columns, and testing various cooling rates. Success was also achieved with showing the effects that different cooling rates and polymer quantities had on the quality of fractionation.

It was concluded from experimental results that the quench cooling forced progressively more crystallizable fraction to elute at a lower temperature in the TREF. Quench cooling also caused broadening in the Prep-TREF fractionated CRYSTAF traces. Further, on-support crystallization in Prep-TREF seemed to be better than off-support crystallization, since with the on-support crystallization a broader Prep-TREF weight fraction curve was obtained, relative to the off-support. This conclusion is further supported by the fact that the CRYSTAF traces for the Prep-TREF fractions of the on-support crystallized LDPE were narrower than the CRYSTAF traces of the Prep-TREF fractions of the off-support crystallized LDPE. If time is not a major factor, and the best possible results are required – as in this study, then on-support crystallization in Prep-TREF was determined to be the most preferable. Off-support crystallization does however have the advantage of a much higher cooling rate and therefore a higher "turnaround" cycle.

Using the newly developed Prep-TREF it was possible to successfully fractionate Plastomers A and B (Dow Chemicals Affinity plastomer range.) Results showed that these two metallocene-catalyzed plastomers had more homogeneity in their molecular structure relative to the LDPE, yet still showed heterogeneity in the molecular structure, as illustrated with the Prep-TREF fractions, showing shifting of the peak maxima in the DSC and CRYSTAF traces. This heterogeneity in the plastomers was further illustrated using the 3-D graphs of the DSC and CRYSTAF traces of the plastomers. Blends of LDPE with the respective plastomers were also fractionated. The results of the fractions obtained from the blends were then interpreted, to try and understand the influences that the molecular structure had on the physical properties of the blends. This was done in conjunction with

143

using the information acquired from the results of the fractionation of the LDPE and plastomers individually.

Further, it was possible to create 3-D graphs for better visualization of the CRYSTAF data and DSC data of the Prep-TREF fractions. This offered a new and useful way to present data since features not easily seen in one dimension were now more apparent.

The 3-D plots showed very good correlation between the TREF elution temperature and the CRYSTAF and DSC results. A comparison between these two plots also showed similar features. The correlation between the TREF elution temperature and the two techniques for monitoring the crystallizability (DSC and CRYSTAF) confirmed that the newly developed Prep-TREF was successfully fractionating according to molecular crystallizability.

It was also shown that different blending ratios of the two plastomers with LDPE had a dramatic effect on the physical properties of the blends. As expected, the higher octene-content plastomer B had the most dramatic effect on the reduction of the amount of crystallinity while simultaneously leading to the best improvement in the mechanical properties, such as impact strength.

5.2) Recommendations for future work

1.) It is recommended that the effects of on-support and off-support crystallization be investigated further. The study should be expanded to include polypropylene polymers since it is possible that there could be additional effects in the fractionation of polyolefins due to a homogeneous (PE) versus heterogeneous (PP) crystallization environment.

2.) The Prep-TREF should be designed or modified to fractionate at sub-ambient temperatures since the 25°C room-temperature fraction still contains crystallizable material. The easiest way to accommodate sub-ambient temperatures would probably be to use one controlled environment for the crystallization and elution steps of the Prep-TREF. The CRYSTAF results for these sub-ambient temperature fractions will not be able to be dissolved in TCB, since TCB freezes at 18°C. A solvent like heptane should be used for the CRYSTAF results.

3.)   The effects of the various plastomer/LDPE blending ratios need to be investigated further. Furthermore, the optimal blending ratios should be determined.

4.)   It is recommended that the Prep-TREF fractions of the 40% Plastomer A blend also be analysed by DSC and 3-D plots, similar to the analyses done for LDPE and Plastomer B.

Appendix A
(Scanning electron microscopy)

In Appendix A the first numerical number illustrates the type of polymer or polymer blend used. The next alphabetical letter shows the time the sample was etched. The final numerical numbers ending with an "x" shows the scale of magnification.

1 = LDPE 100%

2 = XHF77/50+ 10% PL1881

3 = XHF77/50+ 20% PL1881

4 = XHF77/50+ 40% PL1881

5 = XHF77/50+ 10% VP8770

6 = XHF77/50+ 20% VP8770

7 = XHF77/50+ 40% VP8770

8 = PL1881 100%

9 = VP8770 100% (least crystalline)

A = 40 minutes etched

B = 60 minutes etched

C = 90 minutes etched

Thus 1a5000x means pure LDPE etched for 40 minutes and 5000 times enlarged.
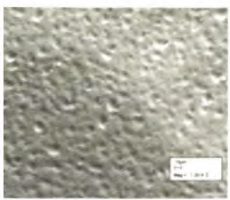
1a1000x

1a5000x

1a20000x

1b1000x
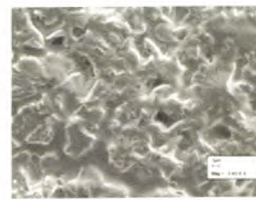
1b5000x

1c400x
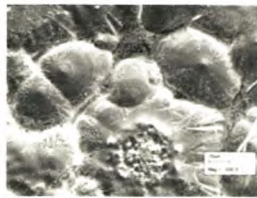
1c500
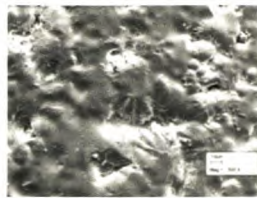
1c500(2)x
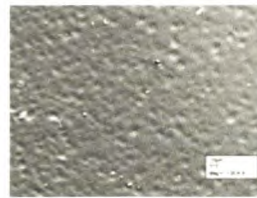
2a1000x
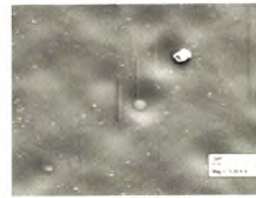
2a5000x
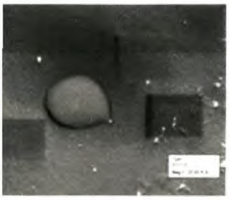
2a20000x
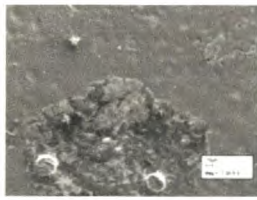
2b1000x
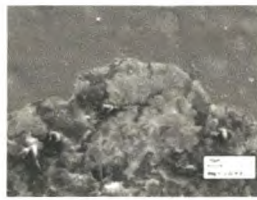
2b2000x
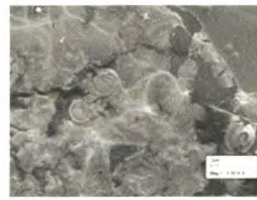
2b5000x
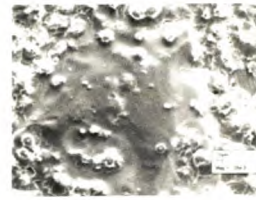
2c250x
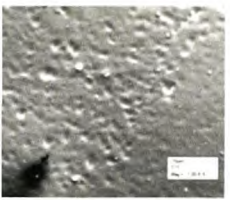
3a1000x
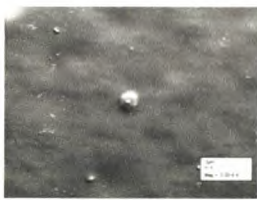
3a5000x

3a20000x
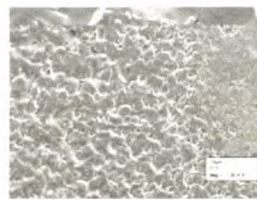
3b1000x
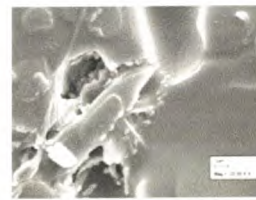
3b20000x
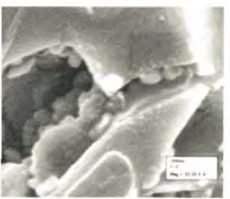
3b50000x
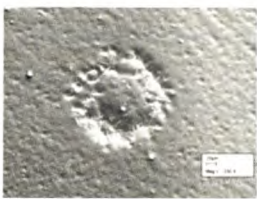
3c250x
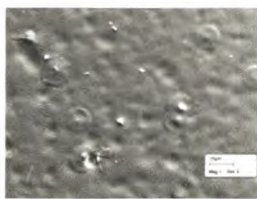
3c500x
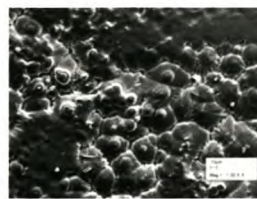
4a1000x

4a5000x

4a20000x
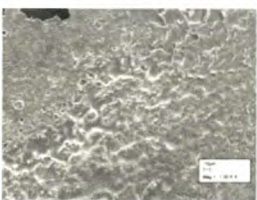
4b1000x
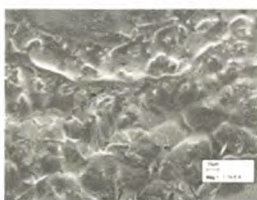
4b1000x2
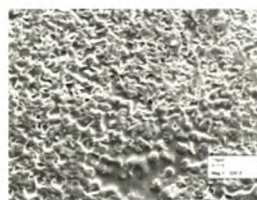
4c500x
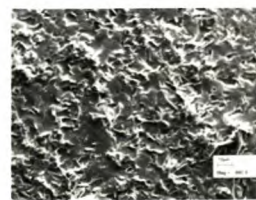
4c660x
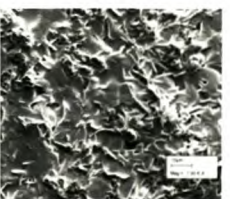
4c1000x

5a5000x
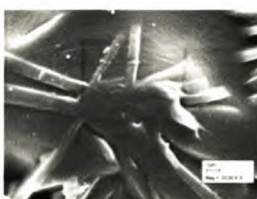
5a20000x
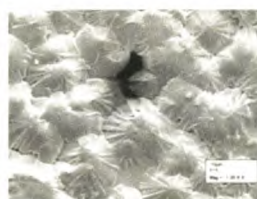
5b1000x

5b5000x
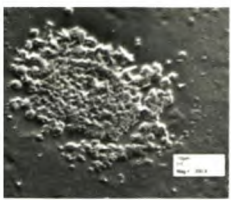
5c200x

5c300x

5c500x
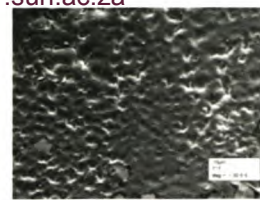
6a1000x
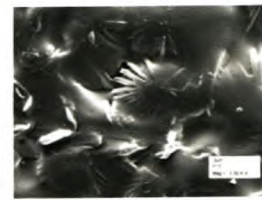
6a5000x
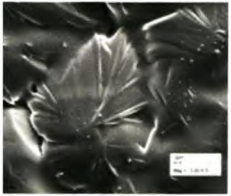
6a5000x2
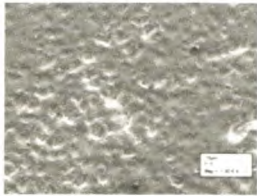
6b1000x
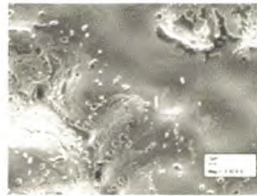
6b5000x
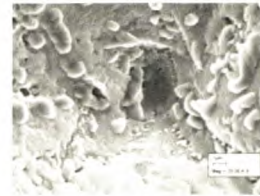
6b20000x
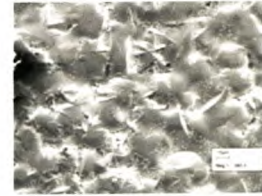
6c500x

6c1000x
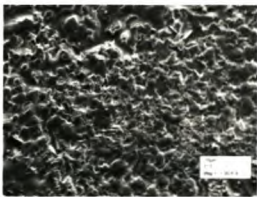
7a1000x
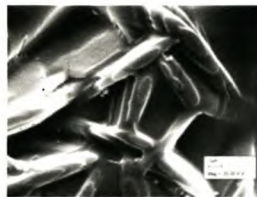
7a20000x

7b1000x
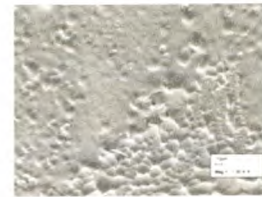
7b1000x2
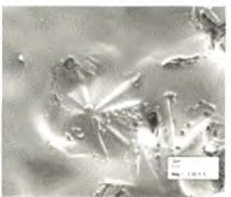
7b5000x
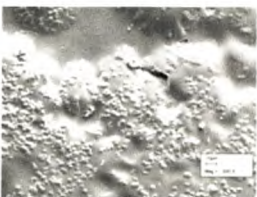
7c500x
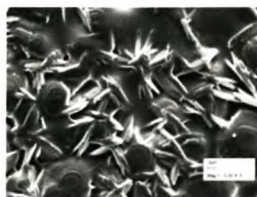
7c5000x

8a1000x
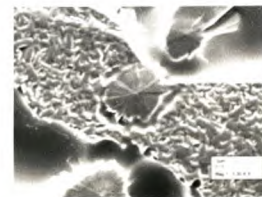
8a5000x

8a5000x2

8a20000x

8b180x
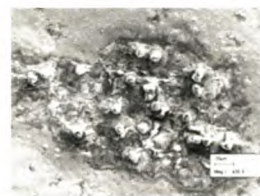
8b500x

8b1000(2)
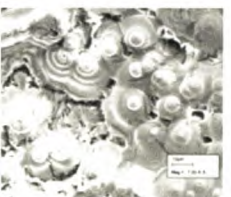
8b1000x

8c250x

8c1000x
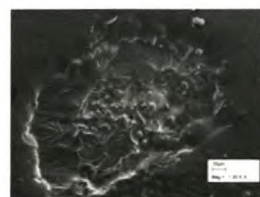
9a1000x
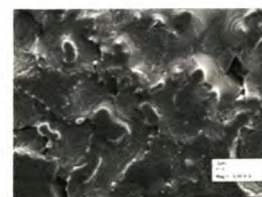
9a5000x
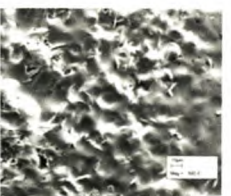
9b500(2)
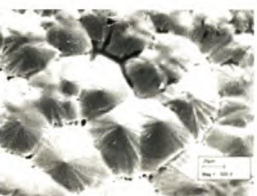
9b500x

9b1000

Appendix B
(NMR results of Plastomer A)
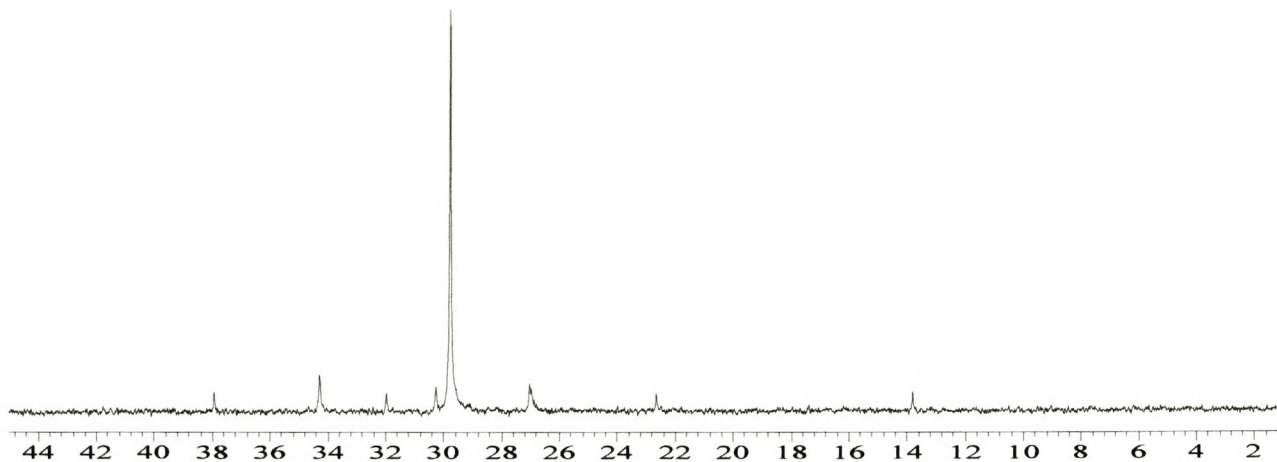
^{13}C NMR of the Prep-TREF 40°C fraction of Plastomer A
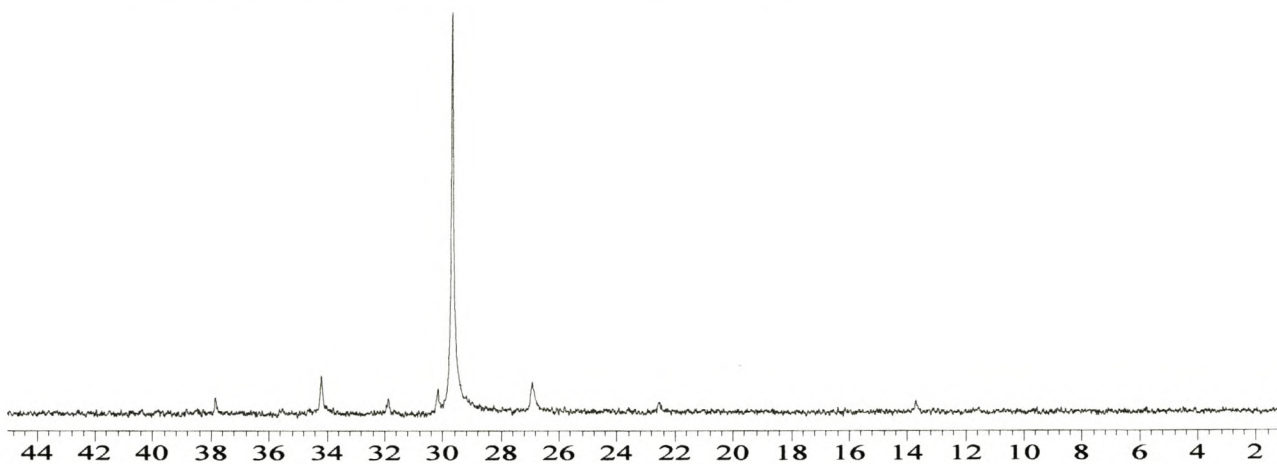
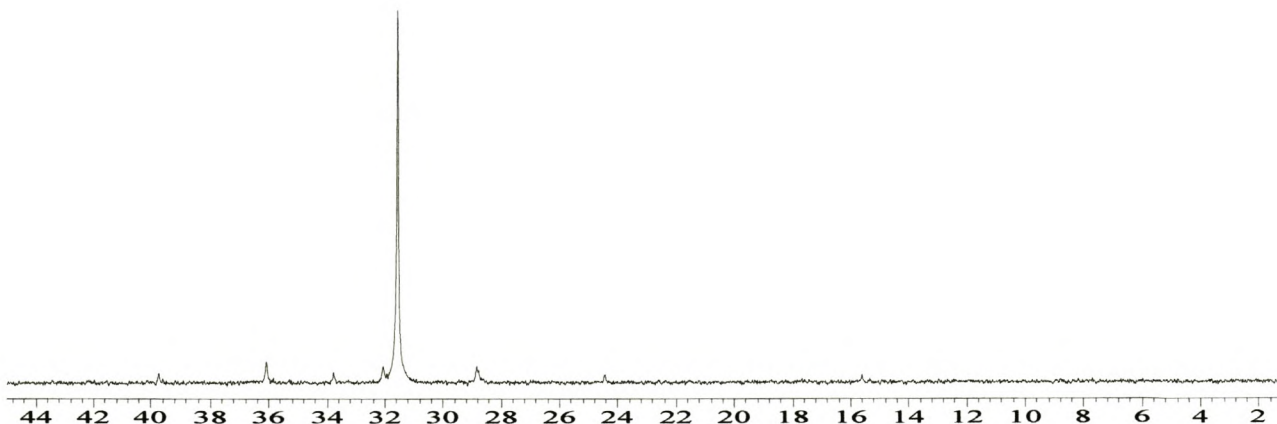**^{13}C NMR of the Prep-TREF 45°C fraction of Plastomer A**
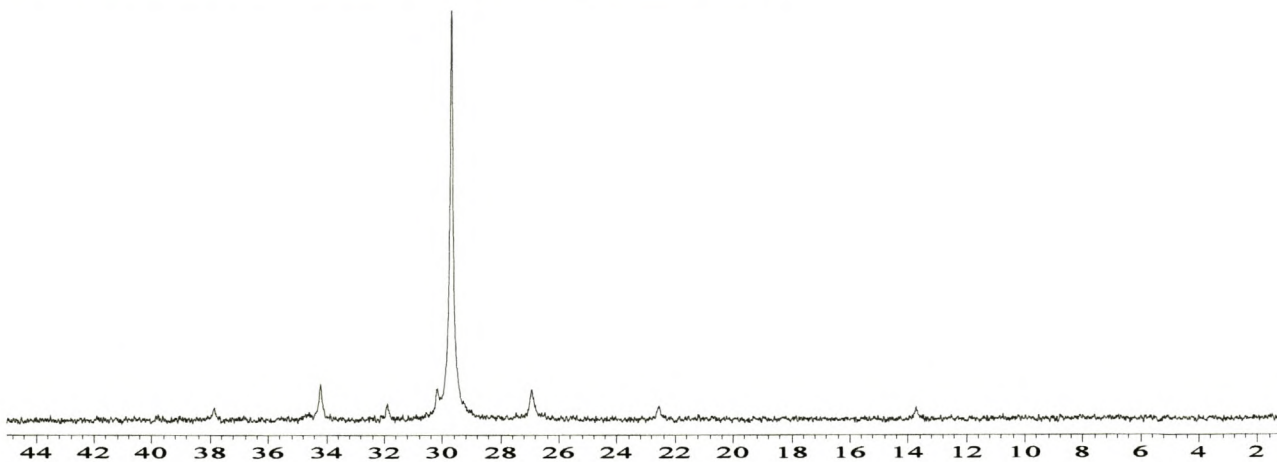
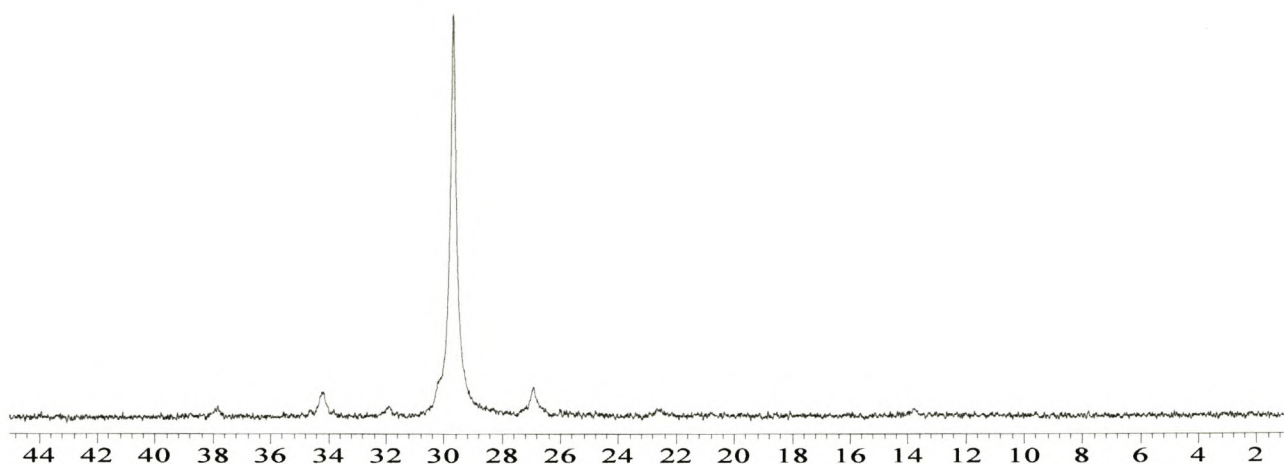**^{13}C NMR of the Prep-TREF 50°C fraction of Plastomer A**
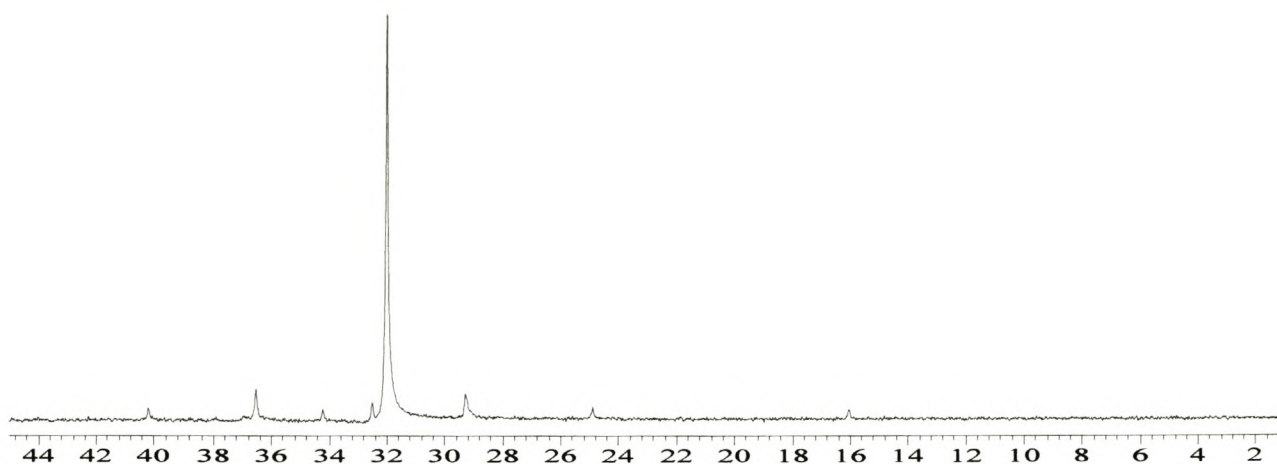
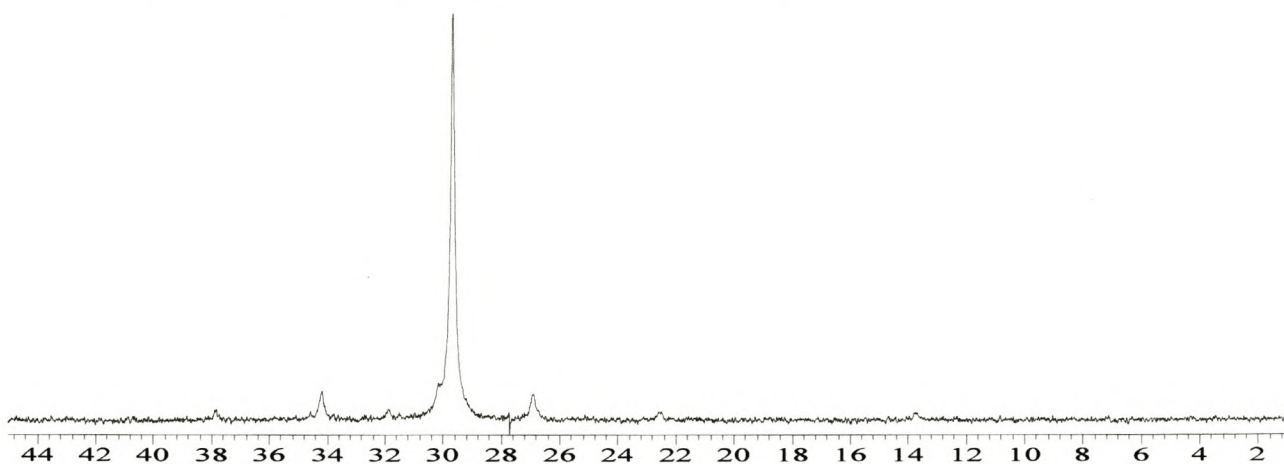**^{13}C NMR of the Prep-TREF 55°C fraction of Plastomer A**
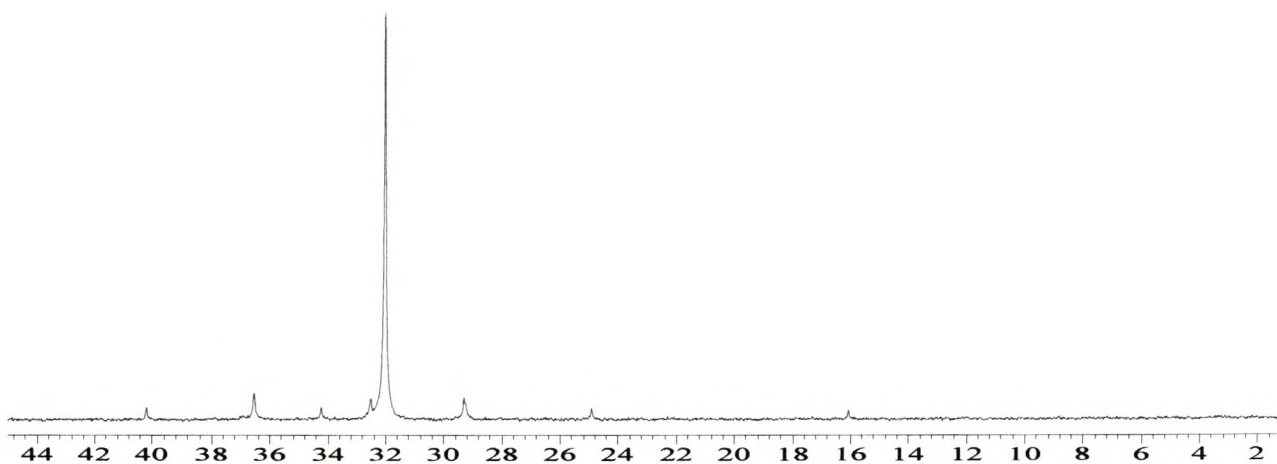
^{13}C NMR of the Prep-TREF 60°C fraction of Plastomer A
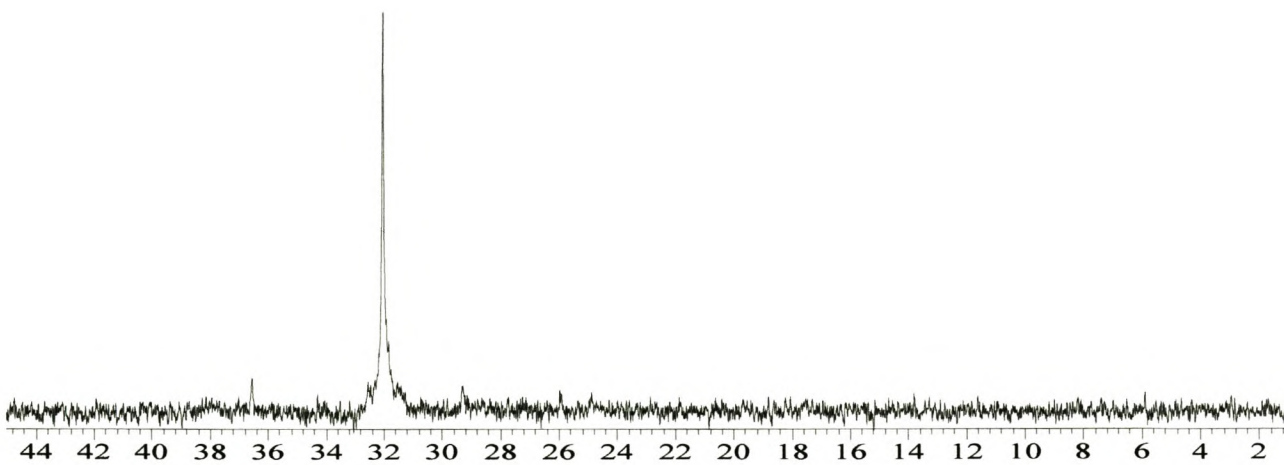

^{13}C NMR of the Prep-TREF 70°C fraction of Plastomer A

^{13}C NMR of the Prep-TREF 80°C fraction of Plastomer A

^{13}C NMR of the Prep-TREF 90°C fraction of Plastomer A

^{13}C NMR of the Prep-TREF 100°C fraction of Plastomer A

153